

# **Crystallization and Solidification Properties of Lipids**

Editors

**Neil Widlak**

Archer Daniels Midland  
Decatur, Illinois

**Richard Hartel**

University of Wisconsin  
Madison, Wisconsin

**Suresh Narine**

M&M/Mars  
Hackettstown, New Jersey



Champaign, Illinois

### **AOCS Mission Statement**

To be a forum for the exchange of ideas, information, and experience among those with a professional interest in the science and technology of fats, oils, and related substances in ways that promote personal excellence and provide high standards of quality.

### **AOCS Books and Special Publications Committee**

G. Nelson, chairperson, University of California at Davis, WRRS, Davis, California  
R. Adlof, USDA, ARS, NCAUR, Peoria, Illinois  
P. Allan-Wojtas, Agriculture and Agri-Canada, Kentville, Nova Scotia  
N.A.M. Eskin, University of Manitoba, Winnipeg, Manitoba  
J. Endres, Fort Wayne, Indiana  
T. Foglia, USDA, ERRC, Wyndmoor, Pennsylvania  
M. Gupta, Richardson, Texas  
C. Hammond, CONDEA Vista Co., Austin, Texas  
L. Johnson, Iowa State University, Ames, Iowa  
H. Knapp, University of Iowa, Iowa City, Iowa  
K. Liu, Hartz Seed Co., Stuttgart, Arkansas  
M. Mathias, USDA, CSREES, Washington, D.C.  
M. Mossoba, Food and Drug Administration, Washington, D.C.  
F. Orthoefer, AC Humko, Cordova, Tennessee  
R. Patzer, Agri. Utilization Research Institute, Marshall, Minnesota  
A. Proctor, University of Arkansas, Fayetteville, Arkansas  
J. Rattray, University of Guelph, Guelph, Ontario  
A. Sinclair, Royal Melbourne Institute of Technology, Melbourne, Australia  
G. Szajer, Akzo Chemicals, Dobbs Ferry, New York  
B. Szuhaj, Central Soya Co., Inc., Fort Wayne, Indiana  
L. Witting, State College, Pennsylvania  
S. Yorston, Shur-Gain, Mississauga, Ontario

Copyright © 2001 by AOCS Press. All rights reserved. No part of this book may be reproduced or transmitted in any form or by any means without written permission of the publisher.

The paper used in this book is acid-free and falls within the guidelines established to ensure permanence and durability.

### **Library of Congress Cataloging-in-Publication Data**

Crystallization and solidification properties of lipids/editors, Neil Widlak, Richard Hartel, Suresh Narine.

p. cm.

Includes bibliographical references and index.

ISBN 1-893997-21-9 (acid-free paper)

1. Lipids—Congresses. 2. Crystallization—Congresses. I. Widlak, Neil. II. Hartel, Richard W., 1951– III. Narine, Suresh.

TP669.5 .C79 2001  
660'.284298—dc21

2001022751  
CIP

Printed in the United States of America with vegetable oil-based inks.

04 03 02 01 5 4 3 2 1

## Preface

The crystallization and solidification properties of lipids are important physical attributes that influence the functional properties of lipids in biological systems, foods, personal care products, pharmaceuticals, and oleo chemicals. A basic understanding of lipid crystallization and solidification is fundamental to understanding and optimizing products or systems containing lipids.

This book is a collection of papers from the American Oil Chemists' Society conference on Crystallization and Solidification Properties of Lipids held in Toronto, Canada, in 2000. The purpose of this conference—as was the purpose of the AOCS conference on Physical Properties of Fats, Oils, and Emulsifiers, which preceded this conference by three years—was to provide the attendee with a combination of

- Plenary papers to provide an overview on the fundamental principles of lipid crystallization
- Original research papers to update the most current research in the area of lipid crystallization
- Papers covering application of lipid crystallization into food, personal care, and pharmaceutical products

Hopefully the papers will be informative and sufficiently thought provoking to stimulate new ideas and research in this field.

We would like to thank all of the authors for their contribution to a very successful conference and for allowing their papers to be published within these proceedings. We would also like to thank the AOCS staff for providing the organization and support to make conferences and books such as this possible.

*Neil Widlak  
Richard Hartel  
Suresh Narine*

# Contents

	Preface .....	v
<b>Phase Behavior and Polymorphism</b>		
Chapter 1	Molecular Aspects in Fat Polymorphism ..... <i>Kiyotaka Sato</i>	1
Chapter 2	Molecular Modeling Applications in Lipid Crystallization ..... <i>James Evans, Alfred Y. Lee, and Allan Myerson</i>	17
Chapter 3	Simultaneous Examination of Structural and Thermal Behaviors of Fats by Coupled X-ray Diffraction and Differential Scanning Calorimetry Techniques: Application to Cocoa Butter Polymorphism ... <i>Michel Ollivon, Christophe Loisel, Christelle Lopez, Pierre Lesieur, Franck Artzner, and Gérard Keller</i>	34
Chapter 4	Effects of Tempering on Physical Properties of Shortenings Based on Binary Blends of Palm Oil and Anhydrous Milk Fat During Storage ... <i>Nor Aini I.</i>	42
<b>Lipid Crystallization Kinetics</b>		
Chapter 5	Triacylglyceride Crystallization in Vegetable Oils: Application of Models, Measurements, and Limitations ..... <i>Jorge F. Toro-Vazquez, Elena Dibildox-Alvarado, Verónica Herrera-Coronado, and Miriam A. Charó-Alonso</i>	53
Chapter 6	Differential Scanning Calorimetry as a Means of Predicting Chocolate Fat-Blooming ..... <i>Imogen Foubert, Inge Van Cauteren, Koen Dewettinck, and André Huyghebaert</i>	79
Chapter 7	Effect of Sucrose Polyesters and Sucrose Polyester–Lecithins on Crystallization Rate of Vegetable Ghee ..... <i>Mohammad Ibrahim Nasir</i>	87
Chapter 8	Experimental Study and Computer Modeling of the Dynamic and Static Crystallization of Cocoa Butter ..... <i>Ph. Rousset and M. Rappet</i>	96
Chapter 9	Crystallization of Palm Oil Products ..... <i>Chiew Let Chong</i>	110
Chapter 10	Comparison of Experimental Techniques Used in Lipid Crystallization Studies ..... <i>A.J. Wright, S.S. Narine, and A.G. Marangoni</i>	120

**Microstructure and Rheology**

Chapter 11	Ultrasonic Characterization of Lipid Crystallization . . . . .	132
	<i>John N. Coupland</i>	
Chapter 12	Solid Fat Index vs. Solid Fat Content: A Comparison of Dilatometry and Pulsed Nuclear Magnetic Resonance for Solids in Hydrogenated Soybean Oil . . . . .	146
	<i>G.R. List, K.R. Steidley, D. Palmquist, and R.O. Adlof</i>	
Chapter 13	Elasticity of Fractal Aggregate Networks: Mechanical Arguments . . . .	153
	<i>Alejandro G. Marangoni and Suresh S. Narine</i>	
Chapter 14	Development and Use of a Novel Technique to Measure Exchange Between Lipid Crystals and Oils . . . . .	160
	<i>Paul Smith, Negin Haghshenas, and Björn Bergenst�hl</i>	

**Crystallization in Emulsions**

Chapter 15	Application of Crystallization Technique for the Lipase-Catalyzed Solid-Phase Synthesis of Sugar Fatty Acid Monoesters . . . . .	168
	<i>Youchun Yan, Uwe T. Bornscheuer, and Rolf D. Schmid</i>	
Chapter 16	Relating Bulk-Fat Properties to Emulsified Systems: Characterization of Emulsion Destabilization by Crystallizing Fats . . . . .	176
	<i>Shawn D. Campbell, H. Douglas Goff, and D�rick Rousseau</i>	
Chapter 17	Crystallization in Emulsion: Application to Thermal and Structural Behavior of Milk Fat . . . . .	190
	<i>Christelle Lopez, Pierre Lesieur, G�rard Keller, and Michel Ollivon</i>	

**Applications**

Chapter 18	Emulsion Partial Coalescence and Structure Formation in Dairy Systems . . . . .	200
	<i>H. Douglas Goff</i>	
Chapter 19	Solidification Processes in Chocolate Confectionary Manufacture . . . .	215
	<i>Gregory R. Ziegler</i>	
Chapter 20	Polymorphism and Texture of Fats . . . . .	225
	<i>J.M. deMan and L. deMan</i>	
	Index . . . . .	237

## Chapter 1

# Molecular Aspects in Fat Polymorphism

Kiyotaka Sato

Hiroshima University, Faculty of Applied Bio Science, Higashi-Hiroshima, Japan 739-8528

### Introduction

Polymorphism of fat crystals is an important phenomenon which relates the molecular structures of fats to their macroscopic physical properties (1–3). This is because melting and solidification behavior, morphology, and aggregation of fat crystals in bulk and emulsions states are determined by the polymorphic modifications of the fats. For example, among the representative polymorphic modifications called  $\alpha$ ,  $\beta'$ , and  $\beta$ , cocoa butter crystals in the confections are in the  $\beta$  modification, the fats in margarine and shortening are of  $\beta'$ , and the  $\alpha$  form was revealed in chilled milk fats in the oil-in-water (O/W) emulsion state (4). Actually, the polymorphic properties of fats in practical applications are determined by multiple factors; cooperating interactions among different triacylglycerols (TAG) involved in every fat material (3), molecular interactions of the individual TAG component (3), influences of crystallization and transformation under various external conditions (in particular, temperature variation and shear) (6), interactions between the fats with the other ingredients such as minor components (7), emulsifiers (8), etc. A lot of work is needed for clarification of the mechanisms controlling the polymorphic behavior of the fat crystals.

In this chapter, molecular factors affecting structural behavior of fat polymorphism are discussed in terms of internal influences of the TAG molecules. In particular, the influences of fatty acid compositions and their positions connected to glycerol carbons on the polymorphism of fat crystals are of primary concern. It has been known that the fats with simple and symmetric fatty acid compositions tend to exhibit typical  $\alpha$ ,  $\beta'$ , and  $\beta$  forms, whereas those with asymmetric mixed-acid moieties often make the  $\beta'$  form more stable (1,9). In the mixed-acid TAG containing unsaturated fatty acid moieties, the number and conformation of the double bond, *cis* or *trans*, give rise to remarkable influences on the polymorphic structures (10–12). The TAG containing different saturated fatty acids with different chain-lengths also revealed quite diversified polymorphism (13–15). Therefore, it may be worthwhile now to discuss the molecular aspects of the polymorphism of fats. This consideration may also be a prerequisite for molecular design of structured fats, in combination with nutritional and metabolic properties.

## Fat Polymorphism: Definition

The nature and compositions of three fatty acid moieties of a TAG molecule, defined  $R_1$ ,  $R_2$ , and  $R_3$ , determine its chemical property (1). The three polymorphs, called  $\alpha$ ,  $\beta'$ , and  $\beta$  are based on the subcell structures, which define cross-sectional packing modes of the zigzag aliphatic chain, as shown in Figure 1A (16). The chainlength structure produces a repetitive sequence of the acyl chains involved in a unit cell lamella along the long-chain axis, playing critical roles in the mixing phase behavior of different types of the TG in a solid-phase. Double chainlength (DCL) structure is formed when the chemical properties of the three acid moieties are the same or very similar. By contrast, when the chemical properties of one or two of the three chain moieties are largely different from the others, a triple chain length (TCL) structure is formed because of chain sorting, as verified by single-crystal analysis of 1,2-dipalmitoyl-3-acetyl-*sn*-glycerol (PP2)  $\beta$  form (17). Quatro-layer and hexa-layer chain-length structures shown in Figure 1B have been reported for the TAG containing asymmetric fatty acid moieties (14), whose details are discussed in this chapter.

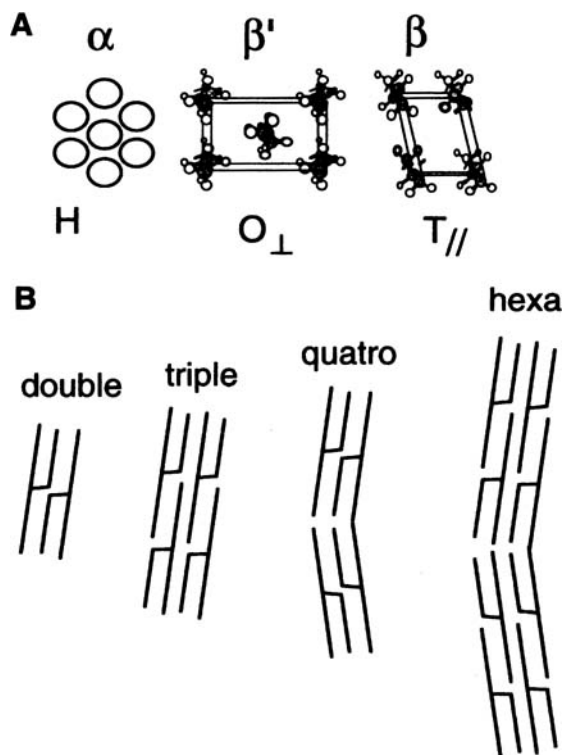


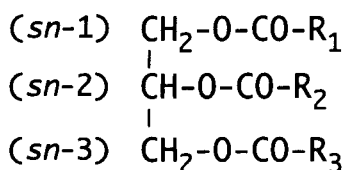
**Fig. 1.** (A) Three typical subcell arrangements and (B) four typical chainlength structures.

## Molecular Interactions in TAG

Figure 2 illustrates diversity in the fatty acid types and compositions of the TAG. The mono-acid and mixed-acid TAG are defined, respectively, on whether the fatty acid chains are of the same fatty acid molecules or not. Even for the mono-acid TAG, the diversity maintains in chainlength and parity (odd or even numbers of carbon atoms) of the fatty acids, the number and position of the double bond and the conformation of the double bond, *cis* or *trans*, etc. As for the mixed-acid TAG, polymorphic diversity is superimposed over that of the mono-acid TAG in the form of *sn* (stereo-specific numbered) position.

The relevance of the molecular structural diversity of the TAG to practical application may be understood by taking some examples of natural fats: cocoa butter with major TAG of POP (1,3-dipalmitoyl-2-oleoyl-*sn*-glycerol), POS (1,3-palmitoyl-stearoyl,2-oleoyl-*rac*-glycerol) and SOS (1,3-distearoyl-2-oleoyl-*sn*-glycerol), milk fats whose major TAG are saturated-unsaturated mixed-acid TAG, and mixed-acid TAG with saturated fatty acids having different chainlengths (2). In these natural fats, few mono-acid TAG are present as major TAG components, and the major fats are composed of the mixed-acid TAG. Therefore, it is required to elucidate for the polymorphic structures of the mixed-acid TAG.

Figure 3 illustrates major molecular interactions which are thought to be most influential in exhibiting the polymorphic structures of the fats: (i) aliphatic chain-packing caused by hydrocarbon chain-chain interactions, as revealed in the subcell structures shown in Figure 1A; (ii) glycerol conformation whose influences may act through dipole-dipole interactions of the glycerol groups; (iii) methyl end stacking whose influences may play important roles in organizing different chain-length structures; and (iv) olefinic interactions which may be predominant in poly-



### mono-acid

\*saturated: chainlength, odd/even

\*unsaturated: chainlength, odd/even,  
number and position of  
double bond, *cis/trans*

### mixed-acid

\*different chainlength

\*saturated/unsaturated

\**sn*-position

**Fig. 2.** Diversity in fatty acid compositions of triacylglycerols.

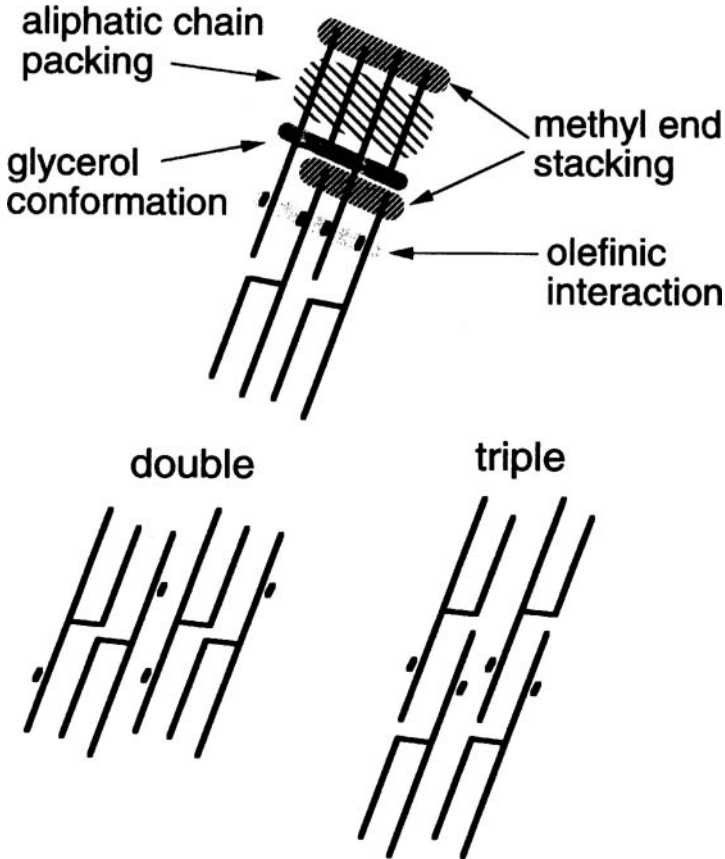


**Fig. 3.** Illustration of molecular interactions most influential to structural stabilization of triacylglycerol crystals.

morphic occurrence of the mixed-acid TAG containing the unsaturated fatty acid moieties.

This category of the molecular interactions and its implication may be well understood, if one thinks of saturated-unsaturated mixed-acid TAG, such as SOS (Table 1, to be further discussed below). SOS has five polymorphs in which the DCL structure appears in the least stable polymorph of  $\alpha$ , and TCL is revealed in the more stable forms of  $\gamma$ ,  $\beta'$ , and two  $\beta$  forms (10). This means that structural stabilization prevails in the TCL structure compared with the DCL structure. Apparently, the modes of the methyl end stacking and glycerol conformation look simpler in the DCL structure than in the TCL structure, since two types of the methyl end stacking are formed, and thereby local molecular packing around the glycerol groups may be destabilized in the TCL structure. However, in the case of SOS, stearic hindrance

around the olefinic groups might make the DCL structure unstable, and the TCL structure may release this instability despite its complicated methyl end stacking and the glycerol conformations.

Taking into account the above category, we will discuss the latest work on the molecular structures of the mixed-acid TAGs in the next sections.

## Molecular Structures of Mixed-Acid TAG

*PP<sub>n</sub>*. In *PP<sub>n</sub>*, the carbon number of the *sn*-3 fatty acid chain (even-numbered, *n*) was varied from 2 to 14, while palmitic acid at the *sn*-1 and *sn*-2 positions was unchanged (13). Likewise, *PP<sub>n</sub>* was not racemic, but optically active. Figure 4 shows the occurrence of polymorphic forms of *PP<sub>n</sub>*, in which the number of polymorphic forms, relative stability of  $\beta'$  and  $\beta$ , and the chainlength structure varied in a drastic manner. For example, the single-chain structure was observed in the  $\alpha$  forms of PP4, PP6, and PP8, hexa-chain, and quatro-chainlength structures were seen in  $\beta'_1$  of PP10 and  $\beta'_2$  of PP14, respectively (15). Interestingly, these unusual chainlength structures were often revealed in the metastable forms. As to the most stable form,  $\beta$  was for PP2, PP4, PP10, and PP12, whereas  $\beta'$  was for PP6, PP8, and PP14. Single-crystal X-ray structural determination proved that PP2  $\beta$  was of the DCL structure with the  $T_{//}$  subcell (17) and PP14  $\beta'_2$  was of the four chainlength structure with the hybrid orthorhombic subcell structure (18). In this section, we discuss the molecular structures of PP2  $\beta$  and PP14  $\beta'_2$  as shown in Figure 5.

PP2  $\beta$  is of the DCL structure (Fig. 5A) in which the palmitic acid chains are packed in the same leaflet, whereas the acetic acid chains are arranged in the same

<i>n</i>	2			4			6, 8	
form	$\alpha$	$\beta'$	$\beta$	$\alpha$	$\beta'$	$\beta$	$\alpha$	$\beta'$
chain-length	2	3	2	1	3	2	1	3

<i>n</i>	10					12				14		
form	$\alpha$	$\beta'_3$	$\beta'_2$	$\beta'_1$	$\beta$	$\alpha$	$\beta'_2$	$\beta'_1$	$\beta$	$\alpha$	$\beta'_2$	$\beta'_1$
chain-length	2	2	2	6	3	2	2	2	2	2	4	2

Fig. 4. Polymorphism in *PP<sub>n</sub>* with different chainlength of the *sn*-3 chains.

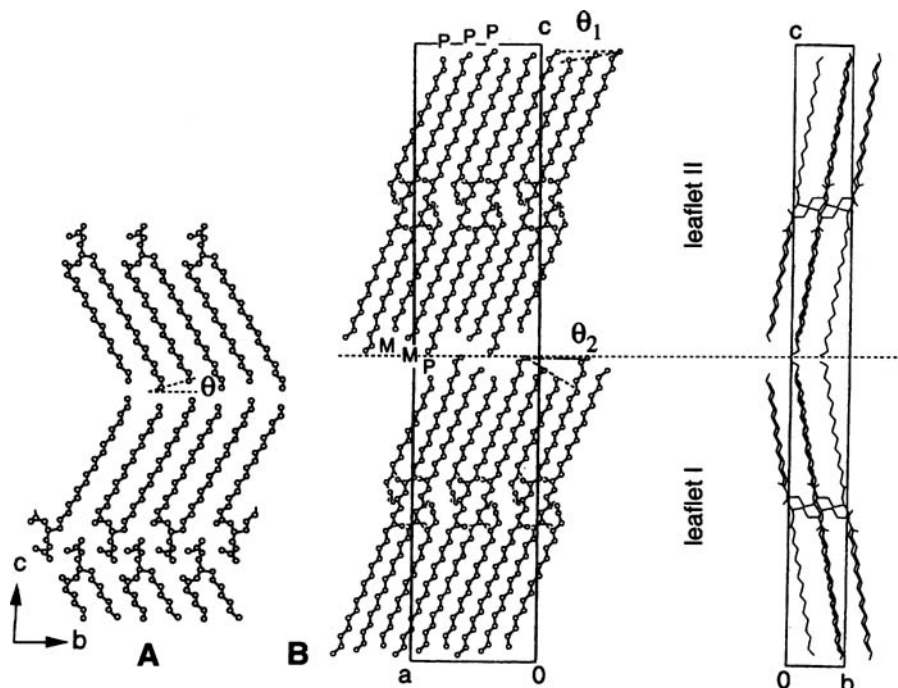


Fig. 5. Crystal structures of (A) PP2  $\beta$ , and (B) PP14  $\beta'_2$ .

plane as the glycerol groups due to its short chainlength (17). In other words, no independent leaflet was formed for the *sn*-3 acetic acid moiety. Therefore, the methyl end stacking is singly defined for the palmitic acid moieties, as shown in Figure 5A. From this, it is found that the glycerol conformation is most influential to stabilization of palmitic-acetic chain-chain interactions at one side, and the methyl end stacking is also influential at the other side in forming the DCL structure.

In contrast to PP2  $\beta$ , the molecular structure of PP14  $\beta'_2$  showed quite unique properties as summarized in the following (Fig. 5B): (i) a unit lamellae reveals quatro chainlength structure consisting of two double-layer leaflets (leaflets I and II); (ii) the two DCL leaflets are combined end-to-end in the unit lamellae; (iii) the chain axes of the two leaflets are alternatively inclined against the lamellar interface, as shown in the (b, c) projection; and (iv) two modes of the methyl end stacking are revealed; deep zigzag stacking at the interior portion of the quatro-layer, and thinner zigzag stacking at the outer portion, as shown in dashed lines of (a, c) projection.

Quite a complicated structure of PP14  $\beta'_2$  is partly explained by defining two asymmetric units, (a and b, Fig. 6A), which form a hybrid-type orthorhombic perpendicular subcell (Fig. 6B). The two asymmetric units reveal different glycerol conformations; *trans* for *sn*-1(P, palmitic) and *sn*-2(P) but *gauche* for *sn*-3 (M,

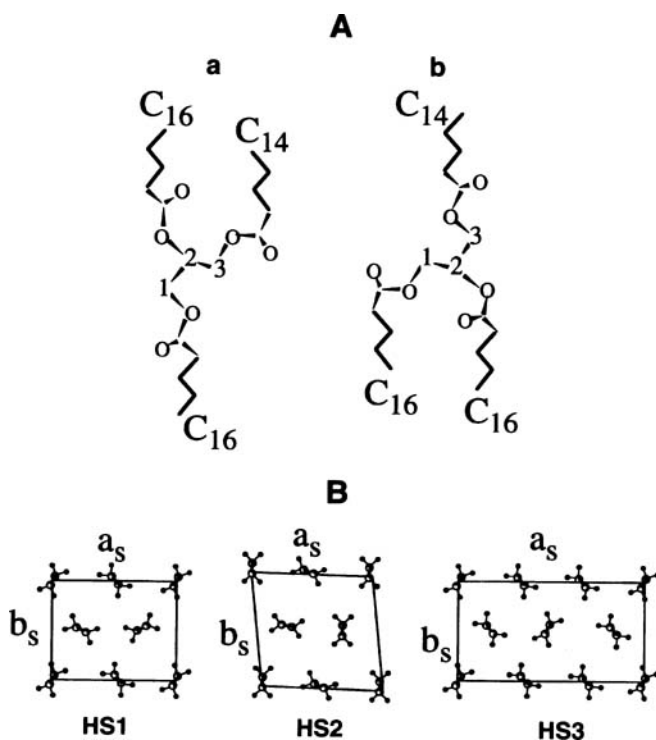


Fig. 6. (A) Two asymmetric units in PP14  $\beta'_2$  and (B) three hybrid-type subcells.

myristic) in A, and *trans* for *sn*-2(P) and *sn*-3(M) but *gauche* for *sn*-1(P) in B. In accordance with the presence of the two asymmetric units, the subcell having the orthorhombic symmetry is not as simple as that shown in Figure 1(A). A hybrid-type subcell with a superimposing periodicity along the  $a_s$  direction as triple that of the usual simple orthorhombic perpendicular subcell was formed, named HS3. In the lipid crystals, hybrid-type subcells have been observed in phospholipid (HS1) (19,20) and cerebroside (HS2) (21).

Two types of methyl end stacking mode were revealed in PP14  $\beta'_2$ : the outer interface composed of PPP and the inner interfaces composed of PMM, as shown in Figure 5. The difference in the two methyl end stacking modes appeared as inclination angles with respect to the lamella plane defined in Figure 5B:  $\theta_1 = 9.6^\circ$  for the PPP interface and  $\theta_2 = 38.0^\circ$  for the PMM interface. The latter value for the PMM interface is quite anomalous, if one compares it with the values of the other crystals:  $11^\circ$  in PP2  $\beta$  ( Fig. 5A) and  $12^\circ$  in tricaprolylglycerol  $\beta$  (22,23). It seems that the instability of the methyl end stacking of the methyl end terrace planes having the large  $\theta$  value for the PMM interface may be compensated by arranging them face-to-face at the interior interfaces of the quatro chain-length structure.

The molecular structure of PP14  $\beta'_2$  shown in Figures 5 and 6 is a good example to understand the effect of combined interactions of the methyl end stacking, the lateral chain packing, and the glycerol conformation on the structural stabilization of the TAG crystals. For the moment, it is rather difficult to assess how these interactions cooperate and which interaction plays the dominant role. It has been widely observed that the  $\beta'$  form is stabilized when a TAG contains different kinds of fatty acid moieties which are connected to the glycerol carbons in an asymmetric manner, like PP14 (9).

In this connection, one may refer to polymorphism of a homologous series of  $C_nC_{n+2}C_n$ , in which  $n$  was even-numbered carbon atoms ranging from 10 to 16 (24,25). In these TAG, the most stable form is  $\beta'$ , and no  $\beta$  form was observed. The crystal structure of the  $\beta'$  form  $C_nC_{n+2}C_n$  may, quite simply and symbolically, be illustrated in Figure 7A, in which the TAG molecules are bent with respect to the lamella plane at the glycerol group (26). In this regard, one may note that vibration spectroscopic (FT-IR) analyses of  $\beta'_1$  in PP14 indicate the structure of the model Figure 7A (27). This makes a clear contrast to the structure of  $\beta'_2$  in PP14 where molecules are bent at the methyl end packing, as modeled in Figure 7B. The two reports on the  $\beta'$  forms in  $C_nC_{n+2}C_n$  and PP14 may raise a concept of "diversity in the  $\beta'$  structures." Further research on the TAG exhibiting  $\beta'$ -stabilized polymorphism is definitely required to enrich the understanding of the  $\beta'$  structure. This is because many food fats are functional in this polymorphic form, and new ways to prohibit the transformation from  $\beta'$  to  $\beta$  may be born from the structural clarification of the  $\beta'$  form.

### Saturated-Unsaturated Mixed-Acid TAG

The mixed-acid TAG containing saturated fatty acids at the *sn*-1 and *sn*-3 glycerol carbon positions and unsaturated fatty acids at the *sn*-2 position, namely the St-U-St TAG, chain-chain interactions among the saturated and unsaturated fatty acid moieties, or within every saturated or unsaturated moieties, play critical roles in their complicated polymorphic transformations. Precise observation was recently

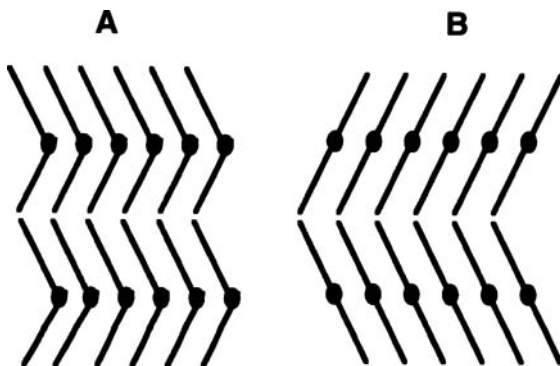


Fig. 7. Two possible structures of  $\beta'$  in triacylglycerols.

TABLE 1

Occurrence and Subcell Structures of Polymorphic Forms of SOS, SRS, and SLS

		$\alpha$	$\gamma$	$\beta'$	$\beta_2, \beta_1$	
						
		TAG <sup>a</sup>			Subcell <sup>b</sup>	
SOS	SRS	SLS	Saturated	Unsaturated		
$\alpha$ -2	$\alpha$ -2	$\alpha$ -2	H	H		
$\gamma_{\perp}$ -3	$\gamma_{\perp}$ -3	$\gamma_{\perp}$ -3	//-type	H		
$\beta'$ -3	$\beta'_2$ -3	—	$O_{\perp}$	H		
	$\beta'_1$ -3					
$\beta_2$ -3	—	—	$T_{//}$	$T_{//}$ or $O'_{//}$		
$\beta_1$ -3			$T'_{//}$	$T_{//}$		

<sup>a</sup>S: stearoyl, O: oleoyl, R: ricinoleoyl, L: linoleoyl.<sup>b</sup>H: hexagonal,  $O_{\perp}$ : orthorhombic perpendicular,  $O'_{//}$ : orthorhombic parallel,  $T_{//}$ : triclinic parallel.

made on the St-U-St TAG having the *sn*-2 acids of oleic (10,28,29), ricinoleic (21), and linoleic (31).

Table 1 shows the polymorphic behavior of the three TAG in which the saturated fatty acid at the the *sn*-1 and *sn*-2,3 positions is stearic and the *sn*-2 acid varied from oleic (SOS), ricinoleic (SRS) to linoleic (SLS). As a reference, a typical feature of polymorphic transformation of SOS from  $\alpha$  to  $\beta_1$  forms through  $\gamma$ ,  $\beta'$  and  $\beta_2$  is illustrated in Table 1 (10). As briefly mentioned in the previous section, one of the unique polymorphic properties in SOS is that the chainlength structure converted from DCL ( $\alpha$ ) to TCL ( $\gamma$ ,  $\beta'$ ,  $\beta_2$ , and  $\beta_1$ ), and the subcell structures of stearic and unsaturated acid leaflets in the TCL polymorphs changed in different manners. This transformation behavior is caused by the steric hindrance of steric and unsaturated acid chains, as well as by the structural stabilization of the aliphatic chains and glycerol groups altogether, as briefly summarized in the following.

**$\phi$  form.** This form appears in SOS, SRS, and SLS. The DCL structure assumes the coexistence of the stearoyl and unsaturated moieties in the same leaflets, where hexagonal subcell leads to a disordered aliphatic conformation.

**$\gamma$  form.** This form appears in SOS, SRS, and SLS, and SLS has this form as the most stable form (31). In the TCL structure, the stearoyl and unsaturated leaflets are separated through the chain sorting during the  $\alpha$ - $\gamma$  transformation. The stearoyl leaflet assumed a specific parallel packing, and hexagonal subcell still remained in the unsaturated leaflets. The TAG molecules are arranged normal to the lamellar interface (10).

**$\beta'$  form.** This form appears in SOS and SRS, and, in the latter, two  $\beta'$  forms are most stable and no  $\beta$  form occurs (30). In the TCL structure, the stearoyl leaflet

assumed the  $O_{\perp}$  subcell and the hexagonal subcell structure still remained in the unsaturated leaflets.

*$\beta$  form.* SOS has two  $\beta$  forms. The subcell structure of the stearyl and oleoyl leaflets was  $T_{//}$  in  $\beta_1$ , whereas  $T_{//}$  or  $O'_{//}$  may be the subcell structure of the oleoyl leaflet in  $\beta_2$ .

As to the molecular interactions, it is worth noting that SRS has no  $\beta$  form but  $\beta'$  is most stable, and neither  $\beta'$  nor  $\beta$  is present in SLS. Correspondingly, thermal data of melting of the polymorphic forms of SRS and SLS, shown in Table 2 together with those of tristearoylglycerol (SSS) and SOS, indicate structural stability of every polymorphic forms. The structural stability can be evaluated by comparing the values of entropy of fusion (DS), which is the difference in entropy between the crystalline form (ordered, and small  $S$  value) and liquid (disordered, and large  $S$  value). Therefore, it follows that the larger the DS values, the more stabilized are the polymorphic structures.

As for the  $\alpha$  form,  $\Delta S$  is largest in SSS. This means that the DCL structure in  $\alpha$  is most stabilized in this TAG, because of minimized chain-chain steric hindrance which is enhanced in the saturated-unsaturated mixed-acid TAG. As for the  $\gamma$  form,  $\Delta S$  is largest in SLS, although there is no  $\gamma$  in SSS. This property is discussed at a molecular level below. The  $\Delta S$  value of  $\beta'$  is largest in SRS, as dramatically shown in its values of  $575.3 \text{ J mol}^{-1} \text{ K}^{-1}$ , which is much larger even than SSS  $\beta$  ( $544.3 \text{ J mol}^{-1} \text{ K}^{-1}$ ). Finally,  $\Delta S$  of  $\beta$  form is larger in SSS than in SOS, indicating that the presence of a *cis*-double bond enlarges the entropy value of SOS  $\beta$ .

**TABLE 2**

Enthalpy ( $\Delta H$ ) and Entropy ( $\Delta S$ ) of Polymorphic Transformations of SSS, SOS, SRS, and SLS<sup>a</sup>

	Form	Melting point (°C)	$\Delta H$ (kJ mol <sup>-1</sup> )	$\Delta S$ (J mol <sup>-1</sup> K <sup>-1</sup> )
SSS	$\alpha$ -2	55.0	109.3	333.1
	$\beta'$ -2	61.6	142.8	426.5
	$\beta$ -2	73.0	188.4	544.3
SOS	$\alpha$ -2	23.5	47.7	160.7
	$\gamma$ -3	35.4	98.5	319.2
	$\beta'$ -3	36.5	104.8	338.5
	$\beta_2$ -3	41.0	143.0	455.2
	$\beta_1$ -3	43.0	151.0	477.6
SRS	$\alpha$ -2	25.8	58.1	194.4
	$\gamma$ -3	40.6	119.6	381.3
	$\beta_2$ -3	44.3	171.2	539.3
	$\beta_1$ -3	48.0	184.8	575.3
SLS	$\alpha$ -2	20.8	40.9	139.2
	$\gamma$ -3	34.5	137.4	448.7

<sup>a</sup>See Table 1 for abbreviations.

The molecular aspect of the structural stabilization of SRS  $\beta'$  may be discussed by taking into account the hydrogen bonding in the ricinoleoyl chains. Figure 8A shows X-ray diffraction (XRD) short spacing and Fourier transform-infrared (FT-IR) spectra of  $\alpha$ ,  $\gamma$ , and two  $\beta'$  forms of SRS. The long-spacing values of the four forms are 4.87 nm ( $\alpha$ ), 7.10 nm ( $\gamma$ ), 6.97 nm ( $\beta'_2$ ), and 6.85 nm ( $\beta'_1$ ). Hence  $\alpha$  is the DCL structure, and the other three forms are of the TCL structure. The XRD short-spacing spectra are quite equivalent to the corresponding poly-

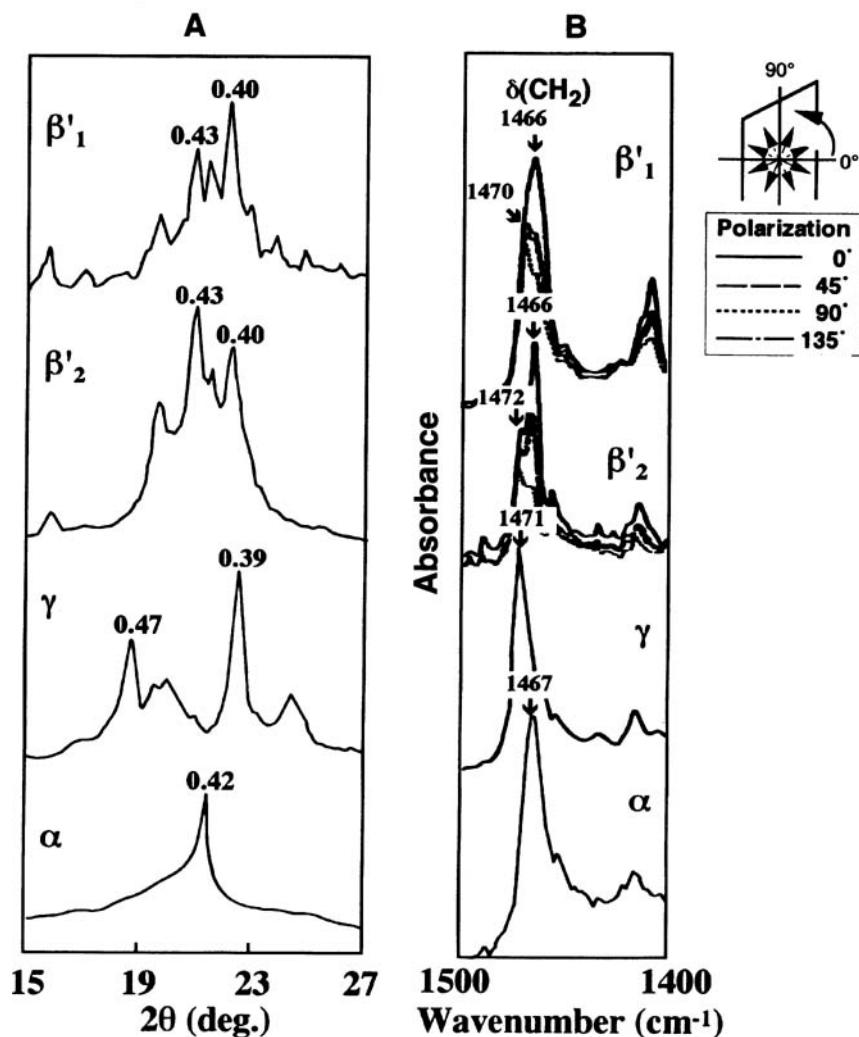
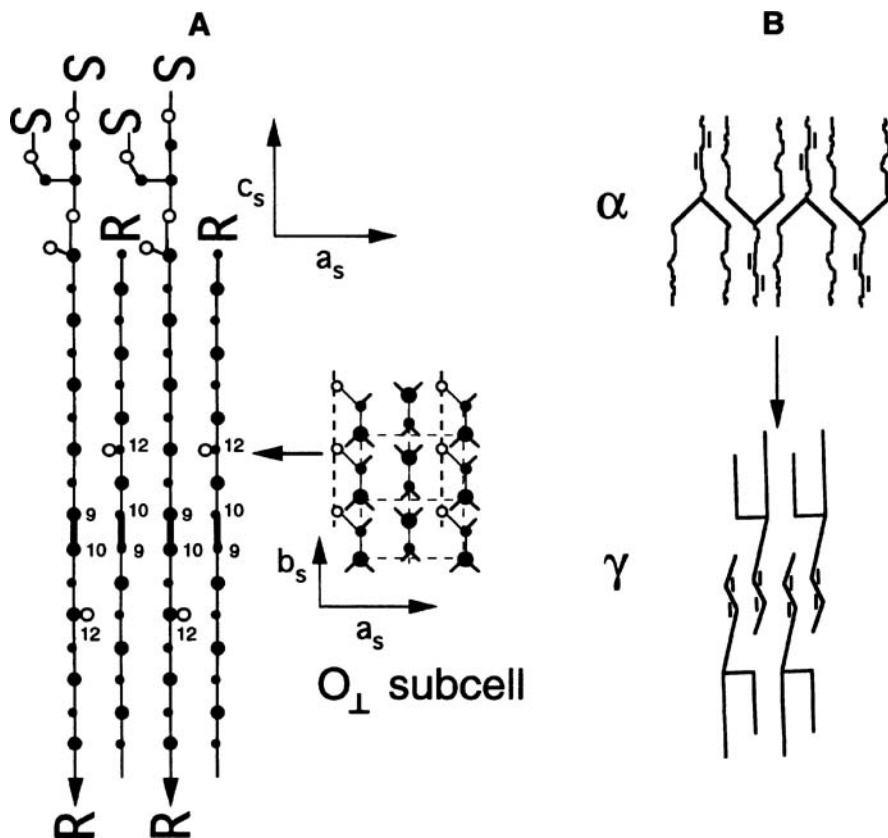


Fig. 8. (A) X-ray diffraction spectra (unit, nm) and (B) polarized Fourier transform-infrared spectra of the four polymorphs in ricinoleic acid (SRS).

morphs of POP (10). The micro-probe polarized FT-IR spectra of  $\text{CH}_2$  scissoring mode show that aliphatic chains in  $\alpha$  and  $\gamma$  are in the disordered state, showing a single absorption spectra (30). However, anisotropic property with respect to the rotation of the polarizing direction of incident beam against the crystal edge direction showed that the subcell structure is of the O type for  $\beta'_2$  and  $\beta'_1$ . Although the detailed structures of the two  $\beta'$  forms are still open to question, it was assumed that the chain packing of the ricinoleoyl chains in SRS  $\beta'$  is so tight that the subcell structure of  $\text{O}_\perp$  is stabilized through the glycerol groups, making  $\beta'$  most stable, as modeled in Figure 9A.

In SLS, the polymorphic transformation from  $\alpha$  to  $\gamma$  proceeded quite fast, because thermal energy easily accelerated the transformation between the two forms having rather low melting points. Therefore, Synchrotron radiation X-ray diffraction (SR-XRD) was employed to monitor the transformation process, since



**Fig. 9.** Molecular models of (A)  $\beta'$  of SRS, and (B)  $\alpha$  and  $\gamma$  forms of linoleic acid (SLS). See Figure 8 for abbreviation.

the time resolution for spectral analysis was so short (10 s) in the *in situ* observation during rapid cooling and heating processes (31). Figure 10 shows the SR-XRD spectra of the  $\alpha$ - $\gamma$  transformation and the melting of the  $\gamma$  form of SLS, during cooling from 50 to 10°C, isothermal transformation at 10°C and subsequent heating to 50°C. The XRD short-spacing spectra of the two forms, both are equivalent to those of SRS shown in Figure 8, converted during the transformation. The melting of  $\gamma$  did not crystallize any more stable forms, such as  $\beta$  and  $\beta'$  as observed in POP and SOS (1) and SRS (30).

In SLS, the steric hindrance caused by the interactions among the stearyl chains at the *sn*-1 and *sn*-3 positions and the linoleoyl chains at the *sn*-2 position may lead to more enhanced destabilization of the DCL  $\alpha$  form, in comparison to the same forms of the other TAG. Hence the  $\Delta S$  value of SLS  $\alpha$  is smallest.

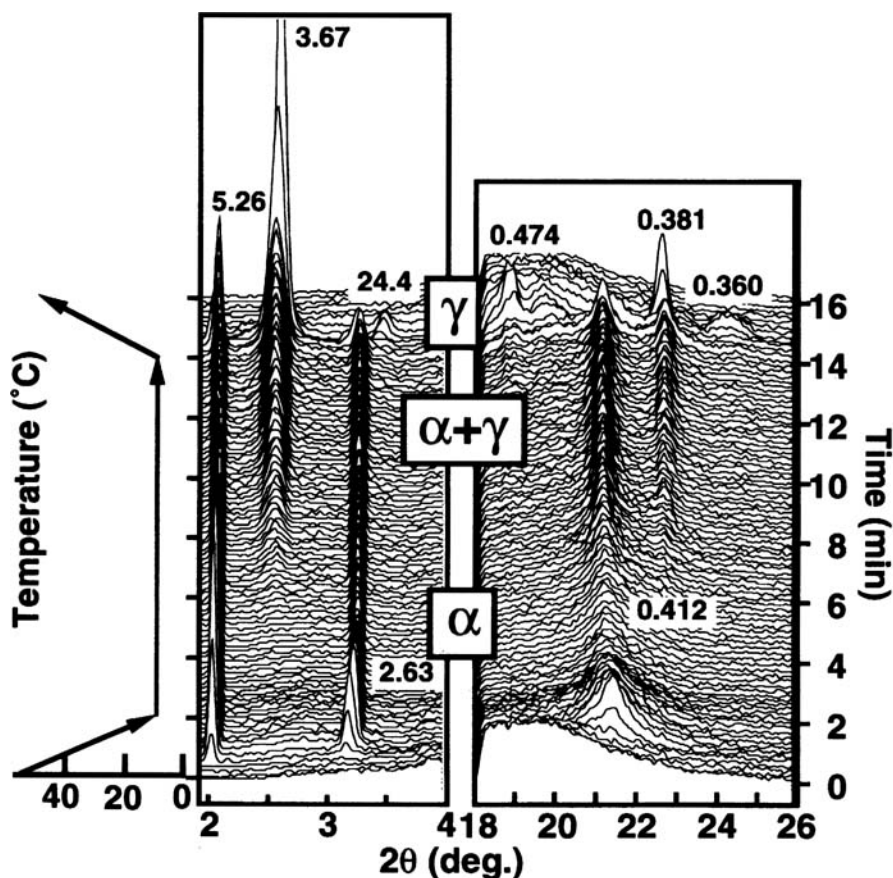


Fig. 10. *In situ* Synchrotron radiation X-ray diffraction spectra of  $\alpha$ - $\gamma$  transformation and melting of  $\gamma$  of SLS (unit, nm). See Figure 9 for abbreviation.

However, the situation may be converted in the  $\gamma$ -3 form, in which the presence of two *cis*-double bonds may stabilize the chain-chain interactions of the linoleic acid leaflet, prohibiting the transformation into more stable forms of  $\beta'$  or  $\beta$  as illustrated in Figure 9B. For this reason, the  $\Delta S$  value of  $\gamma$  of SLS is much larger than those of  $\gamma$  of SOS and SRS. Furthermore,  $\Delta S$  of SLS  $\gamma$  is as large as  $\beta$  forms of SOS. Mechanistically, the transformation from  $\gamma$  to  $\beta'$  or  $\beta$  is associated with an inclined chain arrangement with respect to the lamellar interface (10), which might be prohibited by the chain-chain interactions of the linoleoyl leaflets in SLS.

Table 3 shows the TAG involving elaidic acid placed at different glycerol carbon positions together with stearic and palmitic acids (11,12). Quite curiously,  $\beta'$  is most stable in PEP (1,3-dipalmitoyl, 2-elaidoyl-*sn*-glycerol), EPP, and PEE, whereas SES (1,3-distearoyl, 2-elaidoyl-*sn*-glycerol), ESS, and SEE reveal the most stable form of  $\beta$ . In the series of St. Oleic. St TAG, the replacement of stearic acid with palmitic acid did not show any drastic conversion with respect to relative stabilization of  $\beta'$  and  $\beta$  (10). For example, the  $\beta$  form is most stable both in SOS and POP. Therefore, one may assume that the chain end packing mode composed of the saturated and elaidic acids may be a key factor in controlling the relative occurrence of the  $\beta'$  and  $\beta$  forms in the saturated-elaidic mixed-acid TAG exemplified in Table 3. This problem is completely open to question.

A brief review has been made on the molecular aspects of the polymorphic structures of the TAG containing different fatty acid moieties (mixed-acid TAG). The clarification of the polymorphic properties of the mixed-acid TAG has high implication to real fat systems, since many naturally occurring TAG are the mixed-acid TAG, and the polymorphic stability regarding, in particular, the stabilization of the  $\beta'$  form seems to be tightly related to inter- and intra-molecular chain-chain interactions. Recent work on atomic-level analyses of the crystal structures of the  $\beta'$  forms has given quite informative data as discussed in this chapter. Although the approach so far has been made with experimental techniques (X-ray, FT-IR, etc.), it is of the highest opportunity and challenge to assess the molecular structures using computer modeling techniques based on the atomic-level crystal structures of the model substances.

**TABLE 3**  
Polymorphic Occurrence of Saturated-Elaidic Mixed-Acid Triacylglycerols (TAG)<sup>a</sup>

TAG		Polymorphic forms		
PEP	$\alpha$	$\beta'_2$	$\beta'_1$	—
EPP	$\alpha$	$\beta'_2$	$\beta'_1$	—
PEE	$\alpha$	$\beta'_2$	$\beta'_1$	—
SES	$\alpha$	$\beta'_2$	$\beta'_1$	$\beta$
ESS	$\alpha$	$\beta'_2$	$\beta'_1$	$\beta$
SEE	$\alpha$	—	—	$\beta$

<sup>a</sup>Not detectable. PEP, 3-dipalmitoyl, 2-elaidoyl-*sn*-glycerol; SES, 1,3-distearoyl,2-elaidoyl-*sn*-glycerol.

## References

1. Small, D.M., Glycerides, in *The Physical Chemistry of Lipids, from Alkanes to Phospholipids*, Handbook of Lipid Research Series, Vol. 4, edited by D.J. Hanahan, Plenum Press, New York, 1986, pp. 475–522.
2. Sato, K., Polymorphism of Pure Triacylglycerols and Natural Fats, in *Advances in Applied Lipid Research*, Vol. 2, edited by F.B. Padley, JAI Press, London, 1996, pp. 213–268.
3. Sato, K., S. Ueno, and J. Yano, Molecular Interactions and Kinetic Properties of Fats, *Prog. Lipid Res.* 38: 91–116 (1999).
4. Lopez, C., P. Lesieur, G. Keller, and M. Ollivon, Thermal and Structural Behavior of Milk Fat 1. Unstable Species of Cream, *J. Coll. Interf. Sci.* 229: 62–71 (2000).
5. Kaneko, F., J. Yano, and K. Sato, Diversity in Fatty Acid Conformation and Chain Packing in *cis*-Unsaturated Lipids, *Curr. Opin. Struct. Biol.* 8: 417–425 (1998).
6. Sato, K., Solidification and Phase Transformation Behaviour of Food Fats—A Review, *Fett/Lipid* 101: 467–474 (1999).
7. Tietz, R.A., and R.W. Hartel, Effects of Minor Lipids on Crystallization of Milk Fat-Cocoa Butter Blends and Bloom Formation in Chocolate, *J. Am Oil Chem. Soc.* 77: 763–771 (2000).
8. Katsuragi, T., Interactions Between Surfactants and Fats, in *Physical Properties of Fats, Oils, and Emulsifiers*, edited by N. Widlak, AOCS Press, Champaign, 1999, pp. 211–219.
9. Hagemann, J. W., Thermal Behavior of Polymorphism of Acylglycerols, in *Crystallization and Polymorphism of Fats and Fatty Acids*, edited by N. Garti and K. Sato, Marcel Dekker, New York, 1988, pp. 9–95.
10. Sato, K., T. Arishima, Z.H. Wang, K. Ojima, N. Sagi, and H. Mori, Polymorphism of POP and SOS. I. Occurrence and Polymorphic Transformation, *J. Am. Oil Chem. Soc.* 66: 664–674 (1989).
11. Desmedt, A., C. Culot, C. Deroanne, F. Durant, and V. Gibon, Influence of *cis* and *trans* Double Bonds on the Thermal and Structural Properties of Monoacid Triglycerides, *Ibid.* 67: 653–660 (1990).
12. Elisabetini, P., G. Lognay, A. Desmedt, C. Culot, N. Istasse, E. Deffense, and F. Durant, Synthesis and Physicochemical Characterization of Mixed Diacid Triglycerides That Contain Elaidic Acid, *Ibid.* 75: 285–291 (1998).
13. Kodali, D.R., D. Atkinson, T.G. Redgrave, and D.M. Small, Synthesis and Polymorphism of 1,2-dipalmitoyl-3-acyl-*sn*-glycerol, *Ibid.* 61: 1078–1084 (1984).
14. Kodali, D.R., D. Atkinson, and D.M. Small, Polymorphic Behavior of 1,2-dipalmitoyl-3-lauroyl (PP12)- and 3-Myristoyl (PP14)-*sn*-glycerols, *J. Lipid Res.* 31: 1853–1864 (1990).
15. Kodali, D.R., D. Atkinson, and D.M. Small, Molecular Packing in Fats, Influences of Acyl Chain Length and Unsaturation, *J. Disp. Sci. Technol.* 10: 393–440 (1990).
16. Larsson, K., Classification of Glyceride Crystal Forms, *Acta Chem. Scand.* 20: 2255–2260 (1966).
17. Goto, M., D.R. Kodali, D.M. Small, K. Honda, K. Kozawa, and T. Uchida, Single Crystal Structure of a Mixed-Chain Triacylglycerol: 1,2-Dipalmitoyl-3-acetyl-*sn*-glycerol, *Proc. Natl. Acad. Sci. USA* 89: 8083–8086 (1992).
18. Sato, K., M. Gato, J. Yano, K. Honda, D.R. Kodali, and D.M. Small, Atomic Resolution Structure Analysis of  $\beta'$  Polymorph Crystal of a Triacylglycerol: 1,2-Dipalmitoyl-3-myristoyl-*sn*-glycerol, *J. Lipid Res.* 42: 338–345 (2001).

19. Hitchcock, P.B., R. Mason, K.M. Thomas, and G.G. Shipley, Structural Chemistry of 1,2-Dilauroyl-DL-phosphatidylethanolamine: Molecular Conformation and Intermolecular Packing of Phospholipids, *Proc. Nat. Acad. Sci. USA* 71: 3036–3040 (1974).
20. Elder, M., P. Hitchcock, R. Mason, and G.G. Shipley, A Refinement Analysis of the Crystallography of the Phospholipid, 1,2-Dilauroyl-DL-phosphatidylethanolamine, and Some Remarks on Lipid-lipid and Lipid-protein Interactions, *Proc. Roy. Soc. London, ser. A* 354: 157–170 (1977).
21. Pascher, I., and S. Sundell, Molecular Arrangements in Sphingolipids. The Crystal Structure of Cerebroside, *Chem. Phys. Lipids* 20: 175–191 (1977).
22. Jensen, L.H., and A.J. Mabis, Crystal Structure of  $\beta$ -Tricaprin, *Nature(London)* 197: 681–682 (1963).
23. Jensen, L.H., and A.J. Mabis, Refinement of the Structure of  $\beta$ -Tricaprin, *Acta Crystallogr.* 21: 770–781 (1966).
24. Van Langevelde, A.J., K.F. van Massen, E.D. Sonneveld, R. Pechar, and H. Schenk, Crystal Packing of a Homologous Series  $\beta'$ -Stable Triacylglycerols, *J. Am. Oil Chem. Soc.* 76: 603–609 (1999).
25. van de Streek, J., P. Verwer, R. de Gelder, and F. Hollander, Structural Analogy Between  $\beta'$  Triacylglycerols and *n*-alkanes. Toward the Crystal Structure of  $\beta'$ -2 p.p+2.p Triacylglycerols, *Ibid.* 76: 1333–1341 (1999).
26. Van Langevelde, A.J., Triacylglycerol Structures and Cocoa-Butter Crystallization, Ph.D. Thesis, University of Amsterdam, 2000, pp. 91–110.
27. Yano, J., F. Kaneko, M. Kobayashi, D.R. Kodali, D.M. Small, and K. Sato, Structural Analyses of Triacylglycerol Polymorphs with FT-IR Techniques: II.  $\beta'$  1-form of 1,2-Dipalmitoyl-3-myristoyl-*sn*-glycerol, *J. Phys. Chem. B.* 101: 8120–8128 (1997).
28. Yano, J., S. Ueno, K. Sato, T. Arishima, N. Sagi, F. Kaneko, and M. Kobayashi, FT-IR Study of Polymorphic Transformations in SOS, POP, and POS, *Ibid.* 97: 12967–12973 (1993).
29. Yano, J., K. Sato, F. Kaneko, D.M. Small, and D.R. Kodali, Structural Analyses of Polymorphic Transitions of *sn*-1,3-Distearoyl-2-oleoylglycerol (SOS) and *sn*-1,3-Dioleoyl-2-stearoylglycerol (OSO): Assessment on Steric Hindrance of Unsaturated and Saturated Acyl Chain Interactions, *J. Lipid Res.* 40: 140–151 (1999).
30. Boubekri, K., J. Yano, S. Ueno, and K. Sato, Polymorphic Transformations in SRS (*sn*-1,3-distearoyl-2-ricinoleyl glycerol), *J. Am. Oil Chem. Soc.* 76: 949–955 (1999).
31. Takeuchi, M., S. Ueno, J. Yano, E. Floter, and K. Sato, Polymorphic Transformation of 1,3-Distearoyl-*sn*-2-linoleoyl-glycerol, *Ibid.* 77: 1243–1249 (2000).

## Chapter 2

# Molecular Modeling Applications in Lipid Crystallization

James Evans, Alfred Y. Lee, and Allan Myerson

Department of Chemical Engineering, Illinois Institute of Technology, 3301 South Dearborn St., Chicago, IL 60616

## Introduction

“Molecular modeling” is a term used to describe a series of techniques that employ both quantum and molecular mechanics in conjunction with computer simulations to study the chemical and physical properties of a material (1). This approach offers a wide range of benefits to industry: shortens product development cycles, reduces production costs, improves product properties and key solid-state structures, and properties that cannot be examined by experimental techniques may be predicted and studied by computer. Following is a brief review of the fundamentals of modeling crystalline systems.

## Mechanics

The state of a system may be described by one of two mechanics: quantum or molecular. (i) In quantum mechanics, a wavefunction ( $\psi$ ) is used to describe the state in which an atom/molecule exists. Using this wavefunction and by solving the Schrödinger equations, it is possible to describe any atomic/molecular system. So far, exact solutions have been found for only a few simple systems, e.g., hydrogen, with approximations for structures as their complexity increases. (ii) The molecular mechanics approach to predicting the structure and properties of a molecule is based upon classical laws of physics. Molecular mechanics doesn't explicitly consider the electrons in a molecular system. Instead, calculations are based upon interactions among the nuclei. Molecular mechanics assumes that atoms in a molecule have a natural arrangement (bond lengths and angles) and that they adopt this arrangement relative to each other to produce geometry of minimum energy. There are two key contributions in terms of energy: intramolecular forces—including bond stretching, angle bending, and torsional energy terms; intermolecular interactions—including electrostatic forces and van der Waals forces. In molecular mechanics the electronic effects are implicitly considered via a potential function.

## Potential Function

A potential function consists of one or more parameter sets that fit the equation and atom types to experimental data. Each of these functions usually contains a small number of adjustable parameters that can be used to optimize the simulations. There are five main potential functions: the hard sphere (HS) potential, the soft sphere (SS) potential, Sutherland (S) potential, the Lennard-Jones potential, and the Buckingham (B) potential (2). This section provides a brief review of the most frequently used potential function [Lennard-Jones (LJ) potential] and its application for molecular modeling.

### The Lennard-Jones (LJ) Potential

The LJ potential is given by (2)

$$U_{LJ}(R) = \varepsilon_1 R^{v_1} - \varepsilon_2 R^{v_2} \quad [1]$$

Where the first and second terms correspond to the repulsion and attraction, respectively, to describe repulsion prevailing over attraction at small intermolecular separations and attraction prevailing over repulsion at large intermolecular separations the powers ( $v$ ) in the LJ potential should satisfy  $v_1 > v_2$ . As with other potentials the power  $v_2$  is usually chosen to be equal to 6, whereas  $v_1$  is most widely set to 12.

Therefore the LJ potential is usually given as the form described in Equation 2 (2):

$$U_{LJ}(R) = 4\varepsilon \left[ \left( \frac{D}{R} \right)^{12} - \left( \frac{D}{R} \right)^6 \right] \quad [2]$$

where  $D$  designates the intermolecular separation at which the LJ potential changes sign and parameter  $\varepsilon$  gives the LJ potential minimum value  $-\varepsilon$ , achievable at  $R = 2^{1/5}D$  (Fig. 1).

The potential function allows the crystal growth process to be considered at a molecular level by using the atom-atom approach (3,4), which approximates intermolecular bond strength through the summation of its atom-atom interactions (Eq. 3), described variously as the lattice energy ( $E_{\text{latt}}$ ), binding or cohesive energy, within a sphere of sufficient radius (Fig. 2) that an energy plateau has been reached (5).

$$E_{\text{latt}} = \sum_{k=1}^N \sum_{i=1}^n \sum_{j=1}^{n'} V_{kij} \quad [3]$$

where  $V_{kij}$  is the interaction between atom  $i$  in the central molecule and atom  $j$  in the  $k$ th molecule. Each atom-atom interaction consists of a van der Waals interac-

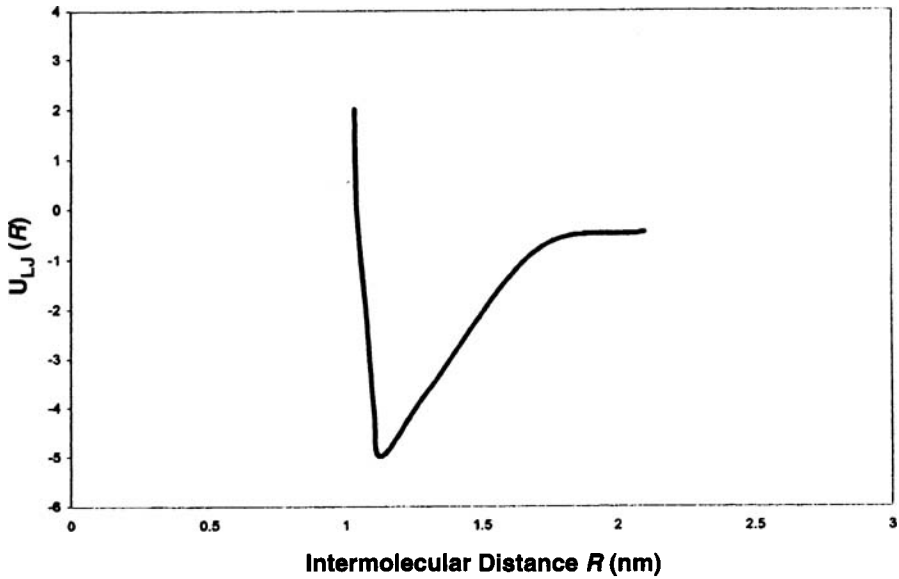


Fig. 1. The Lennard-Jones Potential (Ref. 2), where  $D = 1$  and  $\epsilon = 5$ .

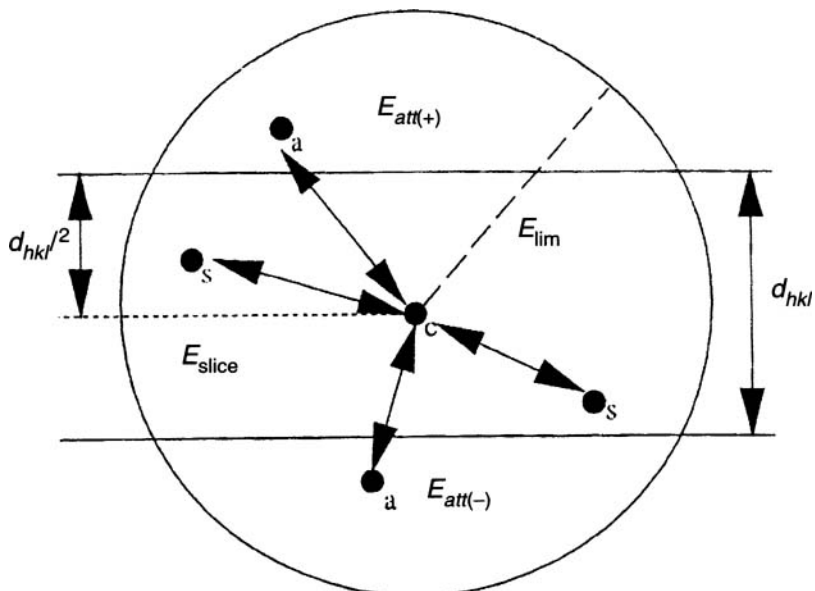


Fig. 2. Calculation of intermolecular interactions, using the atom-atom approach. The slice boundary ( $d_{hkl}$ ) may be shifted along the slice normal to obtain the most energetically stable slice (Ref. 5).

tion and an electrostatic interaction. The van der Waals interactions can be described by various potential functions, all of which have the same basic form. The LJ 6–12 potential (6) is one of the most common, consisting of an attractive and a repulsive contribution (Eq. 4).  $A$  and  $B$  are the atom-atom parameters for describing a particular interaction

$$V_{vdw} = \frac{-A}{r^6} + \frac{B}{r^{12}} \quad [4]$$

Parameters  $A$  and  $B$  are derived from fitting chosen potential to observed properties, i.e., crystal structures, heats of sublimation etc. (4). Ab initio quantum chemistry calculations on interaction energies can also be used as “experimental” data on which to fit these parameters.

The electrostatic interaction (Eq. 5) (4) is described by assigning a fractional charge ( $\pm q$  to each atom, the sign determines whether the atom in the molecular arrangement has an excess or deficiency of electrons compared with the neutral atom. These charges are usually determined from molecular-orbital calculations (7), where  $D$  is the dielectric constant.

$$V_{el} = \frac{q_i q_j}{D r} \quad [5]$$

Hydrogen bonding interactions ( $V_{hb}$ ) are essentially very special van der Waals interactions and modified LJ potential functions, e.g., Momany *et al.* (8), Nemethy *et al.* (9) PF have been used to describe them (Eq. 6) (4). Hydrogen potential functions have a 10–12 rather than a 6–12 potential, where the dependence of the attractive part is  $r^{10}$  rather than  $r^6$  which gives rise to a much steeper potential curve, this helps account for some of the important structural features of hydrogen bonds.

$$V_{hb} = \frac{-A}{r^{10}} + \frac{B}{r^{12}} \quad [6]$$

Inspection of the potential functions shown in Equations 4–6 show that both  $A$  and  $B$  and the fractional charge for a particular atom pair are constant. The interaction energy is, therefore, dependent upon the separation distance  $r$ , while the van der Waals interactions are short-range interactions as they depend on the inverse powers of  $r$ .

Whereas the electrostatic interactions will act over a long range as they depend on  $1/r$ , hence there is the need to carry out the calculation with a sufficient radius to assure that an energy plateau has been reached.

Figure 3 shows an example of calculated lattice energy (oleic acid) (10) and the contribution of the various intermolecular forces. These values were deter-

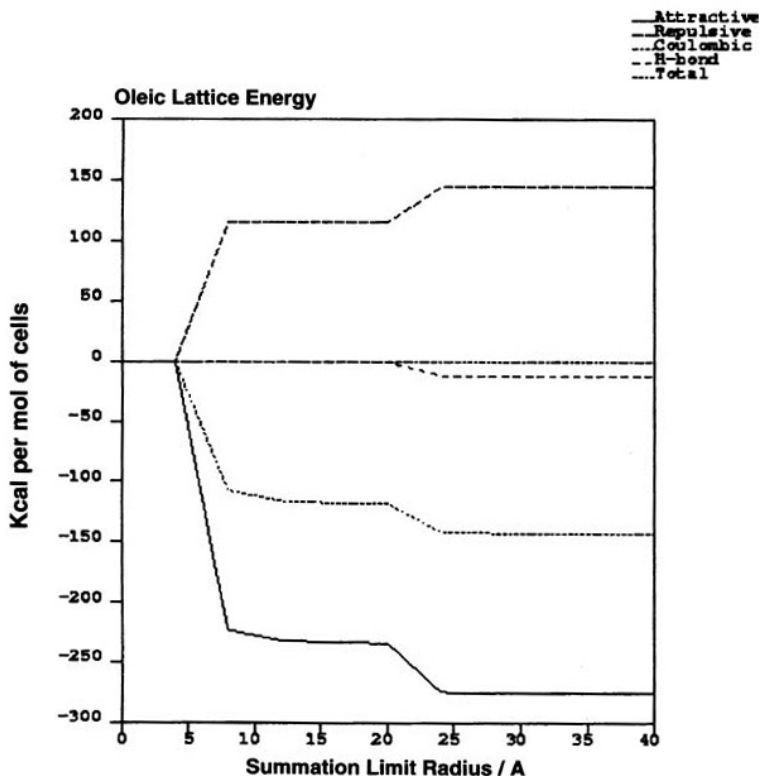


Fig. 3. Oleic acid  $E_{latt}$  using the Drieding II potential set in CERIU2 (Ref. 12).

mined using a modified LJ potential function (Drieding II), which incorporates the electrostatic functionality combined with an angle-dependent potential (11).

$$V_{ij} = \frac{-A}{r_{ij}^6} + \frac{B}{r_{ij}^{12}} + D_{hb} \left[ -6 \left( \frac{r_{hb}}{r_{DA}} \right)^{10} + 5 \left( \frac{r_{hb}}{r_{DA}} \right)^{12} \right] \cos^4(\theta_{DA}) + 332 q_i q_j \epsilon r_{ij} \quad [7]$$

The lattice energy is a crucial parameter to determine as the calculated value can be compared with the experimental sublimation enthalpy (Eq. 8) (13), as a check of the description of intermolecular interactions between the molecules by the defined potential function.

$$V_{exp} = -\Delta H_{sub} - 2RT \quad [8]$$

Where  $2RT$  ( $R$  denotes the universal gas constant) represents a correctional factor for the difference between the gas phase enthalpy and vibrational contribution to the crystal enthalpy.

## Crystal Shape Calculation

Based on crystal lattice geometry, the first morphological simulations were proposed by Bravais (14), Friedel (15), and Donnay and Harker (16). Their works are often known as the BFDH law: it assumes that the linear growth rate,  $R_{hkl}$ , of a given crystal face is inversely proportional to the corresponding interplanar distance,  $d_{hkl}$ , after taking into account the extinction conditions of the crystal space group. In other words, the slowest growing faces, and hence most prominent, are those in which the interatomic spacing is the greatest. This proposal only makes use of the framework of the crystal lattice and gives no consideration to the atom or bond type or partial charge, all of which has an effect on the crystal morphology. In crystal systems with no directional bonding types, the BFDH method often produces a reasonable match with experimental morphologies. However, the presence of directional properties significantly reduces the accuracy of the predictions (17).

In 1955, Hartman and Perdok (18) refined the BFDH model by relating the crystal morphology to its internal structure on an energy basis. They identified that chains of strong intermolecular bonds known as periodic bond chains (PBC) govern the crystal morphology. According to the number of PBC inside a slice of thickness,  $d_{hkl}$ , they classified the crystal faces as: (i) F-faces (flat), two or more PBC, (ii) S-faces (stepped), one PBC, or (iii) K-faces (kinked), zero PBC.

The F-faces have low growth rates due to the existence of a limited number of kink sites, and they grow by lateral extension of the growth layers. Growth of S-faces only needs a unidimensional nucleation and is more rapid than that of F-faces, while, K-faces have an important number of kink sites and consequently higher growth rates. For this reason, F-faces will appear in the crystal morphology since they have the largest slice energy ( $E_{sl}$ ) or lowest attachment energy ( $E_{att}$ ), which is the difference between the crystallization energy and the slice energy, of the three faces. Small attachment energy translates into low growth velocity. The higher growth rates of S- and K-faces mean they rarely (S) and almost never (K) develop. Essentially, the morphology of the crystal can be determined from the slice energy of different F-faces.

Hartman and Bennema (19) found that relative growth rate always increases with  $E_{att}$ . At low supersaturation, they were able to show that the growth rate of a given crystal face,  $R_{hkl}$ , is directly proportional to the attachment energy:

$$R_{hkl} \propto \left| E_{hkl}^{att} \right| \quad [9]$$

Faces with largest  $\left| E_{hkl}^{att} \right|$  will be the fastest growing and therefore will be the least prominent. Since energy is in general a function of interatomic distance, the attachment energy model is consistent with the BFDH law: faces with small interplanar distance have large  $\left| E_{hkl}^{att} \right|$ .

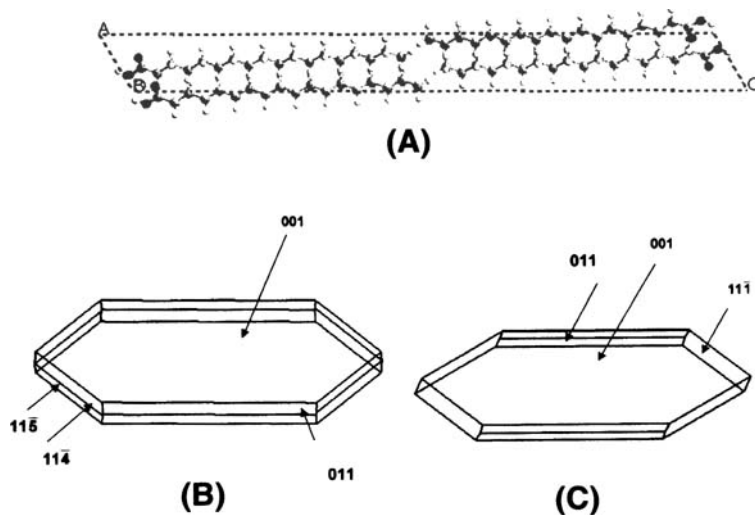


**Fig. 4.** A: Unit cell of stearic acid (E form); while, hydrogen atoms; gray, carbon atoms; and black, oxygen atoms. Theoretical habit of stearic acid B: growth form according to the BFDH law; C: growth form according to the attachment energy model.

Figure 4 shows one polymorph of stearic acid (E form). The molecule crystallizes in the  $P21/a$  space group with four molecules in the unit cell dimensions:  $a = 5.603 \text{ \AA}$ ,  $b = 7.360 \text{ \AA}$ ,  $c = 50.79 \text{ \AA}$  and  $\beta = 119.40^\circ$ . In addition, the crystal habit of stearic acid predicted by the attachment energy model and the BFDH are shown. A slow-growing (001) face dominates both crystals. Table 1 lists the attachment energies and the interplanar spacing of various low-index faces. Both theoretical habits were calculated using the program Cerius2 version 4.2 (12).

## Surface Studies

In reality, very few systems are 100% pure as both solvents and impurities can incorporate into the crystal structure. The incorporation of these molecules onto a

**TABLE 1**  
BFDH and Attachment Energy results for Stearic Acid (E form)

Face ( $hkl$ )	$d_{hkl}$ ( $\text{\AA}$ )	Attachment energy ( $\text{kmol/mol}$ )
001	44.09	-7.34
011	7.17	-74.18
11-1	4.21	-99.33
11-4	4.46	-117.77
11-5	4.46	-118.32

crystal surface can significantly affect both the growth rate and the morphology of a crystal (20). Two types of molecules that can incorporate into a crystalline system have been identified (see Fig. 5) (21): (i) Disrupter molecules tend to be smaller than the host molecule, and they act by incorporating themselves into the crystal and disrupting the intermolecular bonding network. (ii) Blocker molecules tend to be larger than the host; they commonly have the same basic structure with an additional group attached. Once the blocking molecules are incorporated into a system, they simply prevent further host molecules from assuming their correct positions. This can cause vacancies within the system, which in turn can alter the rate of growth that will change the crystal morphology.

The incorporation of either type of molecule onto a crystallographic surface not only alters the growth rate, it also violates the local symmetry of a surface. For

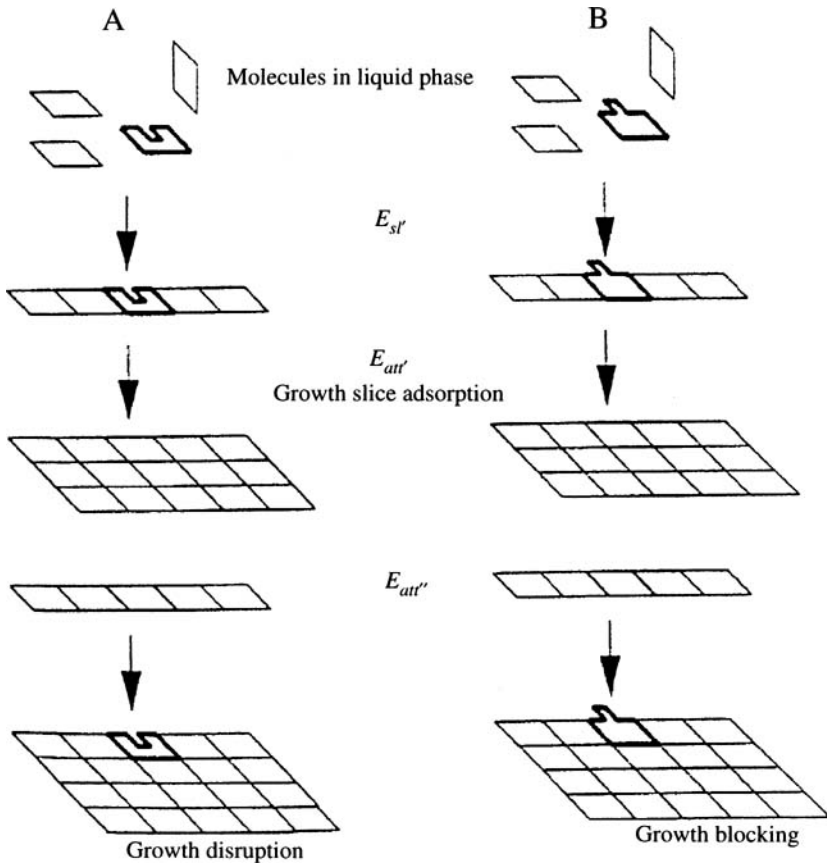


**Fig. 5.** Schematic illustrating the growth of the growth of the crystal interface in a system with the present of (A) disrupter and (B) blocker (Ref. 24).

example in a pure system, Equation 10 (21) is seen to be valid, whereas when impurities of any description are incorporated into a system, the  $E_{att(+)}$  and  $E_{att(-)}$  must be considered separately since preferential adsorption could occur at either one.

Where

$$E_{att} = E_{att(+)} + E_{att(-)} \quad [10]$$

$$E_{att(+)} = E_{att(-)} \quad [11]$$

To quantify the change in growth rate with the presence of these impurities, several new terms were introduced to the Hartman-Perdok model (see Fig. 5) (22,23), which gave rise to the concept of binding energy or incorporation energy:

$$\begin{aligned} \Delta b &= E_{b'} - E_b \\ &= (E_{sl'} + E_{att(+)' } + E_{att(-)' }) - (E_{sl} + E_{att(+)} + E_{att(-)}) \\ &= (E_{sl'} + E_{att'}) - (E_{sl} + E_{att}) \end{aligned} \quad [12]$$

Small  $\Delta b$  values imply a greater likelihood of incorporation of the impurity on a particular face. In certain cases,  $\Delta b$  can be negative, which implies that impurity binding is more favorable than host incorporation. If  $\Delta b$  is very large, then it is unlikely that the impurity will be incorporated. The  $\Delta b$  values are system-specific, and so it is not always entirely clear as to what constitutes a large or a small value.

Therefore, it is often necessary to create a series of models with varying definitions for the  $\Delta b$  values. When considering blocker additives, it is necessary to further modify this approach, as this technique would result in large repulsive interactions when the additive encroaches on a host site. The calculation of  $E_{att}$ , is therefore altered to include vacancies, which are calculated by determining the intermolecular interactions and omitting the vacancies contribution to the energy term if the vacancy contribution arises from the blocking nature of an additive.

The binding energy idea was further developed (24) to enable modified attachment energies to be calculated by comparing the binding energies of the host and the sorbate, which gives rise to the differential interaction energy ( $E_d$ ):

$$E_d = E_{b(\text{sorbate})} - E_{b(\text{host})} \quad [13]$$

If  $E_d$  is negative, then the attachment energy values are modified according to Equation 14, which incorporates proportionality constant.

$$E_{att} = \frac{-E_d}{5} \left[ E_{att} - \frac{E_{att}}{10} \right] \quad [14]$$

The ability to model the impact of impurities on the structure of a crystalline system is crucial: it enables the impact of both solvents and impurities quantified. Both in terms of the overall morphology and where the interactions are likely to occur, thus providing a better understanding of the process chemistry of a system. Two principal techniques exist for simulating the effect of solvents/sorbates on the surface of a crystal: Monte Carlo and Molecular Dynamics and Minimization.

### Monte Carlo Simulations

Monte Carlo simulations use multiple dimensional integrals of statistical mechanics to investigate: in this instance, the potential energy of sorbate molecules in the presence of a molecular surface (25,26).

The Monte Carlo technique can easily be visualized if the particles are assumed to be in a box (Fig. 6). The particles are displaced by a random amount, and the potential energy is calculated using a specified intermolecular potential, and the new configuration is either accepted or rejected, according to the following five-step criteria (24):

- I. Creation—A sorbate molecule was selected and was placed at a random position and orientation within the framework/box. A new configuration is generated based upon the probability.

$$P = \min \left[ 1; \exp \left( -\frac{\Delta U}{kT} - \ln \frac{(N_i + 1)kT}{f_i V} \right) \right] \quad [15]$$

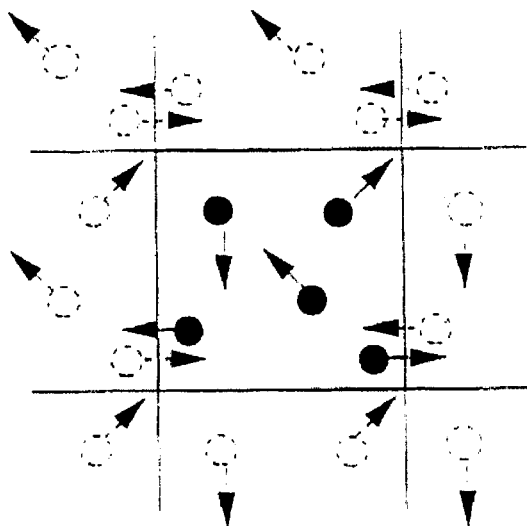


**Fig. 6.** Visualization of the Monte Carlo simulation; periodic boundary conditions are used where the mirror image of a particle enters through the opposite face when a particle leaves (Ref. 24).

- II. Destruction—A molecule is removed from the framework, and the new configuration is accepted based upon the probability shown by:

$$P = \min \left[ 1; \exp \left( -\frac{\Delta U}{kT} + \ln \frac{N_i kT}{f_i V} \right) \right] \quad [16]$$

- III. Translation—A molecule is chosen and translated by a random amount within a cube of size  $2\delta$ ; this configuration is accepted dependent on the probability:

$$P = \min \left[ 1; \exp \left( -\frac{\Delta U}{kT} \right) \right] \quad [17]$$

- IV. Rotation—A random sorbate molecule is chosen from the framework, along with a random axis. The molecule is then rotated randomly within the range  $\pm\delta$ . The new configuration is accepted based on the probability of Equation 17.
- V. Monte Carlo simulation repeated until the system energy converges; it then continues for a significant number of configurations to ensure that the global minimum is achieved.

### ***Molecular Dynamics***

Molecular dynamics simulation determines the dynamics of the interactions between a host crystal surface and a sorbate. The simulation occurs in two stages: (i) The forces are computed and the atoms are moved in response to the forces with a specified potential set used to calculate the atomic motions. This type of simulation is an iterative process that allows the calculation of forces on each atom. (ii) At a time ( $\Delta T$ ), the current position, velocities, and forces were used to calculate new coordinates. This process was repeated for a specified number of iterations.

There are various techniques available for molecular dynamics simulation, i.e., adiabatic, isothermal. The constant volume, temperature (isothermal NVT) method (constant number of atoms, volume, and temperature) is most commonly used. The simulated results obtained from the molecular dynamics studies are then coordinate minimized to ensure that the global minimum has been achieved.

### ***Minimization***

Molecular minimization is applied to a configuration at the end of any simulation, to ensure that the global minimum has been reached.

There are two basic minimization techniques: firstly, coordinate minimization which relies on the calculation of the derivative of the potential energy, with respect to structural parameters, and accordingly, they adjust the atomic/molecular coordinates toward a structure with lower energy (nonperiodic and periodic struc-

tures); secondly, lattice minimization which alters the unit cell parameters to minimize force-field energy (periodic structures only). There are three main algorithms that can be applied during the minimization of a structure. (i) The conjugate gradient algorithm (27) utilizes previous minimization steps along with the present gradient to determine the next step, thus producing rapid convergence. In fact minimum energy converges in the order of  $N$  steps, where  $N$  is the number of degrees of freedom. (ii) The steepest descent algorithm (28) displaces coordinates in a direction opposite to the gradient of the potential energy at each step; the step size is increased if a lower energy is achieved and decreased if a higher energy is obtained. (iii) The Fletcher-Powell algorithm (29) is a pseudo second-order method that generates a second-order derivative matrix by finite differences (coordinate minimization only). There are three main differences between the Monte Carlo and Molecular Dynamics simulations. Firstly the Monte Carlo approach treats the structure as a periodic system i.e. with defined boundaries in the form of a unit cell, whereas Molecular Dynamic approach treats a system as non periodic so there is no boundary effect. Secondly whilst the random nature of the Monte Carlo simulation ensures that the global minimum is achieved, the molecular dynamics approach has the potential for finding a local minimum energy well and not the global energy minimum as the user selects the initial position of the non-host molecule, hence the need to repeat the molecular dynamics simulation to ensure that a global minimum has been achieved. Thirdly in terms of computational cost the Monte Carlo approach is significantly more expensive than the molecular dynamics approach.

However if the simulation is properly parameterized, then either technique is valid, and both systems will produce accurate simulations of the impact of solvents/sorbates on the growth rate and morphology of a crystalline system.

## Structure Solution from Powder

Powder diffraction techniques have become increasingly useful as tools for crystal structure determination especially in cases where it is sometimes difficult to get a single crystal of sufficient size and quality for traditional single-crystal studies. The solution of a structure can be considered as a three-step process: (i) data collection and indexing, (ii) data preparation and Pawley refinement, and (iii) Monte Carlo simulated annealing and rigid-body Rietveld refinement.

In the first step, unit cell parameters are determined by indexing the collected powder pattern with programs such as ITO (30), TREOR90 (31), or DICVOL91 (32). The second step involves further refinement of the lattice parameters, and this can be performed without any knowledge of the atomic positions (33). In addition to lattice parameters, the background coefficients, zero-point shift parameters, and peak width and mixing parameters must be refined to accurately reflect the experimental data. The third step involves a combination of Monte Carlo simulated annealing (34) and rigid-body Rietveld (35) refinement techniques that maximize

the agreement between the calculated and experimental powder patterns. Furthermore, the positions, orientations and intramolecular torsions of the molecular fragments in the asymmetric unit are deduced, and slight changes to the packing arrangement (molecular structure) are carried out, so that the simulated pattern from the proposed structure gets closer to the experimental pattern.

This method has been validated and tested for numerous molecular crystal structures (36). Among the molecules studied was formylurea. Figure 7 shows the simulated formylurea unit cell structure solved by powder diffraction data. This was accomplished using the PowderSolve (36) module in the Cerius2 modeling program (12).

## Polymorphism

A polymorph is defined as a substance that can crystallize out as various different forms that are chemically identical, e.g., carbon graphite and diamond. (It is important to note that we are not talking about hydrate and anhydrate forms of a compound.)

Polymorphism is important as different polymorphic forms of the same compound may have significantly different chemical/physical properties. In terms of polymorphism, computer simulations may be used to either predict the structure of an unknown polymorph or to simulate the potential of a system to exist in other polymorphic forms. In either case the polymorphic simulation is a three-step process.

### Monte Carlo Simulation

The first step of a polymorphic prediction sequence is a systematic simulated annealing search through all of the defined space groups for potential structures.

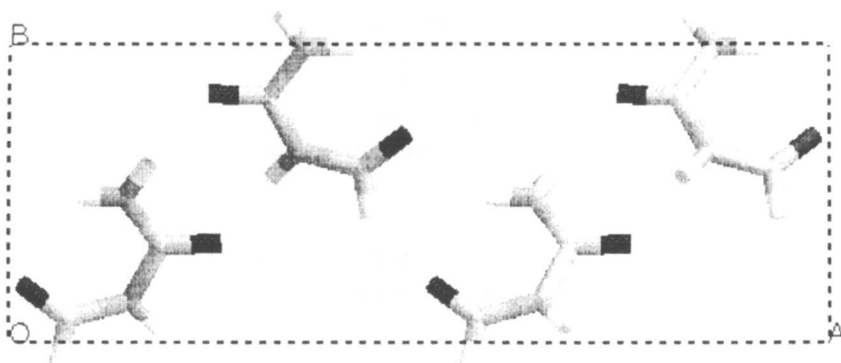


**Fig. 7.** Simulated packing arrangement of formylurea; white, hydrogen atoms; light gray, carbon atoms; dark gray, nitrogen atoms; and black, oxygen atoms.

Potential structures are accepted or rejected according to the Metropolis algorithm (25):

$$P = \min \left[ 1; \exp \left( - \frac{\Delta E}{kT} \right) \right] \quad [18]$$

Simulated annealing search works by treating the search for the global minimum of  $E$  as a thermodynamic problem. At some nonzero temperature, the crystal changes its structure randomly, and its energy fluctuates accordingly. To prevent the simulation from becoming trapped in a local minimum, cooling begins at a relatively high temperature. Therefore every crystal structure (within the constraints of the space group and asymmetric unit contents) can theoretically be reached, and ergodicity ensured. As the temperature is lowered, the algorithm explores the potential energy hypersurface of the crystal with greater precision. At these lower temperatures, movement is restricted to regions where the value of  $E$  is relatively low. The simulation ends when  $T$  is so low that the crystal is frozen and the global minimum of  $E$  has hopefully been found.

### ***Cluster Analysis and Minimization***

The Monte Carlo simulation outputs a large number of unoptimized structures for each space group investigated, which will include low-energy structures and clusters of many similar structures that are obtained at the local minimum of the energy surface of the crystal. Of the various predicted structures, only those with the lowest energy are likely to occur experimentally. To remove the experimentally unlikely structures, cluster analysis is carried out. Cluster analysis identifies all the lowest energy unclustered structures; all other unclustered structures are compared with this via a clustering algorithm which makes its comparison from the partial radial distribution functions between pairs of force-field atom types of the two structures. Structures that are deemed similar are clustered together; this is repeated until all of the unclustered structures have been assigned to a cluster. The structures that are accepted from the cluster analysis are still energetically unrefined and require optimization with respect to all degrees of freedom, and thus undergo both coordinate and lattice minimization. A second clustering step after the minimization removes any duplicate structures.

### ***Confirmation***

The final stage in any polymorphic simulation is to check the reliability of the simulated data. This can be achieved by comparing a variety of data, e.g., density, lattice energies, etc. With the advent of reliable software, a simulated diffraction pattern is now used as the primary comparison with the experimental data. Prior research has shown that computer simulations can successfully predict the structure of an unknown polymorph or determine the potential for polymorphism (37).

## Summary

Molecular modeling is playing an increasingly important role in the study of molecular materials. Molecular modeling has a variety of applications for a crystalline system, and a number of important properties can be simulated or determined from experimental data via computer simulations, thus saving experimental time and money.

Ultimately the aim of molecular modeling is the design (before synthesis) of novel materials. In molecular crystal chemistry, this requires the ab initio prediction of solid-state structures. Although much progress has been made and the potential of such an ability is enormous, progress in this field has been hindered by problems with global minimization and force-field accuracy.

## REFERENCES

1. Myerson, A.S. in *Molecular Modeling Applications in Crystallization*, edited by A.S. Myerson, Cambridge University Press, New York, New York, 1999.
2. Izmailov, A.F., and A.S. Myerson, Introduction to Molecular Modeling, in *Molecular Modeling Applications In Crystallization*, edited by A.S. Myerson, Cambridge University Press, New York, New York, 1999, pp. 29–33.
3. Kitaigorodskii, A.I., K.V. Mirskaya, and A.B. Tovbis, Lattice Energy of Crystalline Benzene in the Atom-Atom Approximation, *Soviet Physics Crystallogr.* 13: 176–180 (1968).
4. Docherty, R., and P. Meenan, The Study of Molecular Materials Using Computational Chemistry, in *Molecular Modeling Applications in Crystallization*, edited by A.S. Myerson, Cambridge University Press, New York, New York, 1999, pp. 117–125.
5. Clydesdale, G., K.J. Roberts, and E. Walker, The Crystal Habit of Molecular Materials: A Structural Perspective, in *Theoretical Aspects and Computer Modeling*, edited by A. Gavezzotti, John Wiley and Sons Ltd., New York, New York, 1997, p. 214.
6. Jones, J.E., On the Determination of Molecular Fields: 1. From the Variation of the Viscosity of a Gas with Temperature, *Proceedings of the Royal Society, A*, 106:441–447 (1923).
7. Stewart, J.J.P., MOPAC: A Semi-Empirical Molecular Orbital Program, *J. Computer-Aided Molecular Design* 4: 1 (1990).
8. Momany, F.A., L.M. Carruthers, R.F. McGuire, and H.A. Scheraga, Intermolecular Potentials for Application to the Packing Configuration and Lattice Energies in Crystals of Hydrocarbons, Carboxylic Acids, Amines and Amides, *J. Phys. Chem.* 78:1595 (1974).
9. Nemethy, G., M.S. Pottle, and H.A. Scheraga, Intermolecular (nonbond and hydrogen-bond) Potentials Applicable to Groups Found in Naturally Occurring Amino Acids, *Ibid.* 87: 1883 (1983).
10. Abrahamsson, S., and I. Ryderstedt-Nahringbauer, The Crystal Structure of the Low-Melting Form of Oleic Acid, *Acta Crystallogr.* 15: 1261–1268 (1962).
11. Mayo, S.L., B.D. Olafson, and W.A. Goddard III, Drieding: A Generic Force Field for Molecular Simulations, *J. Phys. Chem.* 94: 8897 (1990).
12. CERIU2 v 4.2 Molecular Modeling Software for Materials Research by Molecular Simulations Incorporated, San Diego, CA, and Cambridge, UK, 2000.

13. Jang, S.M., *Solvent and Impurity Effects in Crystallization Process*, Polytechnic University, New York, New York, 1996.
14. Bravais, A., *Etudes Crystallographiques*, Gauthiers, Villars, Paris, France, 1866.
15. Friedel, M.G., Etudes sur la loi de Bravais, *Bulletin de la Société Française de Mineralogie* 113: 326 (1907).
16. Donnay, J.D., and D. Harker, A New Law of Crystal Morphology Extending the Law of Bravais, *American Mineralogist* 22: 446 (1937).
17. Docherty, R. and K.J. Roberts, Modeling the Morphology of Molecular Crystals: Application to Anthracene, Biphenyl, and  $\beta$ -Succinic Acid, *J. Crystal Growth* 88: 159–168 (1988).
18. Hartman, P., and W.G. Perdok, On the Relation Between Structure and Morphology of Crystals I, *Acta Cryst.* 8: 49 (1955).
19. Hartman, P., and P. Bennema, The Attachment Energy as a Habit-Controlling Factor, *J. Crystal Growth* 49: 145 (1980).
20. MacCalman, M.L., K.J. Roberts, and B.A. Hendriksen, The Influence of Growth Environment on the Crystallization of Nortriptyline Hydrochloride, a Tricyclic Antidepressant, *J. Crystal Growth* 128: 1218–1224 (1993).
21. Clydesdale, G., K.J. Roberts, and E. Walker, The Crystal Habit of Molecular Materials: A Structural Perspective, in *Theoretical Aspects and Computer Modeling*, edited by A. Gavezzotti, John Wiley and Sons Ltd., New York, New York, 1997, p. 214.
22. Berkovitch-Yellin, Z., J. van Mil, L. Addadi, M. Idelson, M. Lahav, and L. Leiserowitz, Crystal Morphology Engineering by “Taylor-Made” Inhibitors: A New Probe to Fine Intermolecular Interactions, *J. Am. Chem. Soc.* 107: 3111 (1985).
23. Docherty, R., G. Clydesdale, K.J. Roberts, and P. Bennema, Application of Bravais-Friedel-Donnay-Harker, Attachment Energy and Ising Models to Understanding the Morphology of Molecular Crystals, *J. Physics D Appl. Physics* 24: 89 (1991).
24. Walker, E., Modeling the Influence of Growth Environment on the Crystallization of Organic Molecular Compounds, Ph.D. Thesis, University of Strathclyde, 1997.
25. Metropolis, N., A.W. Rosenbluth, M.N. Rosenbluth, and A.H. Teller, Equation of State Calculations by Fast Computing Machines, *J. Chem. Phys.* 21: 1087(1953).
26. Allen, M.P., and D.J. Tildesley, *Computer Simulations of Liquids*, 1989, Oxford UK, Science Publications.
27. Levitt, M., and S. Lifson, Refinement of Protein Conformations Using a Macromolecular Energy Minimization Procedure, *J. Mol. Biol.* 46: 269 (1969).
28. Press, W.H., B.P. Flannery, S.A. Teukolsky, and W.T. Vetterling, *Numerical Recipes, the Art of Scientific Computing*, Cambridge University Press, New York, New York, 1986, 1–994.
29. Fletcher, R., and C.M. Reeves, *Comput. J.* 7: 149 (1964).
30. Visser, J.W., A Fully Automatic Program for Finding the Unit Cell from Powder Data, *J. Appl. Cryst.* 2: 89 (1969).
31. Werner, P.E., L. Eriksson, and M. Westdahl, TREOR, a Semi-Exhaustive Trial and Error Powder Indexing Program for All Symmetries, *Ibid.* 18: 367 (1985).
32. Boultif, A., and D. Louer, Indexing of Powder Diffraction Patterns for Low Symmetry Lattices by the Successive Dichotomy Method, *Ibid.* 24: 987 (1991).
33. Pawley, G.S., Unit Cell Refinement from Powder Diffraction Scans, *Ibid.* 14: 357 (1981).

34. Deem, M.W., and J.M. Newsam, *J. Chem. Soc.* 114: 7189 (1992).
35. Rietveld, H.M., A Profile Refinement Method for Nuclear and Magnetic Structures, *J. Appl. Crystallogr.* 2: 65 (1969).
36. Engel, G.E., S. Wilke, O. König, K.D.M. Harris, and F.J.J. Leussen, Powder Solve—A Complete Package for Crystal Structure Solution from Powder Diffraction Patterns, *J. Applied Crystallogr.* 32: 1169–1179 (1999).
37. Verwer, P., and F.J.J. Leusen, Computer Simulation to Predict Possible Crystal Polymorphs, in *Reviews in Computational Chemistry*, edited by K.P. Lipkowitz and D.B. Boyd, Vol. 12, 1998, Wiley-VCH, New York, New York, pp. 327–365.

## Chapter 3

# Simultaneous Examination of Structural and Thermal Behaviors of Fats by Coupled X-ray Diffraction and Differential Scanning Calorimetry Techniques: Application to Cocoa Butter Polymorphism

Michel Ollivon<sup>a</sup>, Christophe Loisel<sup>a</sup>, Christelle Lopez<sup>a,b</sup>, Pierre Lesieur<sup>c</sup>, Franck Artzner<sup>a</sup>, and Gérard Keller<sup>a</sup>

<sup>a</sup>Equipe Physico-Chimie des Systèmes Polyphasés, 92296 Chatenay-Malabry, France; <sup>b</sup>Arilait Recherches, 75382 Paris, France; and <sup>c</sup>Laboratoire pour l'Utilisation du Rayonnement Electromagnétique, 91898 Orsay, France

## Introduction

The monotropic character of triacylglycerols (TAG) polymorphism renders the study of thermal and structural properties of fats very complex. Both types of properties, largely depending on sample history, are generally determined from differential scanning calorimetry (DSC) and X-ray diffraction examinations, respectively. However, even using the combination of these two techniques, phase and polymorph identifications are still difficult by the closeness of transition temperatures. In this respect, monounsaturated TAG, because of their capability to form both mixed and separate packing of saturated and unsaturated chains (1), display many crystalline varieties in a narrow temperature domain, e.g., 1,3-dipalmitoyl 2-oleylglycerol shows melting and/or transition of at least five crystalline forms within a range of about 20°C (2).

A new instrument allowing simultaneous time-resolved synchrotron X-ray Diffraction at both wide and small angles as a function of temperature (XRDT) and high-sensitivity DSC to be carried out in the same apparatus at rates between 0.01 and 10°C/min from the same sample (typ. 20 mg) in the -30 +150°C range was developed using a single computer for data collection (3). This instrument is used on the D22 and D24 lines of DCI synchrotron of LURE to examine the questioned polymorphism of cocoa butter (CB) (4). The coexistence of three different phases, two solids and one liquid, is established for CB at room temperature. Both solid phases show their own independent polymorphism which only depends on the fat history. Both phases are characterized by XRDT, DSC, and rheological measurements (5). The main solid phase, mainly composed of the three major monounsaturated TAG, displays six different crystalline arrangements while only two have been observed for the minor trisaturated phase. The solubilization of the latter into the liquid issued from the fusion of the former only occurs at about 39°C. The partition of the trisaturated

TAG between the different phases is also addressed. The less stable phase formed by rapid quenching of CB is revealed to be a new liquid crystalline phase. Such a liquid crystalline phase is also observed in palm oil.

## Materials and Methods

The CB used was a standard factory product originating from the Ivory Coast. Its composition, determined by gas chromatography and HPLC for TAG analysis and by atomic absorption for phospholipid content, was as follows: TAG 97%; diacylglycerols 1.1%; monoacylglycerols 0.2%; free fatty acids 1.3%; phosphatides 0.15%; and others 0.25% (4). The TAG composition which is given in detail elsewhere (4) is for main TAG, POP 17.3%, POS 37.3%, and SOS 27.3%; saturated TAG represented 2.3%.

X-ray diffraction was performed using the high-energy of synchrotron beam at L.U.R.E. (Laboratoire pour l'Utilisation du Rayonnement Electromagnétique) using alternately D22 or D24 station operated at  $\lambda = 1.488 \text{ \AA}$  (about  $10^9$  to  $10^{10}$  photons/s/mm<sup>2</sup>). Gas-filled linear detectors (1024 channels, either filled with Ar or a Xe-CO<sub>2</sub> mixture) were used for data collection using sample-to-detector distances of 290 and 1450 mm. Standardization was carried out using the form  $\beta$  of pure tristearin (StStSt) characterized by a long spacing of 44.98  $\text{\AA}$  at room temperature. All X-ray diffraction patterns were recorded by transmission using glass capillaries (GLAS, Berlin, Germany). Samples were prepared by filling these glass capillaries with about 20–30  $\mu\text{L}$  of melted fats, at temperatures about 20°C above their final melting points and centrifuging them immediately, before fat solidification could take place. Quenching of these capillaries containing melted samples was first done either by placing them rapidly in contact with a metal block cooled to –30°C and then transferring them to the precooled sample holder (–10°C) or by direct introduction in the latter. More detailed procedures are given in Reference 4.

The setup of the instrument that allows both small- and wide-angle X-ray diffraction recording as well as DSC is shown below (Fig. 1).

## Results and Discussion

The results and discussion presented here focus on two major points which are: (i) the number of phases coexisting in the CB such as it is found in tempered chocolate and (ii) the liquid crystalline nature of the variety obtained from rapid quenching of CB. A more detailed reexamination of CB polymorphism is given in Reference 4.

### ***How many phases coexist in the CB of a tempered chocolate at room temperature?***

The long and short spacings (LS = 66 and 33  $\text{\AA}$ ; SS = 4.58, 3.98, 3.89, 3.77, and 3.67  $\text{\AA}$ ) observed at 25°C with a short sample-detector distance confirmed, as

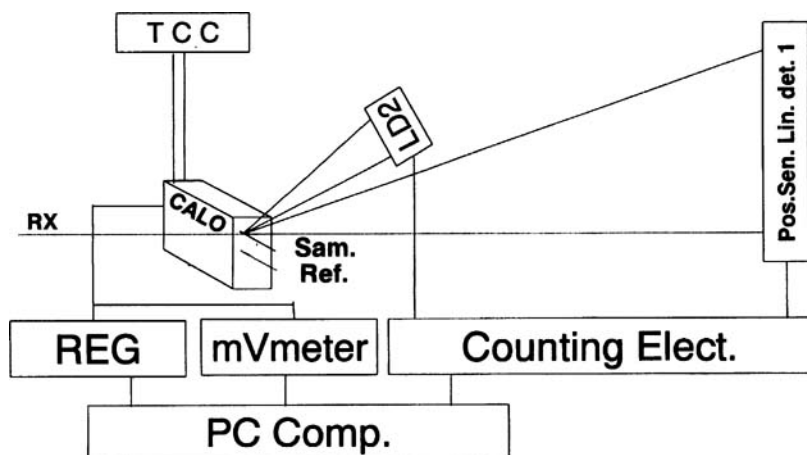


**Fig. 1.** Simultaneous DSC/WAXS/SAXS design. Experimental setup of the microcalorimeter cell in the time-resolved synchrotron X-ray diffraction environment: The cell is positioned with sample-containing capillary perpendicular to the beam in such a way that the diffraction patterns are recorded in the vertical plane including the beam by one or two one-dimensional proportional detectors (Position Sensitive Linear Detector 1 and LD2). Counting Electronic (Counting Elect.), Nanovoltmeter (mVter), and Temperature Controller (T Ctrl) are all monitored by the same PC Computer (PC Comp.). Temperature-Controlled Bath (TCB) is kept at constant temperature (e.g., 20°C). Figure is adapted from Reference 3.

expected, the crystallization of CB into a  $\lambda$ -3L structure corresponding to form V according to Wille and Lutton (6). A weak line at about  $q = 0.14 \text{ \AA}^{-1}$ , corresponding to a long spacing of 44.4 Å, is also observed at 25°C. The presence of this line is confirmed on recordings obtained at a longer sample-detector distance (Fig. 2).

The monitoring at small angles by X-ray diffraction of the melting of this CB sample (form V) was obtained by taking patterns every minute during heating at 1°C/min from 25 to 34°C and at 0.3°C/min from 34 to 41°C. The evolution as a function of temperature (between 25 and 41°C) of the intensity of the line at 44.4 Å was compared to that of the  $\beta$ -3L (V) structure using data recorded with the short sample-detector distance. It was observed that, above 34.5°C, all the lines (LS and SS) characterizing form V disappeared (they were progressively replaced by the bumps corresponding to the scattering from the liquid organization), except that at 44.4 Å, which finally vanished at 37.5°C (4). Then, the observation at 25°C of a line at 44.4 Å is interpreted as the coexistence of trace amount of  $\beta$ -2L form next to the major form  $\beta$ -3L (form V) made by monounsaturated TAG. Thus, a lipid segregation occurs in CB on cooling and/or during storage. The fraction which crystallizes in addition to the usual  $\beta$ -3L form (V) exhibits a higher melting point than the form V and an LS (44.4 Å) corresponding to a 2L packing very close to that of the  $\beta$  form of tristearin (about 45 Å, see above). Taking into

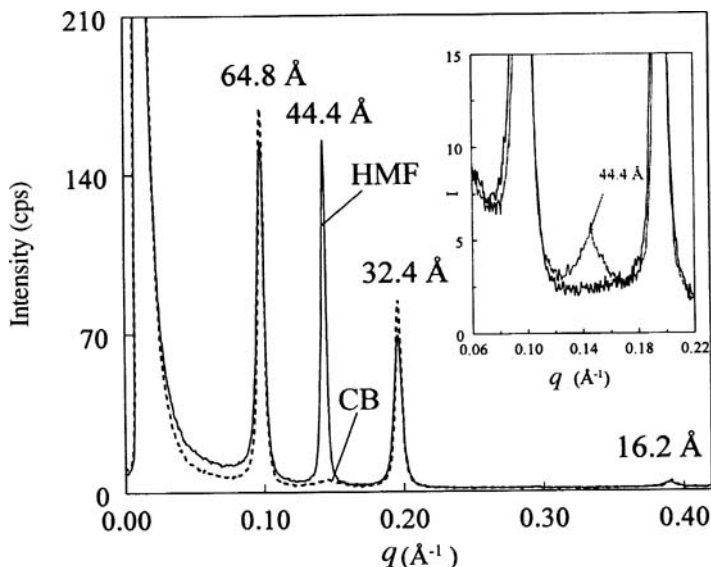


**Fig. 2.** Small-angle X-ray diffraction recordings of form V of cocoa butter (solid line) and of its high-melting fraction (HMF) (dashed line); insert shows form V of cocoa butter on an enlarged  $y$  scale and its low-melting fraction (LMF) which do not display the line at  $44.4\text{Å}$ . Both HMF and LMF fractions are obtained by dry fractionation of BC (4).

account the previous observation of a liquid phase in CB, the amount and the composition of which depend on temperature, this demonstrates that at room temperature three phases coexist in CB. Independent studies of chocolate crystallization in a scraped surface heat exchanger have shown that the crystallization of the minor phase is related to the presence of saturated TAG and is independent of and does not trigger the crystallization of the main solid phase (5). Moreover, it has been found that trisaturated TAG partition between the different phases; trisaturated TAG are likely solubilized in part into the monounsaturated main solid phase. It has been shown previously that the variation of the solubility of the latter as a function of temperature is likely responsible for chocolate bloom (7).

A slow heating scan at  $0.1^\circ\text{C}/\text{min}$  from  $-10$  to  $40^\circ\text{C}$  using coupled DSC and XRDT confirmed the existence of five of the six forms already observed (4). It was also shown that the second solid phase displays at least two polymorphic varieties, the LS and SS of which correspond more or less to the  $\alpha$  and  $\beta$  forms of tristearin (4,8).

### **Liquid Crystalline Structures of CB**

The introduction of a capillary-contained sample of CB melted at  $80^\circ\text{C}$  into the microcalorimeter cell precooled at  $-10^\circ\text{C}$  resulted in its rapid quenching at a rate in

the order of magnitude of about  $1000^{\circ}\text{C}/\text{min}$ . The small-angle X-ray diffraction pattern, recorded immediately after this quenching at  $-10^{\circ}\text{C}$  shows that the LS of CB decompose into two sharp lines corresponding to spacings at about  $52.6 \text{ \AA}$  ( $q = 0.12 \text{ \AA}^{-1}$ ) and  $26.3 \text{ \AA}$  ( $q = 0.24 \text{ \AA}^{-1}$ ) and two broad scattering peaks centered, respectively, at about  $q = 0.17 \text{ \AA}^{-1}$  (intense,  $36.4 \text{ \AA}$ ) and  $q = 0.06 \text{ \AA}^{-1}$  (weak,  $112 \text{ \AA}$ ) (Fig. 3A). SS observed together with LS during a second experiment, per-

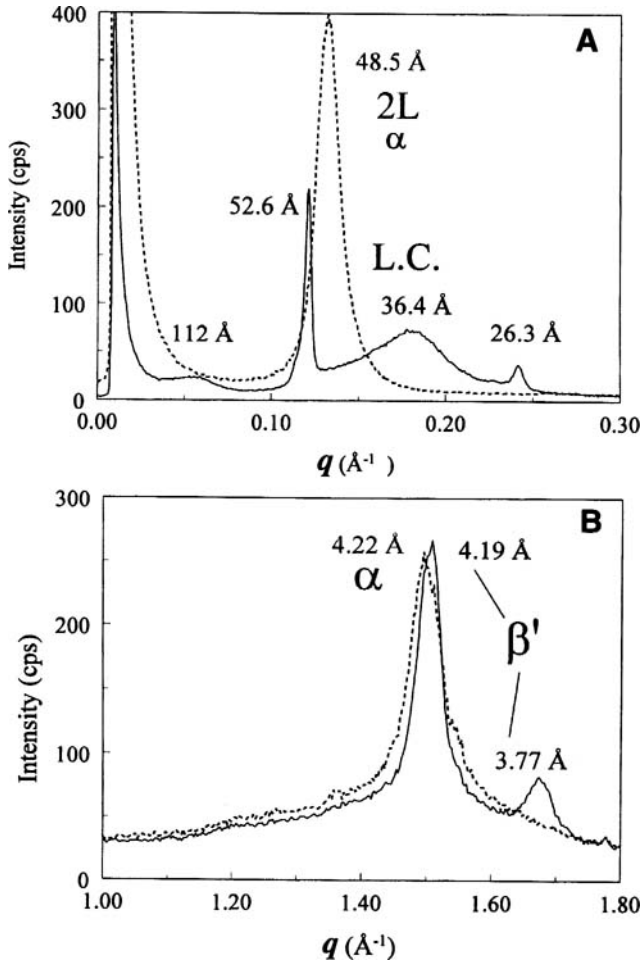


**Fig. 3.** Evolution of the long (A) and short (B) spacings of cocoa butter during heating of a sample obtained by liquid quenching at  $100^{\circ}\text{C}/\text{s}$  from  $-10$  to  $40^{\circ}\text{C}$  at  $1^{\circ}\text{C}/\text{min}$ . Transition from liquid crystalline sample to  $\alpha$  form is observed as determined by small- and wide-angle X-ray diffraction. (A) shows the long spacings observed at  $-10^{\circ}\text{C}$ , before, and at  $20^{\circ}\text{C}$ , after the transition to  $\alpha$  form; (B) corresponding short spacings. Figure is adapted from Reference 4.

formed at a shorter sample-detector distance but under the same conditions, are given in Figure 3B. It shows the existence of two interchain spacings at 4.19 and 3.77 Å above a broad scattering peak at about  $q = 1.4\text{--}1.5 \text{ \AA}^{-1}$ . Figure 3 also shows the evolution of both LS and SS recorded at 20°C/min after heating from -10 to 40°C at 1°C/min. At 20°C, the progressive merging into a single broad peak at 48.5 Å (the third order of which was also observed at 16.1 Å during the second experiment) of all initial sharp diffraction peak and broad-scattering bumps, the initial repeat distances of which were 52.6 and 236.4 Å, and the evolution of the SS at 4.19 and 3.77 Å toward a single line at 4.22 Å were interpreted as resulting from a metastable to a less unstable form transition. A liquid crystalline variety, a possible structure of which is shown Figure 4, self-transforms into an  $\alpha$  form. The structure of the melted TAG is still discussed (9,10) since Larsson proposed a liquid crystal model (1). Both the X-ray pattern observed after CB quenching and its evolution toward an unstable  $\alpha$  form suggest that the liquid crystalline variety is an intermediate form of organization between the liquid crystal corresponding to melt and  $\alpha$  form.

This liquid crystalline structure has also been observed in the CB fractions characterized above as well as in palm and palm fractions. All these fats are monounsaturated TAG rich. Then taking into account the relative scattering and diffraction intensity variations between the different fractions, it is proposed that the sharp lines originate from a  $\beta'$  organization of the saturated chains while the unsaturated ones are left outside of the structure giving a scattering pattern more intense but comparable to that of the liquid TAG (1).

## Conclusion

The presence of one or several long chains, the different packings of which lead to a variety of polymorphic forms, renders the thermal and structural behaviors of lipids rather complex to study. Both types of properties are currently measured by X-ray diffraction and DSC. The use of a new instrument allowing simultaneously time-resolved synchrotron X-ray diffraction at both wide and small angles as a function of temperature (XRDT) and high-sensitivity DSC has been described. The advantages of collecting information from the same sample and from the same acquisition unit were also discussed. The thermal and structural properties of CB are investigated to illustrate the capabilities of the instrument (4). It is shown that in CB at room temperature, and this applies also to tempered chocolate, at least two solid phases corresponding to different TAG compositions coexist beside the liquid fatty phase. The polymorphism of both solid species is also studied. A slow heating scan at 0.1°C/min from -10 to 40°C confirmed the existence of five of the six forms already observed. It is shown from the small-angle X-ray scattering pattern of the first phase that the least stable one, showing the coexistence of sharp lines with broad-scattering bumps, corresponds to a liquid crystalline phase in which likely the saturated chains, perfectly organized in  $\beta'$  form (orthorhombic

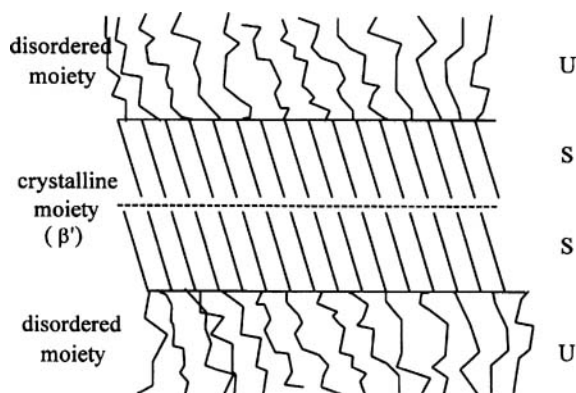


**Fig. 4.** Scheme of a possible arrangement of the triacylglycerol molecules in the liquid crystalline form. A crystalline moiety with a planar organization involves the glycerol backbone and saturated (S) fatty acid chains, while the remaining acyl groups (mono and polyunsaturated, U) adopt a liquid-like structure.

packing), crystallize nearby the melted-like unorganized unsaturated chains. This liquid crystalline phase, which is also observed in palm oil submitted to the same quenching, is also found in the fractions of both fats.

Concerning the second and minor phase of CB, it has been shown that it corresponds to a saturated TAG phase for which two different forms,  $\alpha$  and  $\beta$ , are evidenced. Taking into account that CB is probably one of the fats showing the simplest TAG composition, it is suggested that most of the fats do not crystallize as a single form, as generally considered, but rather as a mixture of different crystals belonging to different phases. This study demonstrates that high resolution obtained at small angles using synchrotron radiation is an absolute requirement for fat polymorphism characterization. The coupling of the three techniques above might be helpful in this respect.

## References

1. Larsson, K., Molecular Arrangement in Glycerides, *Fette Seifen Anstrich.* 74: 136–142 (1972).
2. Sato, K., T. Arishima, Z. Wang, N. Ojima, N. Sagi, and H. Mori, Polymorphism of POP and SOS, I Occurrence and Polymorphic Transformation, *J. Am. Oil Chem. Soc.* 66: 664–674 (1989).
3. Keller, G., F. Lavigne, L. Forte, K. Andrieux, M. Dahim, C. Loisel, M. Ollivon, C. Bourgaux, and P. Lesieur, DSC and X-ray Diffraction Coupling. Specifications and Applications, *J. Thermal Anal.* 51: 783 (1998).
4. Loisel, C., G. Keller, G. Lecq, C. Bourgaux, and M. Ollivon, Phase Transitions and Polymorphism of Cocoa Butter, *J. Am. Oil Chem. Soc.* 75: 425–439 (1998).
5. Loisel, C., G. Lecq, G. Keller, and M. Ollivon, Dynamic Crystallization of Dark Chocolate : Influence of Temperature and Lipid Additives, *J. Food. Sci.* 63: 73–79 (1998).

6. Wille, R.L., and E.S. Lutton, Polymorphism of Cocoa Butter, *J. Am. Oil Chem. Soc.* 43: 491–496 (1966).
7. Adenier, H., H. Chaveron, and M. Ollivon, Mechanism of Fat Bloom Development on Chocolate, in *Shelf-Life Studies of Foods and Beverages; Chemical, Biological, Physical, and Nutritional Aspects*, edited by G. Charalambous, Amsterdam, Elsevier Science Publishers B.V., 1993, pp. 353–389.
8. Sato, K., Polymorphism of Pure Triacylglycerols and Natural Fats, in *Advances in Applied Lipid Research*, Vol. 2, edited by Ed. F. Padley, 1996, Amsterdam JAI Press Inc., pp. 213–268.
9. Larsson, K., On the Structure of the Liquid State of Triglycerides, *J. Am. Oil Chem. Soc.* 69: 835–836 (1992).
10. Cebula, D.J., D.J. McClements, M.J.W. Powey, and P. Smith, Neutron Diffraction Studies of Liquid and Crystalline Trilaurin, *Ibid.*: 130–136 (1992).

## Chapter 4

# Effects of Tempering on Physical Properties of Shortenings Based on Binary Blends of Palm Oil and Anhydrous Milk Fat During Storage

Nor Aini I.

Malaysian Palm Oil Board, P.O. Box 10620, 50720 Kuala Lumpur, Malaysia

## Introduction

Physical properties of a shortening include appearance, consistency, solid fat content, crystal form and size, melting point, and melting behavior. These properties are influenced by the chemical composition which in turn relates to the nature of the fatty acids present and their distribution on the glycerol molecule.

From the palm fruit, two types of oils are obtained, namely palm oil (PO) and palm kernel oil (PKO). PO is obtained from the mesocarp while PKO is derived from the flesh of the kernel. Although they come from the same fruit, they differ in their chemical and physical characteristics. PO and PKO are widely used in various food applications including shortenings (1).

Shortening is a 100% fat product formulated with animal and/or vegetable oil that has been processed for functionality. It is used as an ingredient in bakery products such as bread, cakes, cookies, short pastries, fillings, and icing. It is also used in frying. Anhydrous milk fat (AMF) is made from either butter or directly from milk cream or fresh cream. Traditionally, butter and lard have been the fats used in bakery products. Consumption patterns have shifted away from traditional animal-based fats to vegetable oils and fats due to economics and nutritional considerations. However, the buttery flavor of milk fat is still desirable.

In this study, shortenings based on blends of PO and milk fat were produced to take advantage of the versatility and functionality of PO and the desirable buttery flavor of milk fat. The effects of tempering on the physical properties of these shortenings during storage were investigated.

## Materials and Methods

Refined, bleached, and deodorized PO was obtained from a local refinery, and AMF was obtained from New Zealand Dairy Board, Wellington.

### *Shortening Production*

PO was blended with AMF at the following proportions: 80:20, 60:40, and 40:60. A 100% PO was included as comparison. Final weight of each blend was 30 kg. The

feedstock was melted to a temperature of 57°C and processed on a pilot scale on the Schroeder Kombinator type VUK B 02/60-400 (Lubeck, Germany). The products were run at a pump speed of 300 rpm. The speed of cooler I, cooler II, and working units was 400 rpm, respectively. Back pressure of the pump was 2 kg/cm<sup>2</sup>. Refrigerant temperature was -18°C. The shortenings were filled into cans (filling temperature 16°C). After production, the shortenings were divided into three sets: set A was tempered at 10°C, set B at 23°C, while set C was tempered at 30°C. After 2 days (d), samples in sets A and C were transferred to room temperature (23°C) for further storage and evaluation. Samples in set B remained at 23°C throughout the storage period.

### ***Analysis and Evaluation***

*Consistency Measurement.* The instrument used was Seta Penetrometer-Universal Model 1700 (Stanhope Seta Ltd., Surrey, England). The cone angle used was 40°C, and the penetration time was 5 s. Measurements were taken at ambient temperature (23°C) at intervals of 4 wk. Five penetration readings were taken, and the results were averaged and then converted into yield values using a formula given by Haighton (2).

*Solid Fat Content.* Similar method as described previously (3) was used. In this method, the samples were melted in nuclear magnetic resonance (NMR) tubes; therefore it was essentially the IUPAC method 11.B.6 (4). To measure changes in solid fat content during storage, samples were not melted but instead, they were transferred to the NMR tubes using a rod and a piston. Measurements were taken directly at ambient temperature (23°C) at weeks 4, 8, and 12 of storage.

*Microscopy.* A polarized light microscope (Olympus BH-2) (Olympus, Japan) was used to observe crystal structure and to provide some indication of the relative crystal size of the shortenings. Observations were made at regular intervals. Photomicrographs were taken at 200 magnification.

*X-Ray Diffraction Analyses.* The polymorphic forms of the shortenings were established by x-ray diffraction using procedures as reported previously (5).

## **Results and Discussion**

Table 1 shows effect of the tempering on yield values of PO shortenings during storage. Samples tempered at 10°C for 2 d (set A) were the softest, followed by samples stored at 23°C throughout the study (set B). Samples tempered at 30°C for 2 d (set C) were generally softer than set A samples. On the other hand, shortening based on PO/AMF 80:20 tempered at 10°C for 2 d (set A) were the hardest throughout the entire period with yield values higher than samples in set B or C. Yield values of samples in sets B and C were significantly lower during the first 8 wk of storage than thereafter. In an earlier study, a similar trend in palm stearin-

**TABLE 1**  
Effect of Tempering on Yield Values (g/cm<sup>2</sup>) of Palm Oil Shortening During Storage

Week	Tempering <sup>a</sup>		
	Set A	Set B	Set C
4	173	271	264
8	216	287	352
12	244	374	332
16	244	392	307
20	285	437	392
24	285	480	346

<sup>a</sup>Set A: 2 d at 10°C, then transferred to 23°C; Set B: 23°C throughout; Set C: 2 d at 30°C then transferred to 23°C.

soft milk-fat shortenings was reported (6). Until week 12, Set B samples were softer with lower yield values than set C samples which were tempered at 30°C for 2 d (Table 2). Compared to the other shortening formulation, PO/AMF 80:20 in set A recorded the highest yield values throughout the entire period of the study.

For PO/AMF 60:40 shortening, a trend similar to PO/AMF 80:20 shortening was observed in that set A samples were the hardest throughout the study than those of set B or C samples (Table 3). There was not much difference in yield value between samples in sets B and C. Shortening PO/AMF 40:60 was found to be much softer than the rest of the samples (Table 4). It was noted that the shortenings become softer with a higher amount of AMF in the formulation. Set C samples were slightly softer than set B.

Figure 1 shows solid fat content profiles of the shortenings. PO shortening had the least amount of solid at temperatures below 15°C. Between 15 to 25°C, the solids contents were similar to that of PO/AMF 80:20 shortening. It was noted that with a higher amount (40%) of AMF in the formulation, the solid content increased significantly at lower temperatures. Solid fat content curves of PO and PO/AMF 80:20 shortenings were flatter than those of PO/AMF 60:40 and 40:60.

**TABLE 2**  
Effect of Tempering on Yield Values (g/cm<sup>2</sup>) of Palm Oil:Anhydrous Milk-Fat Shortening 80:20 During Storage

Week	Tempering <sup>a</sup>		
	Set A	Set B	Set C
4	376	57	86
8	478	57	160
12	488	115	240
16	454	260	251
20	474	276	270
24	476	246	277

<sup>a</sup>Tempering conditions as stated in Table 1.

**TABLE 3**Effect of Tempering on Yield Values (g/cm<sup>2</sup>) of Palm Oil:Anhydrous Milk-Fat 60:40 Shortening During Storage

Week	Tempering <sup>a</sup>		
	Set A	Set B	Set C
4	205	42	41
8	260	39	40
12	265	47	61
16	333	69	139
20	463	126	234
24	448	187	340

<sup>a</sup>Tempering conditions as stated in Table 1.

Tempering at 10°C for 2 d (set A) produced shortenings with higher solid contents than tempering at 23°C (set B). On the other hand, tempering the sample at 30°C for 2 d (set C) produced shortenings with less solid contents than those tempered at 23°C for the entire period. For PO shortening (Fig. 2), the changes in solid fat content in the three sets of samples during storage were not significant. The solid fat content ranged between 19.3 to 19.6% (set A), 17.9 to 19.4% (set B), and 14.5 to 15.9% (set C). It was observed that the other shortenings contained less solids than PO at weeks 1 and 4 of storage. There were no significant changes in solid contents of PO/AMF shortenings during the first month (Figs. 3–5). However, at week 8 of storage, there were significant increases in solid contents of the PO/AMF shortenings. For PO/AMF 80:20 shortening, the amount of solids at week 8 in sample sets A, B, and C were less than double the amount at week 4. Larger increases were observed in PO/AMF 60:40 and 40:60 shortenings where the solids contents at week 8 in all three sets of samples were more than double those measured at week 4 of storage. The more the amount of AMF in the formulation, the higher was the amount of solids present at week 8. It should be pointed

**TABLE 4**Effect of Tempering on Yield Values (g/cm<sup>2</sup>) of Palm Oil:Anhydrous Milk-Fat 40:60 Shortening During Storage

Week	Tempering <sup>a</sup>		
	Set A	Set B	Set C
4	71	56	45
8	87	46	39
12	92	57	53
16	103	53	47
20	155	51	43
24	202	48	64

<sup>a</sup>Tempering conditions as stated in Table 1.

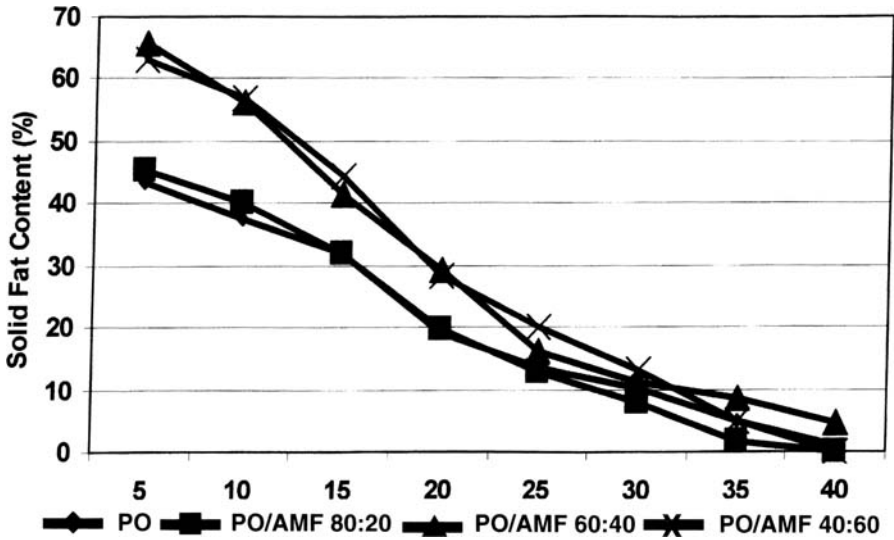


Fig. 1. Solid fat content profiles of palm oil (PO)-anhydrous milk-fat (AMF) shortenings.

out again that in all shortenings, set C samples contained the least amount of solids.

Microscopic observation revealed that PO shortening consisted of small crystals. Crystal size of sample in set C was smaller than in set A or set B (Fig. 6). Upon storage, the crystal grew larger in size. Shortenings made of PO/AMF had

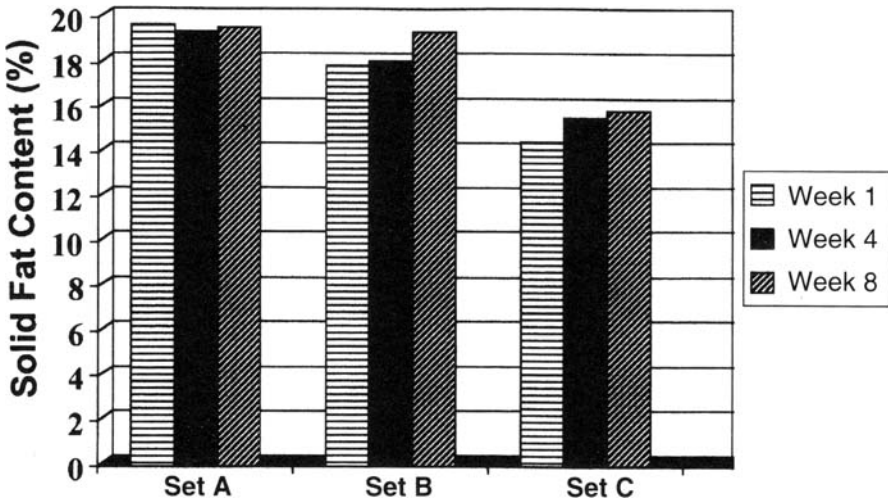


Fig. 2. Changes in solid fat content of palm oil shortenings during storage.

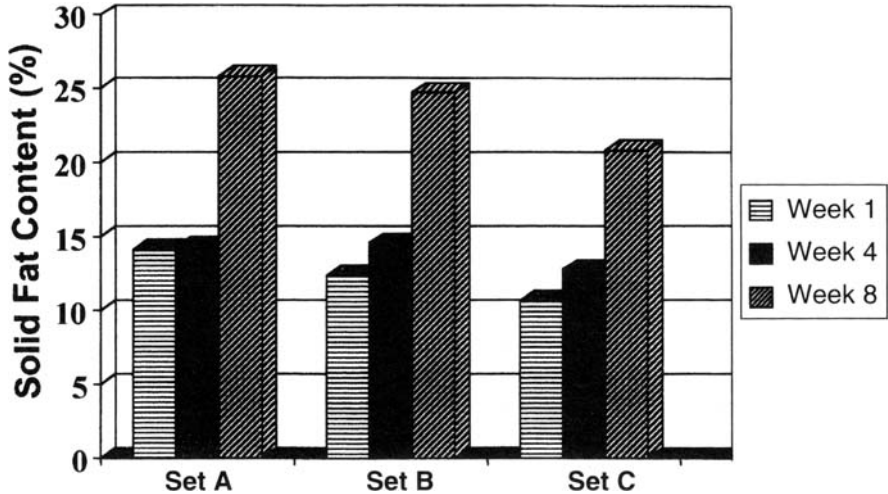


Fig. 3. Changes in solid fat content of palm oil-anhydrous milk-fat 80:20 shortening during storage.

very tiny crystals. The higher the amount of AMF in the formulation, the tinier were the crystals. The crystals in PO/AMF shortening also increased in size upon storage. Figure 7 shows crystals of PO/AMF 60:40 shortenings at 12 wk. Crystals in set A were evenly distributed. Individual crystals formed some clusters in set B. In set C, the crystals seemed to agglomerate into larger clusters. The trend

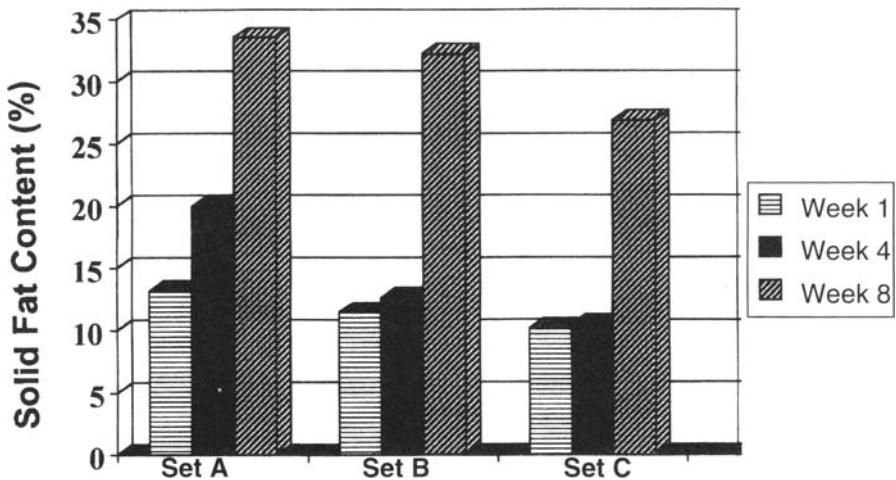


Fig. 4. Changes in solid fat content of palm oil-anhydrous milk-fat 60:40 shortenings during storage.

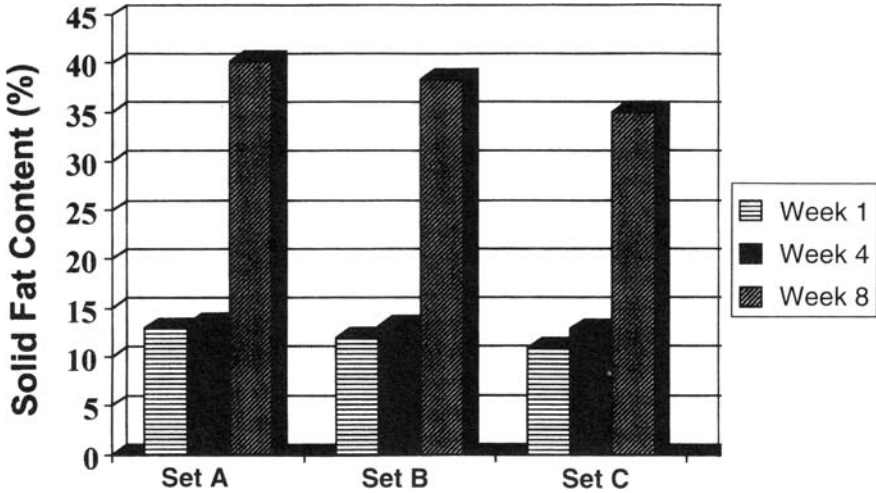
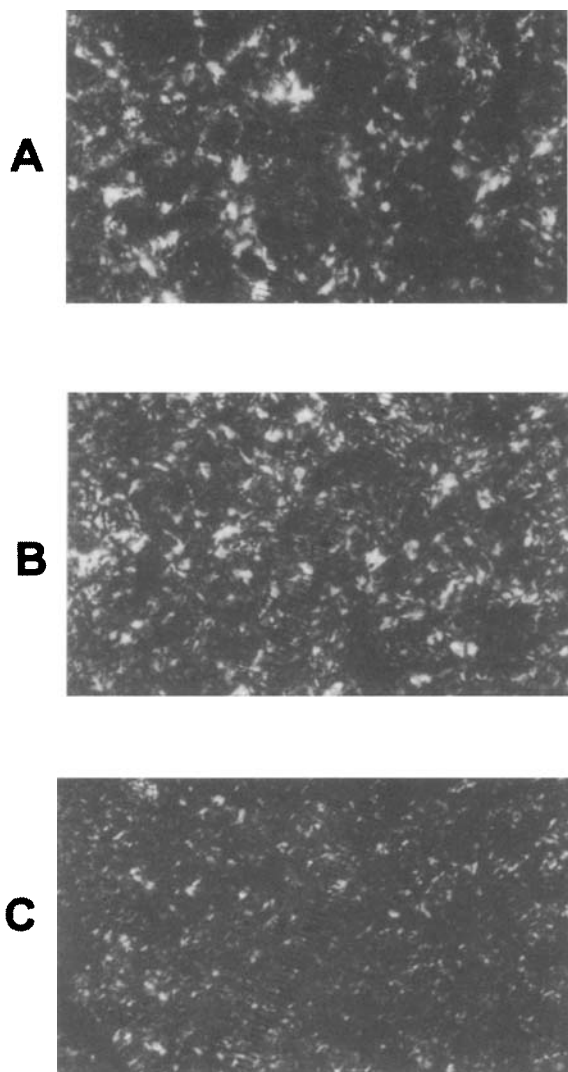


Fig. 5. Changes in solid fat content of palm oil–anhydrous milk-fat 40:60 shortenings during storage.

observed was a reverse of the three sets of PO shortening observed at the first week.

Tempering did not affect the initial polymorphic form of 100% PO shortening. Samples tempered at the three conditions exhibited  $\beta'$  form. Crystallization habit of a fat is dependent on its chemical composition. In general, fats containing uniform triglycerides have the tendency to crystallize in the  $\beta$  form, and those containing a mixture of different types of triglycerides tend to form  $\beta'$  crystals. According to Timms (7), the position of the fatty acid on the glyceride molecule is important in determining polymorphic behavior of oils and fats.  $\beta'$  is prevalent when the triglyceride is “asymmetric,” i.e., two saturated or two unsaturated acids occupy the 1, 2 or 2,3 position, while the remaining position is occupied by an unsaturated or saturated acid. The two major fatty acids in PO (palmitic and oleic) were reflected in the triglyceride composition in that the two major triglycerides POP (31.4%) and POO (19.8%) far exceeded the other triglycerides (8). These were followed by PLP (9.7%) and POS (5.9%). There were moderate amounts of POL, OOO, PLL, and SOO, where P = palmitic, O = oleic, L = linoleic, S = stearic acids. PO forms  $\beta'$  crystal because of the various types of triglycerides present in the oil. It has also been reported that PO, which contains a high level of palmitic acid, promotes the formation of  $\beta'$  crystals (9).

During storage, some changes were observed. PO shortening in sets A and B showed the presence of a small amount of  $\beta$  polymorph at 4 wk and the number of  $\beta$  crystalline formed increased with further storage. However,  $\beta'$  form was still predominant until the end of the study. In set C, equal amounts of  $\beta'$  and  $\beta$  were present at 4 wk and thereafter.



**Fig. 6.** Micrograph of palm oil shortening at 1 wk. A, Set A: Tempered at 10°C for 2 d; B, Set B: Tempered at 23°C throughout the study; and C, Set C: Tempered at 30°C for 2 d.

It has been reported in previous studies that milk fat contained  $\beta' > \beta$  (10,11). Recent investigators (12) reported that milk fat crystallized in  $\beta'$ -2 polymorphic form. In this study, tempering showed some effect on initial polymorphic forms of PO/AMF 80:20 and 60:40 shortenings. In set A of PO/AMF 80:20,  $\beta'$  was predominant, and a small amount of  $\beta$  form was present. In contrast, set B and set C of the same shortenings contained all  $\beta'$  polymorph. In the case of PO/AMF 60:40, set A sample showed equal amounts of  $\beta'$  and  $\beta$ , set B contained only  $\beta'$ , while set C was dominated by  $\beta'$ . On the other hand, there was no effect on PO/AMF 40:60 which showed the presence of  $\beta'$  in all three sets of samples.

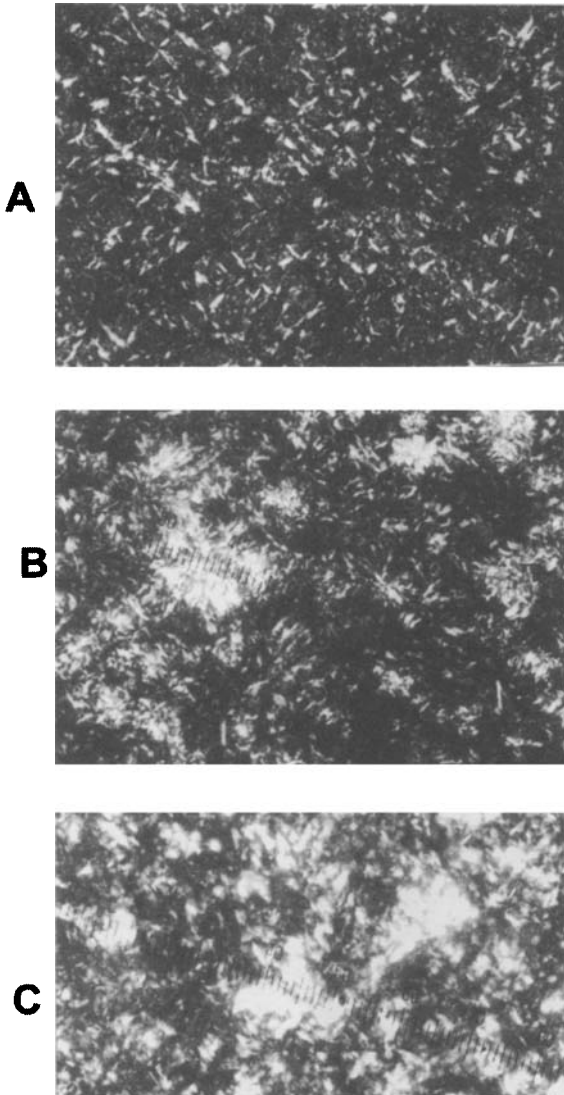


**Fig. 7.** Micrograph of Palm Oil-Anhydrous Milkfat 60:40 Shortenings at 12 wk. A, Set A: Tempered at 10°C for 2 d; B, Set B: Tempered at 23°C throughout the study; and C, Set C: Tempered at 30°C for 2 d.

Several changes occurred during storage (Table 5). Set A of PO/AMF 80:20 and 60:40 shortenings had more  $\beta$  than  $\beta'$  at later storage, while PO/AMF 40:60 contained only  $\beta$  polymorphic form at weeks 8 and 12. Greater  $\beta'$  stability was observed in samples set B and C of PO/AMF 60:40 and 40:60 shortenings where the crystals were still in the  $\beta'$  form until the week 8. Later at week 12,  $\beta$  crystal was predominant in PO/AMF 80:20 and 60:40 shortenings for all three sets of samples. On the contrary,  $\beta'$  was predominant in PO/AMF 40:60 shortening set B and set C at week 12.

**TABLE 5**

Effects of Tempering on Polymorphic Forms of Palm Oil (PO):Anhydrous Milk-Fat (AMF) Shortenings During Storage

Week	Shortening formulation											
	PO			PO/AMF 80:20			PO/AMF 60:40			PO/AMF 40:60		
	A	B	C	A	B	C	A	B	C	A	B	C
1	$\beta'$	$\beta'$	$\beta'$	$\beta' \gg \beta$	$\beta'$	$\beta'$	$\beta' + \beta$	$\beta'$	$\beta' > \beta$	$\beta'$	$\beta'$	$\beta'$
4	$\beta' \gg \beta$	$\beta' \gg \beta$	$\beta' + \beta$	$\beta' + \beta$	$\beta'$	$\beta'$	$\beta \gg \beta'$	$\beta'$	$\beta'$	$\beta' \gg \beta$	$\beta'$	$\beta'$
8	$\beta' \gg \beta$	$\beta' \gg \beta$	$\beta + \beta$	$\beta > \beta'$	$\beta' \gg \beta$	$\beta' \gg \beta$	$\beta \gg \beta'$	$\beta'$	$\beta'$	$\beta$	$\beta'$	$\beta'$
12	$\beta' > \beta$	$\beta' > \beta$	$\beta' + \beta$	$\beta > \beta'$	$\beta > \beta'$	$\beta > \beta'$	$\beta \gg \beta'$	$\beta \gg \beta'$	$\beta \gg \beta'$	$\beta$	$\beta' > \beta$	$\beta' > \beta$

## Summary

In the study, PO/AMF 80:20 shortening set A samples which were tempered at 10°C for 2 d were the firmest with the highest yield values. Tempering at 30°C for 2 d generally resulted in softer products than tempering at 23 or 10°C for 2 d. With higher amount of AMF in the formulation, the samples became softer. There were significant increases in solid contents of PO/AMF shortenings at week 8 of storage. Set A samples contained the highest amount of solid followed by set B and then set C, that is, samples in set C contained the least amount of solids. Set B and set C of PO/AMF shortening samples were generally stable in the  $\beta'$  form until week 4 or 8 of storage. With prolonged storage,  $\beta$  form started to appear, and it was dominant in PO/AMF 80:20 and 60:40 at week 12. Set A of PO/AMF 80:20 and 60:40 contained both  $\beta'$  and  $\beta$  even from the beginning. More  $\beta$  polymorph was formed with longer storage time.

## References

1. Nor Aini, I. and M.S.A. Yusoff, Food Uses of Palm and Palm Kernel Oils, in *Advances in Oil Palm Research*, edited by B. Yusof, B.S. Jalani, and K.W. Chan, Malaysian Palm Oil Board, Bangi, Malaysia, 2000, Vol. II, pp. 968–1035.
2. Haighton, A.J., The Measurement of Hardness of Margarine and Fats with Penetrometers, *J. Am. Oil Chem. Soc.* 36: 345–349 (1959).
3. Oh, F.C.H., and K.G. Berger, in *Proceedings of the International Conference on Palm Oil Product Technology in the Eighties*, edited by E. Pushparajah and M. Rajadurai, Incorporated Society of Planters, Kuala Lumpur, 1983, pp. 383–395.
4. IUPAC, *Standard Analysis of Oils, Fats and Derivatives*, 6th Ed., Pergamon Press, Oxford, 1979.
5. V. D'Souza, L. de Man, and J.M. deMan, Chemical and Physical Properties of the High Melting Glyceride Fractions of Commercial Margarines, *J. Am. Oil Chem. Soc.* 68: 153–162 (1991).
6. Nor Aini, I., M.S. Embong, A. Aminah, A.R. Md Ali, and C.H. Che Maimon, Physical Characteristics of Shortenings Based on Modified Palm Oil, Milkfat and Low Melting Milkfat Fraction, *Fat Sci. Technol.* 7/8: 253–260 (1995).
7. Timms, R.E., Phase Behaviour of Fats and Their Mixture, *Prog. Lipid Res.* 23: 1–38 (1984).
8. Nor Aini, I., Utilization of Palm Oil and Milkfat in Shortening Formulations for Madeira Cake and Short Dough Biscuits, Ph.D. Thesis, University Kebangsaan Malaysia, 1991, pp. 178–179.
9. Rivarola, G.J.A., M.C. Anon Segura, and A. Calvelo, Crystallization of Hydrogenated Sunflower-Cottonseed Oil, *J. Am. Oil Chem. Soc.* 64: 1537–1543 (1987).
10. Woodrow, I.L., and J. M. deMan, Distribution of *Trans* Unsaturated Fatty Acids in Milkfat, *Biochem. Biophys. Acta* 152: 472–478 (1968).
11. Timms, R.E., The Physical Properties of Blends of Milkfat with Beef Tallow and Beef Tallow Fractions, *Australian J. of Dairy Technol.* 34: 257–258 (1979).
12. Wright, A.J., W.H. Hartel, S.S. Narine, and A.G. Marangoni, The Effect of Minor Components on Milkfat Crystallization, *J. Am. Oil Chem. Soc.* 77: 463–475 (2000).

## Chapter 5

# Triacylglyceride Crystallization in Vegetable Oils: Application of Models, Measurements, and Limitations

Jorge F. Toro-Vazquez, Elena Dibildox-Alvarado, Verónica Herrera-Coronado, and Miriam A. Charó-Alonso

Universidad Autónoma de San Luis Potosí, Facultad de Ciencias Químicas-CIEP, Av. Dr. Manuel Nava 6, Zona Universitaria, San Luis Potosí 78210, México

## Introduction

The triacylglycerides (TAG) have several physical chemical properties that determine processing conditions of fats and oils and their functionality in food systems. In the particular case of the phase changes, these are physical properties that determine the solid-to-liquid ratio provided by TAG in fats and oils as a function of temperature. These properties determine much of the functionality of edible vegetable oils in a given food system. However, the relationships of the chemical structure of TAG, their physical properties, and the corresponding functional characteristic of interest in food systems are yet to be established. This is particularly true for complex systems such as vegetable oils, which are composed of mixtures of different families of TAG and consequently do not have specific physical properties. For instance, vegetable oils do not have a particular melting or crystallization temperature. Rather, vegetable oils show a melting/crystallization temperature profile. Thus, when oils are cooled the family of TAG with the highest melting temperature (i.e., the one more saturated) is the first to crystallize, developing a solid within a liquid phase. These lipid systems, generally known as plastic fats, have fractal organization, i.e., a three-dimensional crystal network of TAG in an oil continuum (1,2). The fractal dimension ( $D$ ) has a mathematical relationship with the elastic modulus,  $G'$ , which in turn has a significant linear regression with the hardness provided by crystallized TAG (2). Additionally, TAG crystallize in different polymorph states, with distinctive degrees of thermal stability, crystal size, and shape. These polymorph states for pure TAG crystals (in increasing order of thermal stability) are sub- $\alpha$ ,  $\alpha$ ,  $\beta'$ , and  $\beta$ . Polymorphic forms differ in the geometry of packing of the hydrocarbon chain at the molecular level. At a higher molecular level, the TAG arrangement in the solid state may occur, according to Larsson (3,4) in four different types. Two of these structures depend on the conformation of the fatty acyl groups on the glycerol backbone, each one organizing their hydrocarbon chains across the crystal layers in either of other two structures of TAG (3,4).

Then, the functional properties associated with the use of vegetable oils (i.e., mouthfeel, spreadability, emulsion stability, whippability, and air-bubble retention capacity) in products such as chocolate, butter, low-fat spreads, shortenings, ice cream, and whipped cream depend on the capacity of the TAG in the oil to develop a solid phase, its melting/crystallization temperature profile, polymorph-polytype state, and fractal organization of the crystallized TAG in the oil as affected by the time-temperature conditions. The effect of time-temperature conditions on vegetable oils' functionality is emphasized since TAG organization in the solid state is a thermodynamic metastable process (3,5). Thus, a slight variation in the time-temperature conditions has profound effects on the kinetics of polymorphic transformations and subsequently in the temperature profile of melting/crystallization (i.e., amount of solid phase as a function of temperature) and texture of the product.

In spite of that complexity, the industry uses crystallization of TAG as a process to: (i) eliminate small quantities of high-melting compounds from an oil to improve its appearance and consumer visual appeal particularly at low ambient temperature (i.e., winterization); (ii) obtain TAG fractions from oils or fats through a process known as fractional crystallization; and (iii) modify the texture of food systems.

Although achievement of these objectives is crucial in oils-and-fats processing and in food-industry use, considerable experimental work is still required to understand completely and to further control such process. Three different events are involved during crystallization, namely the induction of crystallization (i.e., nucleation), crystal growth, and crystal perfection or crystal ripening. These events occur nearly simultaneously at different rates, since there is a continuous variation of the thermodynamic condition that produces crystallization, i.e., supercooling or supersaturation. The occurrence of supercooling or supersaturation is a requirement to develop a solid from a liquid phase (i.e., nucleation). The thermodynamic drive brings the molecules into a "liquid structure," until a critical size of monomers aggregates and thermodynamic stable solid nuclei are formed. In the case of vegetable oils, TAG conform lamellar "liquid organizations" which shapes and sizes change as a function of temperature determining oil viscosity (6,7).

Several mechanistic models have been developed to study crystallization. Thus, the Fisher-Turnbull model establishes the dependence of nucleation rate on the activation free energy for nucleation and for molecular diffusion of the crystallizing molecules. In contrast, the mechanism for crystal growth and the overall crystallization rate is described by the Avrami model. However, none of these models was developed considering the particular physicochemical and/or structural characteristics of TAG in pure systems or in vegetable oils. Nevertheless, their application to lipid systems has provided useful information to understand and to describe TAG crystallization in simple and complex systems (i.e., vegetable oils). Our laboratory has been engaged in crystallization experiments with vegetable-oil blends done under several crystallization conditions (i.e., cooling rates, extent of

supercooling), using the Fisher-Turnbull and Avrami models to describe TAG crystallization in vegetable oils. Here, we present some data generated within this context to discuss the application, measurements involved, and physical meaning of the parameter obtained when such models are used in the characterization of TAG crystallization in vegetable oils.

## Supercooling and Supersaturation, the Thermodynamic Drive for Crystallization

Three different events are involved during crystallization: nucleation (solid-phase formation), crystallization (crystal growth), and crystal ripening (crystal perfection). However, before nucleation occurs, the solution must be under supercooling or supersaturation conditions. The supercooling or the supersaturation is the thermodynamic force that drives the formation of a solid nucleus since there is a free energy barrier opposed to the formation of the new phase. A general description of the concepts of supercooling and supersaturation follows.

The relative supercooling,  $\Delta T$ , is defined by  $\Delta T = (T - T_M)$ , where  $T_M$  is the melting temperature of the crystallizing compound and  $T$  is the isothermal crystallization temperature of the system. In the case of pure TAG,  $T_M$  is measured as its melting peak temperature and with mixed TAG and vegetable oils as the melting temperature of the component of highest melting temperature (Fig. 1). In both cases, DSC is used to obtain a dynamic thermogram (e.g., melting thermogram obtained at a specific heating rate), which is used to calculate  $T_M$  (Fig. 1). Relative supercooling, mostly referred to simply as supercooling, is the parameter most commonly used in the literature to evaluate the effect of temperature on TAG crystallization. On the other hand, the effective supercooling,  $(T - T_M^\circ)$ , is the difference between the equilibrium melting temperature,  $T_M^\circ$ , and the isothermal temperature of crystallization,  $T$ . The  $T_M^\circ$  value is the temperature where the smallest aggregation of molecules (i.e., unstable crystal nucleus) is in equilibrium with the molecules in the melt. Thus, small aggregations of molecules without the correct tridimensional arrangement to develop a stable crystal nucleus will melt just above  $T_M^\circ$ . A particular methodology to establish the magnitude of  $T_M^\circ$  in polymers has been described by Hoffman and Weeks (8) and later applied to oil systems by our group (9). The procedure involves the determination of the apparent melting temperature ( $T_M'$ ) of the TAG of interest after its crystallization at different temperatures ( $T$ ). In the absence of secondary crystallization, the experimental plot between  $T_M'$  and  $T$  gives a straight line with positive slope having a crossing point with the equilibrium line  $T_M' = T$  which represents  $T_M^\circ$ . Figure 2 shows the calculation of  $T_M^\circ$  in blends of palm stearin (PS) in sesame oil. It is apparent that in a given crystallizing system and polymorph state,  $T_M^\circ$  is independent of both the concentration of the crystallizing compound in the system (Fig. 2A) and the cooling rate used to achieve isothermal conditions (Fig. 2B). However,  $T_M^\circ$  is affected by the heating rate used during melting, particularly when recrystallization is

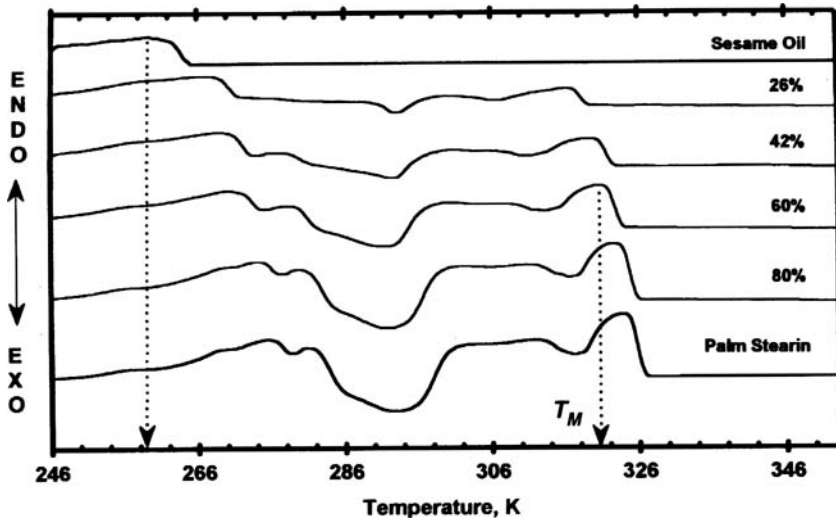


Fig. 1. Dynamic heating (melting) thermograms ( $5^{\circ}\text{C}/\text{min}$ ) for sesame oil, palm stearin, and blends of palm stearin in sesame oil at different proportions.  $T_M$  is the melting temperature of the triacylglycerides (TAG) with highest melting temperature (i.e., tri-palmitin) (adapted from Ref. 9).

involved during heating. Formal studies that evaluate the effect of supercooling on TAG crystallization in vegetable oils require the determination of  $T_M^{\circ}$  (i.e., the effective supercooling).

In contrast, several quantities are commonly used to measure the supersaturation. Some of these are  $\beta$ ,  $\ln \beta$ ,  $(\beta - 1)$  and  $(C - C_s)$ , where  $\beta = C/C_s$  and  $C$  is the concentration of the compound (i.e., TAG) in the solution (i.e., vegetable oil in a solution) at a given temperature. To achieve crystallization,  $C$  always must be higher than the concentration at saturation at the same temperature ( $C_s$ ). In the case of supersaturation, the units used to calculate  $C$  and  $C_s$  differ according to the character of the solute, i.e., electrolyte or nonelectrolyte. The most common units used with TAG are molarities, molalities, and molar fractions.

There are practical differences between the concepts of supercooling and supersaturation. Thus, the concept of supercooling is normally used when crystallization is achieved from a melt of one (i.e., pure TAG) or often two or more components (i.e., vegetable oil). The objective is either a simple solidification of a one-component system, but most times the purification of a multicomponent system (e.g., mixed crystals). In contrast, the term "supersaturation" is used when crystallization of a particular substance (i.e., a given family of TAG) is achieved from a solution (i.e., vegetable oil in hexane or acetone), and its objective is the separation of a pure compound. Additionally, for crystallization from the melt, the composition of the medium surrounding the surface of the growing crystal does not change

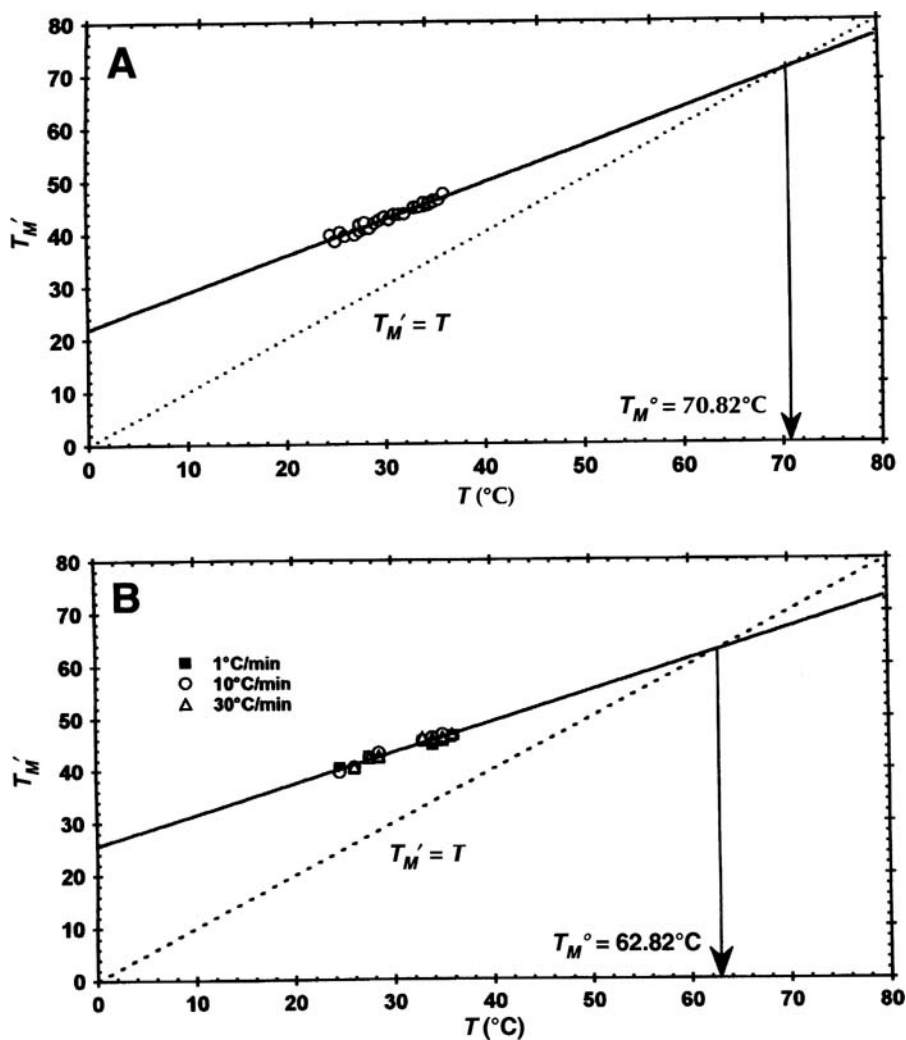


Fig. 2. Determination of the equilibrium melting temperature,  $T_M^0$ . (A) 26–80% blends of palm stearin in sesame oil, cooling rate  $1^\circ\text{C}/\text{min}$ , heating rate  $5^\circ\text{C}/\text{min}$  (adapted from Ref. 9); (B) 26 and 80% blends of palm stearin in sesame oil, cooling rates of 1, 10, and  $30^\circ\text{C}/\text{min}$ , heating rate  $5^\circ\text{C}/\text{min}$ .  $T$  and  $T_M'$  are defined in the text.

as drastically as in crystallization from solution. Therefore, the progress of crystallization is often not controlled by diffusion of the crystallizing molecules toward the growing crystal surface as in crystallization from solution. In crystallization from the melt, the progress of crystallization is controlled mainly by removal of the heat of crystallization ( $\Delta H_{Cp}$ ). Therefore, thermal diffusion effects predominate in

melt crystallization, contrary to crystallization from the solution, where heat transfer is not very important. Nevertheless, there is not a clear distinction between the effect of supercooling and supersaturation on crystallization, especially when the conditions are used at industrial scale (10). The reason for this is that supersaturation is generated by the mixed effect of concentration and temperature, particularly in the processes of cooling and evaporation. In any case, supercooling and supersaturation are associated with the development of thermodynamic conditions needed to structure the molecules in a liquid phase ("lamellar liquid structure"), until a critical size of monomers (i.e., TAG) aggregates and solid nucleuses are formed (3,11). In vegetable-oil crystallization, supercooling is the thermodynamic drive mostly used. Therefore, we discuss just information associated with the concept of supercooling.

During supercooling at temperatures below  $T_M^\circ$ , the system attempts to achieve thermodynamic equilibrium through nucleation and nuclei's growth, and in the absence of foreign particles or crystals of its own type, a solid phase is developed by a process known as homogeneous nucleation. In the research made in the general area of crystallization, including vegetable oil crystallization, homogeneous nucleation conditions are usually assumed. Nevertheless, such experimental conditions are very difficult to achieve, particularly at the industrial level. On the other hand, when nucleation is eased through the presence of foreign particles, which work as nucleating surfaces, the process is known as heterogeneous nucleation. Homogeneous and heterogeneous nucleation are collectively known as primary nucleation. In contrast, in secondary nucleation the presence of a solid phase previously developed in the system or added as seed crystals produces the development of additional solid at lower supercooling than the one needed for primary nucleation.

## The Fisher-Turnbull Equation

When nucleation occurs from the liquid phase of the system, also known as the melt (i.e., a vegetable oil), and in the absence of foreign particles, the rate of nucleation ( $J$ ) depends on the activation free energy to develop a stable nucleus,  $\Delta G_c$ , and the activation free energy for molecular diffusion,  $\Delta G_d$ , which is associated with the work involved in the diffusion of molecules from the bulk toward the crystal interface. Since viscosity is a physical parameter inversely proportional to molecular diffusion, as supercooling increases, the viscosity in the liquid phase might become a limiting factor for nucleation or crystal growth. The Fisher-Turnbull equation (Eq. 1) describes the relationship of  $\Delta G_c$  and  $\Delta G_d$ , with  $J$  through the following expression:

$$J = (N\kappa T/h)\exp(-\Delta G_c/\kappa T)\exp(-\Delta G_d/\kappa T) \quad [1]$$

where  $J$  is the rate of nucleation which is inversely proportional to the induction time of crystallization ( $t_i$ ),  $N$  is the number of molecules per mole,  $\kappa$  is the Boltzman constant,  $T$  is the crystallization temperature, and  $h$  is Planck's constant.

In a spherical nucleus,  $\Delta G_c$  is associated to the supercooling,  $T$ , and the surface free energy at the crystal/ melt interface,  $\sigma$ , through the Gibbs-Thompson equation (Eq. 2):

$$\Delta G_c = (16/3)\pi\sigma^3(T_M^\circ)^2/(\Delta H)^2(\Delta T)^2 \quad [2]$$

where  $(16/3)\pi$  results from the spherical shape attributed to the nucleus,  $\Delta H$  is the heat of fusion,  $T_M^\circ$  is the equilibrium melting temperature of the crystallizing compound, and  $\Delta T$  is the effective supercooling ( $T - T_M^\circ$ ). Working with Equations 1 and 2 and the fact that  $J$  is inversely proportional to  $t_i$ , one can easily prove that from the slope,  $s$ , of the linear regression of  $\text{Log}[(t_i)(T)]$  with  $1/T(\Delta T)^2$  the calculation of  $\Delta G_c$  might be obtained since  $\Delta G_c = s \kappa/(\Delta T)^2$ . With this approach, the only experimental value to be determined besides  $T_M^\circ$  is  $t_i$ , which in vegetable oils might be calculated from the crystallization exotherm as the time from the start of the isothermal process to the beginning of crystallization (i.e., time where the heat capacity of the sample has a significant departure from the baseline) (Fig. 3) (9). Additional methodologies to calculate  $t_i$  have been developed using light transmittance, optical density (6,12), and laser-polarized light turbidimetry (13). Approximations to determine the magnitude of  $\Delta G_c$  with Equation 2 might be obtained with the use of  $T_M$  and the relative supercooling ( $T - T_M$ ).

The  $\Delta G_c$  should not be confused with the heat of crystallization,  $\Delta H_{Cr}$ .  $\Delta G_c$  is the energy required to overcome the thermodynamic forces that oppose to the cre-

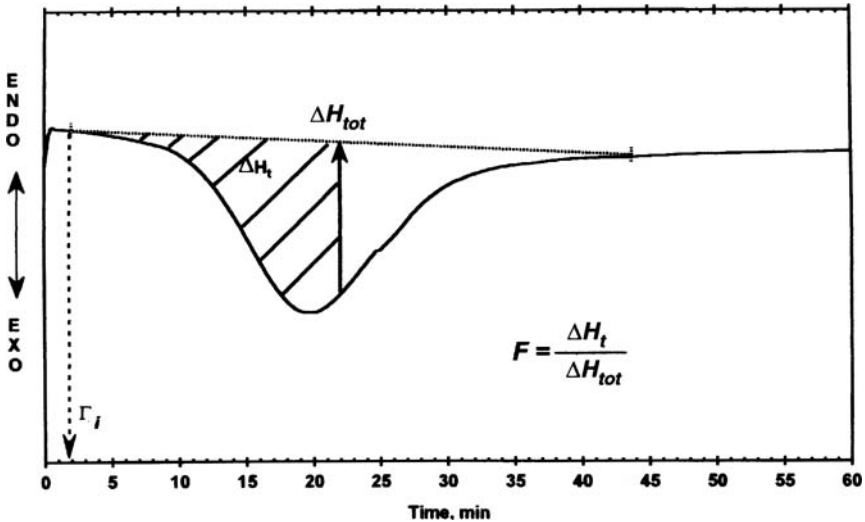


Fig. 3. Isothermal crystallization thermogram obtained by differential scanning calorimetry (DSC) indicating the determination of  $t_i$  and reduced crystallinity ( $F$ ) (adapted from Ref. 9).

ation of a solid phase within the liquid phase, while  $\Delta H_{Cr}$  is the energy added or removed during isothermal crystallization of a given compound. When polymorphic transformations are not involved during the crystallization and melting process of any given compound,  $\Delta H_{Cr} = \Delta H_M$ , where  $\Delta H_M$  is the melting heat of the compound. Both  $\Delta H_{Cr}$  and  $\Delta H_M$  might be easily determined through DSC.

The above description assumes that nucleation occurs directly in the bulk of the mother phase (i.e., the melt, the vegetable oil), which is in contrast to heterogeneous nucleation, a process where the nuclei are developed on substrates. Heterogeneous nucleation introduces a new parameter into the theory, namely, the wetting angle ( $\theta$ ) between the crystallizing molecules and the substrate (i.e., foreign particles, irregularities on the container) (Fig. 4). The heterogeneous nucleation theory follows the same concepts as homogeneous nucleation, except that fewer atoms, and consequently lower supercooling, are needed to achieve nucleation. Then,  $\Delta G_c^* < \Delta G_c$ , since

$$\Delta G_c^* = f[\Delta G_c] \tag{3}$$

where

$$f = (2 + \cos\theta)(1 - \cos\theta)/4 \tag{4}$$

The magnitude of  $f$  is function of the wetting of the foreign particles by the crystallizing molecules (i.e., TAG). A contact or wetting angle of  $180^\circ$  corresponds to

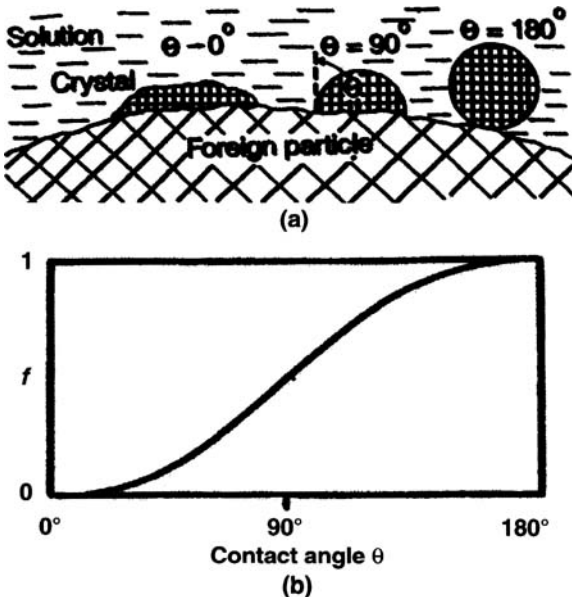


Fig. 4. (a) Nucleation on a foreign particle for different wetting angles  $\theta$ ; (b) factor  $f$  against angle  $\theta$  (from Ref. 10).

nonwettability and thus homogeneous nucleation since  $f = 1$  (Fig. 4). When angle  $\theta$  lies between  $0$  and  $180^\circ$ , the nucleation work is reduced by the wetting surface of the foreign particle (i.e.,  $f < 1.0$ ), consequently heterogeneous nucleation occurs (Fig. 4) (10).

Heterogeneous nucleation is one of the most common processes occurring in vegetable oil crystallization. However, its practical evaluation is complicated due to the difficulty in determining the surface tension components that conform  $\theta$ . The use of Equations 1 and 2 in vegetable oil crystallization without the efficient removal of foreign particles from the oil before crystallization quite probably determines the magnitudes of  $J$  and  $\Delta G_c$  resulting from the combined process of homogeneous nucleation occurring in the bulk and heterogeneous nucleation occurring on foreign substrates (i.e.,  $J^*$  and  $\Delta G_c^*$ ). For example, water that has been carefully purified and cleared of foreign particles by the distillation process and has been maintained out of contact with air to avoid air bubbles can be cooled below  $-30^\circ\text{C}$  without ice forming in it. In contrast, supercooling tap water to  $-5^\circ\text{C}$  is sufficient to freeze some water.

Figure 5 shows the Fisher-Turnbull plot for the crystallization of blends of PS in sesame oil (26, 42, 60, and 80%) (9). This model system is a complex crystallization system. PS is a mixture of TAG obtained through fractional crystallization from refined, bleached, and deodorized palm oil (14). Tripalmitin is the TAG with the highest melting temperature in PS (15), and here its concentration was 16.46% w/w ( $\pm 0.17\%$ ) (9). Our previous research showed that tripalmitin mostly determines the crystallization kinetics of PS and its blends with vegetable oils (i.e.,

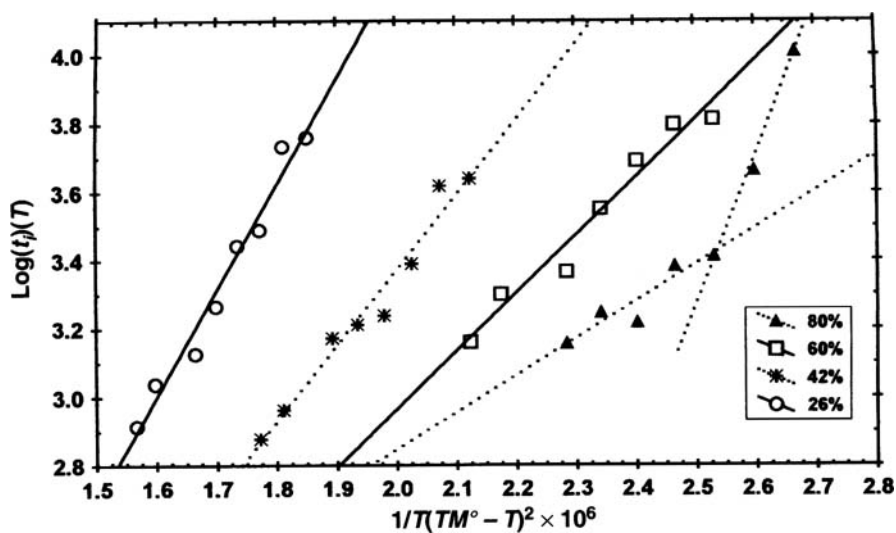


Fig. 5. Fitting of the nucleation kinetics of palm stearin blends in sesame oil according to the Fisher-Turnbull equation (from Ref. 9).

sesame oil) (5,7,9,12). In all these experiments, the crystallization process was evaluated by DSC and involved heating the system for 30 min at 80°C (353.2 K) to erase crystallization “memory” and then cooling to the crystallization temperature at a cooling rate of 1°C/min. The induction time for tripalmitin crystallization,  $t_i$ , was determined from the crystallization exotherm. For these particular blends of PS in sesame oil, the  $T_M^\circ$  was established with a value of 70.82°C (344 K, Fig. 2A) (9).

Then, a good linearity was obtained within the effective supercooling interval investigated ( $r > 0.98$ ,  $P < 0.0001$ ) for the 26, 42, and 60% PS/sesame oil blends (9). However, the 80% PS/sesame oil blend showed a significant change in slope in the plot around 33.8°C (307 K). This behavior is indicative of a change in the free energy required to achieve crystallization and it is associated with the development of a different polymorph state. Then, supported by additional DSC analysis, it was shown that in the 80% solution PS crystallized in two different polymorph states, i.e.,  $\beta_1'$  at  $T \leq 34.5^\circ\text{C}$  (307.6 K) and  $\beta_1$  at  $T \geq 35^\circ\text{C}$  (308.2 K). In contrast, within the interval of effective supercooling investigated the 26, 42, and 60% PS/sesame oil blends crystallized mainly in just one  $\beta_1'$  polymorph state (mixed with some minor quantities of  $\alpha$  crystals, particularly at very low supercooling).

The corresponding  $\Delta G_c$  values for the PS/sesame oil solutions as a function of the crystallization temperature are shown in Table 1. Lower  $\Delta G_c$  values have been obtained for palm oil, PS (16), and hydrogenated sunflower oil (13). However, in these studies a relative supercooling (i.e.,  $T - T_M$ ) rather than the effective supercooling (i.e.,  $T - T_M^\circ$ ) was used in the calculation of  $\Delta G_c$  since the value of  $T_M^\circ$  was not established. As previously indicated, formal studies that evaluate the effect of supercooling require the determination of  $T_M^\circ$ . The analysis of the  $\Delta G_c$  as a function of temperature (Table I) showed that crystallization in the  $\beta_1$  state required more energy for its development than  $\beta_1'$  crystallization (9). The occurrence of the  $\beta' \rightarrow \beta$  polymorphic transition is important to produce value-added products like *trans-free* margarines and vegetable spreads. In general,  $\beta'$  form and small size confer a fine crystal network that incorporates large amounts of liquid oil and provides good spreadability and plasticity to margarines, shortenings, and spreads. In contrast,  $\beta$  form, larger size, and higher melting temperature than  $\beta'$  crystals provide a sensation of sandiness and a dull appearance.

### **The Effect of Viscosity and Cooling Rate**

It is generally accepted that the progress of crystallization from the melt is controlled mainly by the efficient removal of the heat of crystallization. However, it is important to point out that viscosity, in a combined effect with supercooling and cooling rate, determines the magnitude of the  $t_i$  and subsequently the process of nucleation. Some results obtained in that direction are discussed. The effect of the viscosity of the oil phase on  $t_i$ , as a function of the effective supercooling, is shown in Figure 6. Again, the PS/sesame oil blends were used in these DSC experiments using a cooling rate of 1°C/min. The  $T_M^\circ$  for the PS/sesame oil blends was 70.82°C

**TABLE 1**

Free Energy for Nucleation ( $\Delta G_c$ ), Index of Avrami ( $n$ ), and Crystallization Rate Constant ( $z$ ) for Palm Stearin Crystallization in Sesame Oil as a Function of Crystallization Temperature<sup>a</sup>

Crystallization temperature (°C)	Palm stearin (% wt/vol)	$\Delta G_c$ (Kj/mol)	Avrami parameters		
			$n$	$z \times 10^{-8}$ (min <sup>-1</sup> )	
24.5	26	1197	4.4	821.95	
25.0		1224	4.7	249.56	
26.0		1279	4.8	109.69	
26.5		1308	4.6	131.06	
27.0		1338	5.4	5.91	
27.5		1369	5.5	1.31	
28.0		1401	5.1	1.14	
28.5		1434	4.5	7.40	
27.5		42	975	4.3	3095.43
28.0			998	4.0	5858.69
29.0	1046		4.4	649.16	
29.5	1072		4.8	197.29	
30.0	1098		4.7	120.14	
30.5	1026		5.0	9.86	
31.0	1154		5.0	2.81	
31.5	1183		5.2	0.85	
31.5	60		912	5.4	53.34
32.0			936	4.8	81.83
33.0		986	5.3	19.72	
33.5		1013	5.5	1.18	
34.0		1040	3.9	44.46	
34.5		1069	4.6	188	
35.0		1099	4.1	11.64	
33.0		80	629	5.3	30.10
33.5			646	4.8	57.38
34.0			664	5	55.85
34.5	682		5.0	15.18	
35.0	2804		5.5	3.87	
35.5	2884		4.7	3.51	
36.0	2967		5.3	0.03	

<sup>a</sup>Adapted from Reference 9.

(344 K, Fig. 3A). Overall, Figure 6 shows that the effective supercooling was higher for the 26 and 42% PS solutions and lower for the 60 and 80% PS solutions. For a particular PS system, the increment in the effective supercooling produced a higher viscosity of the oil phase and a decrease in the  $t_i$  (Fig. 6). This behavior was explained by the authors as follows (9). Under the supercooling conditions investigated and at the low cooling rate used (i.e., 1°C/min), TAG have enough time to organize in the liquid state in lamellar structures while decreasing the temperature to achieve isothermal conditions (Fig. 7). As a result, an increase in viscosity is

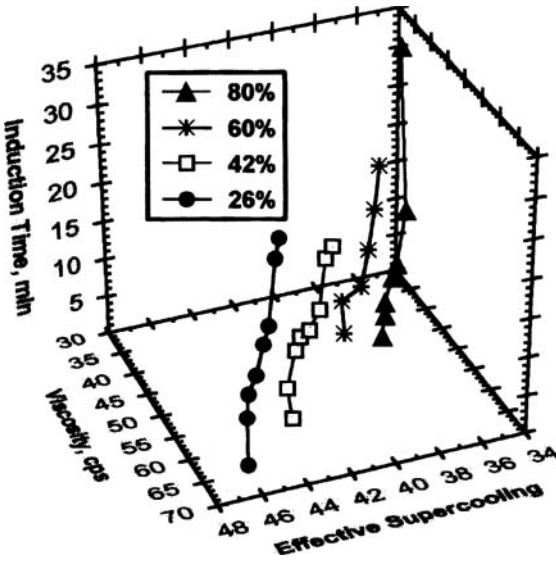


Fig. 6. Relationship among the  $t_i$ , viscosity of the oil phase, and effective supercooling for blends of palm stearin in sesame oil (from Ref. 9).

observed. Thus, once the isothermal conditions have been achieved, TAG lamellar structures further organize and achieve a critical size to develop a stable nucleus. This last process will take place in shorter time (i.e., smaller  $t_i$ ) the longer the system takes to achieve isothermal conditions (i.e., the higher the effective supercool-

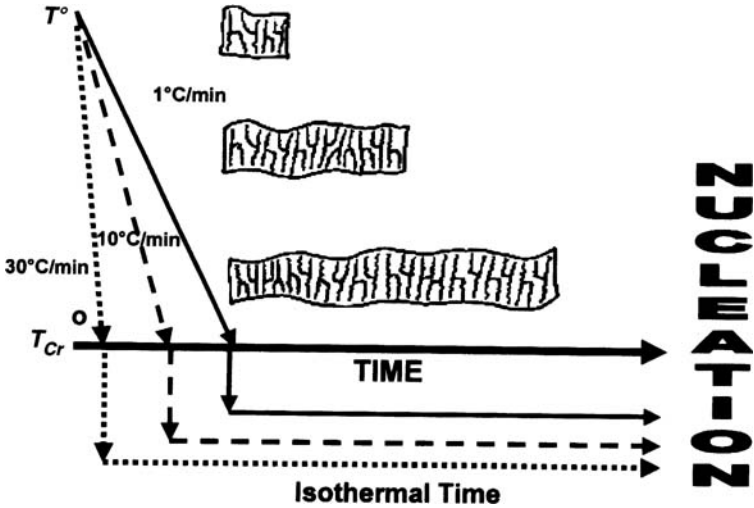


Fig. 7. Schematic diagram showing the effect of cooling rate on the lamellar organization of TAG and the  $t_i$ .  $T^o$  is the initial temperature and  $T_{Cr}^o$  is the isothermal crystallization temperature.

ing and/or the lower the cooling rate) (9). Subsequent studies have been done to evaluate the effect of cooling rate and crystallization temperature on  $t_i$ . The results are shown in Figure 8 for blends of 26 and 80% PS in sesame oil. Again DSC was used in these experiments. However, in this case the  $T_M^\circ$  for the blends was established in 62.8°C (336 K, Fig. 2B). In both systems, the 26 and the 80% PS/sesame oil blends, the increase in the cooling rate from 1 to 10°C/min increased the  $t_i$ . The same effect, although less evident, was observed when cooling rate was further increased to 30°C/min. As previously discussed, at low cooling rates TAG molecular organization is achieved during the cooling period. In contrast, at higher cooling rates (i.e., 10 and 30°C/min), the isothermal conditions are achieved at shorter periods. Therefore, the higher the cooling rate, the less time TAG molecules had to organize during the nonisothermal period. Consequently, when cooling rates are increased to values of 10 and 30°C/min, crystallization takes place after longer  $t_i$  (Figs. 7 and 8). Additional evidence in that direction comes from dynamic rheological measurements done with parallel plates' geometry (50 mm in diameter and a gap of 1 mm) at several cooling rates (1, 10, and 30°C/min) and applying variable strain levels within the linear viscoelastic region (LVR). Blends of 26% PS and 80% PS in sesame oil were used in these experiments. The  $T_M^\circ$  for the blends was established in 62.8°C (336 K, Fig. 2B). The challenge in such determinations is to establish the conditions to apply the appropriate strain level to the oil sample within the LVR and without the occurrence of slippage between the plate and the sample. These conditions vary for each crystallization temperature as a function of time during crystallization. Results are shown in Figure 9 superimposed to the thermograms obtained under the same crystallization conditions. The  $t_i$  obtained by DSC is shown for comparison purposes. The results showed that at the lower cooling rate the viscoelastic component of the blends,  $G'$ , is already the main component in the system before the  $t_i$  was determined by DSC (Fig. 9A). This indicates a more solid-like behavior in the blends before crystallization begins (i.e., higher degree of TAG lamellar organization). In contrast, as the cooling rate increased,  $G'$  was lower than  $G''$  before the induction time of crystallization (i.e., lower degree of TAG lamellar organization), and this relation inverted as the induction time of crystallization approached (Fig. 9B and 9C). Similar results were obtained with the phase shift angle,  $\delta$ , i.e., at the lower cooling rate a solid-like behavior was already in effect ( $\delta \ll 90^\circ$ ) in the PS/sesame oil blends before the induction time of crystallization, while the evolution from liquid toward solid (from  $\delta \approx 90^\circ$  to  $\delta \ll 90^\circ$ ) was observed before the induction time of crystallization at cooling rates of 10 and 30°C/min (Fig. 10). An additional observation is that the peak observed in the rheogram with  $\delta$  has a very good correspondence with the crystallization exotherm obtained by DSC. The  $\delta$  peak is associated with TAG nucleation and crystal growth.

Then, viscosity, supercooling, and cooling rate evidently determine the process of nucleation (i.e.,  $t_i$ ). However, their effect on the free energy for TAG nucleation has not been evaluated. In the same way, the interaction among such

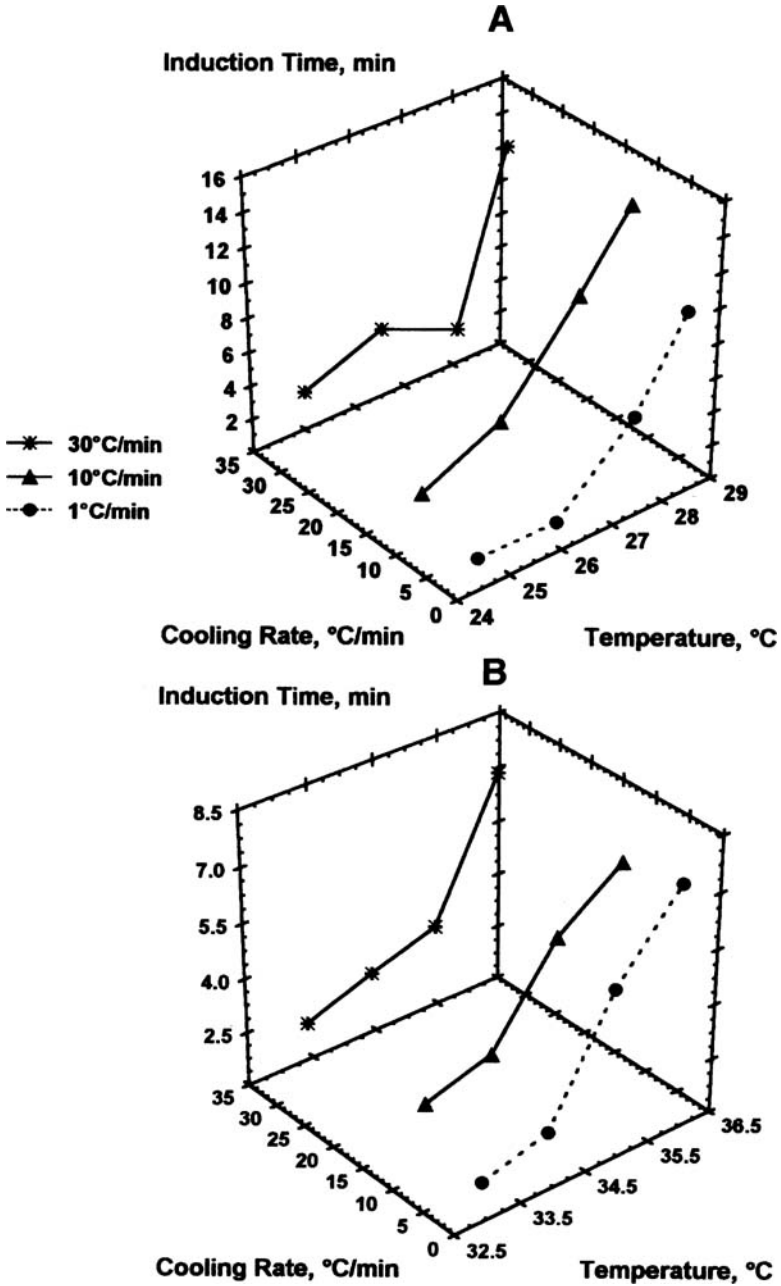
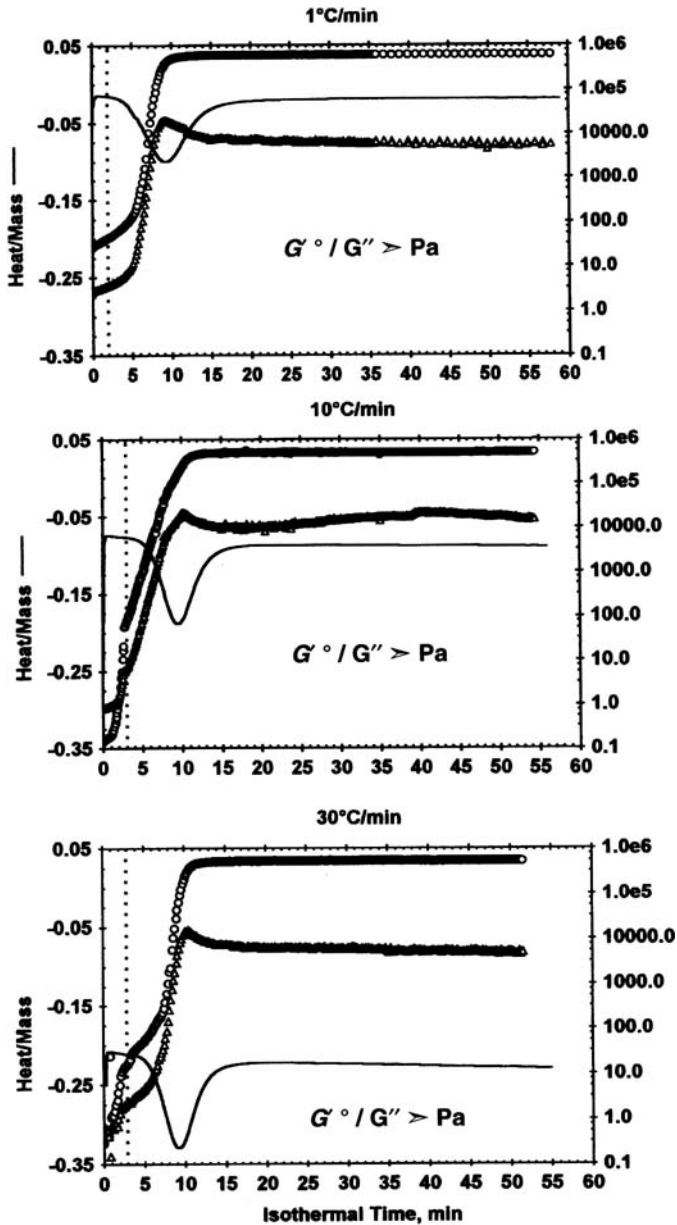
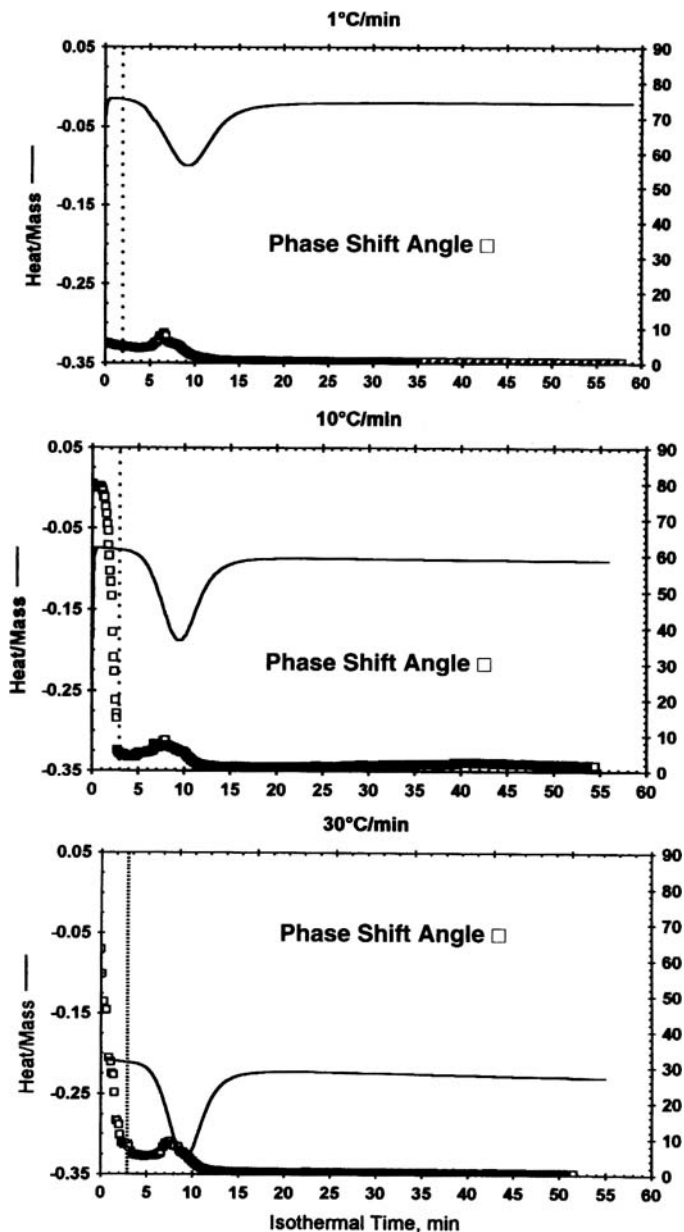


Fig. 8. Effect of cooling rate on the  $t_i$  for the 26% (A) and 80% (B) blends of palm stearin in sesame oil.



**Fig. 9.** Rheograms ( $G'$  and  $G''$ ) and DSC thermograms for an 80% palm stearin blend in sesame oil. The graphs show the 1, 10, and 30°C/min cooling rates used. Crystallization temperature 33°C. The dotted line is the induction time of crystallization by DSC.



**Fig. 10.** Rheograms (phase shift angle,  $\delta$ ) and DSC thermograms for an 80% palm stearin blend in sesame oil. The graphs show the 1, 10, and 30°C/min cooling rates used. Crystallization temperature 33°C. The dotted line is the induction time of crystallization by DSC.

variables during crystallization of TAG and their effect on macroscopic functional properties provided by the three-dimensional fractal network (i.e., texture) have not yet been determined.

## The Avrami Model

During crystallization of most compounds, including TAG, the formation of nuclei and their growth are events that occur nearly simultaneously at different rates, since there is a continuous variation of the conditions that produce crystallization. The Avrami model takes into account the formation of nuclei and their growth. However, is important to indicate that the Avrami model does not provide information regarding the size or the polymorph state of the crystals.

The Avrami model (19,20) states that in a given system under isothermal conditions at a temperature lower than  $T_M^\circ$ , the degree of crystallinity or fractional crystallization ( $F$ ) as a function of time ( $t$ ) (Fig. 11) is described by Equation 5. Although the theory behind this model was developed for perfect crystalline bodies like most polymers, the Avrami model has been used to describe TAG crystallization in simple and complex models (5,9,13,21,22). Thus, the classical Avrami sigmoidal behavior from an  $F$  and crystallization time plot is also observed in TAG crystallization in vegetable oils. This crystallization behavior consists of an induction period for crystallization, followed by an increase of the  $F$  value associated with the acceleration in the rate of volume or mass production of crystals, and finally a metastable crystallization plateau is reached (Fig. 11).

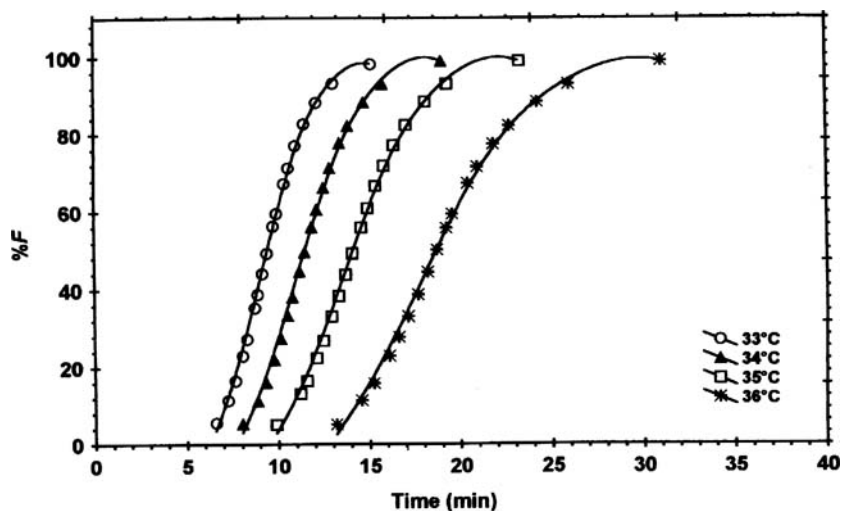


Fig. 11. Reduced crystallinity ( $F$ ) as a function of crystallization time for different temperatures. The system is an 80% palm stearin blend in sesame oil, cooling rate 30°C/min.

$$1 - F = \exp(-zt^n) \quad [5]$$

$$\text{Ln} [-\text{Ln}(1 - F)] = \text{Ln}(z) + n[\text{Ln}(t)] \quad [6]$$

In the Avrami model,  $F$  is, in fact, a reduced crystallinity since it associates the crystallinity of the system at a given time to the total crystallinity achieved under the experimental conditions. The  $F$  value is measured with a property proportional to the change in solid phase or crystallinity developed in the system as a function of time (i.e., light transmitted or reflected, X-ray diffraction, DSC measurements, solid-fat index by nuclear magnetic resonance). In general,  $F$  is calculated as  $F = (X_t - X_0)/(X_\infty - X_0)$  where  $X_0$  is the concentration of solid (i.e., TAG in the solid phase) at time zero,  $X_t$  is the concentration of solid at time  $t$ , and  $X_\infty$  is the maximum concentration of solid obtained in the crystallization process. When DSC is used, the  $F$  values are calculated from the crystallization exotherm as  $F = \Delta H_t / \Delta H_{tot}$ , where  $\Delta H_t$  is the area under the DSC exothermal crystallization curve from  $t = t_i$  to  $t = t$ , and  $\Delta H_{tot}$  is the total area under the crystallization curve (Fig. 3).

According to the theory behind the Avrami model, the  $n$  value describes the crystal growth mechanism process; a crystallization process with a polyhedral crystal growth mechanism (i.e., tridimensional growth) has a value of  $n = 4$ . A value of  $n = 3$  indicates a plate-like crystal growth mechanism (i.e., bidimensional growth), and an  $n = 2$  indicates a linear crystal growth (i.e., unidimensional growth) (21). On the other hand, the value  $z$  (Eq. 5) is the complex rate constant of crystallization, which depends on  $n$  and is a function of the nucleation rate and the linear growth rate of the spherulite (Table 2) (21). This holds as long as conditions assumed by the Avrami model prevail. Such crystallization conditions are: (i) constant radial growth rate, (ii) constant density and shape of the growing nuclei, (iii) no secondary nucleation, (iv) no volume change during crystallization, and (v) free crystal growth (i.e., no impingement between growing crystals).

In Equation 5 the index of the crystallization reaction,  $n$ , and  $z$ , are calculated from its linear format (Eq. 6) as the slope and intercept at  $\text{Ln}(t) = 0$ , respectively. The  $F$  values to calculate by linear regression (Eq. 6)  $n$  and  $z$  are, most of the time, between  $F \leq 0.25$  and  $F \geq 0.75$ . These  $F$  values are considered to assure constant radial growth rate and no crystal impingement.

**TABLE 2**

The  $n$  and  $z$  Constants in Avrami's Equation<sup>a</sup>

Mechanism of crystal growth	Nucleation sporadic in time (primary nucleation)	
	$n$	$z$
Polyhedral	4	$\pi G^3(l/3)$
Plate-like	3	$\pi G^2(l/3)$
Cylindrical	2	$\pi d^2 G(l/r)$

<sup>a</sup>Adapted from Reference 22.  $n$ , index of Avrami's equation;  $z$ , rate constant in Avrami's equation;  $G$ , linear growth rate of crystal spherulite;  $l$ , sporadic nucleation rate in time;  $d$ , width of crystal fibril;  $r$ , crystal radii.

However, in TAG crystallization in vegetable oils, the experimental situation is complicated by different phenomena taking place during crystallization. Consequently, noninteger values of  $n$  are obtained. For instance, in the 26 to 80% PS blends in sesame oil used in Reference 9, the  $n$  (and  $z$ ) values calculated between  $F \geq 0.25$  and  $F \leq 0.75$  are shown in Table 1. In all cases fractional  $n$  values and  $n$  values greater than 4 were obtained. On the other hand, Equation 3 should provide values of  $z$  with a temperature dependence, which within certain temperature interval would allow the calculation of the activation energy for crystallization (e.g., through the Arrhenius Equation). However, with TAG crystallization in vegetable oils, this is not quite the case (23). Additionally, in several crystallizing systems, the resulting plots of the linear format of the Avrami equation,  $\text{Ln}[-\text{Ln}(1 - F)]$  vs.  $\text{Ln}(t)$ , supposed to provide a single slope associated with the value of  $n$ , have given inconsistent results, and most of the times two regions of different slopes are obtained. This last observation is evident in the corresponding plots  $\text{Ln}[-\text{Ln}(1 - F)]$  vs.  $\text{Ln}(t)$  for 26 and 80% (wt/vol) PS/sesame oil blends (Fig. 12). The plot, that was supposed to have provided a single slope associated to the value of  $n$ , resulted in two regions of different slopes (Fig.12). The  $F$  value that limits these two regions varied as a function of the crystallization temperature. Evidently the  $n$  value of the first region is always greater than the one obtained from the second region. Additionally, the fractional values in the Avrami exponents suggest the presence of secondary crystallization. In polymer crystallization, a combination of heterogeneous and homogeneous nucleation along with sec-

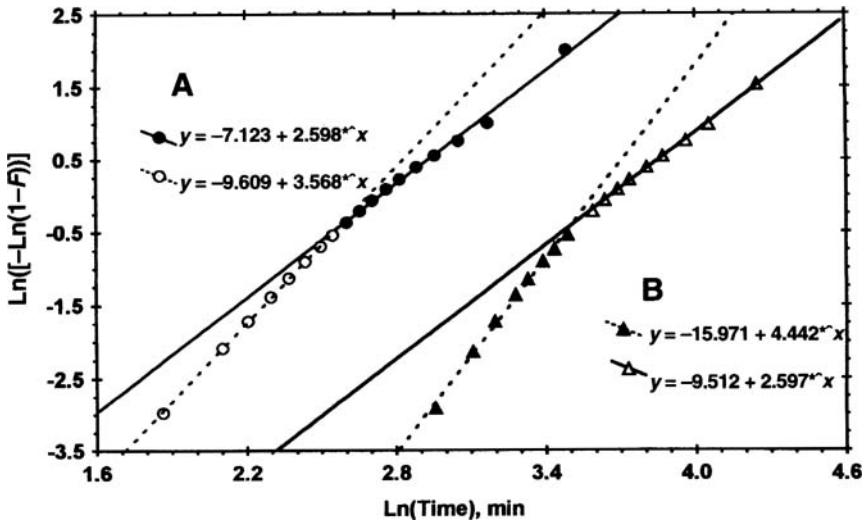


Fig. 12. Linear format of the Avrami equation for crystallization of a 26% blend of palm stearin in sesame oil at 24.5°C (A) and 28.5°C (B). Cooling rate used 1°C/min.  $T_M^\circ = 62.8^\circ\text{C}$ .

ondary crystallization has been associated with this two-region crystallization behavior with different Avrami exponents. This might also be the case with vegetable-oil crystallization.

From dynamic rheological measurements, it has been concluded that at the low cooling rate, such as the one used in the experiments of Figure 12 (1°C/min) (9), TAG molecules have enough time to achieve local-order in the liquid state (i.e., lamellar structures) while decreasing the temperature toward the isothermal crystallization temperature (Figs. 7–9). Once the isothermal conditions have been achieved, TAG lamellar structures further organize and achieve a critical size to develop stable nuclei (i.e., nucleation) (Figs. 7–9). Thus, at low cooling rates, the first region of the Avrami crystallization curve shows the TAG nucleation achieved through molecular organization during the cooling period. Then, the local-order of TAG molecules must be primarily responsible for nuclei formation in the first region of the Avrami curve during vegetable-oil crystallization. However, its effect on TAG crystallization must be reduced as a function of the increase in the cooling rate used to achieve isothermal conditions (i.e., equilibrium conditions). Nevertheless, an additional event taking place in this first region of the Avrami plot is heterogeneous nucleation, an occurrence independent of the cooling rate used.

Within this framework, additional crystallization experiments were carried out with 26 and 80% PS blends in sesame oil using several cooling rates. The results are shown in Figure 13 following the linear format of the Avrami equation (Eq. 6). As before, the slope of the first region is higher than the one in the second region. However, for the same crystallization temperature, the  $n$  value for the second region is independent of the cooling rate used. This suggests that the same mechanism for crystal growth is followed independent of the cooling rate used. In contrast to the first region, in the second region of the Avrami plot, local order of the TAG does not produce additional nucleation since thermodynamic conditions predominate (i.e., isothermal conditions). Thus, as sporadic nucleation gradually begins, the slope of the Avrami plot is affected. Although in this second region the  $n$  values obtained were within the interval accepted by the Avrami theory (i.e., 2.5 to 4.0), their fractional character indicated the occurrence of secondary crystallization. In fact, this has been shown in blends of PS and sesame oil through polarized light microscopy (data not shown). Again, the experimental conditions involved a cooling rate of 1°C/min. The birefringence of TAG crystal is not developed constantly with time. Once the initial solid TAG lamellas have been obtained through the development of local order, subsequent crystallization or crystal growth is achieved by infilling of additional TAG getting the same orientation as the primary lamella. As a result, TAG crystal birefringence increases in a heterogenous way with crystallization time, showing that secondary lamella in these regions has the same orientation as the primary solid structure (i.e., secondary crystallization).

In conclusion, TAG crystallization from the melt involves nucleation mainly by two mechanisms (i.e., local-order of TAG in the liquid state and sporadic nucle-

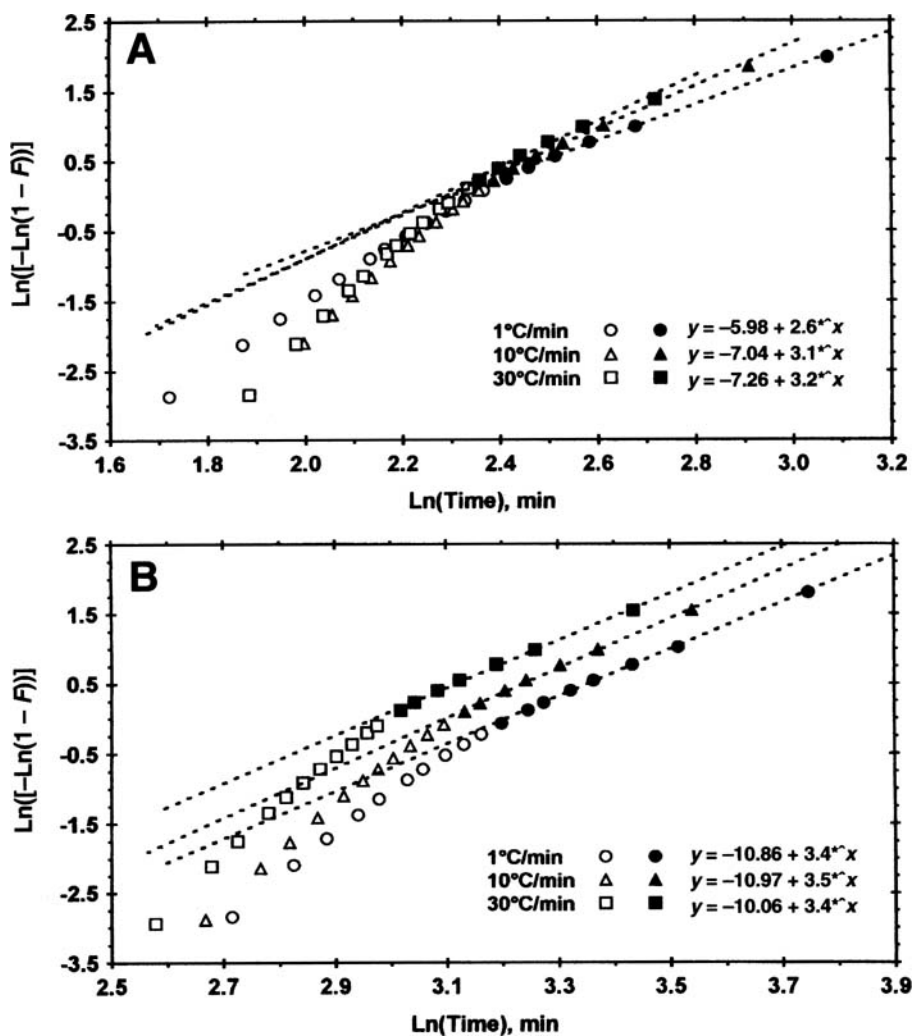


Fig. 13. Linear format of the Avrami equation for crystallization of an 80% blend of palm stearin in sesame oil at 33°C (A) and 36°C (B) at several cooling rates.  $T_M^\circ = 62.8^\circ\text{C}$ .

ation). Additionally, during crystal growth the involvement of secondary crystallization is definite. However, all these processes are engaged during bulk crystallization of TAG in events occurring not sequentially but in parallel. The Avrami model does not consider all these phenomena. Therefore, more complex models have been developed to relax the simplified assumptions considered by the Avrami model. These models, mainly used to describe polymer crystallization, take into

account a variable growth rate, a mixed model of nucleation, a change in the density of the growing nuclei, the time dependence of the nucleation rate, and secondary crystallization (e.g., intra- and inter-secondary crystallization) (24). There are no crystallization studies with TAG or vegetable oils using such models. However, considering the results obtained with polymers (24), it is quite probable that different models have to be employed to describe the crystallization mechanism present among the different families of TAG that constitute the vegetable oil.

### ***The Fractal Organization of TAG During Crystallization***

Our research is now focused in establishing the sequence of factors that determine the macroscopic properties, such as the texture, in vegetable-oil crystallization. Within this framework, the fractal organization of the crystal network and its association with the crystal growth mechanism (i.e., Avrami index) are now investigated. The context of this investigation is based on the elastic properties of fat-crystal networks and their dependence on the fractal nature of the microstructure. Thus, following the analysis of Narine and Marangoni (2) for the elastic shear modulus,  $G'$ ,

$$G' \propto \varphi^m \quad [7]$$

which can be written as (25)

$$G' = \gamma \varphi^m \quad [8]$$

$$\text{Ln}(G') = \text{Ln}(\gamma) + m[\text{Ln}(\varphi)] \quad [9]$$

where  $\varphi$  is the volume fraction of solid fat,  $m$  depends on the fractal dimension, and  $\gamma$  is a constant independent of the volume fraction but dependent on the size of the primary particles and on the interactions between them (i.e., polymorphic nature of the fat) (2). Then assuming that  $F \approx \varphi$ , there is room for discussion regarding the behavior observed by  $G'$  and  $F$  when both are measured as a function of time during the isothermal crystallization process (Fig. 14). In the graphs shown in Figure 14, the  $G'$  values were obtained through dynamic rheological measurements with parallel plates geometry (50 mm in diameter and a gap of 1 mm) and applying variable strain levels within the LVR of the blend. The  $F$  values were calculated by DSC measurements. Thus, the different slopes observed during the process of crystallization are likely associated with stages of the fractal organization achieved by TAG as a function of time. This type of plot might be helpful to evaluate the effect of crystallizing conditions on the fractal dimension of TAG in vegetable oils. In the same way, since  $\gamma$  is a constant dependent on the size of the primary particles and on the interactions between them (i.e., polymorph nature of the TAG crystals), these plots are potential tools to establish the relationship

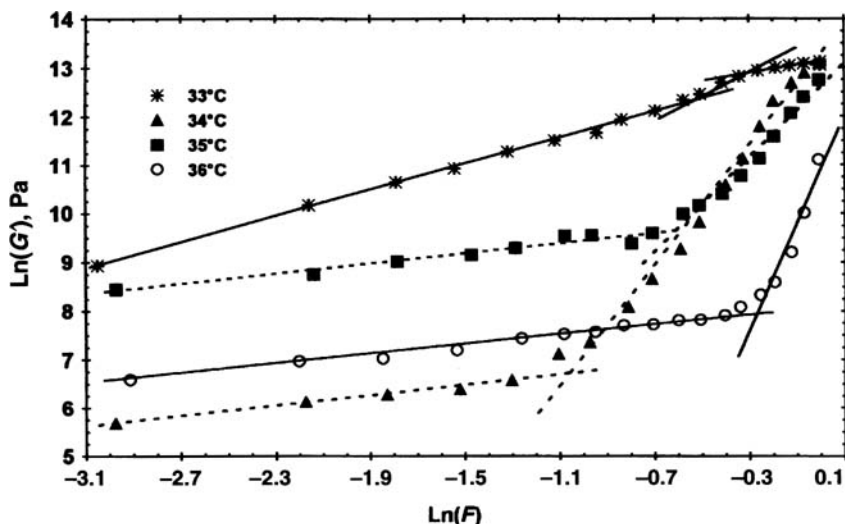


Fig. 14. Relationship between  $G'$  and  $F$  in an 80% blend of palm stearin in sesame oil crystallized at several isothermal temperatures using a cooling rate of  $10^{\circ}\text{C}/\text{min}$ .  $T_M^{\circ} = 62.8^{\circ}\text{C}$ .

among the Avrami index, the polymorph state, and the texture of the system as affected by the crystallizing conditions [i.e., cooling rate (Fig. 15)].

## Summary

The Fisher-Turnbull and the Avrami models have been used to describe TAG crystallization in vegetable oils. However, before applying such models to obtain useful parameters, particular considerations have to be taken. For instance, effective supercooling must be established to calculate with the Fisher-Turnbull equation reliable  $\Delta G_c$  values. Additionally, TAG crystallization from the melt involves nucleation by two mechanisms: local-order of TAG in the liquid state and sporadic nucleation. The results discussed here show that involvement of each mechanism on TAG nucleation is affected by viscosity and cooling rate. The interaction among supercooling, cooling rate, and viscosity during crystallization of TAG and their effect on macroscopic functional properties (i.e., texture) in vegetable oils are areas scarcely investigated. Plots establishing the relationship between  $G'$  and  $F$  (i.e., elastic shear modulus vs. reduced crystallinity in the Avrami equation) are potential tools to study the effect of crystallizing conditions on TAG fractal dimensions in vegetable oils, and subsequently, on texture.

## Acknowledgment

The support from CONACYT through grants and scholarships is greatly appreciated.

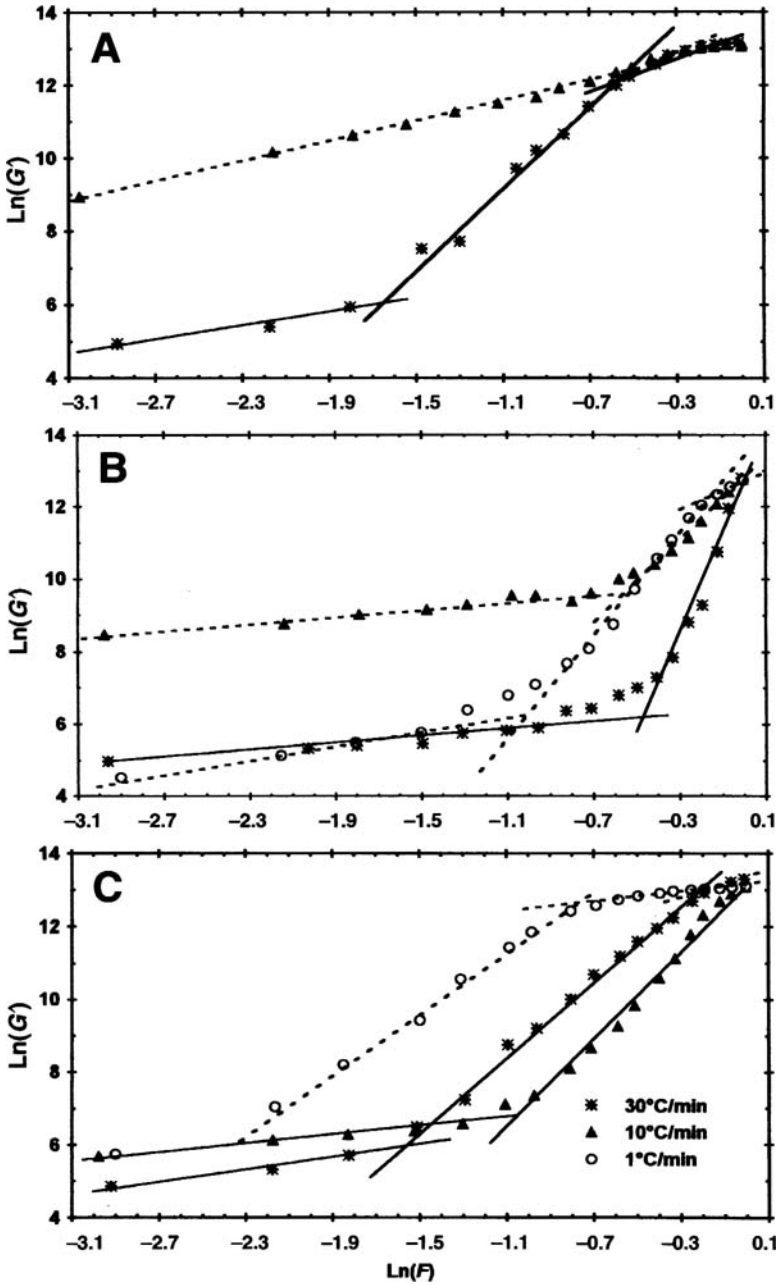


Fig. 15. Relationship between  $G$  and  $F$  in an 80% blend of palm stearin in sesame oil crystallized at 33, 34, and 35°C using several cooling rates.  $T_M^\circ = 62.8^\circ\text{C}$ .

## References

1. Vreeker, R., L.L. Hoekstra, D.C. den Boer, and W.G.M. Agterof, The Fractal Nature of Fat Crystal Networks, in *Food Colloids and Polymers: Stability and Mechanical Properties*, edited by E. Dickinson and P. Walstra, The Royal Society of Chemistry, Cambridge, 1993, pp. 16–30.
2. Narine, S.S., and A. Marangoni, Fractal Nature of Fat Crystal Networks, *Phys. Rev. E*. 59: 1908–1920 (1999).
3. Larsson, K., *Lipids—Molecular Organization, Physical Functions and Technical Applications*, The Oily Press Ltd., West Ferry, Dundee, 1994, pp. 7–45.
4. Larsson, K., Tailoring Lipid Functionality in Foods, *Trends Food Sci. Technol.* 5: 311–315 (1994).
5. Dibildox-Alvarado, E., and J.F. Toro-Vazquez, Isothermal Crystallization of Tripalmitin in Sesame Oil, *J. Am. Oil Chem. Soc.* 74: 69–76 (1997).
6. Toro-Vazquez, J.F., and A. Gallegos-Infante, Viscosity and Its Relationship to Crystallization in a Binary System of Saturated Triacylglycerides and Sesame Seed Oil, *Ibid.* 73: 1237–1246 (1996).
7. Toro-Vazquez, J.F., and R. Infante-Guerrero, Regression Models That Describe Oil Absolute Viscosity, *Ibid.* 70: 1115–1119 (1993).
8. Hoffman, J.D., and J.J. Weeks, Melting Process and the Equilibrium Melting Temperature of Polychlorotrifluoroethylene, *J. Res. Nat. Bur. Std.* 55: 13–28 (1962).
9. Toro-Vazquez, J.F., M. Briceño-Montelongo, E. Dibildox-Alvarado, M.A. Charó-Alonso, and J. Reyes-Hernández, Crystallization Kinetics of Palm Stearin in Blends with Sesame Seed Oil, *J. Am. Oil Chem. Soc.* 77: 297–310 (2000).
10. Mersmann, A., *Crystallization Technology Handbook*, Marcel Dekker, Inc., New York, 1995, pp. 1–78.
11. Boistelle, R., Fundamentals of Nucleation and Crystal Growth, in *Fundamentals of Nucleation and Crystal Growth*, edited by N. Garti and K. Sato, Marcel Dekker, Inc., New York, 1988, Vol. 31, pp. 189–226.
12. Wriath, A.J., R.W. Hartel, S.S. Narine, and A.G. Marangoni, The Effect of Minor Components on Milk Fat Crystallization, *J. Am. Oil Chem. Soc.* 77: 463–475 (2000).
13. Herrera, M.L., C. Falabella, M. Melgarejo, and M.C. Añón, Isothermal Crystallization of Hydrogenated Sunflower Oil: I-Nucleation, *Ibid.* 75: 1273–1280 (1998).
14. Haumann, F.B., Tools: Hydrogenation, Interesterification, *INFORM* 5: 668–678 (1994).
15. Hamm, W., Trends in Edible Oil Fractionation, *Trends Food Sci. Technol.* 6: 121–126 (1995).
16. Ng, W.L., A Study of the Kinetics of Nucleation in a Palm Oil Melt, *J. Am. Oil Chem. Soc.* 67: 879–882 (1990).
17. Dibildox-Alvarado, E., and J.F. Toro-Vazquez, Evaluation of Tripalmitin Crystallization in Sesame Oil Through a Modified Avrami Equation, *Ibid.* 75: 73–76 (1998).
18. deMan, J.M., and L. deMan, Palm Oil as a Component for High-Quality Margarine and Shortening Formulations, *Mal. Oil Sci. Tech.* 4: 56–60 (1995).
19. Avrami, M., Kinetics of Phase Change. I. General Theory, *J. Chem. Phys.* 7: 1103–1112 (1939).
20. Avrami, M., Kinetics of Phase Change. II. Transformation–Time Relations for Random Distribution of Nuclei, *Ibid.* 8: 212–224 (1940).

21. Kawamura, K., The DSC Thermal Analysis of Crystallization Behavior in Palm Oil, *J. Am. Oil Chem. Soc.* 56: 753–758 (1979).
22. Metin, S., and R.W. Hartel, Thermal Analysis of Isothermal Crystallization Kinetics in Blends of Cocoa Butter with Milk Fat or Milk Fat Fractions, *Ibid.* 75: 1617–1624 (1990).
23. Toro-Vazquez, J.F., and E. Dibildox-Alvarado, Parameters That Determine Tripalmitin Crystallization in Sesame Oil, *J. Food Lipids* 4: 269–282 (1997).
24. Ravindranath, K., and J.P. Jog, Polymer Crystallization Kinetics: Poly(ethylene terephthalate) and Poly(phenylene sulfide), *J. Appl. Pol. Sci.* 49: 1395–1403 (1993).
25. Bremer, L.G.B., T. van Vliet, and P. Walstra, Theoretical and Experimental Study of the Fractal Nature of the Structure of Casein Gels, *J. Chem. Soc., Faraday Trans.* 85: 3359–3372 (1989).

## Chapter 6

# Differential Scanning Calorimetry as a Means of Predicting Chocolate Fat-Blooming

Imogen Foubert\*, Inge Van Cauteren, Koen Dewettinck, and André Huyghebaert

Ghent University, Faculty of Agricultural and Applied Biological Sciences, Department of Food Technology and Nutrition, Coupure links 653, B-9000 Gent, Belgium

## Introduction

Fat-bloom, which manifests itself as a white film and general dulling of the characteristic surface gloss, is a major concern to the chocolate industry because it compromises both visual and textural quality (1). The mechanism of fat-bloom formation has been studied intensively. It is rather generally accepted that fat bloom occurs when the chocolate is not properly tempered. In this case, it most probably is the polymorphic transformation from unstable to more stable polymorphic forms during storage that leads to visual fat-bloom formation (2). However, also properly tempered chocolate can develop fat-bloom, and over the years two main mechanisms have been suggested. According to some authors (see for example Refs. 3 and 4), fat-bloom formation can be attributed to a recrystallization from form V to VI. Others (see for example Refs. 5 and 6) suggest that bloom is due to a phase separation of the triglycerides within the crystalline structure of the cocoa butter. Adenier *et al.* (7) suggests that the low-melting liquid-like triglycerides in cocoa butter dissolve a portion of the high-melting triglycerides and carry them to the surface, where they recrystallize in a purified form. Recently Bricknell and Hartel (1) hypothesized a sequence of events for the development of visual bloom in properly tempered chocolates that is also based on this phase-separation theory.

The main aim of this research was to investigate whether differential scanning calorimetry (DSC) measurements performed shortly after production allow the prediction of fat-bloom development at later storage times. Such a prediction tool would have the advantage that the chocolate manufacturer can quickly adjust his production process and that chocolate with a high risk of fat-bloom development can be kept from the market. Besides this, the influence of tempering and cooling time on the visual fat-bloom development and the melting profile of the chocolate was studied to try to better understand the mechanism of fat-bloom development.

## Materials and Methods

Two experimental set-ups with the same general outline were designed. Plain chocolate was produced, but variations were introduced into the conventional

chocolate-making process. In such a conventional process, properly tempered chocolate is produced by cooling the completely molten chocolate of *ca.* 50 to *ca.* 29°C leading to crystallization of the cocoa butter. Then the temperature is increased again to *ca.* 31°C. During this heating stage, the unstable crystals with a melting point lower than 31°C will melt. Thus, after the tempering process (nearly) only crystals in polymorphic form V exist in the chocolate mass. In the conventional process, cooling is performed at 12°C during 20 min.

In a first set-up, properly tempered chocolate was compared with undertempered chocolate (i.e., the temperature of the heating stage was 2°C higher) and with severely undertempered chocolate (i.e., the temperature of the heating stage was 4°C higher). After tempering, the chocolate was cooled at 12°C during 20 min. In a second set-up, properly tempered, slightly undertempered (i.e., the temperature of the heating stage was 1°C higher) and slightly overtempered (i.e., the temperature of the heating stage was 1°C lower) chocolate was cooled at 12°C during 4, 12, and 20 min. After production, the chocolate was stored at room temperature (20°C). It should be stressed that no temperature cycling was performed to induce fat-bloom.

A professional panel assessed the visual fat-bloom development after certain storage times (2, 4, 5, 7, and 9 wk after production in the first set-up and 1 wk, 1 and 3 mon after production in the second set-up). The meaning of the different values for bloom intensity is as follows: 0: the product shows no difference compared to the original product; 1-2: the product loses its gloss, but does not show any white spots; 3: the product starts to show white spots or a gray film; 4: the product clearly shows white spots or a gray film; and 5: the product has turned completely white.

At the following storage times, the solid-fat content and the melting profile were determined: 0, 1, 4, 24, and 48 h, 1 wk, 1 and 3 mon after production in the first set-up and 0, 1, 4, 24, and 48 h and 1 wk after production in the second set-up. The solid-fat content was determined by means of nuclear magnetic resonance (NMR) measurements. The melting profiles were determined using DSC. The samples (sample weight between 2 and 4 mg) were put in the DSC at room temperature, and the following temperature program was used: (i) cooling at a rate of 8°C/min to -20°C; (ii) keeping isothermal for 5 min; and (iii) heating at a rate of 5°C/min to 60°C. From the melting profiles, several parameters were extracted. Apart from determining the peak maximum and the onset temperature, the total area was divided into three by a perpendicular drop at 23.5 and 28.5°C. As such an indication of the heat necessary to melt the unstable,  $\beta'$  and  $\beta$  crystals could be obtained.

## Discussion

*Visual Fat-Bloom Assessment.* Undertempering and shorter cooling lead to a faster and more pronounced fat-bloom development. The slightly overtempered chocolate (second set-up) only shows a loss of gloss when cooled during 20 min.

*Melting Profile (First Set-Up).* Only the peak maximum will be discussed since the other parameters show the same trends. Figure 1 shows the peak maximum as a function of the logarithm of time for the three different tempering conditions. The straight lines represent the best-fit curve (the value 0 h after production was not taken into account to calculate this best fit). The peak maximum shortly after production (up to 48 h after production) is lower as the chocolate is more undertempered. An exception is the peak maximum of the severely undertempered chocolate 0 h after production, which is exceptionally high. The increase of the peak maximum over time is faster as the chocolate is more undertempered, which results in a higher peak maximum for the severely undertempered chocolate at the end of the storage period (from 1 mon after production onward).

A hypothesis explaining these results was formulated. The amount of nuclei after the tempering stage is smaller as the chocolate is more undertempered. This results in a higher amount of liquid chocolate after the cooling stage. Thus, the severely undertempered chocolate contains a few stable nuclei (with a high melting point) and a lot of liquid chocolate (69.7% as measured by NMR) 0 h after production. This might explain the high peak maximum at this moment. During the storage at room temperature, the liquid chocolate will crystallize in unstable forms, since there are not enough stable nuclei to direct the crystallization. This results in a lower peak maximum 1 h after production. During further storage, the unstable forms will transform to stable polymorphic forms, explaining the increase of the peak maximum from 1 h after production onward. In the undertempered chocolates, the main part of the crystallization occurs at room temperature, possibly leading to a coarser structure compared to that of chocolate crystallized at lower temperatures. This coarser structure, possibly together with cracks caused by the transformation from unstable to stable polymorphic forms, might lead to an enhanced

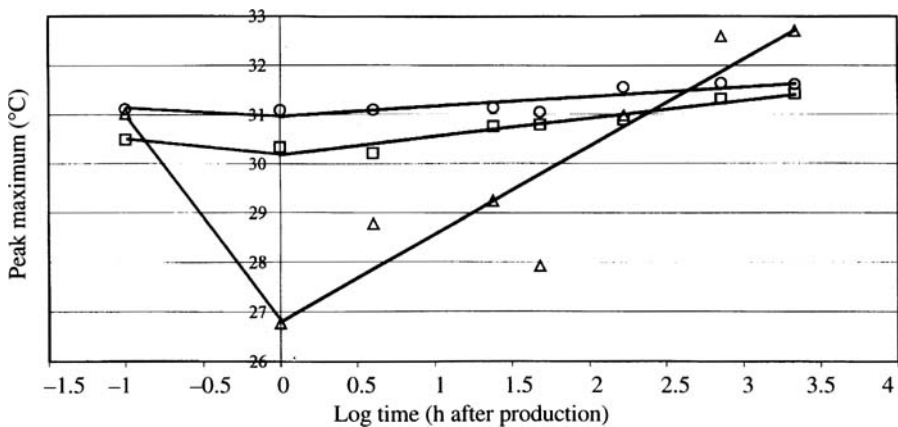


**Fig. 1.** Peak maximum as a function of time for three different tempering conditions (first set up). ○: reference; □: undertempered; △: severely undertempered.

migration of high-melting fractions dissolved in a liquid phase of low-melting triglycerides (1). These high-melting fractions will recrystallize at the surface (1), and this might explain the higher peak maximum at the end of the storage period. An enhanced transformation to polymorphic form VI caused by the coarser structure and/or the cracks is another possibility. A combination of both phenomena is a third possible hypothesis.

*Melting Profile (Second Set-Up).* In the second set-up, tempering has no significant ( $P = 0.05$ ) effect on the peak maximum. Therefore Figure 2 only represents the effect of cooling time. The straight lines represent the best-fit curve (the value 0 h after production was not taken into account to calculate this best fit). It can be noticed that except for the value 0 h after production the chocolate cooled for 4 min has a higher peak maximum than the chocolate cooled for 12 or 20 min. The difference between the chocolates is smaller than in the first set-up, but this could be expected since the visual fat-bloom is also less pronounced in the second set-up (a maximum visual fat-bloom of 2 in the second set-up compared to 5 in the first set-up). There is no significant ( $P = 0.05$ ) difference between 12 and 20 min cooling.

A hypothesis explaining these results was formulated. The chocolate which was only cooled for 4 min has more liquid chocolate left after the cooling phase, as confirmed by NMR measurements. Thus, in this chocolate, more crystallization takes place during the storage at room temperature. As already described in the discussion of the first set-up, this might lead to a coarser structure of the final chocolate, which in turn might lead to an enhanced migration and/or transformation to polymorphic form VI. Each phenomenon or the combination of both might result in an increased peak maximum from 1 h after production onward.

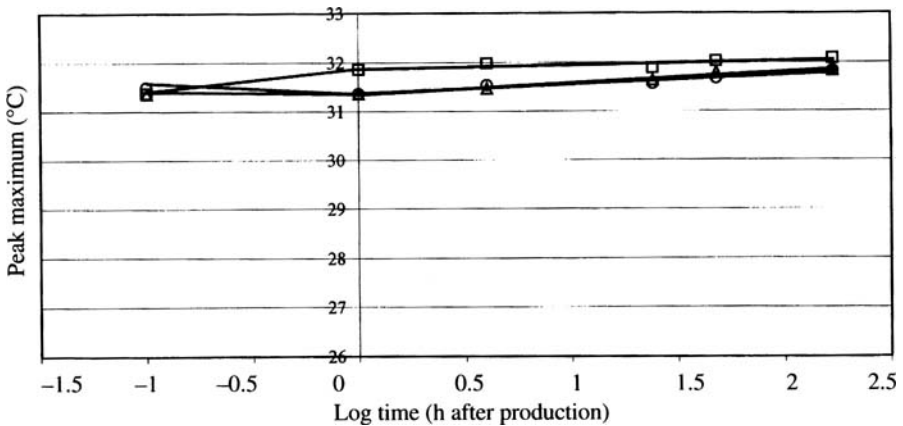


**Fig. 2.** Peak maximum as a function of time for three different coding times (second set up). □: 4 min cooling at 12°C (all tempering conditions); ○: 12 min cooling at 12°C (all tempering conditions); △: 20 min cooling at 12°C (all tempering conditions).

From both experimental set-ups, it could be concluded that chocolates with a different fat-bloom development also show differences in their melting profile. Since distinguishing all the degrees of fat-bloom development on the basis of one parameter at one storage time would be difficult, it was decided to use discriminant analysis as a statistical technique. This allows the simultaneous use of several parameters.

*Introduction to Discriminant Analysis (8).* The problem that is addressed with discriminant analysis is how well it is possible to separate two or more groups of individuals, given measurements for these individuals on several parameters. Discriminant analysis generates a set of discriminant functions based on linear combinations of the parameters. The distance of the individuals to the group means can be calculated based on these discriminant functions, and each individual is then allocated to the group it is closest to. This may or may not be the group the individual actually belongs to. The percentage of correct allocations is an indication of how well groups can be separated using the available parameters. However, a moment's reflection will suggest that allocating the individuals using this procedure must tend to have a bias in favor of allocating individuals to the group to which they belong. After all, the group means are determined from the observations in that group, and it is not surprising to find that an observation is closest to the group mean which it helped to determine. To overcome this bias a "jackknife classification" can be performed. This involves allocating each individual to its closest group without using that individual to help determine the group means.

*Results of the Discriminant Analysis.* For each of the two set-ups, the following parameters were used: peak maximum, onset temperature, heat necessary to melt the unstable,  $\beta'$  and  $\beta$  crystals (absolute and relative values). This leads to eight parameters per storage time, which, multiplied by four storage times (0, 1, 4, and 24 h after production), leads to 32 parameters per individual. However, some parameters failed the tolerance test. This means that for that parameter the variance within a group was too big compared to the variance between the groups. These parameters were left out because they would not increase the prediction quality.

In the first set-up, three groups of chocolates were taken into account: the chocolates that did not develop any fat-bloom, chocolates that attained a bloom intensity of 3 after 2 wk and 5 after 5 wk, and chocolates that already attained a bloom intensity of 5 after 2 wk. All the variance between the groups can be explained by two discriminant functions. Using the regular classification method, 100% of the individuals is correctly allocated; using the "jackknife classification," this value decreases to 41.7%. A better representation of the separation quality is presented in Figure 3. This graph displays the value of the second discriminant function vs. that of the first discriminant function for each of the individuals. It can be derived from Figure 3 that a very good separation between the groups is possible.

In the second set-up, the visual fat-bloom after 1 wk, 1 and 3 mon is taken into account to create groups of chocolates, irrespective of the tempering and cooling

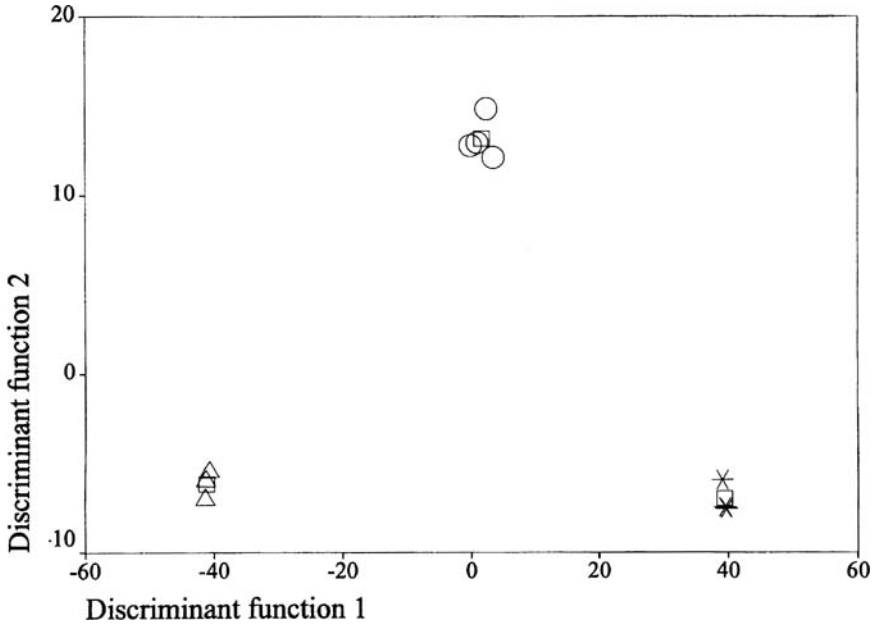
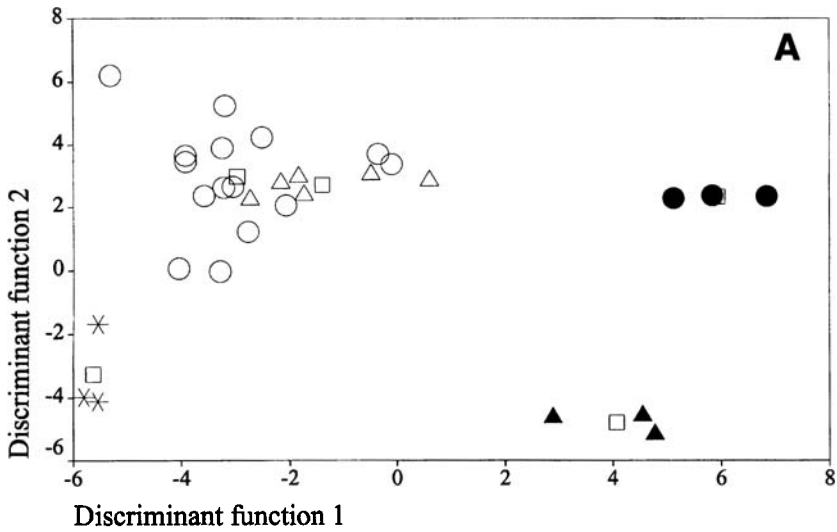


Fig. 3. \*: no fat-bloom development; Δ: bloom intensity 3 after 2 wk and 5 after 5 wk; □: group centroid; ○: bloom intensity 5 after 2 wk.

conditions. This leads to five groups: no fat-bloom development, bloom intensity 0 after 1 wk and 1 after 1 and 3 mon, bloom intensity 1 after 1 wk, 1 and 3 mon bloom intensity 1 after 1 wk and 1 mon and 0 after 3 mon and intensity 1 after 1 wk and 1 mon and 0 after 3 mon and bloom intensity 1 after 1 wk and 2 after 1 and 3 mon. In this case, four discriminant functions are necessary to explain all the variance. Using the regular classification method, 98.7% of the individuals is correctly allocated; using the “jackknife classification,” this value decreases to 79.3%. Again, a graph (Fig. 4) gives a better idea of the separation quality. Figure 4A displays the value of the first two discriminant functions for each of the individuals. It can be seen that three groups can be separated well from the rest of the individuals. However, no good separation is possible between the group with no fat-bloom development, and the group attaining a bloom intensity of 1 after 1 wk, 1 and 3 mon. When the value of the third discriminant function is plotted against that of the first (Fig. 4B), a much better separation between these two groups is possible. A fairly good separation between the five groups is thus possible when more than two discriminant functions are taken into account.

### Summary

From this research, it can be concluded that varying the tempering conditions and/or the cooling time at 12°C influences both the visual fat-bloom development



**Fig. 4A.** ○: no fat-bloom development; ●: bloom intensity 0 after 1 wk and 1 after 1 and 3 mon; △: bloom intensity 1 after 1 wk, 1 and 3 mon; \*: bloom intensity 1 after 1 wk and 1 mon and 2 after 3 mon; ▲: bloom intensity 1 after 1 wk and 2 after 1 and 3 mon; □: group centroid.

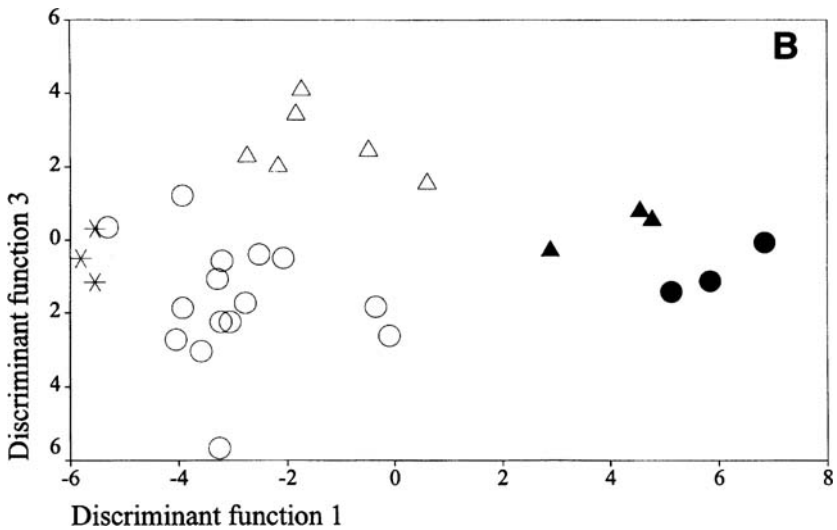


**Fig. 4B.** ○: no fat-bloom development; ●: bloom intensity 0 after 1 wk and 1 after 1 and 3 mon; △: bloom intensity 1 after 1 wk, 1 and 3 mon; \*: bloom intensity 1 after 1 wk and 1 mon and 2 after 3 mon; ▲: bloom intensity 1 after 1 wk and 2 after 1 and 3 mon.

and the melting profile as assessed by means of DSC. Also, this research pointed out that the combination of DSC as an analytical technique and discriminant analysis as a statistical technique shows possibilities as a prediction tool for fat-bloom development.

### Acknowledgments

Imogen Foubert benefits from a scholarship from the Flemish Community (aspirant FWO-Vlaanderen). The authors would like to thank Barry Callebaut Belgium (especially Mr. De Clercq and Mr. De Schepper) for the excellent cooperation in providing the samples and discussing the results. They would also like to thank dr. ir. Stephan Dierckx and ir. Bert Vanhoutte for the help with the DSC.

### References

1. Bricknell, J., and R.W. Hartel, Relation of Fat Bloom in Chocolate to Polymorphic Transition of Cocoa Butter, *J. Am. Oil Chem. Soc.* 75: 1609–1615 (1998).
2. Seguire, E.S., Tempering—The Inside Story, *Manufact. Confect.* 71: 117–125 (1991).
3. Wille, R.L., and E.S. Lutton, Polymorphism of Cocoa Butter, *J. Am. Oil Chem. Soc.* 43: 491–496 (1966).
4. Cebula, D.J., and G. Ziegleder, Studies of Bloom Formation Using X-Ray Diffraction from Chocolates After Long-Term Storage, *Fat Sci. Technol.* 95: 340–343 (1993).
5. Becker, K., Die Ursachen der Fettreifbildung bei Schokoladen: Pralinen, *Rev. Int. Choc.* 8: 246–249 (1958).
6. Schlichter-Aronhime, J., and N. Garti, Solidification and Polymorphism in Cocoa Butter and the Blooming Problem, in *Crystallization and Polymorphism of Fats and Fatty Acids*, edited by N. Garti and K. Sato, Marcel Dekker Inc., New York, 1988, pp. 363–393.
7. Adenier, H., H. Chaveron, and M. Ollivon, Mechanisms of Fat Bloom Development in Chocolate, in *Shelf Life Studies of Foods and Beverages*, edited by G. Charalambous, Elsevier Science, London, 1993, pp. 353–389.
8. Manly, B.F.J., *Multivariate Statistical Methods: A Primer*, 2nd Edn., Chapman & Hall, London, 1994, pp.107–126.

## Chapter 7

# Effect of Sucrose Polyesters and Sucrose Polyester–Lecithins on Crystallization Rate of Vegetable Ghee

Mohammad Ibrahim Nasir

Research Department, Jahan Vegetable Oil Company, Tehran - 19697, Iran

## Introduction

Vegetable ghee or vanaspati is mostly vegetable fat in composition with a melting point of 34–40°C. Vanaspati is a shortening and can be considered as a substitute for ghee as margarine is for butter. Ghee is butter fat obtained from the milk of cows or buffalo by boiling and draining off the aqueous phase (1,2). It is added to tin cans in its liquid state and allowed to crystallize very slowly under well-controlled conditions. In the Jahan plant, it is kept in cold storage at 12–16°C for 20 h in winter and 48 h in summer. Large crystals and grainy texture develop. Some countries such as India, Pakistan, and those in central Asia prefer a coarse appearance.

It is desirable that the vanaspati have a homogeneous consistency with no phase separation. It should be stored undisturbed at the required temperature until a stable crystal form is reached.

Constant-temperature rooms for tempering vegetable ghee are expensive to operate and create logistic problems in maintaining and rotating inventories (3). Although it cannot be eliminated, the tempering time can be reduced.

Some oil-soluble emulsifiers affect the crystallization process and development of polymorphic forms of fats (4–8). Sucrose fatty acid ester or sucrose polyesters (SPE) and lecithins are well-known food emulsifiers (9,10). The main characteristics of lecithins and SPE useful in food applications are their oil-in-water and water-in-oil emulsifying properties, that result in dispersion with condensed milk and coffee whitener, and prevention of blooming in candy products and chocolate (7,9–11). But there are very few reports about two effects of SPE on the crystallization of fats and oils, i.e., enhancement and inhibition (12,13).

The purpose of this work, therefore, was to evaluate the effect of several SPE, lecithins, and SPE–lecithin mixtures on the crystallization of fat and to determine the one that accelerated the crystallization in the vegetable-ghee processing, thus reducing the tempering time.

## Materials and Methods

**Materials.** The hydrogenated blend of soybean (90%)/cottonseed (10%) oil, and food-grade lecithin was from Jahan Vegetable Oil (Teheran). The sucrose tetrastearate (SPE) used were DK Ester F-10 (70% stearate–30% palmitate), sucrose tetrastearate was obtained from Daiichi Kogyo Seiyaku Co. (Tokyo, Japan), P-170 (80% palmitate) and S-170 (70% stearate) were from Mitsubishi-Kagaku Foods Corporation (Tokyo, Japan). All of the SPE used were hydrophilic-lipophilic balance (HLB) = 1. Acetone and ethanol used for lecithin fractionation were of analytic reagent (AR) grade from E. Merck (Darmstadt, Germany).

**Differential Scanning Calorimetry (DSC).** A Rheometric Scientific DSC-Gold (Surrey, United Kingdom), programmed with the COMPAQ Prolinea 4/255 database (COMPAQ Computer Corp., Houston, TX, USA), was used to measure isothermal crystallization curves. Samples (ranging from 7.5 to 9.7 mg) were placed in a standard aluminum sample pan. The procedure of DSC isothermal analysis followed the method of Kawamura (14) with little modification. Melting profiles of the crystallized fat were obtained by heating at a constant rate of 5°C/min, starting from about 20°C. Then the fat sample was held at 89°C for 10 min, rapidly cooled at a constant rate of 80°C/min or 100°C/min, and held finally at the programmed temperature of 17°C. Heat flow (mcal/s) was plotted as a function of time (Fig. 1) and a function of temperature (Fig. 2).

Sample preparation followed the method described by Ryoto (13). One gram SPE or dry deoiled lecithin was dissolved in 100 g of oil and heated to 60–80°C for complete dispersion of the emulsifier. Ethanol-insoluble lecithin was added at a level of 1 mg/100 g oil and any residual to the ethanol was removed by heating a water bath. Samples with 0.5 and 0.25% SPE or dry lecithin were prepared by diluting the original sample with oil. Deoiling and fractionation of lecithin were done with acetone and ethanol, respectively, as reported by Ziegelitz (15). Turbidity test was conducted on 70 mL oil in a 100-mL tube at different concentrations of DK F-10 (0.0, 0.5, and 1.0%) at several temperatures.

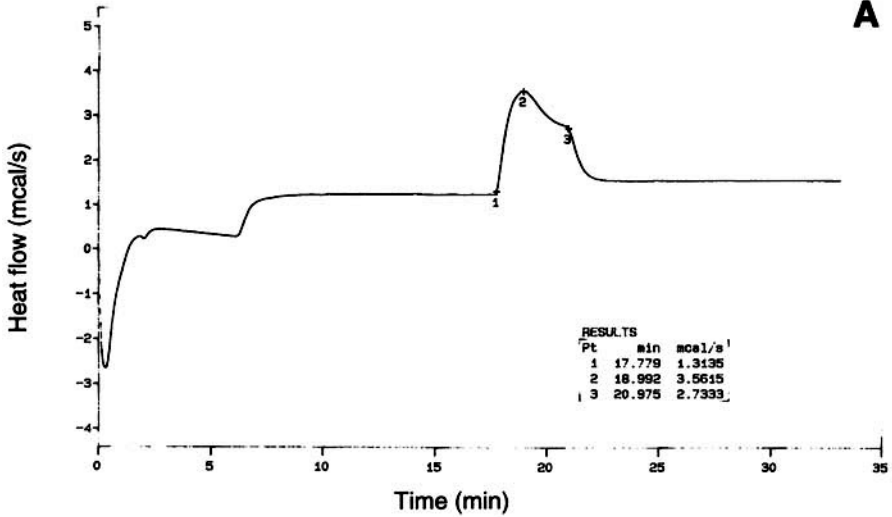
## Results and Discussion

It has been reported previously that SPE palmitate- and stearate-types have an effect on the crystallization rate of fat (6,12).

In the present study, the effect of the addition of various SPE on the DSC isothermal curves of fat is shown in Figure 1. The rapid cooling of the melted fat to the programmed temperature (17°C) gave two exothermic peaks (three peaks in the case of P-170 sample) due to the heat of crystallization.

The interval between the moment crystallization temperature is reached (point 1 diagrams) and the appearance of the second exothermic peak (point 3) is termed  $T_c$  ( $T_c$  = point 3–point 1), and is a measurement of the crystallization rate.

## Tarbait Modares



## Tarbait Modares

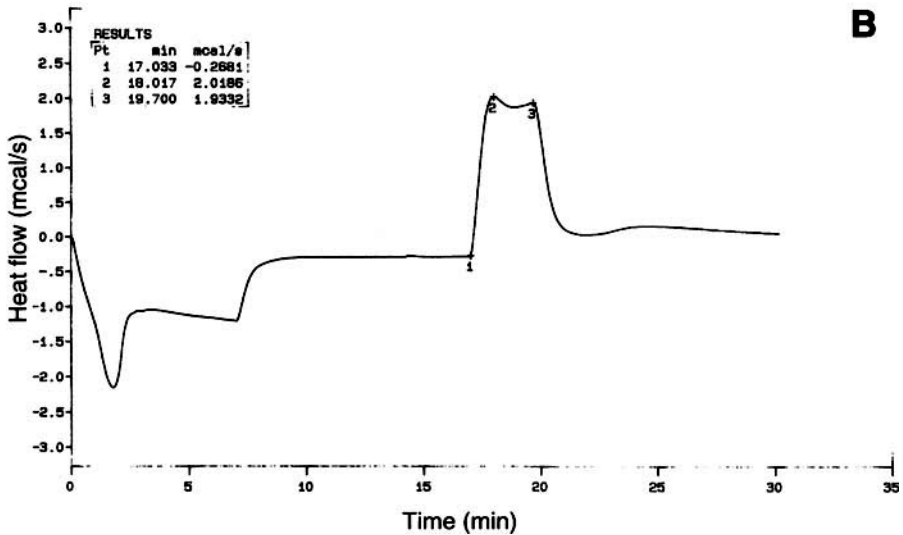
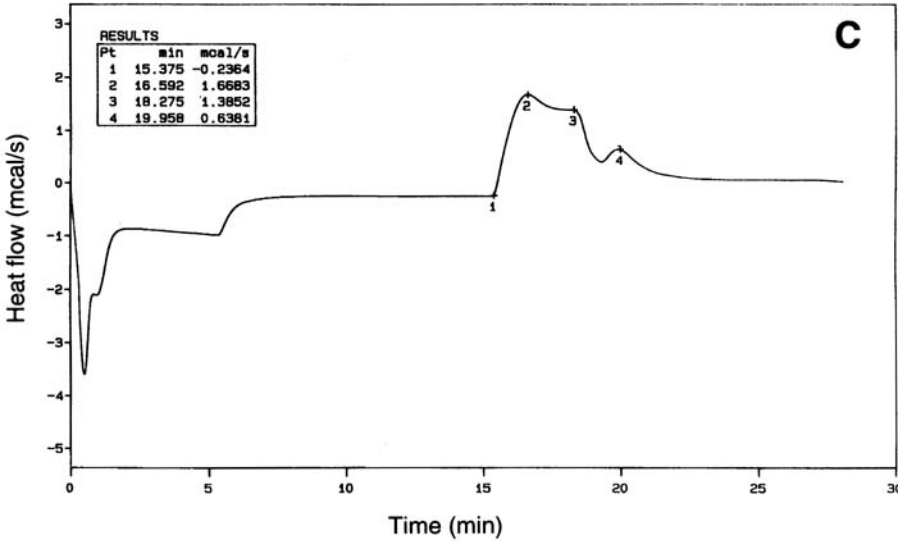


**Fig. 1.** Differential scanning calorimetry (DSC) isothermal analysis curves of fat: A. blank sample, B. sample with DK F-10, C. sample with P-170, D. sample with S-170 (Emulsifier concentration is 0.5%). Isothermal crystallization at 17°C (right side), and heating curves (left side), start at about 20°C at a rate of 5°C/min (rapidly cooled at a rate of 80°C/min). (Continued)

Tar bait Modaress



Tar bait Modaress

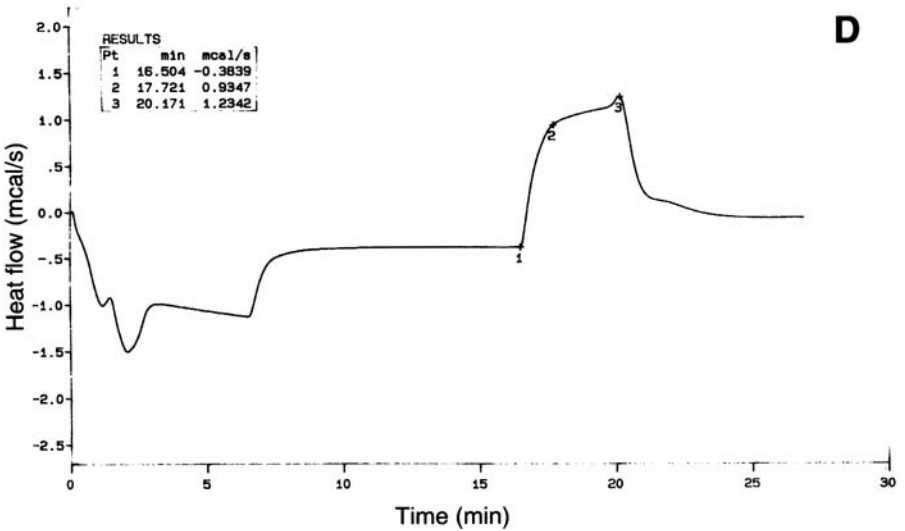
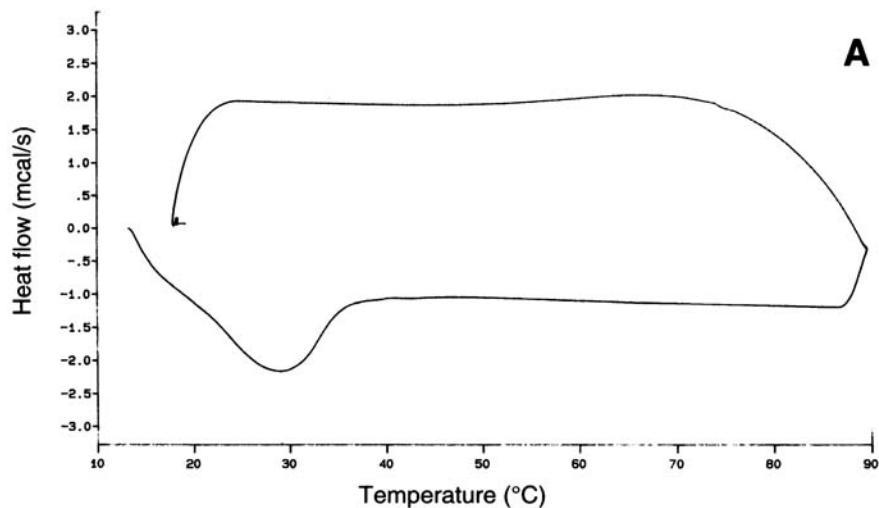


Fig. 1. (Continued)

The addition of DK F-10 and P-170 reduced the value of  $T_C$  by 17 and 10%, respectively, in comparison to the fat sample without the emulsifier. S-170 prolonged  $T_C$  by 15% in comparison to the control fat sample. It seems that the first peak in the exothermic curve represents the  $\alpha$ -form crystal, which transformed to the  $\beta$ -form as

Tarbait Modaress



Tarbait Modaress

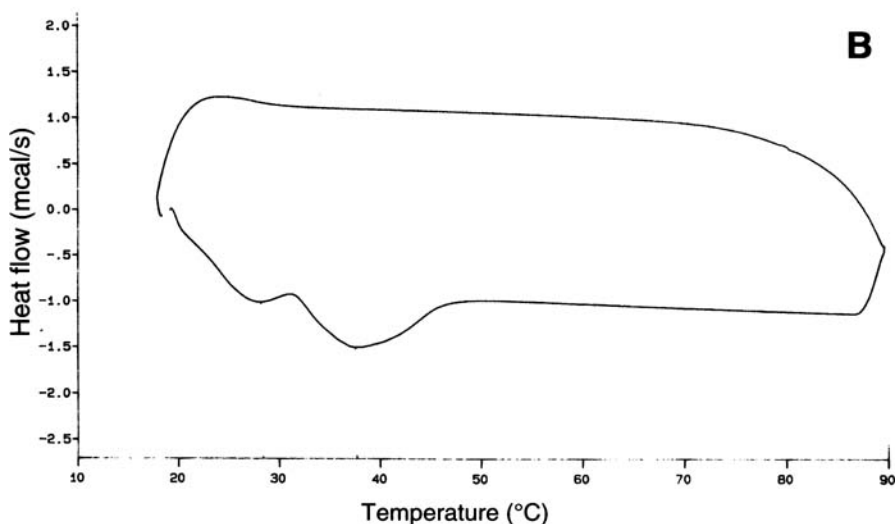


**Fig. 2.** Heat flow as a function of temperature: A. sample with DK F-10, B. sample with S-170 (it is the same isothermal curve of Figure 1 with the function differing.)

the second peak in the same curve (6,14,16). The appearance of the third peak in Figure 1C corresponds to the  $\beta$ -form from  $\beta'$ -form crystal (second peak), in which P-170 has facilitated the polymorphic transition, probably due to structure similarity and its ability to co-crystallize with the fat (4,16). The bulkiness of the lipophilic group. i.e., fatty acid ester, and the length of the lipophilic chain as well as struc-

**TABLE 1**The Effect of the Addition Different Concentrations of DK F-10 on  $T_c$  Values of Fat<sup>a</sup>

DK F-10 Concentration (%)	$T_c$ (min)
0.25	3.51
0.50	3.53
1.00	3.28

<sup>a</sup>The rapid cooling was at a constant rate of 100°C/min; the other conditions are as in Figures 1 and 2.  $T_c$  is a measure of the crystallization rate.

ture similarity are probably the factors behind the effectiveness of DK F-10 in increasing crystallization (decreasing  $T_c$ ) (4,16,17). On the other hand, S-170 delayed the crystallization probably due to its structurally dissimilarity with the fat and its lower degree of ester composition (4,17). DKF-10 has been reported to be an inhibitor of crystallization in hydrogenated soybean oil (18), whereas it promotes crystallization in the blend of hydrogenated soybean/cottonseed oil. The addition of cottonseed oil to soybean oil alters the fat composition and thus changes the activity of the emulsifier (4,6).

Table 1 shows the effect of the addition of DK F-10 at different concentrations on  $T_c$  values. At levels of 0–25 and 50%,  $T_c$  values were similar but there was a decrease of  $T_c$  at 1% concentration. This observation indicates that the emulsifier at the level of 1% was absorbed by the fat during crystallization in sufficient amount to affect the crystallization, whereas at 0.25 to 0.50% levels, there was an insufficient amount to cause an effect.

The effects of the addition to the fat of DK F-10, lecithins, and DK F-10/lecithin mixture on  $T_c$  values are shown in Table 2. Addition of both deoiled and ethanol-insoluble lecithins (1%) to the oil produced higher  $T_c$  values compared to that of DK F-10, due to the known inhibitory effect of lecithin on crystallization of fat (5,19). Deoiled lecithin is more effective in delaying crystallization of fat than the ethanol-insoluble lecithin fraction, probably due to the lower HLB of the ethanol-insoluble fraction (mostly phosphatidylinositol) compared with deoiled lecithin (10). The mixture of DK F-10/lecithins had an intermediate effect on crystallization of fat.

**TABLE 2**The Effect of the Concentration of DK F-10, and DK F-10/Lecithins on  $T_c$  Values<sup>a</sup>

Emulsifiers and concentration (%)	$T_c$ (min)
DK F-10 1	3.75
DK F-10-Deo L (50:50) 1	4.52
Deo L 1	5.72
DK F-10-E-I L (50:50) 1	4.11
E-I L 1	5.29

<sup>a</sup>Deo L = deoiled Lecithin; E-I L = ethanol-insoluble lecithin. The conditions are the same as those in Table 1.

In looking at the DSC melting profiles of the crystals (endothermic peak) in Figure 1 A–D, the sample with DK F-10 has a higher crystallization rate because only the first peak is evident whereas the second melting peak has disappeared (Fig. 1B). The sample containing S-170 has a lower crystallization rate (Fig. 1D), with a very small first peak and a large second peak. This indicates that DK F-10 and S-170 have opposite effects on fat crystallization. Melting peaks of the control and sample containing P-170 were intermediate in size between samples containing DK F-10 and S-170. The disappearance of the second melting peak (Fig. 1B) indicates that the  $\beta$ -form crystals were not obtained and the less stable  $\alpha$ -form crystals melted directly without being first converted into  $\beta$ -form crystals. Figure 1D shows that  $\alpha$ -form crystals (first peak) converted rapidly into the more stable  $\beta$ -form crystals before being transformed into the liquid phase (19).

Figure 2A and B show the effect of temperature on heat flow of fat samples containing either 0.5% DK F-10 or S-170. One endothermic peak is apparent in Figure 2A, as is the case in Figure 1B and 1D at around 28°C, whereas in Figure 2B there are two endothermic peaks, which appear around 27 and 37°C.

Turbidity of the oil is caused by its crystallization. The effects of 0.0, 0.50, and 1.0% DK F-10 addition and temperature on the appearance of full turbidity (nontransparent) are shown in Table 3. The turbidity appearance rate increased with increasing DK F-10 concentration in the oil. The differences in the rate are high at a higher temperature, i.e., 25°C and reduced at a lower temperature. Consequently, the addition of DK F-10 will allow the oil to temper at a relatively high temperature (around 25°C) will be more useful and effective in saving time and energy than that at a low temperature (around 12°C).

A practical scaled-up study was performed on samples of 3 kg of fat in square tin cans: one with 1% DK F-10 in vegetable ghee and the other as control. The sample containing DK F-10 reached complete solidification after 13 h, whereas the control did not solidify until 5 h later. In the sample containing Dk F-10, solidification took place in all parts of the oil simultaneously, whereas in the control, solidification occurred from bottom to top. This fact indicates that the emulsifier was absorbed in the fat during crystallization in sufficient amounts to bring about a faster solidification process.

**TABLE 3**

Effect of DK F-10 Concentration and Temperature on the Turbidity Time of Fat Used in Vegetable Ghee Production

Sample no.	DK F-10 (%)	Temperature (°C)		
		25	19	12
1	0.0	>420 min	91 min	25 min
2	0.5	28 min	19 min	11 min
3	1.0	21 min	10 min	7 min

## Summary

This study is on the effect of various food emulsifiers on the fat used in the production of vegetable ghee and shows that DK F-10 is the most effective in increasing the crystallization rate and speeding up the solidification process. This approach will save 5 h of work and contribute to increased production compared to the production without DK F-10. This is in addition to the emulsifying properties of DK F-10. The composition of fat used with the emulsifier is important in determining its effect. Deoiled lecithin is the most effective in delaying the crystallization process and can inhibit fat-blooming in chocolate and other fat food.

## References

1. Berger, K.G., *Food Uses of Palm Oil. Palm Oil Information Series*, Malaysian Palm Oil Promotion Council, Kelane Jaya, Malaysia, 1996, pp. 12–14.
2. Gander, K.F., Margarine Oils, Shortenings, and Vanaspati, *J. Am. Oil Chem. Soc.* 58: 417–420 (1976).
3. Metzroth, D.J., Shortening: Science and Technology, in *Bailey's Industrial Oil and Fat Products*, edited by Y.H. Hui, John Wiley & Sons, New York, 1996, Vol. 3, pp. 115–160.
4. Lee, S., and J.M. de Man, Effect of Surfactants on the Polymorphic B Behaviour of Hydrogenated Canola Oil, *Fette Seifen. Anstrichm.* 86: 460–465 (1984).
5. Rivarola, G., M.C. Anon, and A. Calvelo, Influence of Phospholipids on the Crystallization of Waxes in Sunflowerseed Oil, *J. Am. Oil Chem. Soc.* 65: 1771–1773 (1988).
6. Herrera, M.L., and F.J. Marquez Rocha, Effects of Sucrose Ester on the Kinetics of Polymorphic Transition in Hydrogenated Sunflower Oil, *Ibid.* 73: 321–326 (1996).
7. Nakamura, S., Using Sucrose Ester as Food Emulsifiers, *INFORM* 8: 866–874 (1997).
8. Sato, K., Solidification and Phase Transformation Behaviour of Food Fats—A Review, *Fett/Lipid* 101: 467–474 (1999).
9. Lauridsen, J.B., Food Emulsifiers: Surface Activity, Edibility, Manufacture, Composition, and Application, *J. Am. Oil Chem. Soc.* 53: 400–407 (1976).
10. Stauffer, C.E., Emulsifiers for the Food Industry, in *Bailey's Industrial Oil and Fat Products*, edited by Y.H. Hui, John Wiley & Sons, New York, 1996, Vol. 3, pp. 483–522.
11. DKS, *Application of DK-Esters to Processed Foods of Fat and Oil*, Daiichi Kogyo Seiyaku Co., Kyoto, Japan, 1979.
12. Yuki, A., K. Matsuda, and A. Nishimura, Effect of Sucrose Polyesters on Crystallization Behavior of Vegetable Shortening and Margarine Fat, *J. Jpn. Oil Chem. Soc.* 39: 236–244 (1990).
13. RYOTO, *Ryoto Sugar Ester Technical Information; Nonionic Surfactant/Sucrose Fatty Acid Ester/Food Additive*, Mitsubishi-Kagaku Food Corporation, Tokyo, Japan, 1996, pp. 9.
14. Kawamura, K., The DSC Thermal Analysis of Crystallization Behavior in Palm Oil, *J. Am. Oil Chem. Soc.* 56: 753–758 (1979).
15. Ziegelitz, R., Lecithin Processing Possibilities, *INFORM* 6: 1224–1230 (1995).
16. Kawamura, K., The DSC Thermal Analysis of Crystallization Behavior in Palm Oil, II, *J. Am. Oil Chem. Soc.* 57: 48–52 (1980).

17. Timms, R.E., Phase Behaviour of Fat and Their Mixtures, *Prog. Lipid Res.* 23: 1–38 (1984).
18. DKS, *DK Ester Sucrose Fatty Acid Ester*, Daiichi Kogyo Seiyaku Co., Tokyo, Japan, 1998.
19. Garti, N., E. Wellner and S. Sarig, Crystal Structure Modification of Tristearin by Food Emulsifiers, *J. Am. Oil Chem. Soc.* 59: 181–185 (1982).

## Chapter 8

# Experimental Study and Computer Modeling of the Dynamic and Static Crystallization of Cocoa Butter

Ph. Rousset<sup>a</sup> and M. Rappaz<sup>b</sup>

<sup>a</sup>Nestec S.A., Nestlé Research Center, 1000 Lausanne 26, Switzerland, and <sup>b</sup>Département des Matériaux, Ecole Polytechnique Fédérale de Lausanne, MX-G, CH-1015 Lausanne, Switzerland

## Introduction

Close control of fat crystallization is often a key parameter for the processing of food containing a significant level of fat. For example, chocolate, which is made of a continuous fat matrix of mainly cocoa butter enrobing the other ingredients, must be tempered before molding (1). This stage is necessary for cocoa butter to crystallize in the right form to get the desired final properties for the chocolate: contraction at demolding, gloss, stability during storage, high melting point, fine texture, hardness.

Fat is mainly composed of triacylglycerol (TAG) molecules. These TAG are polymorphic, i.e., they can crystallize under several crystalline forms (2). To get a stable food at the end requires the fat to be crystallized in the stable polymorphic form to avoid possible further transformation. Cocoa butter does not form in the stable Form V by simple cooling. It needs a well-controlled thermal path, performed under shearing conditions, called tempering. This specific temperature program is necessary to first nucleate enough crystals and then only keep the Form V crystals and melt the other metastable ones. Shear is also required during this process to get sufficiently rapid and intense nucleation of the stable forms.

Polymorphism and kinetics of crystallization of TAG and fat under static conditions (e.g., in differential scanning calorimetry [DSC] apparatus) have been studied for a long time and are summarized in many reviews (2–6). Yet, these conditions are far-removed from industrial applications, where crystallization is usually achieved under shear (dynamic). Shearing has a major effect on crystallization kinetics: it induces a faster and more homogeneous crystallization, often in the stable form and with a refined grain size. Yet, its effect is far from being fully understood. Recently, several studies of dynamic crystallization of lipids have been reported (7–12).

In the first part of this work, static, dynamic, and intermediate dynamic–static crystallization kinetics of cocoa butter measured under isothermal conditions are reported. The effect of shear rate and time is analyzed using a kinetics theory previously developed for polymers. In the second part, these isothermal experimental

data are used in a computer model that has been developed for the simulation of the crystallization kinetics of TAG $\Delta$  (13,14). This model allows the modeling of the crystallization of cocoa butter samples under complex static or dynamic–static crystallization conditions.

## Materials and Methods

### Experiments

Fat studied was pure prime-pressed cocoa butter from de Zaan B.V., Koog aan de Zaan, Holland. Cocoa butter was crystallized under either static or shearing conditions using two different apparatus. Static isothermal crystallization was investigated using a DSC Mettler FP900 instrument (Greifensee, Switzerland), which allowed simultaneous calorimetric measurements and *in situ* microscopy observations. The same device was used for the study of TAG $\Delta$ , and details can be found in References 13–15. The cocoa butter sample (between 1 and 2.5 mg) was placed in a small glass pan, and formation of crystals in the sample was directly observed in transmission with a polarized-light microscope (PLM). The following thermal path was used: first, the sample was kept at 100°C for 3 min to ensure a completely liquid state; then it was rapidly cooled (10°C/min) to the desired temperature,  $T_{\text{iso}}$ , at which crystallization was allowed to proceed. After complete solidification, the sample was heated at 2 or 5°C/min in order to measure the melting range (MR) and the latent heat of fusion,  $\Delta H_f$ , for each solid phase formed. For unambiguous identification of the phases formed during isothermal crystallization of cocoa butter, X-ray diffraction (XRD) measurements (Siemens Kristalloflex 805, Muenchen, Germany) were done in parallel to the DSC fusion curves.

For each isothermal experiment, the evolution of the mass fraction of solid,  $f_s(t)$ , could be obtained by numerical integration of the DSC exothermal peaks of solidification, after correction for the baseline and normalization with the value of  $\Delta H_f$  of the phase(s) formed. As cocoa butter is composed of many TAG $\Delta$ , its maximum solid fraction at equilibrium,  $f_{s,\text{max}}$ , is not unity and depends on the crystallization temperature. Therefore, the crystallinity ratio,  $f_s(t)/f_{s,\text{max}}$ , was used to follow the advance of the liquid–solid transformation, during which it varies from 0 to 1. From the evolution of  $f_s(t)/f_{s,\text{max}}$ , the onset time,  $t_{\text{onset}}$ , and the finish time,  $t_f$ , of the transformation were estimated. They corresponded to  $f_s(t_{\text{onset}})/f_{s,\text{max}} = 1\%$  and  $f_s(t_f)/f_{s,\text{max}} = 99\%$ , respectively. Temperature–time–transformation (TTT) diagrams, which represent the kinetics of the phase transformations under isothermal conditions, were also constructed, as previously described in Reference 13. For each isothermal solidification plateau,  $t_{\text{onset}}$  and  $t_f$  of the various phase transformations were reported on the diagram, thus delimiting the time domain when liquid and solid coexist. The morphology of the crystals that formed on the isothermal plateau was also observed. Maps of crystal morphology as a function of the temperature of solidification were constructed.

Dynamic crystallization under precise control of shear and temperature was studied in a prototype apparatus specially developed. The whole cell, similar to a Couette viscometer, was made out of glass. The inner cylinder rotated at a controlled speed,  $\omega$ , while the outer wall was fixed. A double-mantel with a circulation of water allowed precise control of the temperature. Temperature of cocoa butter in the cell was measured with a chromel-alumel thermocouple. Measures were recorded with a data acquisition system. Shear rate imposed to cocoa butter in the system could be estimated from the rotation speed of the inner cylinder, assuming that the fluid is Newtonian and incompressible. There is no normal speed, only tangential speed. The shear rate,  $\dot{\gamma}$ , in the specimen is a single function of the radius. In the rest of this work, shear in the cell was characterized by its average value,  $\bar{\dot{\gamma}}$ , calculated by integration over the cell thickness (7).

Three different isothermal crystallization experiments were performed in this work: classical static (i.e., quiescent) crystallization in the DSC apparatus, dynamic crystallization with the apparatus described above, and dynamic-static crystallization. Dynamic isothermal crystallization consisted in completely solidifying cocoa butter under a shear in the Couette apparatus. Comparison of shear effect with results from literature was done using the average shear rate  $\bar{\dot{\gamma}}$ . This experiment did not allow direct measurement of the solid content in the sample. However, characteristic times of crystallization were estimated. The  $t_{\text{onset}}$  corresponded visually to the cloud point and to an increase of the cocoa butter temperature  $T(t)$  due to latent heat release. The finish time,  $t_f$ , was evaluated from the temperature evolution in cocoa butter. At  $t_f$ , the temperature  $T(t)$  suddenly increases sharply because of the apparition of a coherent crystalline structure in cocoa butter. This induces a loss of contact with the outer wall and a sharp decrease in the heat extraction.

Dynamic-static crystallization is a combination of the two first techniques. Cocoa butter was partially solidified under shear in the glass cell at constant temperature during a shear time,  $t_\omega$ , shorter than the time,  $t_{\text{onset}}$ , of the dynamic crystallization. Then a small sample was taken out and put in the DSC apparatus, where crystallization was achieved under static conditions at the same temperature. In this way, the same parameters as those used under static crystallization could be observed but with a preliminary shearing period of the liquid. During the shearing period, the sample was characterized by the average shear rate,  $\bar{\dot{\gamma}}$ . This procedure in two steps reproduces somehow the industrial processing of chocolate, in which chocolate is first pre-crystallized under shear (i.e., tempering stage with the appearance of a sufficiently large density of stable nuclei), before it completes its crystallization quiescently (cooling tunnel after molding).

### Model

As for pure TAG or binary mixtures (13,14), a numerical model called FEM-TTT and previously developed for phase transformations in steel (16) was adapted in the case of crystallization of cocoa butter during any cooling cycle. A finite ele-

ment (FEM) code was used to calculate the evolution of the temperature in the DSC sample, knowing the physical properties of the material as well as the initial and boundary conditions. This calculation was coupled with a macroscopic model of crystallization, which uses an additivity principle and the isothermal data presented in the form of TTT diagrams to simulate the solidification path at any node of the finite element mesh. For this purpose, the corresponding cooling curve at a given node was decomposed into small steps, during which the temperature was held constant and isothermal solidification data could be used to estimate the evolution of the solid fraction. As a result, the evolution of the latent heat or of the fraction of each phase in the sample could be calculated. Details of the model can be found in References 7 and 16.

## Results and Discussion

### Static Crystallization

Figure 1 presents the TTT diagram determined with the FP900 DSC apparatus under static conditions. The temperature–time domain shown corresponds to the domain of stability of Form II. Above 16°C, for a time longer than 20 min, Form

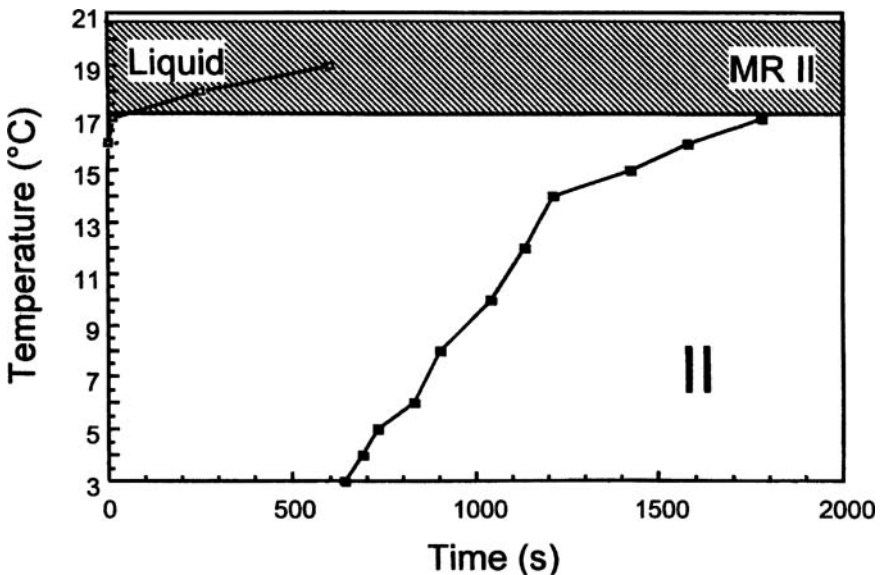


**Fig. 1.** Estimated static temperature–time–transformation (TTT) diagram of cocoa butter obtained with the FP900 apparatus. Open and filled symbols correspond to values 1 and 99% of the liquid–solid transformation achieved. Hatched domain corresponds to the melting range (MR) of Form II.

III starts to form simultaneously with Form II. In this diagram, the hatched region (MR II) corresponds to the melting range measured for this phase upon heating. The corresponding morphology of the crystals formed during static isothermal holding is shown in Figure 2 as a function of the solidification temperature. Below 18°C, crystals of Form II grow under the form of a fine equiaxed morphology, appearing as white spots dispersed in a dark liquid. Above this temperature, the density of nuclei is low and spherulites are observed as a result of the smaller undercooling available for the formation of Form II. These spherulites are fuzzier than those observed for pure TAGΔ (13,14). This might be caused by irregularities of crystalline layers due to the incorporation of molecules of various composition and length.

### ***Dynamic Crystallization***

To study crystallization conditions closer to industrial processes, shearing was imposed on the sample in a series of experiments using the Couette apparatus described above. For dynamic crystallization, cocoa butter was completely crystallized isothermally under shear. The dynamic TTT diagram obtained at 600 rpm is presented in Figure 3. The phases formed were identified by DSC and XRD. For all the crystallization temperatures between 17 and 23°C, only the Form V is found in the samples after complete solidification. The melting ranges measured during heating for Phases IV and V are shown as hatched regions. Crystallization kinetics is accelerated, and formation of stable phases is favored as compared with static crystallization (see Fig. 1). This shows the large effect of shearing, which enhances

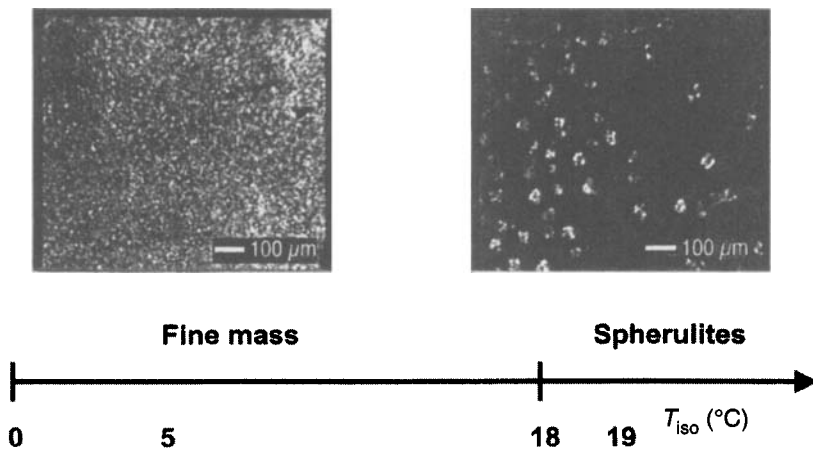


**Fig. 2.** Morphology map of Form II of cocoa butter obtained during the isothermal experiments of the static TTT diagram presented in Figure 1. Polarized light microscope (PLM) views illustrate the morphology observed in each domain. See Figure 1 for other abbreviation.

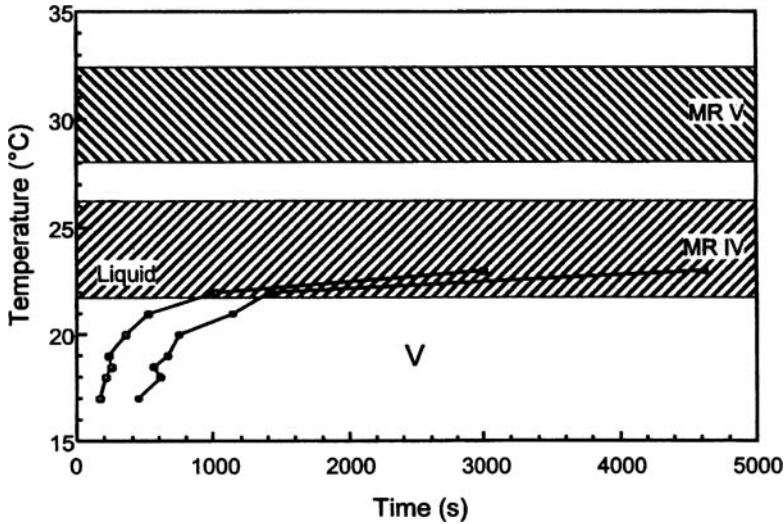
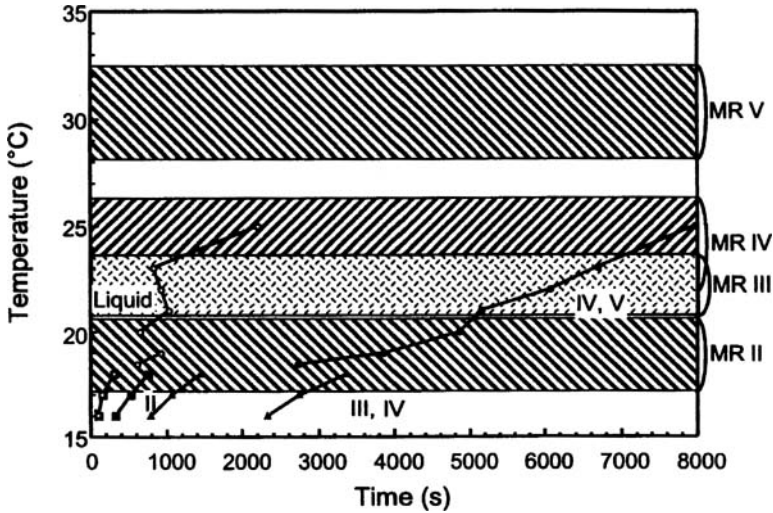


Fig. 3. Dynamic TTT diagram of cocoa butter at a rotation rate of 600 rpm. Hatched domains correspond to the MR of Forms IV and V. See Figure 1 for abbreviations.

the mobility of molecules, thus helping them to overcome the kinetic barriers for nucleation and growth. As a result, stable crystals are formed within a much shorter time range.

### **Dynamic–Static Crystallization**

The dynamic–static TTT diagram of cocoa butter presented in Figure 4 was constructed from DSC isothermal data, after a preliminary shearing of the melt at 600 rpm for a time  $t_{\omega}$  just lower than the  $t_{\text{onset}}$  of the dynamic experiment at the same temperature,  $T_{\text{iso}}$ . In the upper part of the diagram, Form V crystallizes but together with some Form IV, contrary to what is observed under purely dynamic conditions (Fig. 3). These two phases were unambiguously identified with both DSC and XRD (7). During the dynamic stage, nucleation and growth of the stable phase V are favored. But, when shearing is stopped and the specimen is further crystallized under static conditions, crystals of Form IV can appear and grow as the temperature is lower than the liquidus of this phase (i.e., the upper value of the melting range [MR IV]). They are metastable, but their growth rate is higher than that of Form V. At lower temperatures, the dynamic stage is too short to allow the liquid to transform into the most stable phases. Phase II first crystallizes (lower left corner of the TTT diagram); then mainly Form III appears and grows very quickly in the whole sample. Phase II only crystallizes at a low percentage because the temperatures studied are just below its liquidus. The remaining liquid crystallizes in a mixture of Forms III (main phase) and some Form IV. Compared with purely static



**Fig. 4.** Dynamic–static TTT diagram of cocoa butter. Dynamic stage is under a rotation rate of 600 rpm during a time  $t_{\omega}$  just smaller than the dynamic onset time,  $t_{\text{onset}}$ . Static crystallization is performed in the FP900 differential scanning calorimetry (DSC) apparatus. Hatched domains correspond to the MR of the various polymorphs observed. See Figure 1 for other abbreviations.

crystallization, the kinetics is more rapid and the growth of more stable phases is favored. Such dynamic–static crystallization in the upper temperature domain studied here is comparable with the industrial tempering process for chocolate. Ziegleder (17) observed that chocolate contains a mixture of Forms IV and V just after solidification. Then, Form IV transforms into Form V within a few days during storage.

Morphology map of the crystals observed simultaneously with the dynamic–static DSC measurements is presented in Figure 5. The mixture of Forms III and IV crystallizes in a fine equiaxed mass (lower temperature range of Fig. 4), as does the mixture of Forms IV and V just above 18°C. For higher solidification temperatures, Forms IV and V appear also as a mass growing radially from several nucleation centers. This morphology becomes dominant as the temperature increases.

### **Effect of Shear Rate and Time**

Figure 6 presents the dependence of  $t_{\text{onset}}$  with the average shear rate,  $\bar{\dot{\gamma}}$ , for three temperatures of crystallization, 18, 20, and 23°C. All the experiments were performed under shear. The behavior is similar for the three temperatures. Below a critical shear,  $\bar{\dot{\gamma}}_c$ ,  $t_{\text{onset}}$  is independent of the shear rate, where above it,  $t_{\text{onset}}$  is found to decrease as  $\bar{\dot{\gamma}}_m^{-1}$ , where the exponent  $m$  is close to  $-1$ . Lagasse and Maxwell (18) observed the

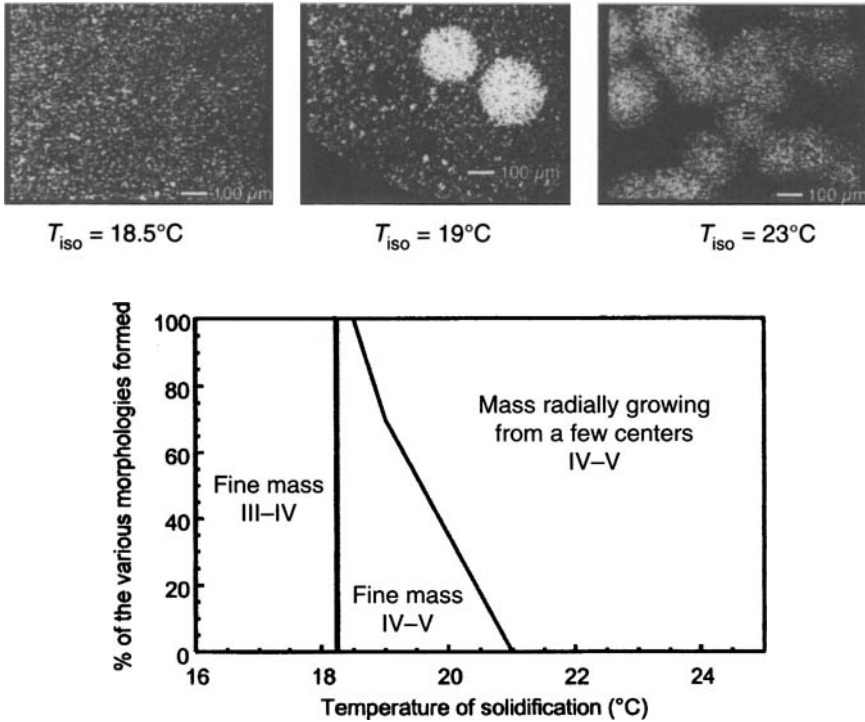
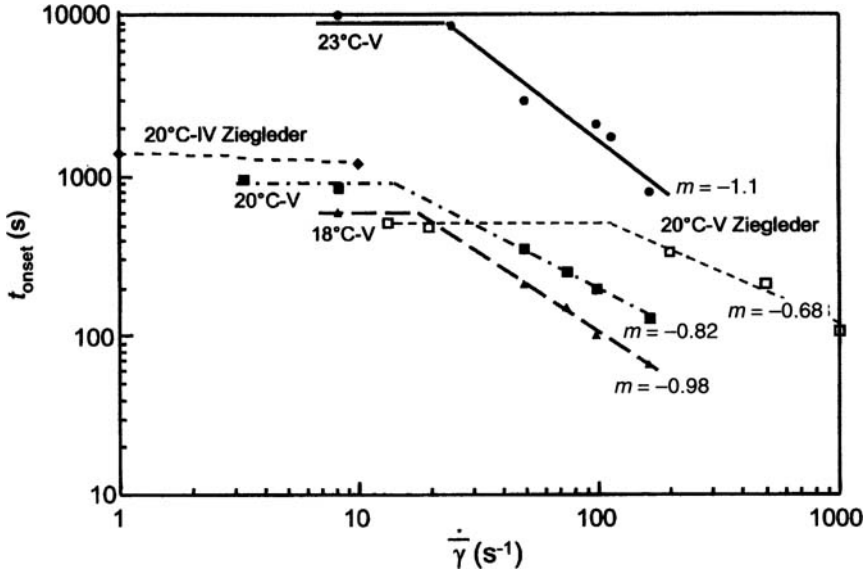


Fig. 5. Morphology map of cocoa butter crystals forming during the isothermal experiments of the dynamic-static TTT diagram presented in Figure 4. PLM views illustrate the morphology observed in each domain. See Figures 1 and 2 for abbreviations.

same phenomenon on polyethylene. Eder *et al.* (19) explained this behavior for polymers by a theory considering a dependence of the nucleation and its induction time with the shear rate. They found two nucleation domains. At low  $\dot{\gamma}$ , nucleation is often independent of  $\dot{\gamma}$ . At high  $\dot{\gamma}$ , the induction time is inversely proportional to  $\dot{\gamma}$ . Therefore, the effect of shear on nucleation seems to be similar for cocoa butter and for polymers.

Regardless of the shear rate and temperature, only the Form V is observed at the end of crystallization. Results obtained by Ziegler (12) for similar experiments done at 20°C are also reported in Figure 6. This author identified Form IV at the lowest shear rates and Form V at higher values. He also measured slightly slower crystallization kinetics. This is certainly due to the different experimental apparatus used in his study, since kinetics is very sensible in particular to the surface of the container in contact with the fat (13).

The effect of the shearing time,  $t_{\omega}$ , of the dynamic-static experiments was also investigated. Since  $t_{\text{onset}}$  could not be measured when it was shorter than the time for the DSC system to be equilibrated, the  $t_f$  was instead selected as an indicator of the



**Fig. 6.** Evolution of the dynamic onset time,  $t_{\text{onset}}$ , as a function of the average shear rate. Results are compared with those of Ziegler (Ref. 12) shown in dashed lines. The slope of the lines is estimated with least squares.

crystallization kinetics. If it is assumed that the growth rate is only a function of the temperature and not of other parameters such as grain morphology, then  $t_f$  is only a function of the nuclei density during the isothermal trials. For three temperatures (20, 23, and 25°C), a series of experiments was performed varying  $t_\omega$  and keeping  $\omega$  constant at 600 rpm. In all cases, liquid transforms in a mixture of forms IV and V, as identified by both DSC and XRD. The melting range of this mixture and its latent heat do not change much with  $t_\omega$ . They are in between the values of Forms IV and V. This indicates that the proportion of Phases IV and V formed does not depend on  $t_\omega$ . Yet, it depends on the temperature of solidification: the higher the temperature, the greater the proportion of Form V, as  $T_{\text{iso}}$  is closer to the liquidus of Form IV. Morphology of the crystal is a directed mass growing from a few nucleation centers (see Fig. 5). The number of nucleation sites of this mass strongly depends on  $t_\omega$ . Figure 7A and B present the variations of  $t_f$  and of the final density of nuclei,  $N_f$  respectively, as a function of  $t_\omega$  for the three crystallization temperatures. Horizontal lines in Figure 7A correspond to the minimum value of  $t_f$  that can be reached when purely dynamic crystallization is performed, assuming that Phase V only forms. These times can be found in Figure 3 (solid symbols). The big dots on these horizontal lines have been placed at  $t_\omega = t_{\text{onset}}$ , where  $t_{\text{onset}}$  is again the onset value of the purely dynamic crystallization.

The density of nuclei in Figure 7B has been evaluated by counting the number of sites on the microscopic views, when the nuclei were distinguishable, that is for

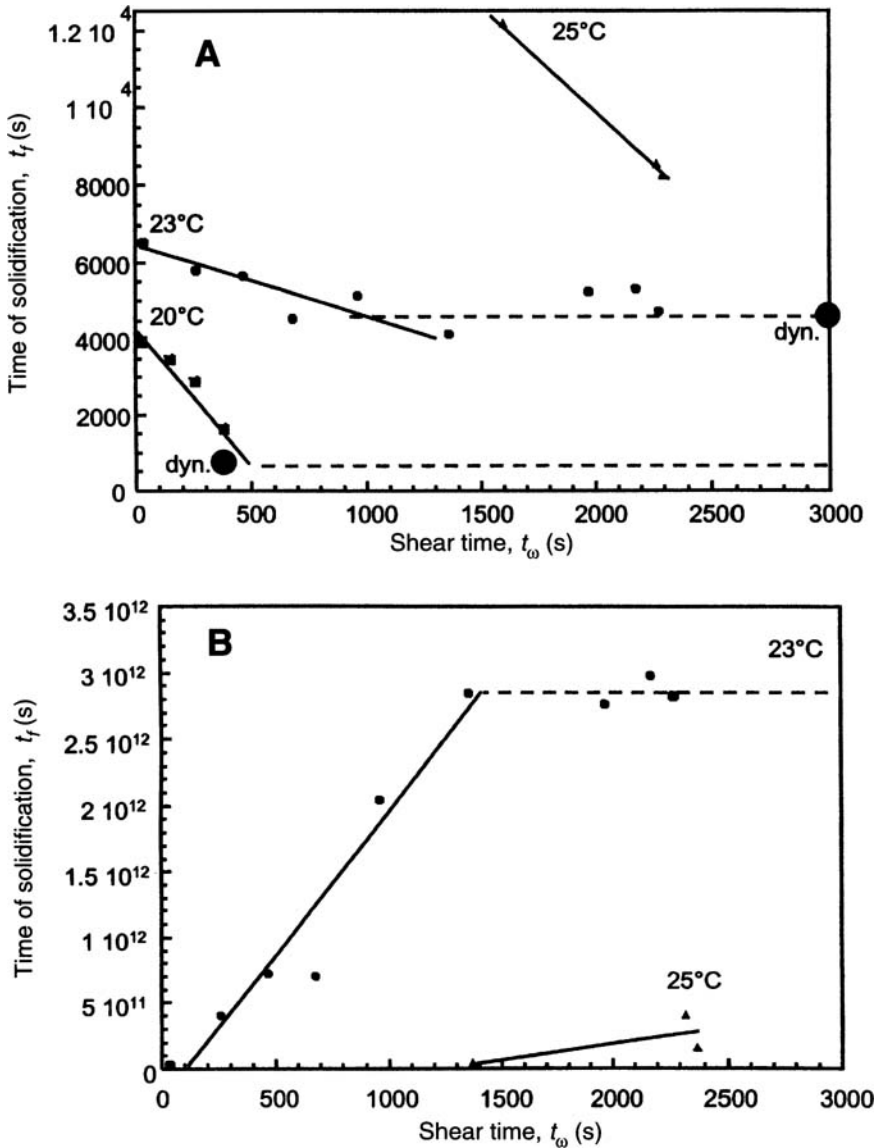


**Fig. 7.** Dynamic–static crystallization of cocoa butter. Effect of the shear time,  $t_w$  on: A. finish time of solidification,  $t_f$  B. density of nuclei sites. Dynamic stage is at 600 rpm, and large dots are the results for purely dynamic experiments.

23 and 25°C. As predicted by Eder *et al.* (19),  $t_f$  decreases, and the nuclei density increases with increasing values of  $t_w$ , up to the saturation limit, where all the

nucleation sites have been exhausted. The minimum value of the solidification time was then reached, for  $t_{\omega} < t_{\text{onset}}$ .

### Modeling of Anisothermal Crystallization

The FEM-TTT model, based on the use of TTT diagrams and an additivity principle, was applied to the complex cocoa butter system. Two cases of cocoa butter crystallization were simulated. First, static crystallization at constant cooling rate of a cocoa butter sample in a DSC pan was studied. Experiments were done in a Perkin-Elmer (Norwalk, CT) DSC7 apparatus. Isothermal kinetic data used for the simulation were also acquired on the same apparatus. The corresponding TTT diagram is not shown here but can be found in Reference 7. The following thermal path was applied to the sample. Initially the sample was fully liquid at 37°C; then it was cooled at a constant rate between 0.5 and 4°C/min. Figure 8 presents the experimental and simulated evolutions of the latent heat released by the sample due to crystallization, for the four cooling rates considered. As expected for a static case, a mixture of Forms II and III crystallizes. The simulation is in good agreement with the experiment. Simulated curves are interrupted before the end of the solidification, when the sample temperature reached 14°C. Indeed, isothermal measurements could not be obtained below, due to a kinetics which was too fast compared with the apparatus stabilization time. The small bumps observed in the

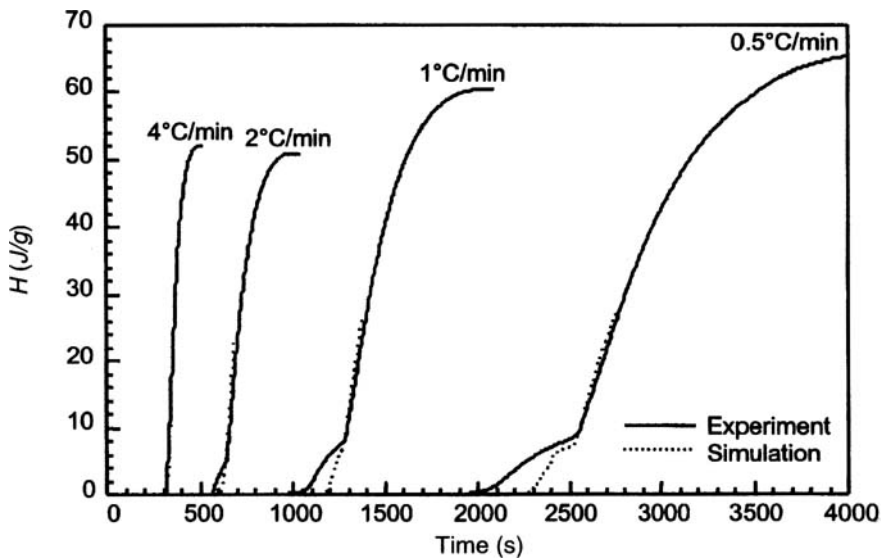


**Fig. 8.** Comparison between experimental and simulated evolutions of the latent heat of a cocoa butter sample in a DSC pan cooled at various cooling rates starting from a completely liquid state at 37°C. See Figure 4 for abbreviation.

enthalpy evolutions for both experiment and simulation at the slow cooling rates (below  $1^{\circ}\text{C}/\text{min}$ ) correspond to an arrest in the crystallization of Phase II, when the sample is cooled between  $17$  and  $16^{\circ}\text{C}$ . In this temperature domain, the DSC peak of crystallization measured under isothermal condition corresponds to a maximum crystallizable fraction,  $f_{s,\text{max}}$ , of about  $8\%$  and is almost independent of  $T$ . It is only below  $16^{\circ}\text{C}$ , that the maximum crystallizable fraction increases again with a decrease in temperature and that further crystallization occurs.

For the second example, cocoa butter was dynamically cooled from an initial liquid state at  $42^{\circ}\text{C}$ , under three cooling conditions. Just before the dynamic time  $t_{\text{onset}}$  was reached (the dynamic  $t_{\text{onset}}$  was first determined for each of the three cooling rates), a sample was taken and put in the DSC FP900 apparatus, where it was submitted to an isothermal plateau at the last temperature it was taken. The complete thermal paths for the three cases considered are presented in Figure 9. For the three cases, a mixture of Forms IV and V crystallizes. The same crystal morphology as for the isothermal dynamic–static crystallization is observed, i.e., masses growing radially from nucleation centers. The number of nuclei decreases when the cooling rate is smaller.

The crystallization of the three cases was simulated with the same FEM-TTT model, using the isothermal data presented in the dynamic–static TTT diagram of Figure 4. Figure 10 shows the experimental and simulated onset and finish times of crystallization. The model provides a good estimation of the crystallization kinetics.

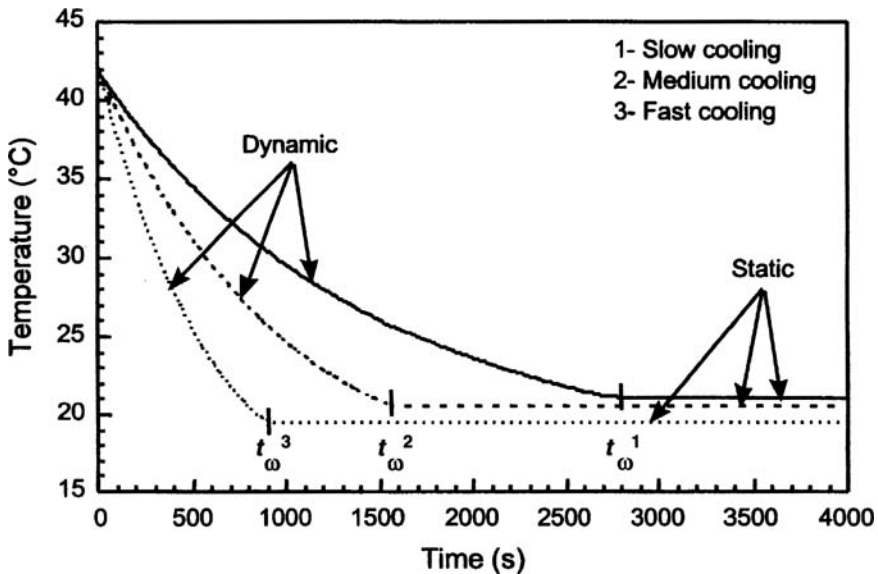


Fig. 9. Cooling curves of a cocoa butter sample for three cases of dynamic–static crystallization. Anisothermal part is under shear at  $600$  rpm. Isothermal part is static in the DSC apparatus. See Figure 4 for abbreviation.

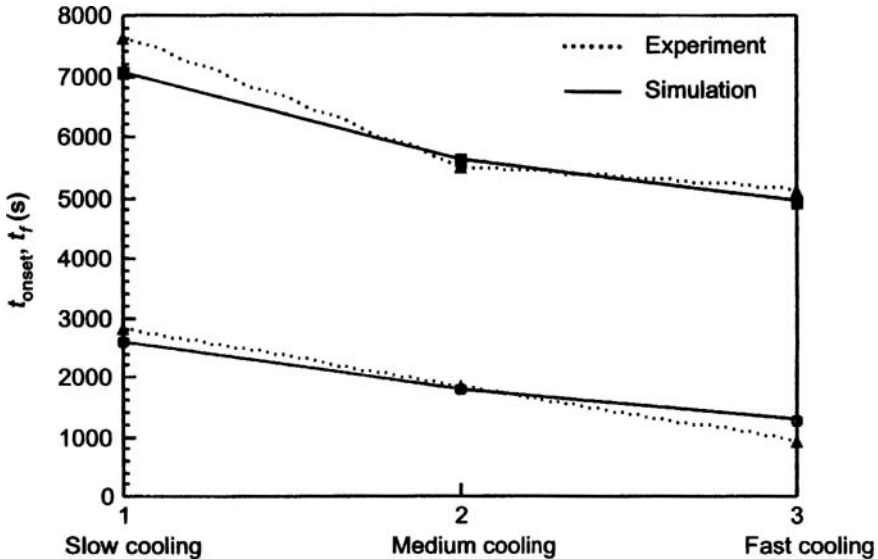


Fig. 10. Onset and finish times of dynamic-static crystallization of cocoa butter samples for the three cooling curves presented in Figure 9, measured experimentally, and simulated with the FEM-TTT model.

In the case of complex crystallization cycles of cocoa butter, the two preceding examples have shown that the macroscopic approach of the FEM-TTT model allowed a satisfactory prediction of the crystallization kinetics. The model simply needs to first establish the TTT diagrams corresponding to the experimental conditions used. Therefore, computer modeling can become a tool for quantitative simulation of the crystallization kinetics of fat (e.g., estimation of percentage of phases formed and crystallization times) under complex cooling and shear conditions.

### Acknowledgments

The authors thank the Commission pour la Technologie et l'Innovation (CTI), Bern, Switzerland, and the Nestlé Research Center, Vers-chez-les-Blanc, Switzerland, for their financial support (CTI project 2944.1).

### References

1. Talbot, G., Chocolate Temper, in *Industrial Chocolate Manufacture and Use*, edited by S.T. Beckett, Blackie Academic & Professional, Glasgow, 1994, pp. 156–166.
2. Garti, N., and K. Sato, *Crystallization and Polymorphism of Fats and Fatty Acids*, edited by N. Garti and K. Sato, Surfactant Science Series, Vol. 31, Marcel Dekker, Inc., New York, 1988, pp. 3–137.
3. Hernqvist, L., Polymorphism of Triglycerides: A Crystallographic Review, *Food Structure* 9: 39–44 (1990).

4. Sato, K., S. Ueno, and J. Yano, Molecular Interactions and Kinetic Properties of Fat, *Progress in Lipid Res.* 38: 91–116 (1999).
5. Sato, K., Polymorphism of Pure Triacylglycerols and Natural Fats, *Advances in Lipid Res.* 2: 213–268 (1996).
6. Sato, K., Solidification and Phase Transformation Behaviour of Food Fats, A Review, *Fett/Lipid* 101: 467–474 (1999).
7. Rousset, Ph., *Etude Expérimentale et Modélisation de la Cristallisation de Triacylglycérols et du Beurre de Cacao*, Ph.D. Thesis 1718, EPFL, Lausanne, 1997.
8. Stapley, A., H. Tewkesbury, and P. Fryer, The Effects of Shear and Temperature History on the Crystallization of Chocolate, *J. Am. Oil Chem. Soc.* 76: 677–685 (1996).
9. Loisel, C., G. Lecq, G. Keller, and M. Ollivon, Dynamic Crystallization of Dark Chocolate as Affected by Temperature and Lipid Additives, *J. Food Sci.* 63: 73–79 (1998).
10. Loisel, C., G. Keller, G. Lecq, B. Launay, and M. Ollivon, Tempering of Chocolate in a Scraped Surface Heat Exchanger, *Ibid.* 62: 773–780 (1997).
11. Ziegleder, G., Verbessertes Kristallisationsverhalten von Kakaobutter unter dem Einfluss eines Schergefälles, *Int. J. Food Technol.* 36: 412–416 (1985).
12. Ziegleder, G., Kristallisation von Kakaobutter unter Statischen und Dynamischen Bedingungen (DSC, Rheometer), *Süßwaren* 32: 487–493 (1988).
13. Rousset, Ph., and M. Rappaz, Crystallization Kinetics of the Pure Triacylglycerols Glycerol-1,3-Dipalmitate-2-Oleate, Glycerol-1-Palmitate-2-Oleate-3-Stearate, and Glycerol-1,3-Distearate-2-Oleate, *J. Am. Oil Chem. Soc.* 73: 1051–1057 (1996).
14. Rousset, Ph., M. Rappaz, and E. Minner, Polymorphism and Solidification Kinetics of the Binary System POS-SOS, *Ibid.* 75: 857–864 (1998).
15. Rousset, Ph., and M. Rappaz,  $\alpha$ -Melt-Mediated Crystallization of POS, *Ibid.* 74: 693–697 (1997).
16. Jacot, A., M. Swierkosz, J. Rappaz, M. Rappaz, and D. Mari, Modelling of Electromagnetic Heating, Cooling, and Phase Transformations During Surface Hardening of Steels, *J. de Physique* 4(C1): 203–213 (1996).
17. Ziegleder, G., Kristallisation von Kakaobutter und Schokoladenmassen, *Proceedings of 2nd International Congress on Cocoa and Chocolate*, Munich, 1991, Behrs Verlag, Hamburg, 1992.
18. Lagasse, R., and B. Maxwell, *Polym. Engng. Sci.* 16: 189 (1976).
19. Eder, G., H. Janeschitz-Kriegl, and S. Liedauer, Crystallisation Processes in Quiescent and Moving Polymer Melts Under Heat Transfer Conditions, *Prog. Polym. Sci.* 15: 629–714 (1990).

## Chapter 9

# Crystallization of Palm Oil Products

### Chiew Let Chong

Product Development and Advisory Services Division, Malaysian Palm Oil Board (MPOB),  
P.O. Box 10620, 50720 Kuala Lumpur, Malaysia

## Introduction

The Avrami equation (1), originally developed for the crystallization of metals from melt, has been applied by many researchers to the crystallization of oils and fats in order to elucidate information on their crystallization mechanism. The Avrami equation is based on the model of a growing sphere crystallizing from a melt of uniform density without impingement. The usual Avrami exponent, used to draw conclusions with respect to the crystallization mechanism of the system, is observed to be about three or four for oils and fats after rounding off to whole integers.

In the work reported by Ng and Oh (2), an Avrami exponent of three was observed for palm oil from solid fat content (SFC) measurements. Using differential scanning calorimetry (DSC) to monitor the isothermal crystallization of palm oil, Kawamura (3) reported an Avrami exponent of four for palm oil.

For a mixture of cocoa butter with milk fat and milk-fat fractions using DSC measurements, Metin and Hartel (4) observed that: (i) cocoa butter crystallization was by heterogeneous nucleation and spherulitic growth with an Avrami exponent  $n$  of four, (ii) anhydrous milk-fat crystallization is by instantaneous nucleation followed by spherulitic growth with an Avrami exponent of three, (iii) for milk-fat fractions the crystallization mechanism was observed to have a high nucleation rate at the beginning of the crystallization which decreased with time followed by plate-like growth with  $n$  values of about two for the high-melting fractions. (iv) the addition of milk-fat fractions did not cause any significant changes in the suggested nucleation and growth mechanism of cocoa butter. The range of  $n$  observed for the cocoa-butter/milk-fat mixtures was four to seven.

In the work reported by Wright *et al.* (5) on milk-fat crystallization using SFC measurements, the following observations were made: (i) for anhydrous milk fat, the Avrami exponent  $n$  was observed to change from less than one at 5°C to 1.5 at 20°C and to three or four after 20° up to 27°C, (ii) for milk-fat triacylglycerol, the Avrami exponent  $n$  was observed to change from below one at 5°C to 2.41 at 20°C and from then to four or five up to 27°C, and (iii) for milk-fat triacylglycerol mixed with diacylglycerol, the  $n$  values changed from less than one at 5°C to 1.33 at 20°C and then to between four to six up to 27°C.

Observed good fit of SFC data was reported by Herrera *et al.* (6) for the fitting of SFC data of hydrogenated sunflower oil using Avrami exponent of three and one. In the work reported by Dibildox-Alvarado and Toro-Vazquez (7) on the isothermal crystallization of tripalmitin in sesame oil using ultraviolet (UV) measurement, the tripalmitin solutions were observed to crystallize with Avrami exponents of three and four in the temperature range of 285 K to 295 K.

Marangoni (8) has warned of the misuse of a modified form of the Avrami equation.

From reported literature values, it can be seen that the Avrami exponent for crystallizing oils and fats is usually about three or four with the exceptions of anhydrous milk fat, its triacylglycerols, and its mixtures with diacylglycerol at temperatures below 20°C, where an exponent of three is more common.

### **Avrami Equation for DSC measurement**

For DSC measurements, the area under an exothermal curve corresponds to the heat of crystallization,  $\Delta H$ . The fraction of crystals  $f$  at any time  $t$  during the crystallization process is given by Equation 1:

$$f = \left[ \int_{t=0}^t \frac{d\Delta H(t)}{dt} \cdot dt \right] / \Delta H \quad [1]$$

The equation developed by Evans for DSC measurements based on the Avrami equation is:

$$1 - f = e^{-kt^n} \quad [2]$$

where  $k$  is the rate constant and  $n$  is the Avrami exponent related to the crystallization mechanism. The previous equation can be expressed in logarithmic form as:

$$\ln [-\ln(1 - f)] = \ln k + n \ln t \quad [3]$$

$n$  can be obtained from a plot of  $\ln[-(1 - f)]$  vs.  $\ln t$ .

Values for the Avrami exponent  $n$  for various types of nucleation and growth are as shown in Table 1.

## **Experimental Procedures**

### **Materials**

Crude and refined palm oils, refined palm kernel oil, and refined palm stearin of iodine value (IV) 35 and 41 are commercial samples obtained from various refineries around the Klang Valley region and used without any treatment.

**TABLE 1**

Values of the Avrami Exponent  $n$  for the Various Types of Nucleation and Growth Mechanisms<sup>a</sup>

Avrami exponent $n$	Type of crystal growth and nucleation expected
$3 + 1 = 4$	Spherulitic growth from sporadic nuclei.
$3 + 0 = 3$	Spherulitic growth from instantaneous nuclei.
$2 + 1 = 3$	Disc-like growth from sporadic nuclei.
$2 + 0 = 2$	Disc-like growth from instantaneous nuclei.
$1 + 1 = 2$	Rod-like growth from sporadic nuclei.
$1 + 0 = 1$	Rod-like growth from instantaneous nuclei.

<sup>a</sup>Source: Reference 5.

### Methods

Isothermal crystallization of the oil or fat was monitored by a Perkin Elmer DSC 7 differential scanning calorimeter. Sample sizes range from 5 to 10 mg. The oil sample is heated to a temperature of 80°C at a heating rate of 5°C/min from ambient and held at that temperature for at least 10 min in order to totally erase all past crystallization memories. The sample was then cooled at a rate of 5°C/min until the desired crystallization temperature had been reached. The sample temperature was then maintained at this crystallization temperature for 2 h to monitor the complete crystallization behavior of the sample. Partial areas under the thermal curve were determined by means of the Perkin Elmer Pyris partial area analysis software.

Crystal polymorphic analyses were determined by means of X-ray diffraction on an Enraf-Nonius FR 590 diffractometer equipped with a Guinier camera. Visual crystal observations were made using a Leica DMLP polarizing microscope equipped with a CCTV camera. Suppliers were Golden JoMalina, Lam Soon Sdn. Bhd., and Felda Vegetable Oils Products Sdn. Bhd., all of Malaysia.

### Observations and Discussion

In plotting the DSC isothermal data points (Figs. 1–4) to obtain the Avrami exponent  $n$  for the various types of palm products, it was observed that only the crystallization fractional range of 2–70% can be utilized to obtain the straight-line plot required to determine the exponent. This is in line with the observation by Ng and Oh (2) that only 70% of the SFC values could be fitted. Data from higher degree of crystallization (>70%) were observed to deviate from the straight line. From the figures, it can be seen that very good straight lines are obtained for the data range plotted for all the samples at all the crystallization temperatures investigated. Deviations from a straight line can be observed in some of the plots even at the 70% of crystallization level.

Table 2 shows the results for the effect of sample cooling rate for refined palm oil at 293 K. The cooling rates investigated are in the range normally used for most DSC analysis of oils and fats. From the results, it can be deduced that DSC cooling rates in the range of 5 to 20°C per minutes do not have any effect on the Avrami exponent determined.

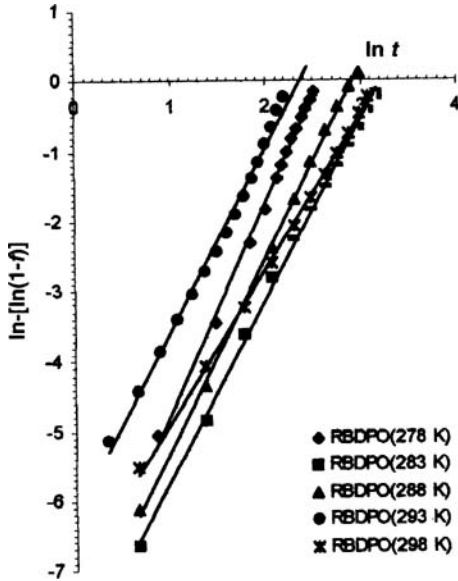


Fig. 1. Avrami equation plots for refined, bleached, deodorized (RBD), palm oil (PO) under isothermal.

Table 3 shows the crystal polymorphic form and Avrami exponent observed for crude and refined palm oil and refined palm kernel oil at the isothermal crystallization temperature indicated. An Avrami exponent of three was observed for all the temperatures for the three types of oil even though the crystal may be in different polymorphic form as in the case of crude and refined palm oils.

Table 4 shows the results for two palm stearins with IV of 35 and 41. The stearin with IV of 41 is a soft stearin and appears to behave in a manner similar to

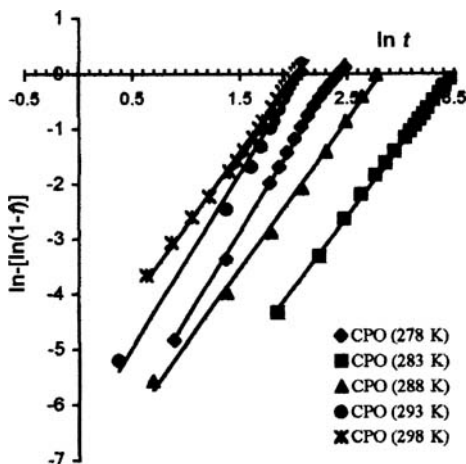


Fig. 2. Avrami equation plots for crude palm oil (CPO) under isothermal crystallization.

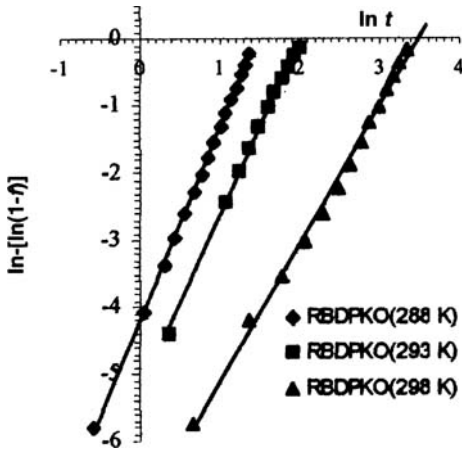


Fig. 3. Avrami equation plots for refined palm kernel oil (PKO) under isothermal crystallization. See Figure 1 for other abbreviation.

that of palm oil showing the same polymorphic forms and Avrami exponents at all the temperatures investigated. The stearin with IV 35 is a sample of medium hardness. From the results it can be seen that as the isothermal crystallization temperature increases some of the crystals are transformed from the  $\beta'$  form into the  $\beta$  form with the  $\beta$  form dominating at 308 K. The Avrami exponent was observed to increase from a value of three at 298 K to five or six at higher temperatures.

In applying the Avrami equation to the crystallization of metals, for which the equation was originally developed, experimental data would give exponents which are whole numbers. When applied to polymers, it was observed that although

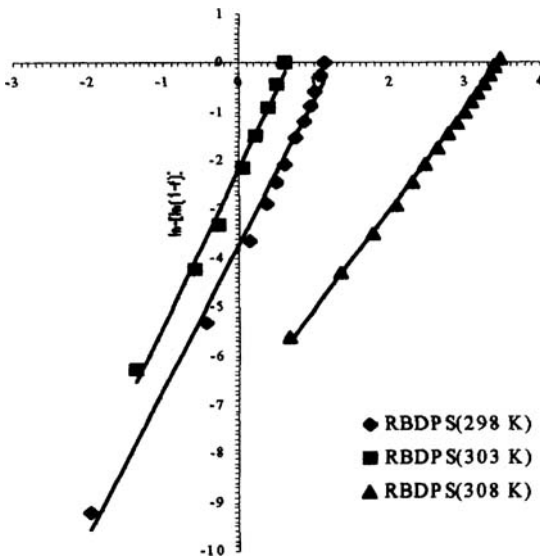


Fig. 4. Avrami equation plots for refined palm stearin (PS) with an iodine value of 41 under isothermal crystallization. See Figure 1 for other abbreviation.

**TABLE 2**Effect of Differential Scanning Calorimetry Cooling Rate on the Determination of the Avrami Exponent<sup>a</sup>

Cooling rate	Avrami exponent $n$	Regression equation
5°/min	3	$Y = 2.627X - 6.2006$
10°/min	3	$Y = 2.6212X - 5.7109$
15°/min	3	$Y = 2.6457X - 6.1482$
20°/min	3	$Y = 2.7152X - 6.3106$
Where	$Y = \ln[-\ln(1 - f)]$ and $X = \ln t$	

<sup>a</sup>RBD, refined, bleached, deodorized.

whole number exponents were obtained in most cases, fractional exponents were sometimes observed. However in the case of crystallizing oils and fats, the exponents obtained are seldom whole integers, and rounding off to obtain whole numbers will have to be effected. Generally, only the rounded exponents are reported in literature although in certain instances the fractional exponents have been reported (4,5). This will give rise to ambiguities when the integers fall within gray areas such as those between the 0.45–0.49 decimal range.

From theoretical considerations, an Avrami exponent of four would imply three-dimensional growth with sporadic nucleation. For an Avrami index of three, the implication can either be spontaneous or instantaneous homogeneous nucleation with three-dimensional growth or a sporadic heterogeneous nucleation followed by two-dimensional growth (Table 1). From theoretical considerations (9–11), it was stated that spontaneous or homogeneous nucleation should rarely occur in fats. Hence from theoretical considerations, oils and fats should crystallize with Avrami exponent of four. However, from literature it can be seen that most oils and fats tend to have an Avrami index of three, including the work on palm oil

**TABLE 3**Avrami Exponents and Polymorphic Forms of Crude and Refined Palm Oil and Refined Palm Kernel Oil<sup>a</sup>

Temp/ K	Crude/palm oil		Refined (RBD) palm oil		Refined palm kernel oil	
	Polymorphic form	Avrami exponent $n$	Polymorphic form	Avrami exponent $n$	Polymorphic form	Avrami exponent $n$
278	$\alpha$	3	$\alpha$	3		
283	$\alpha$	3	$\alpha$	3		
288	$\alpha \rightarrow \beta'$	3	$\alpha \rightarrow \beta'$	3	$\beta'$	3
293	$\beta'$	3	$\beta'$	3	$\beta'$	3
298	$\beta'$	3	$\beta'$	2	$\beta'$	3

<sup>a</sup>See Table 2 for abbreviation.

**TABLE 4**  
Avrami Exponents and Polymorphic Forms of Refined Palm Stearin<sup>a</sup>

Temp (K)	IV = 41		IV = 35	
	Polymorphic form	Avrami exponent <i>n</i>	Polymorphic form	Avrami exponent <i>n</i>
298	β'	3		3
303	β'	3		5
308	β'	3	β' >>> β	4
313	β'	2		6
318		3		
315			β >>> β'	5

<sup>a</sup>IV, iodine value.

products reported here. This would imply that the growth of the crystals of oils and fats is in two dimensions, not three.

For the work reported here, the polymorphic forms of the crystals of all the palm oil products at the temperatures measured are either in the β or β' form or a mixture of both. The β polymorphic crystal form is plate-like while the β' crystal form is spherulitic with needle-like projections from the center of the crystal as can be seen from the electron microscope pictures published by van Putte and Bakker (12). Therefore it can be seen that for the β polymorph, although the final overall shape of the crystal assumes the shape of a sphere in three dimensions, the plates or leaves that form the crystal are thin. This shows that as far as the actual growing sites of the crystal are concerned, growth is in two and not in three dimensions.

For the β' polymorphic crystals, they assume a spherulitic shape with needle-shaped protrusions radiating from the center. These needle-like protrusions from the center of the crystals are the actual growing sites of the crystals as can be observed under the microscope. The distribution of these needles around the center of the crystal gives the final spherulitic shape of the β' polymorphic form. As in the case of the β polymorph, the growing needles of the β' polymorph can also be considered as two-dimensional as it is only radiating outward from its own center and upward. From the above considerations, it can be seen that the more commonly observed Avrami exponent of three will be inconsistent with the theoretical considerations for oils and fats nucleation.

The exponent values of more than three, i.e., five or six observed for the stearin sample with IV of 35, were observed to occur in the presence of a mixture of β and β' crystals. These values could possibly be the sum of the exponents from both the β and β' crystals. However, more data will have to be obtained to support this hypothesis.

As mentioned earlier, the Avrami exponent values commonly observed for oils and fats crystallization appear to be inconsistent with theoretical considerations. Why is this so?

This could be due to the fact that the original Avrami equation was developed for the crystallization of metals with conditions that are not fulfilled in the case of oils and fats crystallization as compared to those of metals from melt. In those crystallizing systems, the materials are more homogeneous with constant concentration or density of the crystallizing material. However, this is not the case for crystallizing oils and fats systems. Oils and fats are made up of a mixture of different types of triacylglycerols, each with its own distinctive melting point. Under isothermal crystallizing conditions, the density or concentration of the crystallizable component is not constant but is diminishing in concentration with time or the degree of crystallization.

In addition, the original equation developed was based on a model where the crystal growth is over a solid sphere. In the case of the so-called three-dimensional spheres assumed by the  $\beta$  and  $\beta'$  crystals of oils and fats, it can be seen from the electron microscope pictures (12) that the spheres are not solid but contain a lot of empty spaces or voids.

It can be observed from microscope observations that as the crystal spherulites grew in size they began to impinge on each other at advance degree of crystallization. The form of the Avrami equation applied by most researchers to the crystallization of oils and fats does not take this impingement into consideration. This impingement at higher degree of crystallization could account for the deviations in the plots after the 70% crystallization level.

These deviations from the original concept could probably account for the deviation observed in the case of oils and fats crystallization and the fractional Avrami exponents obtained. This can also account for the observation that only the data obtained from 70% of the crystallization process can be utilized to determine the exponent, i.e., the deviation from the theory is still small enough at this degree of crystallization for the theory to hold. This would also imply that the amount of empty spaces in the crystallizing spherulite is still small compared to a solid sphere of crystal. The results obtained showed that where the fractional exponent is close to a whole integer the assignation of the Avrami exponent is more certain. Ambiguous assignations can occur if the fractional exponent is halfway between two integers. Added to this ambiguity is the "loss" of information or contribution from the last 30% of the crystallization process where large deviations from theory were observed. The question that needs to be answered is whether the data from the first 70% of the process is sufficient to represent the whole crystallization process. Further work in this area will have to be carried out to resolve this as well as to improve on the Avrami equation, taking into account the deviations from theory mentioned above.

The caution by Marangoni (8) on the misuse of a modified form of the Avrami equation is rightly justified within the context of the warning. However, if the equation is to be applied to the crystallization of oils and fats in order to elucidate information on the mechanisms of their nucleation and growth, the equation will have to be modified to suit the conditions prevailing in the system.

## Summary

From the above discussion, it can be seen that palm oil products tend to crystallize with an Avrami exponent of three except for palm stearin with an IV of 35 at higher temperatures where exponents higher than three were observed. From the Avrami exponent values observed, it can be concluded that the crystallization process of palm oil products is by sporadic or heterogeneous nucleation followed by two-dimensional growth, from the point of view of the growing site, although the final shape of the crystal mass is a sphere. However, the sphere is not solid, having empty spaces occurring within the sphere.

In calculating the Avrami exponent from DSC data, it was observed that fractional Avrami exponents are obtained, and not whole numbers, as is observed for the application of the equation to metal melts for which the theory was developed or in the majority of cases for polymeric crystallization from melts. In certain instances the practice of rounding off the Avrami exponent value could lead to ambiguity, especially where rounding off intermediate values between two integers, e.g., where exponents of 2.45 or 2.48 are obtained.

The Avrami equation can be used to probe the crystallization process of oils and fats up to a certain level of crystallization (70% in the case of palm oil products). Data from higher degrees of crystallization may distort the value of the Avrami exponent due to the large amount of empty spaces in the crystal mass as well as the other deviations from original theory. This may lead to a misinterpretation of the actual crystallization mechanism. A modified form of the Avrami equation will have to be derived for the conditions prevailing in oils and fats crystallization if the equation is to be fully exploited for the elucidation of information on their crystallization process.

## References

1. Avrami, Melvin, Kinetics of Phase Change I: General Theory, *J. Chem. Physics* 7: 1103–1112 (1939).
2. Ng, G.L., and C.H. Oh, Kinetic Study on Isothermal Crystallization of Palm Oil by Solid Fat Content Measurements, *J. Am. Oil Chem. Soc.* 71: 1135–1139 (1994).
3. Kawamura, K., The DSC Thermal Analysis of Crystallization Behavior in Palm Oil, *Ibid.* 56: 753–758 (1979).
4. Metin, Serpil, and Richard W. Hartel, Thermal Analysis of Isothermal Crystallization Kinetics in Blends of Cocoa Butter with Milk Fat or Milk Fat Fractions, *Ibid.* 75: 1617–1624 (1998).
5. Wright, A.J., R.W. Hartel, S.S. Narine, and A.G. Marangoni, The Effect of Minor Components on Milk Fat Crystallization, *Ibid.* 77: 463–475 (2000).
6. Herrera, M.L., C. Falabella, M. Melgarejo, and M.C. Anton, Isothermal Crystallization of Hydrogenated Sunflower Oil: II. Growth and Solid Fat Content, *Ibid.* 76: 1–6 (1999).
7. Dibildox-Alvarado, E., and T. Toro-Vazquez, Isothermal Crystallization of Tripalmitin in Sesame Oil, *Ibid.* 74: 69–76 (1997).
8. Marangoni, A.G., On the Use and Misuse of the Avrami Equation in Characterization of the Kinetics of Fat Crystallization, *Ibid.* 75: 1465–1467 (1998).

9. Timms, R.E., Crystallization of Fats, in *Developments in Oils and Fats*, edited by R.J. Hamilton, Blackie Academic & Professional, 1995, pp. 204–223.
10. Boistelle, R., in *Crystallization and Polymorphism of Fats and Fatty Acids*, edited by N. Gardi, and K. Sato, Marcel Dekker, New York, 1998, pp. 189–226.
11. Van den Tempel, M., in *Surface-Active Lipids in Foods*, SCI Monograph no. 32, Society of Chemical Industry, London, 1968, pp. 22–36.
12. Van Putte, K.P.A.M., and B.H. Bakker, Crystallization Kinetics of Palm Oil, *J. Am. Oil Chem. Soc.* 64: 1138–1143 (1987).

## Chapter 10

# Comparison of Experimental Techniques Used in Lipid Crystallization Studies

A.J. Wright, S.S. Narine, and A.G. Marangoni

Department of Food Science, University of Guelph, Guelph, Ontario, N1G 2W1, Canada

### Introduction

Crystallization of fats encompasses two distinct events: nucleation and crystal growth. While a stable nucleus must be formed before crystal growth can occur, these events are not mutually exclusive. Nucleation may take place while crystals grow on existing nuclei (1). In our investigations into the effects of minor components on milk-fat crystallization, it became clear that minor components delayed crystallization of the milk-fat triacylglycerols (TAG) (2). However, it was difficult to discern whether the effects were at the nucleation or crystal growth level. Distinguishing between nucleation and crystal growth constitutes a major challenge in lipid crystallization studies.

The shape of a crystallization curve can provide some insight into the mode of crystal growth (3). However, the nucleation step is more elusive because the methods typically used in these studies are relatively insensitive. Pulsed nuclear magnetic resonance (pNMR), which measures solid fat content (SFC), and light-scattering techniques, which measure absorbance or transmittance of light, are commonly used to monitor lipid crystallization. Anyone familiar with the pNMR method knows that, at times, small amounts of crystals are visible in the melt before any solids are detected. Clearly, at this stage, well beyond the induction time for nucleation, the pNMR signal is measuring crystal growth. Turbidimetry, while more sensitive than pNMR, *e.g.*, shorter induction times are obtained, also has its limitations. Crystallization times determined by turbidimetry correlated well with the mass deposition of fat (4). A very strong correlation was found between induction times by pNMR and turbidimetry for the three fat systems used in the minor components study, suggesting that increases in turbidity are also due to mass deposition of crystals and not only nucleation (2).

It would be beneficial to have a convenient way of unambiguously determining nucleation induction times when seeking to understand the effects of varying composition and processing conditions on nucleation, and it is essential if the induction times are used in mathematical models such the Fisher-Turnbull equation (5). In the Fisher-Turnbull model, activation energies of nucleation are calculated from nucleation induction times. The usual assumption is that the experimental

technique used to determine the induction time provides an accurate measure of the nucleation rate.

Induction times for this purpose have been determined using light-scattering techniques (6). Herrera *et al.* (7) used a modified laser-polarized light turbidimetric approach to obtain induction times, the details of which were described by Herrera (8). Polarized light microscopy (PLM) has also been used to visually observe the onset of nucleation (7,9). Similarly, nucleation and growth rates in palm oil were determined microscopically using polarized light in conjunction with a counting cell and graduated ocular (10). A similar method was automated using PLM in conjunction with a CdS photosensor. Instead of observing the sample visually, the sensor monitored the transmission of light through the crystallizing sample on a microscope slide (11). This is a very sensitive approach; however, the specialized equipment required is not commonly available. Differential scanning calorimetry (DSC) has also been used to monitor isothermal crystallization of lipids (12-14).

Induction times determined by pNMR, turbidity, and light-scattering measurements are compared to those determined using PLM in conjunction with image analysis. Isothermal DSC was attempted as a fifth method for comparison. However, because of the inherent lack of sensitivity at the high cooling rates required to obtain isothermal crystallization conditions, it was abandoned. This research was carried out in the context of our milk-fat minor components study (2).

## Experimental Procedures

Minor components (non-triacylglycerol species) were removed from anhydrous milk-fat (AMF) to obtain purified milk-fat TAG (MF-TAG) by column chromatography using Florisil as the stationary phase (2). As previously described, the crystallization behavior of the original AMF, the MF-TAG, and MF-TAG to which 0.1% milk-fat diacylglycerol was added (MF-DAG) was studied by pNMR and turbidimetry (2). Although crystallization was studied between 5.0 and 27.5°C, we will concentrate only on data collected at 22.5°C.

In addition, crystallization was followed using PLM at 22.5°C. AMF, MF-TAG, and MF-DAG were preheated to 80°C for 10 min before a drop of each was placed on a preheated (80°C) glass microscope slide and covered with a preheated (80°C) glass coverslip. The samples were imaged with a Zeiss polarized light microscope (Oberkochen, Germany) using a 10x objective and equipped with a CCD Video Camera (Sony, Tokyo, Japan). Temperature of the slide was maintained at 22.5°C. Crystallization was followed by capturing an image every 15 s for 30 min. The images were processed using Image Tool (The University of Texas Health Science Center, San Antonio, TX). A background subtraction was performed initially by subtracting the initial image (time = 0 s) for each AMF, MF-TAG, and MF-DAG from every other image in the respective crystallization run. The images were manually thresholded, using the same value for every image in each AMF, MF-TAG, and MF-DAG. The threshold level was that which was found to most accurately reflect the original

greyscale images. Once the images were thresholded, the relative amounts of black-and-white pixels in each image were determined. The amount of black (representing crystal mass) was plotted as a function of crystallization time.

For the light-scattering studies, a phase-transition analyzer (Phase Technology, Richmond, B.C., Canada) was used; 150  $\mu\text{L}$  of sample, preheated at 80°C for 30 min, was pipetted into the sample container of the analyzer, which was preheated and maintained at 75°C, using a thermoelectric cooler. Thereafter, the sample was rapidly cooled from 75 to 22.5°C at a controlled rate of 50°C/min. When the sample reached 22.5°C, it was held at this temperature, and crystallization was continuously monitored using an optical-scattering approach. In this set-up, a beam of light impinges on the sample from above. A matrix of optical sensors, in tandem with a lens system, is also placed perpendicularly above the sample. When crystals start to appear in the sample, the incident beam is scattered by the solid-liquid phase boundaries, and scattered light impinges via the lens onto the detectors. As more and more crystal mass develops, the signal output increases and is automatically recorded.

Crystallization curves for pNMR, turbidity, light-scattering, and image analysis were normalized by dividing each value by the maximum crystallization value. The resulting fractional crystallization values were compared. Induction times were determined by extrapolating the linear portion of the crystallization curves to the time axis and by baseline deviation as shown in Figure 1.

Induction times were taken as the time from when the samples were placed at 22.5°C until crystallization began. Strictly speaking, however, induction times

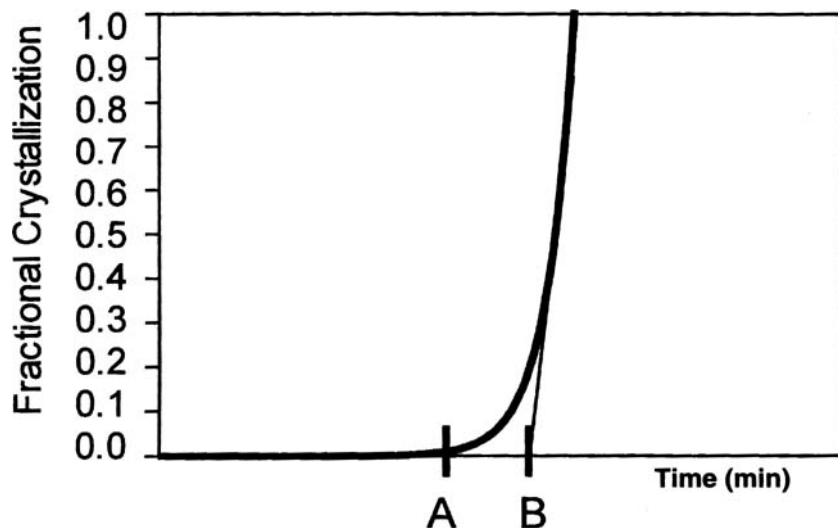


**Fig. 1.** Determination of crystallization induction times by baseline deviation (A) and linear extrapolation to the time axis (B).

should be taken from the point at which the sample reaches the crystallization temperature until crystallization is detected. In all experiments, however, it takes some time for isothermal conditions to be established. It is possible that differences in the cooling rates between the four methods could influence crystallization. This will be true regardless of how induction time is defined. Considering time zero as the point at which 22.5°C is reached ignores the fact that crystallization will occur between the melting temperature and 22.5°C. AMF, MF-TAG, and MF-DAG have Mettler dropping points of *ca.* 34°C (2). Therefore, during cooling below 34 and at 22.5°C, the fats experience the same degree of supercooling. This eliminates concerns of having different thermodynamic factors at work in the three fats and makes the comparison of their crystallization behaviors much easier to define. However, there are very real concerns regarding differences in cooling rates between the different experimental methods. The cooling curves for the pNMR, turbidity, and light-scattering are shown in Figure 2. A cooling curve was not determined for the microscopy experiment, although the temperature was found to equilibrate at 22.5°C within *ca.* 30 s. The rate constants of cooling for the initial decrease in temperature to the dropping point (34°C) are shown in Table 1.

Figure 2 and Table 1 show that the cooling for the pNMR and light-scattering is reasonably rapid and linear to 22.5°C. Similarly, the microscope slides reached the crystallization temperature very rapidly. This makes it easier to assign any differences observed between these experimental methods to the sensitivity of the

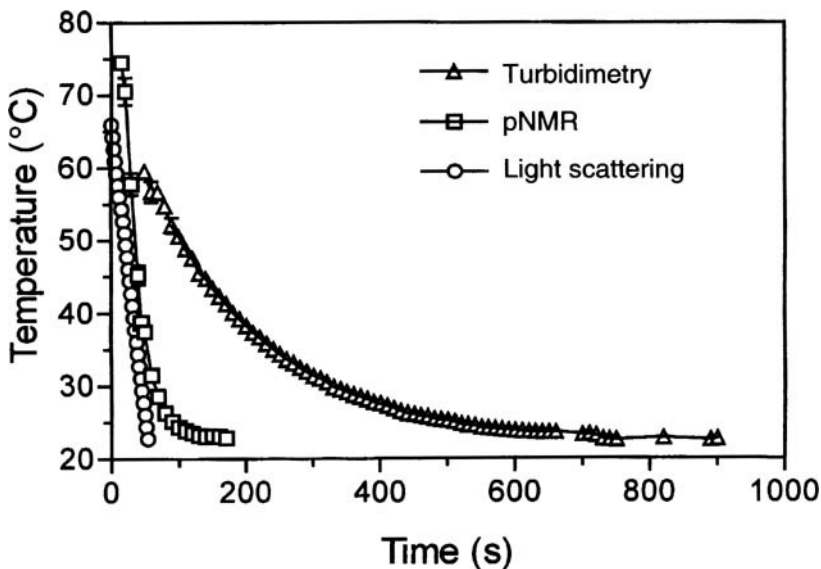


Fig. 2. Cooling curves for samples in pulsed nuclear magnetic resonance (pNMR), turbidimetric, light-scattering, and image analysis experiments.

**TABLE 1**

Rate of Cooling Determined from the Initial Linear Decrease in Temperature to 34°C for pNMR, Turbidimetry, and Light-Scattering Spectroscopy<sup>a</sup>

Experimental method	Cooling rate (°C/s)
pNMR	-1.060 ± 0.119
Turbidimetry	-0.156 ± 0.008
Light scattering	-0.774 ± 0.000

<sup>a</sup>pNMR, pulsed nuclear magnetic resonance.

methods, and not specifically to different cooling rates. Newtonian type cooling was observed for the turbidity experiments. This meant that 22.5°C was not reached for nearly 15 min. This is longer than most of the induction times determined for turbidimetry (Table 2). Therefore, these induction times actually correspond to crystallization at temperatures higher than 22.5°C, and we must be careful in drawing information from the results. In the cases where the crystallization temperature was attained very quickly and within approximately the same time frame (pNMR, light-scattering, and microscopy), the comparison between the methods is more appropriate. Every effort should be made to achieve rapid and linear cooling during crystallization experiments to avoid such complications. In the case of turbidimetry, this resulted because of the poor heat transfer between the sample and the surrounding metal cell holder through which cooling water was circulated. More efficient heat transfer was achieved when the glass pNMR tubes were plunged into a water bath at the crystallization temperature, in the chamber of the phase transition analyzer, and when the glass microscope slides were placed on a metal platform.

**TABLE 2**

Induction Times (min) Determined by Linear Extrapolation and Baseline Deviation for AMF, MF-TAG, and MF-DAG Monitored by pNMR, Turbidimetry, Light-Scattering Spectroscopy, and by Polarized Light Microscopy Coupled to Image Analysis. Average and Percent Error Reported<sup>a</sup>

By extrapolation	pNMR	Turbidimetry	Light-scattering	Microscopy
AMF	28.2 (4.2%)	14.9 (8.4%)	9.9 (0.5%)	3.0 (3.8%)
MF-TAG	14.7 (6.2%)	12.3 (11.8%)	6.7 (1.1%)	1.5 (3.0%)
MF-DAG	33.3 (4.9%)	12.9 (11.0%)	7.1 (0.7%)	5.3 (1.8%)
By baseline deviation				
AMF	21.7 (4.1%)	16.3 (8.1%)	7.5	3.0
MF-TAG	11.0 (9.1%)	11.8 (3.7%)	5.0 (10.0%)	1.5
MF-DAG	34.0 (5.9%)	12.7 (9.5%)	6.5	3.5

<sup>a</sup>AMF, anhydrous milk-fat; MF-TAG, milk-fat triacylglycerol; MF-DAG, milk-fat triacylglycerol with 0.1% milk-fat diacylglycerol. See Table 1 for other abbreviation.

## Results and Discussion

Figure 3 shows thresholded polarized light micrographs of MF-TAG at various crystallization times at 22.5°C. Crystallization curves for AMF, MF-TAG, and MF-DAG by pNMR, turbidity, and PLM-image analysis are shown in Figure 4. MF-TAG crystallized first, followed by AMF and MF-DAG. MF-DAG had the longest induction times determined by pNMR, while by turbidimetry and microscopy, AMF had the longest induction times. Crystallization curves for

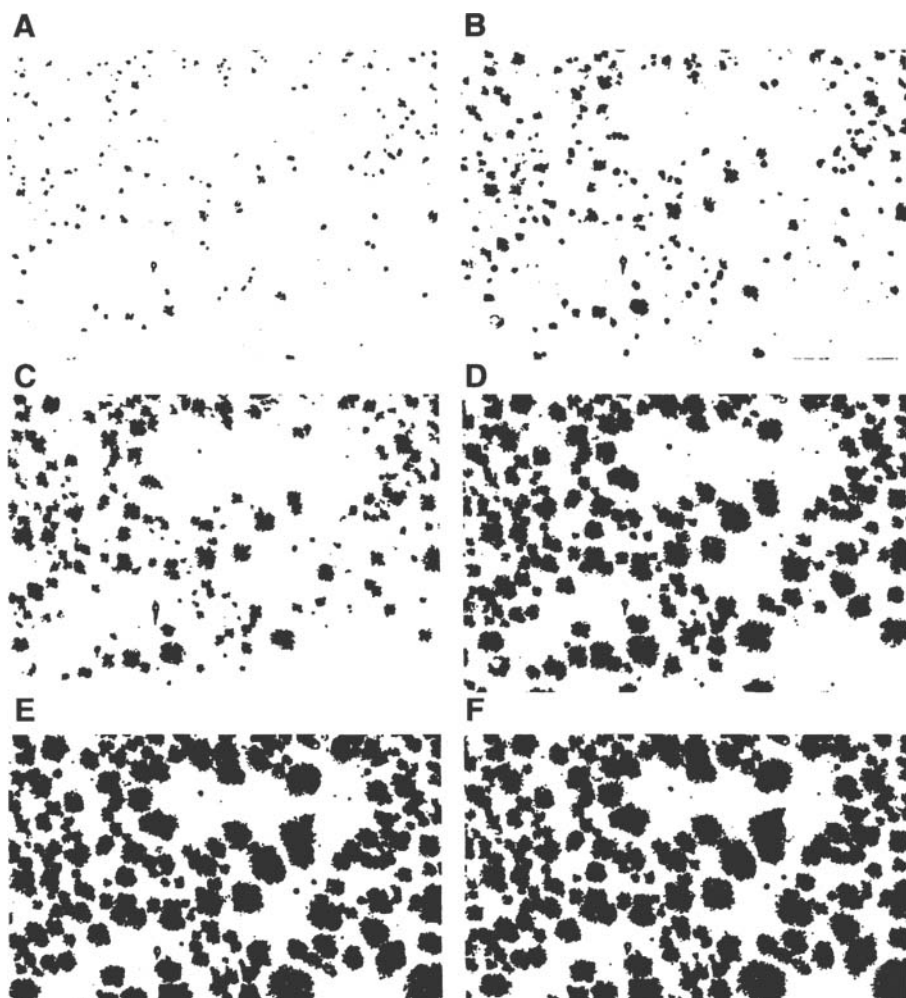


**Fig. 3.** Thresholded polarized light micrographs of milk-fat triacylglycerol (MF-TAG) at various crystallization times at 22.5°C: (A) 1 min, (B) 3 min, (C) 5 min, (D) 10 min, (E) 20 min, (F) 28 min.

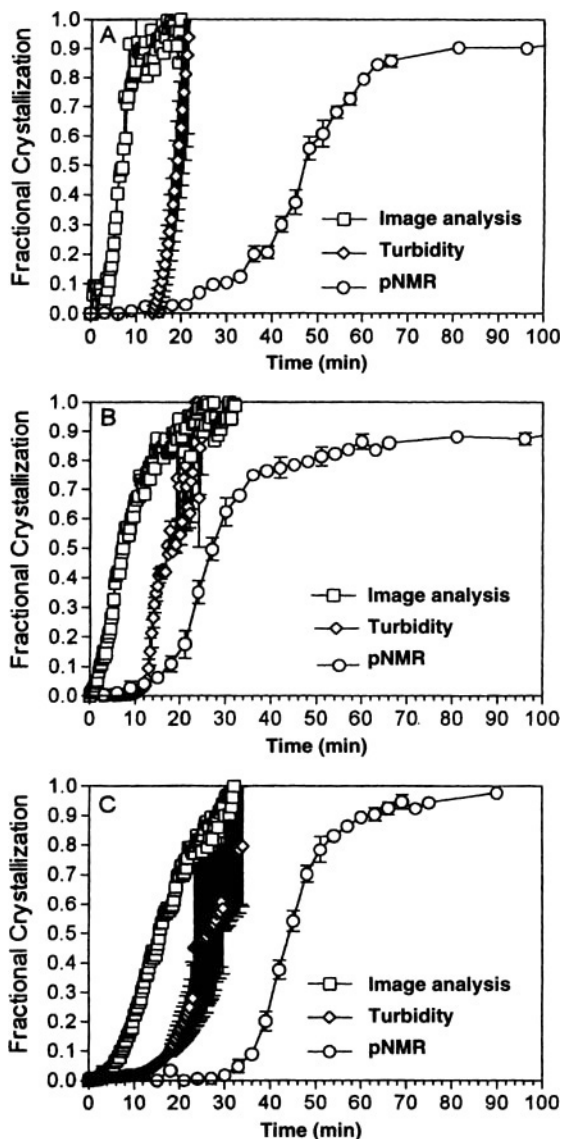


**Fig. 4.** Fractional crystallization of anhydrous milk-fat (AMF) (A), MF-TAG (B), and milk-fat MF-TAG with 0.1% milk-fat diacylglycerol (MF-DAG) (C) determined by pNMR measurements of solid fat content, turbidity measurements, and polarized light microscopy coupled to image analysis at 22.5°C. Symbols in (A) and (B) represent the average and standard errors of three replicates. See Figures 2 and 3 for other abbreviations.

AMF, MF-TAG, and MF-DAG obtained from measurements of light-scattering intensities are shown in Figure 5. In this case, MF-TAG crystallized first, and AMF had the longest induction times. The induction times for the crystallization curves are reported in Table 2.

Induction times determined as the time of deviation from the baseline were shorter than those calculated by extrapolation of the linearly increasing curves,

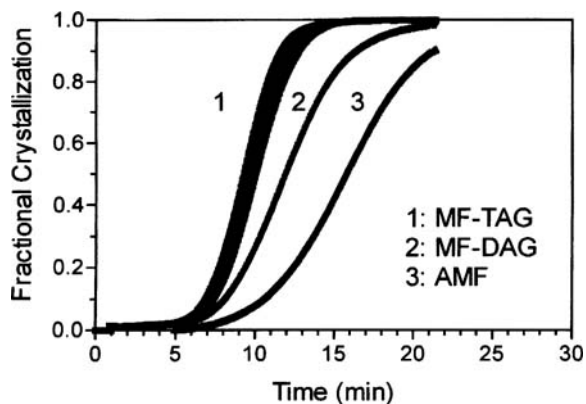


**Fig. 5.** Fractional crystallization of AMF, MF-TAG and MF-DAG determined by light-scattering spectroscopy. See Figures 3 and 4 for abbreviations.

although the same trends were observed. Also, Table 2 shows that while the relative trends were similar, there were large differences in the absolute value of onset times of crystallization between the four methods. Despite the fact that the absolute values for the induction times differed, removal of the minor components consistently decreased the induction times of the TAG. We can thus be certain that milk-fat minor components exhibit an inhibitory effect on TAG crystallization.

Table 2 shows that the induction times determined by pNMR were the longest, while those determined by the image analysis technique were the shortest. Therefore, with the image analysis approach, we were able to detect some early crystallization events beyond the sensitivity of the other methods. The higher sensitivity demonstrated allowed for the detection of early crystallization events, possibly in the vicinity of the true nucleation events.

A simple calculation can highlight the reason why the microscopic technique is more sensitive than pNMR and turbidity measurements. Solids in a 30-mg fat sample ( $\rho = 0.90 \text{ g/cm}^3$ ) with an SFC of 0.1% (w/w) occupy a volume of  $3.33 \cdot 10^{-11} \text{ m}^3$ . The volume of a spherical nucleus of 0.5  $\mu\text{m}$  diameter is  $6.54 \cdot 10^{-20} \text{ m}^3$ . If all of this solid mass corresponded to nuclei,  $5.1 \cdot 10^8$  nuclei would be present in this sample. An SFC of 0.1% is below the detection threshold of a pNMR machine. Two obvious conclusions can be drawn from these calculations. Even at 0.1% SFC, the solids present in the sample cannot solely correspond to nuclei, since their number would be too great. Microscopic observation of a typical 30-mg sample of crystallizing fat (0.1% SFC) should convince any skeptic that  $5.1 \cdot 10^8$  nuclei cannot possibly be present. This suggests that by the time SFC values reach 0.5-1.0%, a typical detectable level in a pNMR machine, significant amounts of crystal growth must have necessarily taken place. Therefore, an induction time of crystallization determined by pNMR does not correspond to the induction time for nucleation.

If cooling rates could be controlled in a better fashion, turbidimetry could be a more sensitive technique for the study of the early stages of a crystallization

process than pNMR. Poor heat transfer was the major disadvantage with the turbidimetric experiments, although there are other inherent limitations (see below). Turbidimetry relies on the scattering of light by newly formed, or growing crystals. Scattering produces two effects on the transmitted beam: (i) a loss of transmitted intensity due to scattering of the radiation at angles other than  $0^\circ$  (turbidity) and (ii) an apparent change in velocity of the transmitted beam (refraction). A change in the velocity of the transmitted beam due to scattering results in a change in the refractive index of the medium, which will itself affect the measured turbidity (see below).

The ratio of the intensity of the light beam after its passage through a sample ( $I$ ) over the intensity of the incident light beam ( $I_o$ ) is related to the concentration of scattering material by Beer's law:

$$\frac{I}{I_o} = e^{-\tau lc} \quad [1]$$

where  $\tau$  is a turbidity parameter ( $m^2/kg$ ) similar to an extinction coefficient,  $l$  is the sample thickness (m), and  $c$  is the concentration of scattering material ( $kg/m^3$ ). The signal measured in a common spectrophotometer is the absorbance (or transmittance) due to scattering,  $A_s = -\ln(I/I_o)$ . Hence,

$$A_s = \tau lc \quad [2]$$

The turbidity parameter ( $\tau$ ) is related to the Raleigh ratio at  $90^\circ$  ( $R_{90}$ ) by (15):

$$\tau = \frac{16\pi}{3} R_{90} \quad [3]$$

And the Raleigh ratio for a solution containing  $N$  scattering centers per unit volume is given by (15):

$$R_{90} = \frac{8\pi^4 \alpha^2}{\lambda^4} N \quad [4]$$

where  $\alpha$  is the molecular polarizability of the system, which is a function of the shape of the electron cloud and the frequency of the applied radiation, and  $\lambda$  is the wavelength of the applied radiation. Hence,  $\tau$  is proportional to the number of scattering centers per unit volume.

The molecular polarizability is related to the difference in refractive indices of the pure solvent and the solution/suspension by the relationship (15):

$$\alpha = \frac{n_s^2 - n_o^2}{4\pi N} \quad [5]$$

where  $n_s$  corresponds to the refractive index of the solution/suspension, and  $n_o$  corresponds to the refractive index of the pure solvent. Substituting Equations 3, 4, and 5 into Equation 2, we obtain the following expression for  $A_s$ :

$$A_s = \frac{8\pi^3 l (n_s^2 - n_o^2)^2}{3\lambda^4} \left( \frac{c}{N} \right) \quad [6]$$

The absorbance of light due to scattering is proportional to the ratio of the concentration of crystallized material to the number of scattering centers per unit volume. Hence, in the vicinity of a nucleation event, a small amount of mass is distributed among a large number of nuclei, resulting in a small value of  $c/N$ . This, in turn, results in a small value of  $A_s$ , which implies an inherent physical limitation in the ability of the technique to detect nucleation events. The reader should keep in mind that the simplified treatment shown above applies only to dilute solutions/suspensions, where scattering centers are small relative to the wavelength of the incident light.

Another complicating factor in the measurement of turbidity is the absorption of light by colored materials in the sample, thus reducing the intensity of the measured signal, and therefore the sensitivity of the technique. Impurities such as dust can contribute to high background scattering, reducing the signal-to-noise ratio. If the light used is not monochromatic, such as in the case of diode-array spectrophotometers, a distribution of scattering events at different wavelengths will take place. Signal intensity can be lost due to the presence of slits on the detector side of the spectrophotometer, which cut out much of the transmitted beam. As well, only a small volume element is sampled during measurement, roughly the diameter of the light beam. All of these factors result in a decrease in the sensitivity of the technique and its ability to detect nucleation events.

Light-scattering spectroscopy proved to be a more sensitive method than turbidimetry and pNMR. In this method, the intensity of scattered light, rather than the attenuation of the signal intensity ( $I/I_o$ ) is measured. The particular geometry of the sample cell and positioning of the detectors also maximize the collection of the scattered light. This technique proved to be very convenient, user-friendly, and reproducible.

PLM has inherent advantages over turbidimetry. The PLM technique exploits the difference in refractive index of a beam of incident light polarized in two perpendicular directions. This phenomenon is known as birefringence. Anisotropic materials, such as a fat crystal, will display birefringence. Since fat crystals are birefringent, they will appear as sharp bright objects in a nonbirefringent, and therefore dark, background. The use of polarizers set at  $90^\circ$  removes most of the nonbirefringent background signal (colored melt and scattering impurities), thereby considerably increasing the signal-to-noise ratio. As well, since all of the transmitted light beam in the field of view is collected by the lenses and focused on the camera, signal intensity and therefore sensitivity are increased.

Ultimately, the experimental technique of choice will depend on the application. pNMR provides the best method to characterize the overall crystallization process. For this reason it is suitable for use in the Avrami analysis. The water-bath-based cooling used in the pNMR experiments also offered rapid cooling and accurate temperature control. Both turbidity and scattering intensity signals tend to become saturated prior to the completion of the crystallization process. Thus, it is not possible to obtain reliable data on the latter stages of crystallization. Although turbidity seems to offer the advantage of improved sensitivity, in our experience there can be major errors associated with its measurement, concerns with poor reproducibility, and major challenges with temperature control. Light-scattering improves on this because it measures reflectance of light as opposed to transmittance. It offers extreme sensitivity to early crystallization events, is easy to use, and requires only a small volume of sample. Cooling rates and temperature can also be accurately controlled in the instrument. Microscopy coupled with image analysis also proved to be sensitive and had good temperature control, although it was the most cumbersome technique. It does have the advantage that morphological information can be acquired simultaneously as the kinetics are quantified.

### Acknowledgments

The authors would like to acknowledge Dr. Gorgon Chiu from Phase Technology (Richmond, B.C., Canada) for the light-scattering analysis.

### References

1. Sato, K., Crystallization Phenomena in Fats and Lipids, *J. Dispersion Sci. Technol.* 10: 363–392 (1989).
2. Wright, A.J., R.W. Hartel, S.S. Narine, and A.G. Marangoni, The Effect of Minor Components on Milk Fat Crystallization, *J. Am. Oil Chem. Soc.* 77: 463–475 (2000).
3. Sharples, A., *Introduction to Polymer Crystallization*, Edward Arnold Ltd., London, 1966, pp. 44–63.
4. Wang, F.S., and C.W. Lin, Turbidimetry for Crystalline Fractionation of Lard, *J. Am. Oil Chem. Soc.* 72: 585–589 (1995).
5. Strickland-Constable, R.F., Nucleation of Solids, in *Kinetics and Mechanism of Crystallization*, Academic Press, London, 1968, pp. 74–129.
6. Herrera, M.L., M. de Leon Gatti, and R.W. Hartel, A Kinetic Analysis of Crystallization of a Milk Fat Model System, *Food. Res. Int.* 32: 289–298 (1999).
7. Herrera, M.L., C. Falabella, M. Melgarejo, and M.C. Anon, Isothermal Crystallization of Hydrogenated Sunflower Oil: I-Nucleation, *J. Am. Oil Chem. Soc.* 75: 1273–1280 (1998).
8. Herrera, M.L. Crystallization Behaviour of Hydrogenated Sunflowerseed Oil: Kinetics and Polymorphism, *Ibid.* 71: 1255–1260 (1994).
9. Ng, W.L., A Study of the Kinetics of Nucleation in a Palm Oil Melt, *Ibid.* 67: 879–882 (1990).
10. van Putte, K.P.A.M., and B.H. Bakker, Crystallization Kinetics of Palm Oil, *Ibid.* 64: 1138–1143 (1987).

11. Koyano, T., I. Hachiya, T. Arishima, K. Sato, and N. Sagi, Polymorphism of POP and SOS. II. Kinetics of Melt Crystallization, *Ibid.* 66: 675–679 (1989).
12. Dibildox-Alvarado, E., and J.F. Toro-Vazquez, Isothermal Crystallization of Tripalmitin in Sesame Oil, *Ibid.* 74: 69–76 (1997).
13. Metin, S., and R.W. Hartel, Thermal Analysis of Isothermal Crystallization Kinetics in Blends of Cocoa Butter with Milk Fat or Milk Fat Fractions, *Ibid.* 75: 1617–1624 (1998).
14. Ng, W.L., and C.H. Oh, A Kinetic Study of Isothermal Crystallization of Palm Oil by Solid Fat Content Measurements, *Ibid.* 71: 1135–1139 (1994).
15. Campbell, I.D., and R.A. Dwek, Scattering, in *Biological Spectroscopy*, The Benjamin Cummings Publishing Company, Inc., Menlo Park, CA, 1984, pp. 217–238.

## Chapter 11

# Ultrasonic Characterization of Lipid Crystallization

**John N. Coupland**

Department of Food Science, The Pennsylvania State University, 103, Borland Lab,  
University Park, PA 16802

## Introduction

Food oils are mixtures comprised of a range of structurally similar triacylglycerol molecules with differing fatty acid substituents along with several other types of dissolved molecules (1). Because of the range of mutually soluble materials present in the melt, fats can have a range of solid-to-liquid ratios, depending on the composition, current environment, and history of the sample. The solid fat content is a crucial factor, determining various aspects of quality in many foods. While the details of crystallization are dealt with elsewhere in this volume and in the literature (1), it is important to note that, in many cases, there is no way to adequately predict the solid fat content of an unknown sample. Therefore a range of analytical methods has been developed capable of measuring the solids content of an oil mixture.

The earliest developed and frequently most precise technique is dilatometry. In this method the changes in volume on freezing of a fixed amount of oil is used to measure solid fat content. The equipment costs of a dilatometric method are relatively modest, but the experiments are often laborious and messy. Dilatometry remains a recommended method (Cd10-57) of the American Oil Chemists' Society (2) but has been largely replaced by various nuclear magnetic resonance methods (AOCS methods Cd16-81 and Cd16b-93). Nuclear magnetic resonance (NMR) exploits the differences in nuclear decay time of hydrogen nuclei in the solid and liquid phases. "Solid" nuclei decay in the order of a few ms while "liquid" remains can be polarized for several 100 ms. By making measurements at different times after the excitation pulse, it is possible to distinguish and quantitate the solid/liquid ratio. NMR is a true measure of solid fat content, whereas dilatometry is a relative method that provides only a related solid fat index. NMR instruments are frequently very expensive, but the experiments are easier than dilatometry and many samples can be rapidly measured on a single machine. Solid fat content can also be measured by differential scanning calorimetry (3), but this is not a standard method of the AOCS.

While these methods serve useful roles in research, product development, and quality-control laboratories, they are significantly limited. One important gap in the present techniques is that they cannot be adequately applied on-line. On-line measurements are always useful for automated control systems, but in the case of

lipid crystallization they are even more valuable because the extreme sensitivity of the material to small changes in temperature can bias even at-line measurements. In principle it would be possible to construct an on-line NMR coil, but an adequately large magnet would be prohibitively expensive. It would be impossible to use if the sample were contained in metal or was rapidly moving along a production line so any instrument could often not be applied in a real process environment.

Ultrasonics is in many ways the ideal measurement method for fat crystallization studies. The ultrasonic properties of a fat are strongly sensitive to solids content and can be measured in opaque fats and through container walls. In the present work I will describe the basic physics of ultrasonic waves, their interactions with matter (particularly with semi-solid fats), and their measurement. I will then describe ultrasonic studies of fat crystallization in bulk and emulsified fats. Finally I will use some measurements of the effect of applied shear on fat crystallization as an illustration of a study that could not be easily undertaken by other methods.

## Ultrasonics

### *Fundamentals of Sound Waves*

Sound is transmitted through materials as mechanical waves in physical structure. Because the material is being mechanically deformed by the passing wave, its ultrasonic properties contain useful information about its macroscopic and microscopic composition and structure.

Ultrasound is very high frequency sound (>20 kHz, often ~MHz) beyond the range of human hearing. Sound at high frequencies can often behave as a beam and can offer a usefully high degree of spatial resolution. The power levels used in sensing ultrasonics are low, and the deformations induced by the wave are small and reversible. In the sensing context, ultrasonics is therefore nondestructive and should not be confused with high power applications such as homogenization, welding, and cell disruption (4).

There are two distinct types of ultrasonic waves; the most commonly used in fats characterization are longitudinal waves (Fig. 1A) where deformations occur in the direction of propagation of the wave. It is also possible to generate shear waves with deformations normal to the direction of propagation (Fig. 1B). Shear waves do not travel macroscopic distances in fluids so it is often impossible to make good measurements in foods. Throughout this work I will exclusively focus on longitudinal waves.

A wave can be characterized by an amplitude, frequency, and wavelength which may change with time or distance traveled from the source. We can express both the storage and loss properties of a sonic wave moving in a material concisely as the real and imaginary parts of a complex wavenumber:  $k = \omega/c + i\alpha$ , where  $c$  is the speed of sound,  $\omega$  is the angular frequency ( $=2\pi f$ ),  $f$  is frequency,  $i = \sqrt{-1}$ , and  $\alpha$  is the attenuation coefficient. Ultrasonic properties are often frequency dependent so it is necessary to define the wavelength at which  $k$  is reported. The dependency of  $k$  on frequency is the basis of ultrasonic spectroscopy.

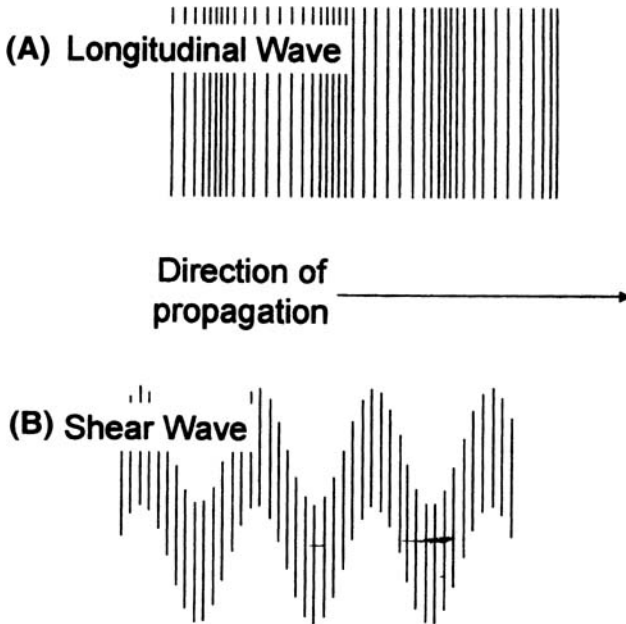


**Fig. 1.** Schematic diagram showing the features of a (A) longitudinal and (B) shear longitudinal wave. The solid lines represent the instantaneous positions of elements of the material structure as a sinusoidal acoustic wave passes.

### **Interactions with Food Materials**

The speed and attenuation of sound in a food material are of no practical value in themselves but only as they relate to other relevant material properties. Fundamentally, wavenumber is related to material properties *via* the Wood equation (5):

$$\left(\frac{k}{\omega}\right)^2 = \frac{\rho}{E} \quad [1]$$

where  $E$  is the adiabatic elastic modulus of the material, which is equivalent to the bulk modulus,  $K$ , for a fluid. When a beam of ultrasound passes through a bulk material (i.e., beam width less than sample width), there is some shearing at the beam edges because the compressed material has to move laterally against the uncompressed material, and  $K$  is replaced by  $K + 4/3 G$  where  $G$  is the shear modulus. Because  $K \gg G$ , longitudinal ultrasonic properties have only a weak and hard-to-measure dependence on bulk shear rheology. Although all of the material parameters in Equation 1 are complex, in many cases it is possible to neglect the imaginary component and rewrite it in the more widely known form ( $\kappa$  is the adiabatic compressibility =  $K^{-1}$ ):

$$c^2 = \frac{1}{\kappa\rho} \quad [2]$$

Speed of sound is thus directly and analytically related to bulk-material properties and becomes a useful measure of fat structure.

Ultrasonic velocity has been almost exclusively measured in ultrasonic studies of fat crystallization, but the attenuation coefficient also can reveal interesting information. As the sound wave passes, the fluid is alternately compressed and rarefied which results in the formation of rapidly varying temperature gradients. Heat energy is lost because the conduction mechanisms are inefficient (thermal losses) and together with molecular friction (viscous losses) cause an attenuation of the sound given by classical scattering theory (5):

$$\frac{\alpha_c}{f^2} = \frac{4\pi^2}{\rho c} \left( \frac{4\eta}{3} + \frac{(1-\gamma)\zeta}{C_p} \right) \quad [3]$$

where,  $\alpha_c$  is the classical attenuation coefficient,  $\gamma = C_p/C_v$ ,  $C_p$  and  $C_v$  are the specific heat at constant pressure and volume, respectively,  $\zeta$  is the thermal conductivity and  $\eta$  the viscosity. Classical scattering is often a severe underestimate of the attenuation of real lipid systems where scattering or the perturbation of certain fast physical and chemical reactions can cause much more significant losses (6,7).

### Measurement Methods

Various types of commercially available and specially constructed equipment are available for the measurement of the ultrasonic properties of fluids (8,9) including semi-solid fats. All require an electrical signal generator to excite ultrasonic vibrations in a transducer that propagate into the sample and are detected by another transducer (or the same one after a time interval). Some sort of time/voltage measuring apparatus, typically a digital storage oscilloscope, is required to measure the electrical signals.

The changes in the ultrasonic properties of fats on crystallization are so large that it is not always necessary to use the most precise ultrasonic equipment, and it is possible to use the more robust pulsed methods where the ultrasonic velocity is calculated from the time taken for the pulse to travel the known pathlength (from a water calibration) and attenuation from the logarithmic decrease in energy with distance (5). If required, the frequency dependence can be calculated from a Fourier transformation of the detected, board-band echo (10) or by using a series of single-frequency tone bursts. More precise measurements can be made using an interferometer (5) or a fixed pathlength resonator (11,12).

If transmission measurements are impossible, another approach is to measure the amount of sound reflected at the interface between the sample and a known solid—often the container wall. The amount of sound reflected is a function of the impedance mismatch between sample and solid defined by a reflection coefficient,  $R_{12}$ : where  $z$  is the acoustic impedance of the material ( $= cp$ ) (5).

$$R_{12} = \left( \frac{z_1 - z_2}{z_1 + z_2} \right)^2 \quad [4]$$

Whether constructing purpose-built apparatus or using off the shelf instrumentation, a certain amount of care is required to make good quality measurements. Good temperature control ( $\pm 0.1^\circ\text{C}$ ) is essential in precise ultrasonic experiments because the ultrasonic properties of fluids, and also the solids content of fats, are strongly temperature-dependant, e.g., the speed of sound in liquid oil changes *ca.*  $3 \text{ ms}^{-1}$  per  $1^\circ\text{C}$  temperature (13). When temperature control is not possible, good temperature measurements should be made and reported with the ultrasonic data. It is crucial that the reported temperature is homogeneous over the entire acoustic pathlength. Finally, perhaps the most common reason for poor acoustic data is the presence of entrained air bubbles in a food sample. Because bubbles attenuate sound so strongly, even 1 vol% of the correct-sized bubbles can make a material acoustically opaque. Smaller amounts, which may not be visible on casual inspection, will dominate the signal and overwhelm the effects of varying fat composition. Air cells can often be removed by gentle centrifugation or by degassing before an experiment.

## Measurements of Fat Crystallization

### *Bulk Fats*

Sound travels more quickly in solids than liquids, and by measuring the time for an ultrasonic pulse to move through a fixed pathlength of oil as a function of temperature, it is possible to measure the solids content (14). In a model system study, McClements and Povey (14) showed that each percentage of insoluble triacyl glycerol added to paraffin oil gave an increase of about  $3.1 \text{ ms}^{-1}$  in the speed of sound. The technique was relatively insensitive to the type of triglyceride and thus a useful general measurement of solid fat content. Modern instrumentation is capable of an accuracy of *ca.*  $\pm 0.1 \text{ ms}^{-1}$  corresponding to *ca.* 0.03% solid fat content. While it may not be possible to realize this precision in a real processing environment, even if it were an order of magnitude worse, it would be comparable to an off-line NMR measurement (2).

It is relatively easy to determine an empirical correlation line to measure the solids content of a mixture of soluble and insoluble fats (a good straight line was shown up to  $\phi = 0.5$ ), but these authors (14) were also able to show that the Wood equation (Eq. 2) may also be used to give some theoretical basis to the measurement. For a two-phase system with small density differences between the phases and particle sizes less than ultrasonic wavelength, the density ( $\rho$ ) and adiabatic compressibility ( $\kappa$ ) in Equation 2 are given by volume fraction ( $\phi$ ) weighted averages:  $\kappa = (1 - \phi)\kappa_1 + \phi\kappa_2$  and  $\rho = (1 - \phi)\rho_1 + \phi\rho_2$  (subscripts 1 and 2 refer to the

dispersed and continuous phases, respectively). By substituting  $\kappa = c^{-2}\rho^{-1}$  (Eq. 2) for each phase, the volume fraction is given as the solution of the following quadratic equation:

$$\phi = \frac{-B - \sqrt{B^2 - 4AC}}{2A} \quad [5]$$

where

Volume fraction can be converted into the more familiar solid fat content from the

$$A = c_1^2 \left( 1 - \frac{\rho_1}{\rho_2} \right) + c_2^2 \left( 1 - \frac{\rho_2}{\rho_1} \right) \quad [6]$$

$$B = c_2^2 \left( \frac{\rho_2}{\rho_1} - 2 \right) + c_1^2 \frac{\rho_1}{\rho_2} \quad [7]$$

$$C = c_2^2 \left( 1 - \frac{c_1^2}{c_2^2} \right) \quad [8]$$

densities of the component fats as solid fat content =  $100 \phi \rho^2 \rho^{-1}$ . The extended Wood equation worked well up to  $\phi = 0.2$  (14).

Comparisons of ultrasonic with NMR methods have shown that the former perform at least as well and better in the case of low levels of solids (15). The measurements are insensitive to the type of triglyceride used (14) but may show some dependency on any polymorphic transitions that may occur (16). However this technique has not been widely adopted nor has it received detailed review by the AOCS.

Ultrasonic measurements can also be used to estimate solids content by plotting speed of sound as a function of temperature. The speed of sound in lipids decreases with temperature, and overlaid on this, there is a sigmoidal increase in speed of sound on crystallization due to change in solid fat content. Results of a typical experiment are shown in Figure 2, where the speed of sound in a chocolate sample is measured as a function of temperature. The solid fat content can be measured by extrapolating the solid and liquid lines over the transition range. The solid fat content can then be calculated as:

where  $c$  is the measured ultrasonic velocity,  $c_s$  ( $c_l$ ) the velocity in pure solid fat

$$\text{SFC} = \frac{\frac{1}{c^2} - \frac{1}{c_1^2}}{\frac{1}{c_s^2} - \frac{1}{c_1^2}} \quad [9]$$

(liquid oil) extrapolated to the measurement temperature, and SFC = solid fat content. This equation was again derived from Equation 2 by assuming solid fats and liquid oils have similar density and behave ideally as a mixture (17). It should be noted that this approach is similar to differential scanning calorimetry in that it assumes that the extrapolations drawn are from pure liquid or solid fat.

Acoustic reflectance can also be used to estimate the onset of crystallization. In Figure 3 the reflection coefficient from the surface of a confectionary coating fat was measured as a function of temperature during cooling. As the solids content increases, the fat becomes more acoustically similar to solid used to transmit the solid (Eq. 4), and the reflection coefficient decreases. An important advantage of a reflectance method is that it is no longer necessary to maintain a fixed and known pathlength to measure the ultrasonic properties of the fat. It is therefore easier to noninvasively retrofit ultrasonic reflectance sensors on existing process equipment

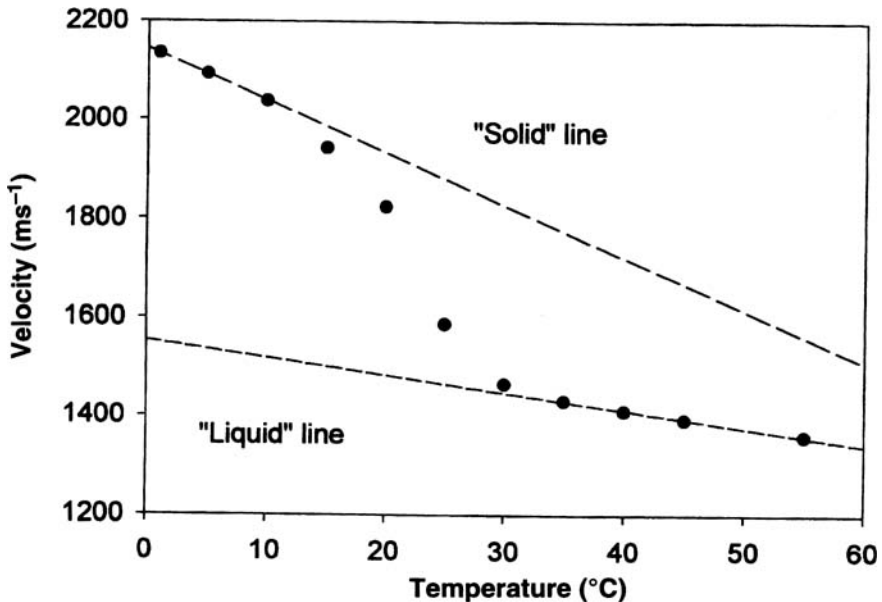


**Fig. 2.** Ultrasonic velocity in a commercial milk chocolate sample on cooling. The speed of sound increases from a low "liquid" value to a high "solid" value as the fat crystallized. The construction lines show how this curve can be used to measure solid fat content (see text for details).

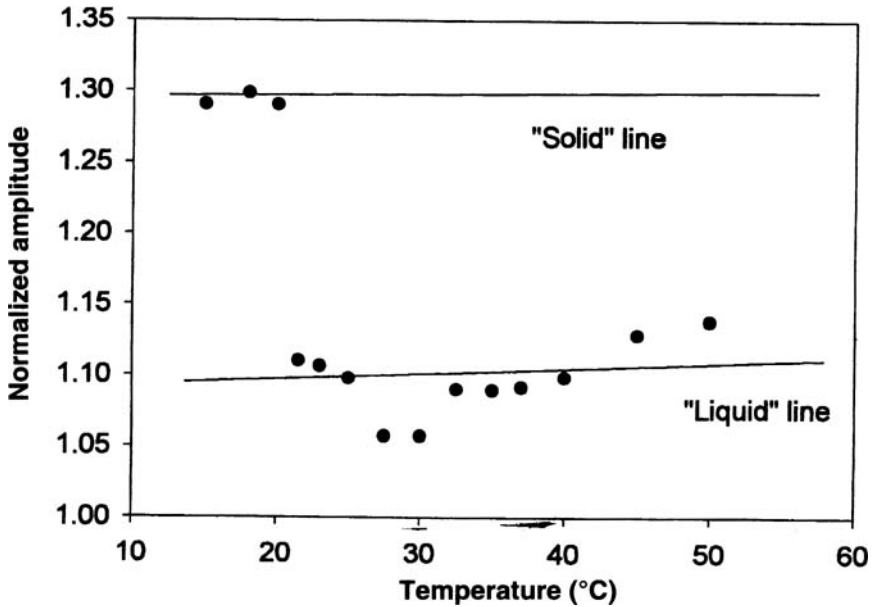


Fig. 3. Ultrasonic reflectance amplitude from the interface between a piece of Plexiglas and sample of confectionary coating fat during cooling. As the sample crystallized, it became more acoustically similar to the Plexiglas and less sound was reflected.

where there may be no appropriate pathlength available without extensive machine-shop work.

### ***Dispersed Fats***

The same techniques developed for bulk fats can be equally employed to measure the crystallization of emulsified oils. In these cases, the experiments tend to be easier as the contraction of the fat on freezing does not lead to the formation of air spaces in the sample, but, on the other hand, because a smaller volume of material is undergoing a phase transition, the magnitude of the signal change, and thus the precision, is lower.

Figure 4 shows the speed of sound in a 20 wt% emulsified hexadecane sample. There is a large hysteresis loop with a significant decrease in ultrasonic velocity at the bulk melting point and a similar increase several degrees below. The hysteresis is indicative of the high degree of supercooling frequently observed in fine emulsions (18). By extrapolating the solid and liquid portions of the lines to get a value of  $c_s$  or  $c_l$  at any temperature, it is possible to measure the solid fat content of the emulsion droplets (Eq. 9).

Analysis of the attenuation of a melting sample of emulsified fat gives some

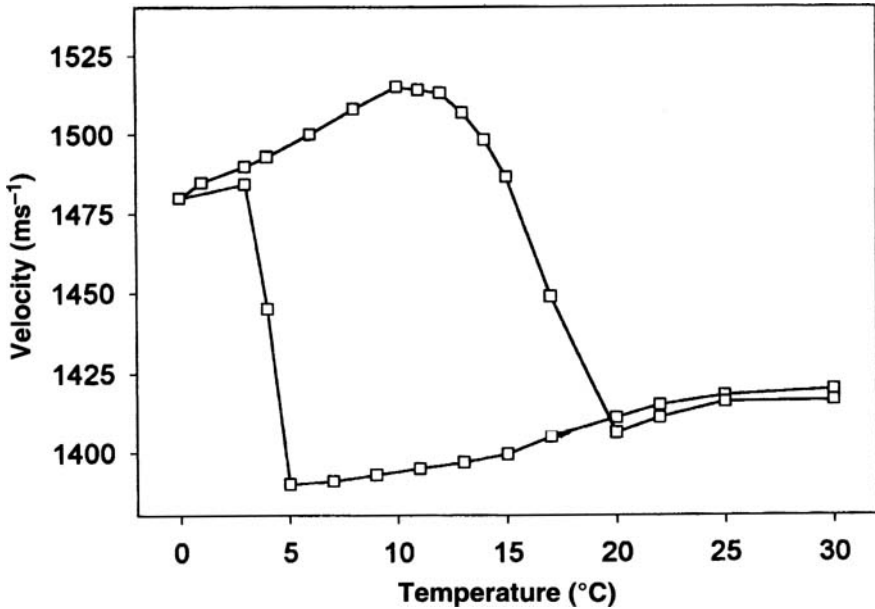


**Fig. 4.** Speed of sound in a sample of emulsified *n*-hexadecane (20 wt%). The ultrasonic velocity increases on freezing and decreases on melting. Note the large separation of freezing and melting points due to the extensive supercooling of emulsified fat.

indication of the molecular dynamics of the process. For example, the attenuation of a moderately concentrated emulsion is low except close to the melting point when there is also a large attenuation peak (and extensive velocity dispersion) (18). The pressure-temperature waves of the sound disrupt the solid-liquid equilibrium at the growing crystal surface, and some of the ultrasonic energy is lost as heat. The attenuation is strongly frequency-dependent in this temperature region because only over an intermediate region are the temperature-pressure gradients sufficiently large and persist for a sufficiently long time that an appreciable amount of material is able to undergo an ultrasonically induced phase transition. The excess absorption (and velocity dispersion) is related to the kinetics of the phase transition (6) and could be exploited to probe the molecular dynamics of the system.

### **Crystallization Under Shear**

The principles outlined in the above studies constitute the basics of ultrasonic measurements of fat crystallization. We now proceed to an investigation of the effect of changing model process conditions (shear rate) on fat crystallization behavior. These studies are facilitated by the relative ease by which ultrasonic sensors could be applied to a processing operation.

In order to study the effect of known shear on a fluid, it is necessary to control

the geometry through which deformation occurs and the rate of deformation. This is commonly achieved in rheometer design, but in order to study the effects of an applied shear field on a phase transition, it is necessary to incorporate some other solids-sensing principle. Garbolino and co-workers (19) constructed a shear rheometer with ultrasonic sensors to measure the crystallization of bulk and emulsified fat under shear illustrated in Figure 5. The ultrasound was transmitted from the transducer to the sample through a Plexiglas delay line. The ultrasonic part of the instrument was effectively a modified ultrasonic pulse-echo reflectometer similar to those described above (10), and the shearing part was the rotating inner cylinder of a concentric cylinder viscometer.

The results of a typical crystallization experiment for a confectionery coating fat are shown as Figure 6. The speed of sound in the liquid fat decreased approximately linearly with decreasing temperature consistent with data reported in the literature for liquid vegetable oils (13). At the crystallization point, there was a rapid decrease in signal with the increasing solids content. The onset of crystallization was seen as a discontinuity in the ultrasonic velocity with respect to temperature

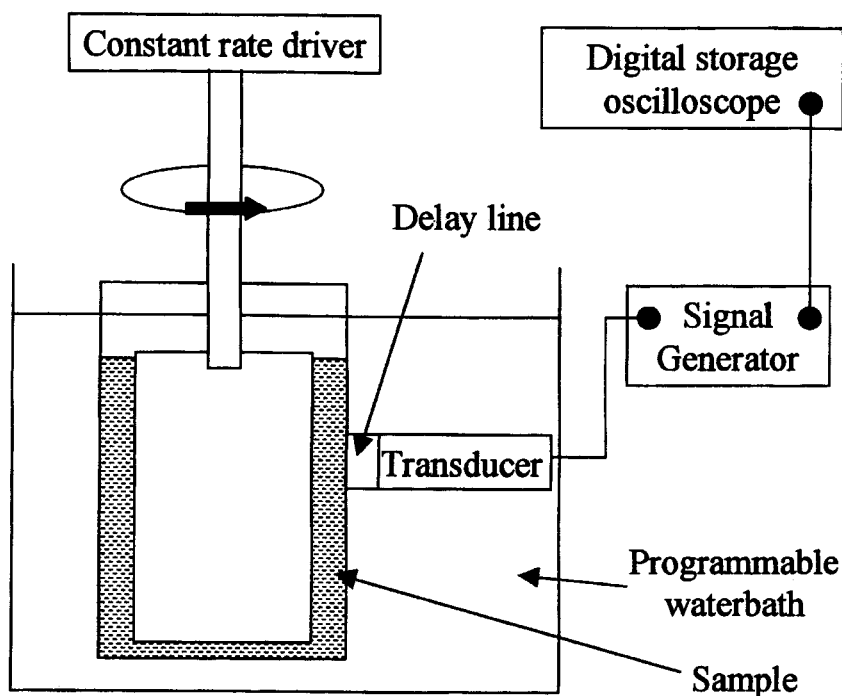


**Fig. 5.** Diagram illustrating an ultrasonic instrument designed to measure the speed of sound in a fluid under known shear conditions. The design is based on a combination of a pulse-echo ultrasonic reflectometer and a controlled-strain concentric cylinder rheometer.

(shown as arrows in Fig. 6). The temperature of the onset of crystallization increased with shear rate.

The same apparatus was used to measure the kinetics of emulsion crystallization under shear. McClements and co-workers (20) showed that supercooled liquid *n*-hexadecane droplets crystallize more rapidly when a population of solid *n*-hexadecane droplets are present. They hypothesized that a collision between a solid and liquid droplet could be sufficient to act as a nucleation event in the liquid. The frequency of collisions increases with the intensity of applied shear field, and hence shearing should increase the crystallization rate. A 50:50 mixture of solid and liquid *n*-hexadecane emulsion droplets was stored at  $6 \pm 0.01^\circ\text{C}$  in a water bath (i.e., between the melting points and freezing points of emulsified *n*-hexadecane). A constant shear rate ( $0$ – $200 \text{ s}^{-1}$ ) was applied to the emulsion in the shear cell, and ultrasonic velocities were determined as a function of time. The change in speed of sound was used to calculate the percentage solids in the system (Fig. 7). Surprisingly, there was no clear effect of increased shear rate. This could either be because increase in collision rate was relatively modest for the small particles used (in the order of 30% at the fastest rate) or because the time the interacting droplets remain in proximity is not affected by the applied shear.

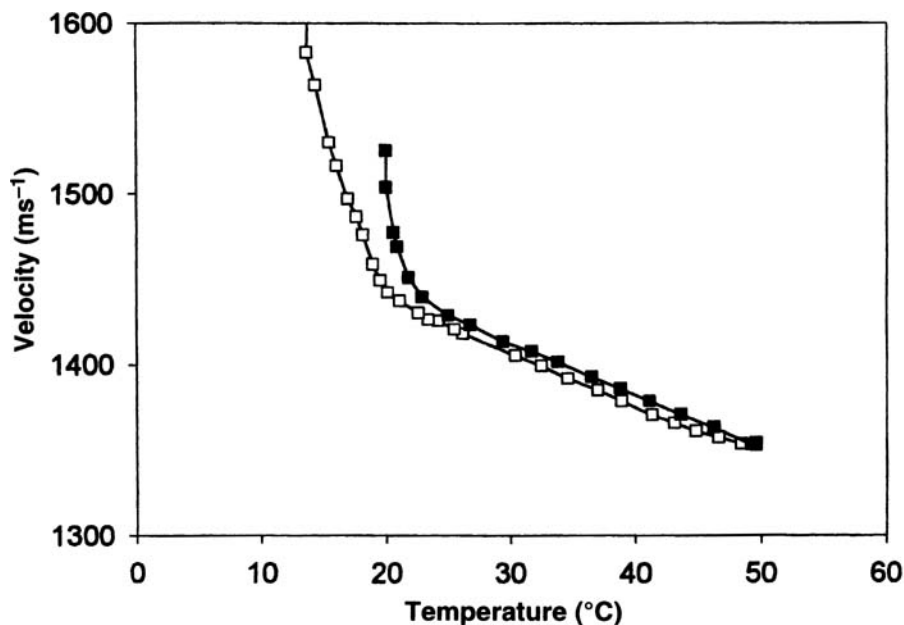


Fig. 6. Speed of sound during cooling of a sample of confectionary coating fat at a shear rate of  $0$  ( $\square$ ) or  $100 \text{ s}^{-1}$  ( $\blacksquare$ ).

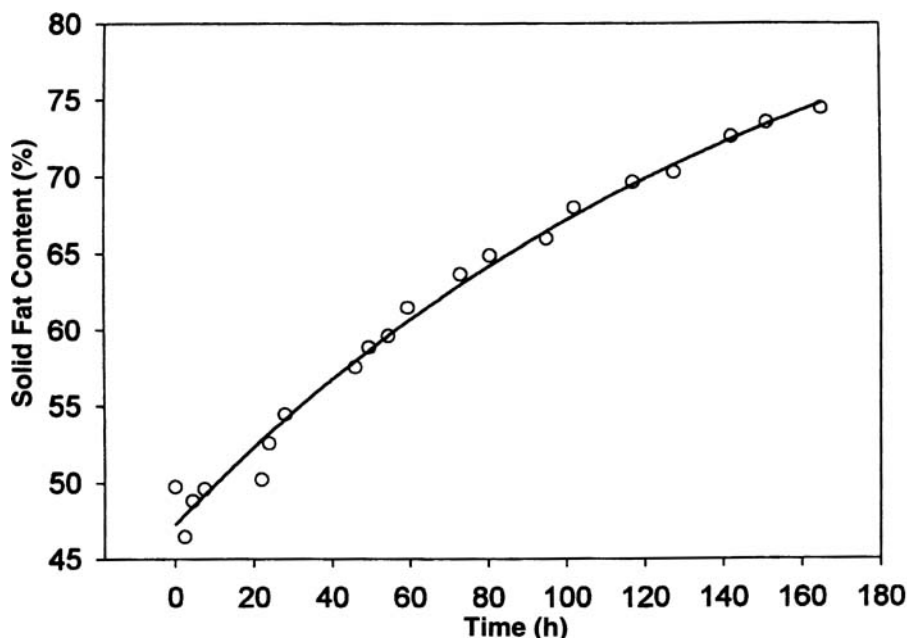


Fig. 7. Crystallization kinetics of mixtures 10 wt% liquid *n*-hexadecane emulsion droplets in the presence of 10 wt% solid *n*-hexadecane emulsion droplets at 6°C. Measurements were conducted at a shear rate of 100 s<sup>-1</sup>.

## The Future

Ultrasonic methods are perhaps the best tools available for studying fat crystallization under certain circumstances. They surpass the precision available with NMR, yet the experimental operation is as simple and the equipment costs are lower. Uniquely, ultrasonic sensors can be readily applied on-line with little cost in precision and, particularly using the new reflectance approach, minimal modification of existing process equipment.

The question remains: Why is this powerful method still seen as esoteric? The techniques discussed in this paper are largely based on 15-yr-old science. Many of the applications are new, and advances in electronics have made the experimental protocols easier, but still ultrasonic techniques have not been widely adopted. At least part of the answer is the home-made nature of much ultrasonic equipment means developing a method requires a significant time and monetary investment from an individual researcher.

Another reason is that ultrasound remains underappreciated. The scientific literature of 30 yr ago is full of hopeful arguments on the superiority of NMR to the then-preferred solid fats methods. Ultrasonics is in a similar position now. Wider acceptance and use of ultrasound will allow better study of the processes of lipid

crystallization. It will only come about with concerted action between respected professional groups (most usefully the AOCS), to establish protocols, and instrument manufacturers, to make easy-to-use instruments.

Ultrasound offers more to the lipid chemist than simple determination of solid fat content. By considering the frequency-dependency of the acoustic signals, it is possible to resolve many other aspects of crystallization. For example, McClements (18) convincingly argues that the attenuation peak seen in melting fat droplets is due to molecular relaxation at the solid surface, but there have been no subsequent efforts to use the relaxation time to characterize how fat melts. Another intriguing omission from current literature is that no studies have considered scattering of sound to be a solid-in-liquid fat dispersion. As well as relaxations due to physicochemical reactions, dispersed systems may scatter sound in a size-number-frequency-dependent manner. Measurement of a scattering profile has been successfully used to size emulsion droplets, but there has been no real effort to use ultrasonic spectroscopy to measure the size and microstructure of semi-solid fats.

I encourage lipid chemists to invest the resources to develop ultrasonic measurement methods. Existing technology can compete with existing solid fat measurement methods, and new theoretical developments offer the promise of much more.

### Acknowledgments

I am grateful to Chiara Garbolino, Raffaella Saggin, and Siva Vanapalli for making many of the measurements reported here and to Julian McClements and Gregory Ziegler for many helpful discussions.

### References

1. Lawler, P.J., and P.S. Dimick, Crystallization and Polymorphism of Fats, in *Food Lipids: Chemistry, Nutrition, and Biotechnology*, edited by C.C. Akoh and D.B. Min, Marcel Dekker, New York, 1998, pp. 229–250.
2. AOAC, *Official Methods of Analysis of AOAC International*, 16th Edn., AOAC International, Arlington, 1995.
3. Wunderlich, B., *Thermal Analysis*, Academic Press, San Diego, 1990.
4. Mason, T.J., Power Ultrasound in the Food Industry—The Way Forward, in *Ultrasound in Food Processing*, edited by M.J.W. Povey and T.J. Mason, Blackie Academic and Professional, London, 1998, pp. 105–126.
5. Blitz, J., *Ultrasonics: Methods and Applications*, Butterworths, London, 1971.
6. Matheson, A.J., *Molecular Acoustics*, John Wiley and Sons, London, 1971.
7. McClements, D.J., Comparison of Multiple Scattering Theories with Experimental Measurements in Emulsions, *J. Acoust. Soc. Am.* 91: 849–853 (1992).
8. Papadakis, E.P., The Measurement of Ultrasonic Velocity, in *Ultrasonic Measurement Methods*, edited by R.N. Thurston and A.D. Pierce, 1990, Academic Press, San Diego, 1990, pp. 81–106.
9. Papadakis, E.P., The Measurement of Ultrasonic Attenuation, in *Ibid.*, pp. 107–155.
10. McClements, D.J., and P. Fairley, Ultrasonic Pulse Echo Reflectometer, *Ultrasonics* 29: 58–62 (1991).

11. Eggers, F., and T. Funck, Ultrasonic Measurements with Milliliter Liquid Samples in the 0.5–100 MHz Range, *Rev. Sci. Instrum.* 44: 969–977 (1973).
12. Sarvazyan, A.P., Development of Methods of Precise Ultrasonic Measurements in Small Volumes of Liquids, *Ultrasonics*, 1982, pp.151–154.
13. Coupland, J.N., and D.J. McClements, Physical Properties of Liquid Edible Oils, *J. Am. Oil Chem. Soc.* 74: 1559–1564 (1997).
14. McClements, D.J., and M.J.W. Povey, Solid Fat Content Determination Using Ultrasonic Velocity Measurements, *Int. J. Food Sci. Tech.* 22: 491–499 (1987).
15. McClements, D.J., and M.J.W. Povey, Comparison of Pulsed NMR and Ultrasonic Velocity Measurements for Determining Solid Fat Contents, *Ibid.* 23: 159–170 (1988).
16. Kloek, W., P. Walstra, and T. Van Vliet, Nucleation Kinetics of Emulsified Triglyceride Mixtures, *J. Am. Oil Chem. Soc.* 77: 643–652 (2000).
17. Miles, C.A., G.A.J. Fursey, and R.C.D. Jones, Ultrasonic Estimation of Solid/Liquid Ratios in Fats, Oils, and Adipose Tissue, *J. Sci. Food Agric.* 36: 218–228 (1985).
18. McClements, D.J., M.J.W. Povey, and E. Dickinson, Absorption and Velocity Dispersion Due to Crystallization and Melting of Emulsion Droplets, *Ultrasonics* 31: 433–437 (1993).
19. Garbolino, C., G.R. Ziegler, and J.N. Coupland, Ultrasonic Determination of the Effect of Shear on Lipid Crystallization, *J. Am. Oil Chem. Soc.* 77: 157–162 (2000).
20. McClements, D.J., S.W. Han, and S.R. Dungan, Interdroplet Heterogeneous Nucleation of Supercooled Liquid Droplets by Solid Droplets in Oil-in-Water Emulsions, *Ibid.* 71: 1385–1389 (1994).

## Chapter 12

# Solid Fat Index vs. Solid Fat Content: A Comparison of Dilatometry and Pulsed Nuclear Magnetic Resonance for Solids in Hydrogenated Soybean Oil

G.R. List, K.R. Steidley, D. Palmquist, and R.O. Adlof

Food Quality and Safety Research, National Center for Agricultural Utilization, ARS, USDA,  
1815 N. University St., Peoria, IL 61604

## Introduction

The determination of solid fats is one of the most important tests employed by the edible oil industry. Historically the SFI introduced in the 1940s has been replaced by NMR methods now referred to as SFC (1–19). We report here a comparison of solid fat determinations based on official AOCS methods using dilatometry and pulsed NMR (1).

## Experimental Procedures

SFI determinations were conducted according to the official AOCS method at temperatures of 10, 21.1, 26.7, 33.3, and 40°C. SFC was determined by pulsed NMR according to the official AOCS method at the aforementioned temperatures. The instrument was a Bruker Minispec (Bruker Instrument Company, Toronto, Ontario, Canada).

The margarine/spread oils were isolated by heating the formulated products in a microwave oven for a short time, followed by centrifugation. The margarine [iodine value (IV) 69] and shortening (IV 83) basestocks were commercially prepared products supplied by C&T Refinery (Charlotte, NC). Simulated margarine oils were prepared by blending 40% IV 69 hydrogenated basestock with 60% unhydrogenated, refined, bleached, and deodorized soybean salad oil (C&T Refinery). The emulsifiers used in this study were fluid lecithin (Lucas Meyer, Decatur, IL), mixed mono and diglycerides (Eastman Kodak, Rochester, NY), and sunflower oil monoglycerides (Archer Daniels Midland, Decatur, IL).

## Results and Discussion

The study focused on four types of samples formulated from hydrogenated and liquid soybean oil: (i) margarine/spread oils isolated from commercially formulated products, (ii) commercially hydrogenated margarine (IV 69) and shortening (IV 83) basestocks, (iii) margarine/spread oils formulated in the laboratory by blending

the IV 69 soybean oil with additional liquid soybean oil, and (iv) margarine/spread oils containing added emulsifiers, i.e., lecithin, mono/diglyceride, monoglycerides. Results are presented in Tables 1–4, respectively. Data given in Tables 1–3 show that solid content at 10°C is consistently higher by NMR than by dilatometry, which is in agreement with other studies (15,19). In general, measurements made at 21.1–40.0°C are in closer agreement by both methods. The effects of emulsifiers on the dilatometric method were investigated, and the results are shown in Table 4. Although the relative concentrations of emulsifiers had little, if any, effect on SFI values, their presence has a tendency to yield higher SFI values at all temperatures compared to the control not receiving added emulsifiers. However, these differences are not statistically significant. The observation that emulsifiers can be a source of errors in SFI measurements has been attributed to migration of the indicator from the oil interface within the dilatometer tube (2).

## Statistics

A statistical summary comparing the dilatometric—SFI and (NMR methods is shown in Table 5 where standard deviations at 5 temperatures (10–40°C) are

**TABLE 1**

Solid Fat Content<sup>a</sup> of Commercial Margarine Spread Oils by Dilatometry (SFI) and Pulsed NMR (SFC)<sup>b</sup>

Sample	Solid fat at temperature (°C)									
	10.0		21.1		26.7		33.3		40.0	
	SFI	SFC	SFI	SFC	SFI	SFC	SFI	SFC	SFI	SFC
1	9.9	12.1	5.4	5.0	3.9	3.4	1.9	1.2	0.3	0.1
2	9.7	12.7	5.1	5.4	3.8	3.9	2.0	1.7	0.6	0.5
3	8.3	10.4	5.2	5.5	3.8	3.7	2.3	1.6	0.5	0.2
4	8.7	11.0	5.2	5.5	3.9	3.5	1.9	0.9	0.4	0.2
5	11.3	14.7	6.3	6.5	3.9	3.9	1.5	1.1	0.0	0.0
6	9.0	10.7	5.5	5.2	4.0	3.9	2.2	1.3	0.5	0.4
7	9.7	12.8	4.4	5.0	2.8	3.1	1.4	1.2	0.0	0.0
8	13.9	18.1	8.0	8.8	4.8	5.1	0.9	0.8	0.0	0.0
9	13.5	18.0	7.5	8.3	4.7	4.8	1.0	0.9	0.0	0.0
10	25.1	33.5	13.0	14.6	7.8	8.2	1.7	1.5	0.0	0.0
11	20.1	26.3	10.6	12.1	7.4	6.8	3.0	2.7	0.0	0.0
12	19.6	26.4	10.2	11.3	5.2	6.0	0.3	0.4	0.0	0.0
13	15.0	20.7	8.0	9.2	5.0	5.4	2.5	2.1	0.2	0.0
14	19.5	24.9	9.8	10.2	5.9	5.2	1.6	0.9	0.1	0.0
15	19.6	24.9	12.4	13.0	8.6	8.5	3.0	2.3	0.1	0.0
16	21.1	27.4	12.2	13.1	7.8	7.8	2.2	1.6	0.0	0.1
17	21.7	27.8	12.2	13.5	8.4	8.8	2.9	2.6	0.0	0.0

<sup>a</sup>Means of triplicates—three different days.

<sup>b</sup>SFI by AOCS Method Cd 10-57, SFC by AOCS Method Cd 16-81 (Ref. 1). SFI, solid fat index; NMR, nuclear magnetic resonance; SFC, solid fat content.

**TABLE 2**

SFC and Shortening Basestocks by Dilatometry (SFI) and Pulsed NMR (SFC)

Oil <sup>b</sup>	Solid fat <sup>a</sup> at Temperature (°C)									
	10.0		21.1		26.7		33.3		40.0	
	SFI	SFC	SFI	SFC	SFI	SFC	SFI	SFC	SFI	SFC
Margarine	59.1 ± 1.1	73.7 ± 0.3	46.5 ± 1.3	54.1 ± 0.3	40.5 ± 0.9	44.7 ± 0.3	22.1 ± 0.8	22.3 ± 0.0	3.2 ± 0.3	3.3 ± 0.1
Shortening	26.5 ± 1.0	36.3 ± 0.1	11.7 ± 0.5	13.7 ± 0.5	4.1 ± 0.3	4.6 ± 0.2	0.0 ± 0.5	0.0 ± 0.1	0.0 ± 0.6	0.0 ± 0.0

<sup>a</sup>Means of triplicates—SFI by AOCS Method Cd 10-57, SFC by AOCS Method Cd 16-81 (Ref. 1).<sup>b</sup>Hydrogenated soybean oil. See Table 1 for abbreviations.**TABLE 3**SFC of Blends of Margarine Basestocks and Liquid Soybean Oil by Dilatometry (SFI) and Pulsed NMR (SFC)<sup>a</sup>

% Hyd. oil	% Liq. oil	Solid fat <sup>a</sup> at temperature (°C)									
		10.0		21.1		26.7		33.3		40.0	
		SFI	SFC	SFI	SFC	SFI	SFC	SFI	SFC	SFI	SFC
5	95	0.5	1.4	0.1	0.4	0.0	0.2	0.0	0.0	0.0	0.0
10	90	2.9	4.6	1.0	1.2	0.0	0.3	0.0	0.0	0.0	0.0
15	85	5.4	7.8	2.4	2.7	0.7	1.0	0.0	0.3	0.0	0.0
20	80	7.8	10.8	4.1	4.4	1.5	2.1	0.0	0.0	0.0	0.0
25	75	10.5	14.0	5.7	6.7	2.9	3.4	0.6	0.5	0.0	0.0
30	70	13.7	17.2	7.9	8.6	4.5	5.0	0.9	1.0	0.0	0.0
40	60	19.4	24.2	12.3	13.4	8.2	8.8	2.4	2.8	0.0	0.0
50	50	25.5	31.5	17.2	19.0	12.5	13.3	4.4	4.0	0.0	0.0

<sup>a</sup>SFI by AOCS Method Cd 10-57, SFC by AOCS Method Cd 16-81 (Ref. 1). See Table 1 for abbreviations.

**TABLE 4**Effect of Emulsifiers on SFI Values by Dilatometry<sup>a</sup> (Simulated Margarine Oil—40% Margarine Basestock/60% Soybean Oil)

Emulsifier <sup>b</sup>	Conc. %	Solid fat <sup>a</sup> at temperature (°C)				
		10.0	21.1	26.7	33.3	40.0
None/Control	0	18.6 ± 0.1	11.1 ± 1.2	8.0 ± 0.3	2.2 ± 0.0	0.0 ± 0.3
Lecithin	0.1	19.8 ± 0.2	12.7 ± 0.2	8.7 ± 0.3	2.6 ± 0.2	0.0 ± 0.4
Lecithin	0.2	19.8 ± 0.4	12.4 ± 0.2	8.6 ± 0.4	2.5 ± 0.5	0.0 ± 0.6
Lecithin	0.3	19.4 ± 0.3	12.2 ± 0.4	8.3 ± 0.5	2.4 ± 0.4	0.0 ± 0.4
Mono/diglycerides	0.1	19.4 ± 0.6	12.3 ± 0.3	8.2 ± 0.1	2.3 ± 0.3	0.0 ± 0.2
Mono/diglycerides	0.2	20.3 ± 0.4	12.6 ± 0.2	8.6 ± 0.2	2.4 ± 0.4	0.0 ± 0.3
Mono/diglycerides	0.3	19.5 ± 0.6	12.0 ± 0.6	8.2 ± 0.3	2.6 ± 0.3	0.0 ± 0.3
Lecithin/mono/digly.	0.1	19.5 ± 0.1	12.4 ± 0.1	8.4 ± 0.3	2.4 ± 0.1	0.0 ± 0.3
Lecithin/mono/digly.	0.2	19.2 ± 0.6	12.3 ± 0.3	8.3 ± 0.6	2.2 ± 0.5	0.0 ± 0.3
Lecithin/mono/digly.	0.3	19.6 ± 1.0	12.3 ± 0.5	8.5 ± 0.7	2.5 ± 0.4	0.0 ± 0.7
Monoglycerides	0.3	19.6 ± 0.4	12.2 ± 0.3	8.5 ± 0.2	2.5 ± 0.2	0.0 ± 0.3
Monoglycerides	0.4	19.5 ± 1.0	12.3 ± 0.5	8.5 ± 0.5	2.3 ± 0.1	0.0 ± 0.1
Monoglycerides	0.5	19.1 ± 0.3	12.0 ± 0.1	8.1 ± 0.2	2.1 ± 0.1	0.0 ± 0.4

<sup>a</sup>Triplicate determination, AOCS Method Cd 10-57 (Ref. 1).<sup>b</sup>Lecithin fluid, Myverol mono/diglycerides, monoglycerides distilled from sunflower.

**TABLE 5**  
Statistical Evaluation of SFI and SFC Data<sup>a</sup>

Sample	Method	Standard deviation range					Equations for SFI/SFC correlation	R <sup>2</sup>
		Temperature (°C)						
		10.0	21.1	26.7	33.3	40.0		
Commercial spreads	SFI	0.0–1.1	0.1–0.8	0.1–0.4	0.1–0.5	0.0–0.8	SFI = 1.98 + 0.72*SFC – 0.035*Temp	0.98**
	SFC	0.1–0.5	0.1–0.9	0.0–1.9	0.1–0.4	0.1–0.3		
Basestocks	SFI	1.0–1.1	0.5–2.1	0.3–0.9	0.5–0.8	0.3–0.6	SFI = –40.94 + 1.22*SFC + 1.03*Temp	0.99**
	SFC	0.1–0.3	0.1–0.5	0.2–0.3	0.0–0.3	0.1–0.2		
Blends (basestocks/liquid oil)	SFI	0.1–1.1	0.1–1.2	0.0–0.8	0.1–0.4	0.1–0.5	SFI = –0.94 + 0.82*SFC + 0.02*Temp + 0.02*%	0.99**
	SFC	0.0–0.5	0.0–0.5	0.0–0.7	0.0–0.4	0.1–0.5		

<sup>a</sup>See Table 1 for abbreviations.

given. In general, the accuracy of the methods is equivalent, and standard deviations for each method fall within the ranges reported in the official AOCS methods. Equations are given for converting SFC data to SFI data, and the correlation coefficients of 0.98–0.99 are highly significant.

## References

1. *Official and Tentative Methods of the American Oil Chemists' Society*, 4th Edn., edited by D. Firestone, American Oil Chemists' Society, Champaign, IL, 1989 rev. to 1995/99. Solid Fat Index Cd 10-57, Dropping Point Cc 18-80, Solid Fat Content (SFC) Cd 16-81 SFC, Low-Resolution NMR Cd 16-93.
2. *Solid Fat Content by Pulsed NMR*, Bruker Minispec Group, Toronto, Ontario, 1998–2000.
3. Fulton, N.D., E.S. Lutton, and R.L. Willie, A Quick Dilatometric Method for Control and Study of Plastic Fats, *J. Am. Oil Chem. Soc.* 31: 98–103 (1954).
4. Bailey, A.E., and E.A. Kraemer, Dilatometric Investigation of Fats I. Apparatus and Techniques for Fat Dilatometry, *Oil and Soap* 21: 251–253 (1944).
5. Singleton, W.S., and A.E. Bailey, Dilatometric Investigations of Fats, Estimation of Solids and Liquid in Some Plastic Fats, *Ibid.* 22: 295–299 (1945).
6. Kraemer, E.A., and A.E. Bailey, Dilatometric Investigations of Fats VI. Dilatometric Behavior of Some Plastic Fats Between °C and Their Melting Points, *Ibid.* 21: 254–256 (1944).
7. Bailey, A.E., and W.S. Singleton, Dilatometric Investigations of Fats III. The Density, Expansibility, and Melting Dilation of Some Simple Triglycerides and Other Fats, *Ibid.* 22: 265–271 (1945).
8. Craig, B.M., W.O. Lundberg, and W.F. Geddes, Dilatometric Studies of Pure Triglycerides and Mixtures, *J. Am. Oil Chem. Soc.* 29: 128–133 (1952).
9. Houghton, A.J., K. VanPutte, and L.F. Vermas, Determination of the Solid Content of Fats by Wide Line Nuclear Magnetic Resonance: The Signal of Liquid Oils, *Ibid.* 49: 153–156 (1972).
10. Walker, R.C., and W.A. Bosin, Comparison of SFI, DSC and NMR Methods for Determining Solid-Liquid Ratios in Fats, *Ibid.* 48: 50–53 (1971).
11. Anon., Report of the Instrumental Techniques Committee, AOCS 1971–1972, *Ibid.* 49: 431A–433A (1972).
12. VanPutte, K., L.F. Vermas, J. VanDerEnden, and C. DerHollander, Relations Between Pulsed NMR, Wide Line NMR, and Dilatometry, *Ibid.* 52: 179–181 (1975).
13. Mills, B.L., and F.R. VanDeVoort, Comparison of the Direct and Indirect Wide Line Nuclear Magnetic Resonance Methods for Determining Solid Fat Content, *Ibid.* 58: 776–778 (1981).
14. Houghton, A.J., L.F. Vermas, and C. DerHollander, Determination of Solid-Liquid Ratio of Fats by Wide Line Nuclear Magnetic Resonance: The Signal of Liquid Oils, *Ibid.* 48: 7–9 (1971).
15. Pohle, W.D., J.P. Taylor, and R.L. Gregory, A Comparison of Nuclear Magnetic Resonance and Dilatometry for Estimating Solid Contents of Fats and Shortenings, *Ibid.* 42: 1075–1078 (1965).
16. VanDunhoven, J., G. Goedappel, C.M. Grobnan, and V.K.S. Shukla, Solid Fat Content Determination by NMR, *Inform* 10: 479–484 (1999).

17. Ferken, W.P., and R.E. Morse, Wide-Line Nuclear Magnetic Resonance of Liquid/Solid Content of Soybean Oil at Various Degrees of Hydrogenation, *Food Technol.* 17: 1099–1068 (1963).
18. Chapman, D., R.E. Richards, and R.W. Yorke, A Nuclear Magnetic Resonance Study of the Liquid/Solid Content of Margarine Fat, *J. Am. Oil Chem. Soc.* 37: 243–246 (1960).
19. Taylor, J.R., W.D. Pohle, and R.L. Gregory, Measurements of Solids in Triglycerides Using Nuclear Magnetic Resonance Spectroscopy, *Ibid.* 41: 177–180 (1964).

## Chapter 13

# Elasticity of Fractal Aggregate Networks: Mechanical Arguments

Alejandro G. Marangoni and Suresh S. Narine

Center for Food and Soft Materials Science, University of Guelph, c/o Department of Food Science, Guelph, ON N1G 2W1, Canada

## Introduction

The structural network of many soft viscoelastic materials of industrial interest is the product of an aggregation process of molecules into particles and of particles into increasingly larger clusters, until a space-filling three-dimensional network is formed (Fig. 1). Macroscopic properties such as hardness, opacity, and structural stability are directly influenced by this underlying network. Of particular importance is the relationship between network structure and elastic properties. Mathematical formulations for the relationship of the elastic modulus of an aggregate network to the amount and spatial distribution of network mass have been

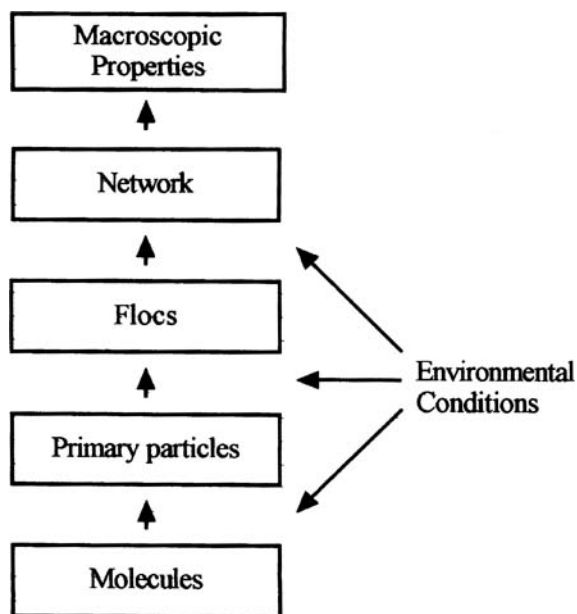


**Fig. 1.** Structural hierarchy of a particulate aggregate network.

developed using fractal scaling relationships (1–10). However, elasticity is not solely influenced by the amount and spatial distribution of network mass, but also by particle properties, including size, shape, mechanical properties, and particle-particle interactions (5,7–9). A general and exact formulation for the relationship between the elastic modulus and the amount of solid material in an aggregate network, considering both particle properties and their spatial distribution in the network, is therefore required.

Early developments of a theory to explain the elastic properties of colloidal gels were carried out by W.D. Brown and R.C. Ball at Cambridge (1). Brown and Ball formulated a power-law relationship of the shear elastic modulus ( $G$ ) to the volume fraction of network mass ( $\Phi$ ), namely  $G \sim \Phi^\mu$ , where  $\mu$  was related to the mechanism of particle aggregation, which ultimately determines the final spatial distribution of network mass. This formulation was subsequently verified experimentally, and the theory further developed by other groups (3–5,7). In 1990, Shih *et al.* (6) outlined the development of a scaling theory to explain the elastic properties of colloidal gels by again considering the structure of the gel network, like their predecessors did, as a collection of close-packed fractal flocs of colloidal particles (Fig. 2). However, these authors also defined two separate rheological regimes, depending on the relative strength of the interfloc links *vis-a-vis* that of the flocs. Their formulation of the strong-link regime (applicable at low-volume fractions), where the flocs yield under an applied stress, was identical to that of Brown and Ball. Their formulation of the weak-link regime (applicable at high-volume fractions), where the interfloc links yield under an applied stress, differed from that suggested by Brown and Ball. The main objectives of the above-mentioned studies were to explore the influence of spatial distribution of network mass on elastic properties and to infer a particle aggregation mechanism responsible for network formation. However, the elastic properties of such materials are not solely influenced by the amount and spatial distribution of network mass, but also by particle properties, including size, shape, mechanical properties, and particle-particle interactions (5,7–9). A general and exact formulation for the relationship between the  $G$  and the volume fraction of gel network material, considering both particle properties and their spatial distribution within the network, is therefore required. In this letter we develop such a model, maintaining consistency with the models developed by Shih *et al.* (1).

## Model

In this treatment we will consider the case where spherical particles are distributed in an aperiodic, fractal fashion within flocs. These flocs form chains which pack in a space-filling (close-packed), periodic fashion, forming a three-dimensional network. The volume fraction of particles in the network ( $\Phi$ ) is given by:

$$\Phi = \frac{V_a N_a N_c N_\xi}{V} \quad [1]$$

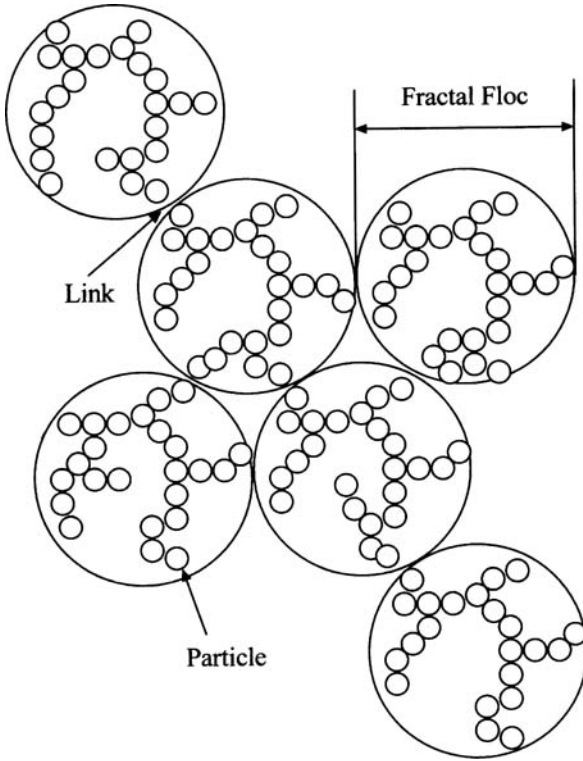


**Fig. 2.** Putative microstructure of a fractal colloidal aggregate network.

where  $V_a$  is the volume of an individual particle,  $N_a$  is the number of particles in a floc,  $N_c$  is the total number of chains of flocs in the system,  $N_\xi$  is the number of flocs per chain, and  $V$  is the volume of the network. The number of particles in a floc scales as (5):

$$N_a \sim \left(\frac{\xi}{a}\right)^D \quad [2]$$

where  $\xi$  is the diameter of the flocs,  $a$  is the diameter of the particles within the floc, and  $D$  is the fractal dimension for the arrangement of particles within the floc. The volume fraction of particles within the floc ( $\Phi_\xi$ ) is therefore given by:

$$\Phi_\xi \sim \frac{N_a V_a}{N_s V_s} \sim \left(\frac{\xi}{a}\right)^{D-d} \quad [3]$$

where  $N_s$  is the number of available embedding space elements within the floc ( $N_s \sim (\xi/a)^d$ ),  $V_s$  is the volume of an element of embedding space, and  $d$  is the Euclidean dimension. In this treatment we have assumed that the volume of a parti-

cle volume is equal to the volume of an element of embedding space, namely  $V_a = V_s$ . Thus, the diameter of the flocs varies with the volume fraction of particles within the floc as:

$$\xi \sim a\Phi_\xi^{\frac{d}{d-D}} \quad [4]$$

Flocs pack in a space-filling, Euclidean fashion; hence, at the floc level of structure, the material can be considered as an orthodox amorphous substance. Within the flocs, however, particles pack in a non-Euclidean, fractal fashion. For such a structural arrangement, the volume fraction of particles in a floc ( $\Phi_\xi$ ) is equivalent to the volume fraction of particles in the entire system ( $\Phi$ ), namely  $\Phi_\xi = \Phi$ . This well-known relation of polymer physics (11) has been experimentally shown to also apply to colloidal aggregates above their gelation threshold (12).

For a one-dimensional compression, where the flocs deform under an applied stress (strong-link regime), the Young's modulus of the system ( $\epsilon$ ) is equal to  $\epsilon = (1/3)N_c\epsilon_c$ , where  $\epsilon_c$  corresponds to the Young's modulus of a chain of flocs. Moreover, the Young's modulus of a chain of flocs, where the flocs correspond to springs, is given by  $\epsilon_c = \epsilon_\xi/N_\xi$ , where  $\epsilon_\xi$  is the Young's modulus of an individual floc (spring), and  $N_\xi$  is the number of flocs (springs) per chain. For spherical particles within a fractal floc, an expression for the  $G$  of the system can be obtained considering Equations 1, 2, and 4, namely:

$$\epsilon \sim \frac{2VE_\xi}{\pi a^3 N_\xi^2} \Phi^{\frac{d}{d-D}} \quad [5]$$

In this treatment, we will consider a square network of volume  $L^3$ . The area of one floc face scales as  $\xi^2$ , and the number of flocs per chain ( $N_\xi$ ) is approximated by  $L/\xi$ . Also, the Young's modulus of the flocs is related to the corresponding force constant of the flocs by  $\epsilon_\xi = k_\xi \xi / A_\xi$ , where  $A_\xi$  corresponds to the area of a floc face upon which the force is applied ( $A_\xi \sim \xi^2$ ). Considering the above in light of Equations 4 and 5, the  $G$  of the system in the strong-link regime can then be expressed as:

$$\epsilon \sim \frac{2k_\xi \xi L}{\pi a^3} \Phi^{\frac{d}{d-D}} \quad [6]$$

The elastic properties of a fractal floc are dependent on the elasticity of the effective backbone for stress transduction (6,10). This tortuous chain of particles serves as a pathway for the transduction of stress across the floc. Shih *et al.* (6) used an expression for the force constant of a long chain of springs derived by Kantor and Webmann (13) in their theoretical development of the strong-link rheological regime of colloidal gels. The force constant of an infinitely long chain of particles

( $k_c$ ) where only bending of bonds (springs) between particles is allowed, i.e., no bond stretching allowed, has the form:

$$k_c = \frac{B_c}{N_{bb} S_{\perp}^2} \quad [7]$$

where  $B_c$  is the bending elastic energy of the chain,  $N_{bb}$  is the number of springs per chain, and  $S_{\perp}^2$  is the radius of gyration of the projection of the chain nodes in the (Force  $\times$  (normal displacement) plane).

Shih *et al.* (1) proposed that this expression could be used to represent the force constant of an entire fractal floc. The assumption made is that the elastic properties of the floc are given by an effective backbone of stress transduction—a tortuous long chain of particles within the floc. Shih *et al.* (1) thus modified Kantor and Webman's expression, making the substitutions  $B_c = B_{\xi}$ ,  $N_{bb} \sim (\xi/a)^x$ , and  $S_{\perp} = \xi$ , to:

$$k_{\xi} = \frac{B_{\xi}}{\left(\frac{\xi}{a}\right)^x \xi^2} \quad [8]$$

where  $B_{\xi}$  is the bending elastic energy of the backbone,  $\xi$  is the diameter of the floc, and  $x$  is the tortuosity, or chemical length exponent, of the effective backbone ( $1 \leq x < 2$ ). By combining Equations 4 and 8 and introducing them into Equation 6, one obtains an expression for the Young's modulus of the network in the strong-link regime:

$$\varepsilon_{SLR} \sim \frac{2B_{\xi}L}{\pi a^3 \xi} \Phi^{\frac{d+x}{d-D}} \quad [9]$$

The main assumption made in this treatment is that the number of particles belonging to the effective backbone of stress transduction remains constant within the range of volume fractions studied.

For a one-dimensional compression, where the links between flocs deform under an applied stress (weak-link regime), it can be easily shown that the Young's modulus of the network is given by:

$$\varepsilon_{WLR} \sim \frac{2k_L d_o L}{\pi a \xi^2} \Phi^{\frac{1}{d-D}} \quad [10]$$

where  $k_L$  corresponds to the force constant of the inter-floc links, and  $d_o$  corresponds to the interfloc separation distance in the absence of an applied stress.

The expressions derived above for the weak and strong-link regimes are valid only in the region of particle volume fractions where  $\xi$  remains approximately constant.

The power of the theory developed by Shih *et al.* (1) lies in the fact that it is possible to experimentally determine if a system is in the strong- or weak-link. The strain at the limit of linearity increases as a function of the volume fraction of network material for the weak-link regime while it decreases for the strong-link regime. Below we derive expressions for the relationship between the strain at the limit of linearity and network material volume fraction.

The macroscopic strain on the network is given by:

$$\gamma = \frac{F}{A\varepsilon} \quad [11]$$

where  $F$ ,  $A$ , and  $\varepsilon$  correspond, respectively, to the force, area, and Young's modulus of the network. It is straightforward to show that:

$$\frac{F}{A} = \frac{F_c}{\xi^2} \quad [12]$$

where  $F_c$  is the force exerted on a chain of fractal flocs, which is equal to the force exerted on the springs within this chain of fractal flocs. This force would be transduced via deformation of interfloc links (weak-link regime) or by deformation of the flocs themselves (strong-link regime). By combining Equations 11 and 12, introducing the final expressions for the  $G$  in the strong- or weak-link rheological regimes and setting  $F_c = 1$  as the force at the limit of linearity, the following expressions are obtained for the relationship between the strain at the limit of linearity ( $\gamma_o$ ) and the volume fraction of network material:

$$\gamma_o(SLR) \sim \frac{\pi a \xi}{2B_\xi L} \Phi^{\frac{(1+x)}{d-D}} \quad [13]$$

$$\gamma_o(WLR) \sim \frac{\pi \xi^2}{2k_L d_o a L} \Phi^{\frac{1}{d-D}} \quad [14]$$

Thus, the strain at limit of linearity decreases as a function of increasing volume fraction of solids for networks in the strong-link regime, while it increases for networks in the weak-link regime.

In conclusion, exact relationships between the Young's modulus and the microstructure of particulate aggregate networks have been obtained. The elastic properties of such materials are a function of the total amount of solid material present, the properties of the particles which make up the solid, and the spatial distribution of solid particles within the network. This model can be utilized to better understand and modify the macroscopic rheological properties of soft materials and fat crystal networks in particular.

## Acknowledgment

This work was funded by the Natural Sciences and Engineering Research Council of Canada.

## References

1. Brown, W.D., The Structure and Physical Properties of Colloids, Doctoral Thesis, Department of Physics, University of Cambridge, Cambridge, England, 1987.
2. Ball, R.C., Fractal Colloidal Aggregates: Consolidation and Elasticity, *Physica D* 38: 13–15 (1989).
3. Sonntag, R.C., and W.B. Russel, Elastic Properties of Flocculated Networks, *J. Colloid Interface Sci.* 116: 485–489 (1987).
4. Buscall, R., P.D.A. Mills, J.W. Goodwin, and D.W. Lawson, Scaling Behaviour of the Rheology of Aggregated Networks Formed from Colloidal Particles, *J. Chem Soc. Faraday Trans. 1* 84: 4249–4260 (1988).
5. Bremer, L.G.B., T. van Vliet, and P. Walstra, Theoretical and Experimental Study of the Fractal Nature of the Structure of Casein Gels, *Ibid.* 85: 3359–3372 (1989).
6. Shih, W.H., W.Y. Shih, S.I. Kim, J. Liu, and I.A. Aksay, Scaling Behavior of the Elastic Properties of Colloidal Gels, *Phys. Rev. A* 42: 4772–4779 (1990).
7. Bremer, L.G.B., B.H. Bijsterbosch, R. Schrijvers, T. van Vliet, and P. Walstra, On the Fractal Nature of the Structure of Acid Casein Gels, *Colloids and Surfaces* 51: 159–170 (1990).
8. Narine, S.S., and A.G. Marangoni, Fractal Nature of Fat Crystal Networks, *Phys. Rev. E* 59: 1908–1920 (1999).
9. Narine, S.S., and A.G. Marangoni, Mechanical and Structural Model of Fractal Networks of Fat Crystals at Low Deformations, *Ibid.* 60: 6991–7000 (1999).
10. Urieu, N.B., and I. Ya Ladyzhinsky, Fractal Models in Rheology of Colloidal Gels, *Colloids and Surfaces A: Physicochem. Engineering Aspects* 108: 11 (1996).
11. De Gennes, P.G., *Scaling Concepts of Polymer Physics*, Cornell University Press, Ithaca, New York, 1979.
12. Dietler, G., C. Aubert, D.S. Cannell, and P. Wiltzius, Gelation of Colloidal Silica, *Phys. Rev. Lett.* 57: 3117–3120 (1986).
13. Kantor, Y., and I. Webman, Elastic Properties of Random Percolating Systems, *Ibid.* 52: 1891–1894 (1984).

## Chapter 14

## Development and Use of a Novel Technique to Measure Exchange Between Lipid Crystals and Oils

Paul Smith<sup>a</sup>, Negin Haghshenas<sup>a</sup>, and Björn Bergenståhl<sup>b</sup>

<sup>a</sup>The Institute for Surface Chemistry, Box 5607, S-114 86 Stockholm, Sweden, and

<sup>b</sup>Department of Food Technology, The University of Lund, S-221 00 Lund, Sweden

### Introduction

#### *Interactions Between Solid and Liquid Triglycerides*

Interactions between lipid crystals and liquids are very important industrially. Critical interactions can occur over the short term during the manufacture of a product, and control of these is vital in producing a desired product. However longer-term interactions over the lifetime of a product can lead to a severe loss in its quality.

A particular problem is the phenomenon of chocolate bloom. This is caused by an unwanted polymorphic change of the crystals of cocoa butter from Form V to Form VI (1,2). Mechanisms for this polymorphic transformation are currently being developed by various authors (3,4). The transformation causes a loss of gloss and a subsequent graying of the chocolate's surface (5). While this process does exist in solid chocolate bars and other "chocolate only" products, the problem is exacerbated by the presence of an oily filling (e.g., praline, nut, or truffle) in a chocolate product (6). This is because the polymorphic transformation appears to be *via* the liquid phase (7). Thus the migration of the oil from the filling through the chocolate and its interaction with the fat crystals are critical to the process. This behavior in chocolate systems has been characterized by Ziegleder *et al.* (8–10). However there has been little attempt to monitor oil migration and crystal–liquid interactions in pure systems, and thereby to determine the underlying mechanisms fundamental to the process.

In order to monitor the interactions of fats in pure systems, it is necessary to find species that can be easily handled and analyzed. One possible technique is by the use of microscopy and fluorescence-labeled species. However, this leads to the problem of the behavior of the large chemically distinct fluorescent tails that must be added to the molecules in order to detect them. Another way of detecting molecules is by radiolabeling and radiodetection. This technique has the advantage that the labeled molecules are chemically identical to the unlabeled ones, therefore, unwanted artifacts should not be present.

## **Experimental Development**

An experimental set-up was devised that allows for the monitoring of interactions between liquid oils and solid fat crystals. A saturated solution of  $^{14}\text{C}$  labeled triglyceride oil is added to a controlled amount of triglyceride crystals. There is then an exchange between the radiolabeled triglyceride in the solution and the triglyceride from the crystals (Fig. 1). Because only the triglyceride in the original solution is radiolabeled by measurement of the change in radioactivity of the solution with time, it is possible to measure the rate of interaction of the oil and fat. Thus the rate of interaction between the two phases can be determined. The experimental plan is illustrated schematically in Figure 2. It can be used to monitor interactions between any liquid and solid triglyceride.

As a first experiment, it was decided to measure the interaction of liquid and  $\beta$ -tripalmitin in a medium-chain triglyceride (MCT) oil.

## **Materials and Methods**

### **Materials**

*Lipid Crystals.* Tripalmitin (>99% pure) (PPP; obtained from Sigma Chemical Co., Stockholm, Sweden) was used. Crystals were recrystallized in hexane to give well-characterized  $\beta$ -crystals. Their surface area was measured by Brunauer, Emmett, and Teller analysis to be  $2.077\text{ m}^2/\text{g}$ .

*Oil.* MCT oil (supplied by Karlshamns AB, Karlshamn, Sweden) was used.

*Radiolabeled Fats.* Radiolabeled PPP ( $^{14}\text{C}$ -PPP obtained from American Radio Chemicals, St. Louis, MO) was used as probe.

*Organic Solvents.* Analytical-grade hexane was used for recrystallization of PPP crystals and also as part of the mobile phase of the radiodetector. It was mixed with Ultima-Flo AP (supplied by Packard Instruments, Meriden, CT) in the radiodetector.

### **Methods**

*$^{14}\text{C}$ -Detector.* A Packard Radiomatic 150TR  $^{14}\text{C}$ -radiodetector (Packard Instruments, Meriden, CT) was used for detection of the radiolabeled compounds.

*Preparation of the Saturated MCT Oil with  $^{14}\text{C}$ -Labeled PPP.* Oversaturated solutions of  $^{14}\text{C}$ -PPP in MCT oil (20 mL) were prepared by adding an excess amount of  $^{14}\text{C}$ -PPP (supplied in organic solvents) to the oil. The organic solvents were then vaporized over several hours, and the dispersion of  $^{14}\text{C}$ -PPP crystals in MCT oil was centrifuged for about 30 min. The upper phase was then removed and used as the liquid phase in the experiments. Saturated solutions of  $^{14}\text{C}$ -PPP in MCT oil were prepared at temperatures from 7 to  $25^\circ\text{C}$ .

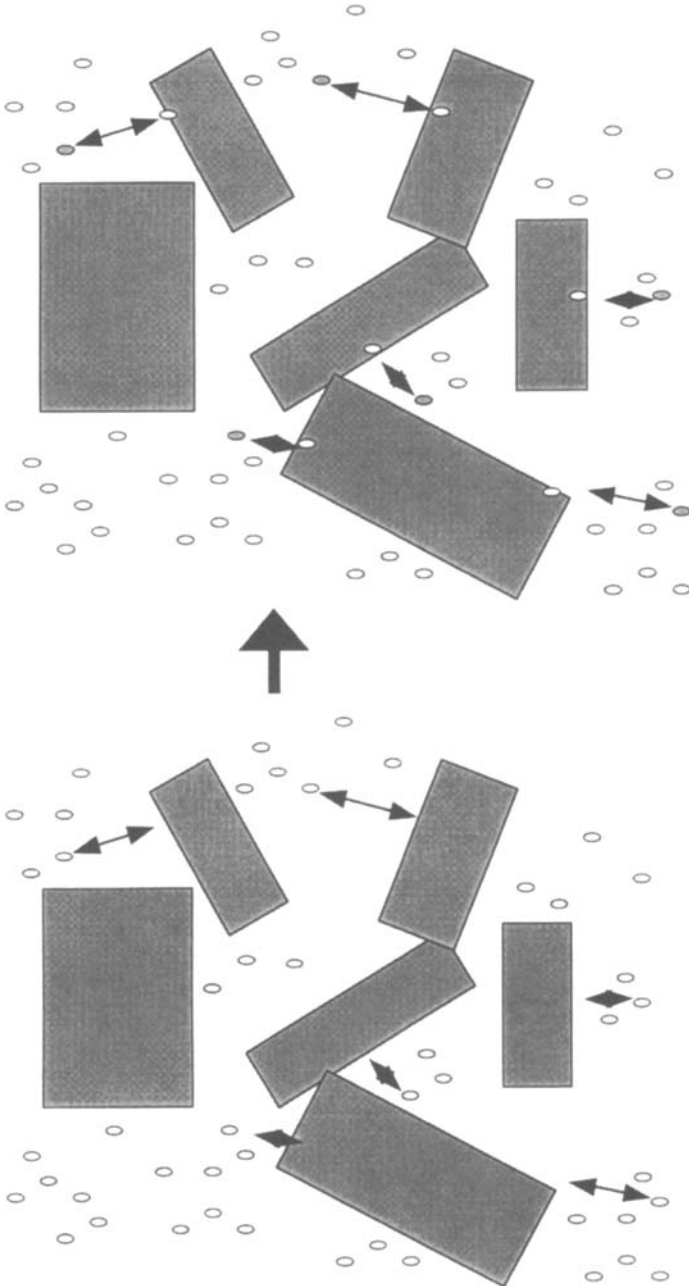


**Fig. 1.** Exchange between labeled triglyceride molecules in solution and unlabeled triglyceride molecules in the crystals. ○, a labeled molecule and ●, a labeled molecule.

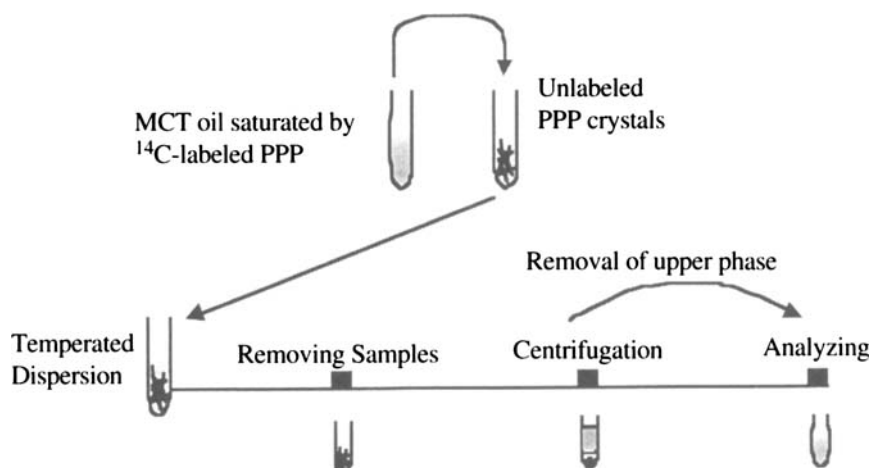


**Fig. 2.** Schematic representation of the experimental plan. PPP, tripalmitin. MCT, medium-chain triglyceride.

*Experimental Procedure.* A dispersion of fat crystals in oil was obtained by adding 5 mL of the preprepared oil solution (saturated by  $^{14}\text{C}$ -PPP, as above) to a controlled amount of unlabeled PPP crystals (either 10 or 20 mg). The polymorphic form of the PPP crystals was determined to be  $\beta$  [from differential scanning calorimetry (DSC)]. The dispersion was gently agitated and the temperature controlled at the temperature of interest. At regular intervals, a sample (150  $\mu\text{L}$ ) of the dispersion was removed and centrifuged. The clear upper phase of this sample was then analyzed by the detector, and so the residual  $^{14}\text{C}$ -PPP in the oil at that time was measured. The method is further described in a previous paper.

## Discussion

### Results

For the experiments performed at 25°C, the results are shown in Figure 3. The loss in intensity of the signal corresponds to depletion of the radiolabeled PPP in solution as it is exchanged with unlabeled PPP in the crystals. It should be noted that as the solution is saturated the concentration of PPP (labeled plus unlabeled) in solution is unchanged at any time. Doubling the concentration of PPP crystals, therefore doubling the surface area, doubles the rate of reaction.

Figure 4 shows the behavior at temperatures from 7 to 25°C. In this case the decay has been normalized. This is to account for the different concentrations of PPP in the oil in each case. Different concentrations are required because of the difference in concentration required for saturation in each case. In all cases the shape of the curve is very similar, revealing that the same mechanisms are occurring at all temperatures measured.

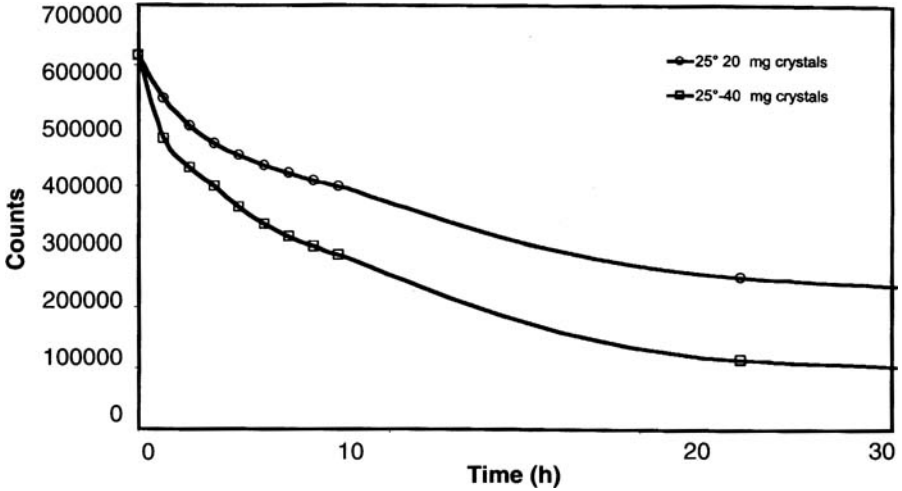


Fig. 3. Change in the solution concentration of radiolabeled PPP with time. See Figure 2 for abbreviation.

**Calculations**

The exchange reaction is defined as follows:

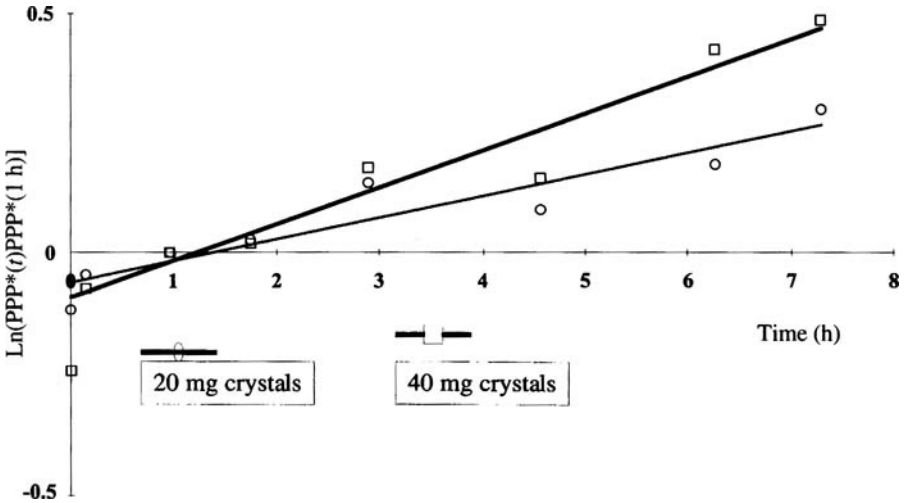


Fig. 4. Analysis of the results at 25°C. Plot of  $\ln ([PPP^*]_{t_2}/[PPP^*]_{t_1})$  against time.

where  $[PPP]_{\text{liquid}}$  is concentration of tripalmitin in the liquid. Both the forward and reverse reactions are first-order. The total volume of the system and its crystal content are constant. From Figure 3 the mass transfer is proportional to the concentration of PPP, with the proportionality constant  $k$ . The overall rate of reaction has two contributions. It is depleted by the forward reaction at a rate  $v_1 = k_1 \cdot [PPP]$ , but is replenished by the reverse reaction at a rate  $v_2 = k_2 \cdot [PPP]$ , with  $v_1$  and  $v_2$  being equal at equilibrium. The overall rate of the loss of  $^{14}\text{C}$ -labeled PPP,  $[PPP^*]$ , is defined as Equation 2.

$$\frac{d[PPP]_{\text{liquid}}}{dt} = -k_1[PPP^*]_{\text{liquid}} + k_2[PPP^*]_{\text{solid}} \quad [2]$$

In the first few hours the concentration of  $^{14}\text{C}$ -PPP in the solid is very low. Thus the rate of dissolving of the labeled  $[PPP^*]_{\text{solid}}$  (reverse reaction) can be assumed to be neglected.

$$\frac{d[PPP]_{\text{liquid}}}{dt} = -k_1[PPP^*]_{\text{liquid}} + k_2[PPP^*]_{\text{liquid}} \quad [3]$$

In order to determine the variation of the exchange rate with time, integration is required.

$$\int_{[PPP]_{t_1}}^{[PPP]_{t_2}} \frac{d[PPP^*]_{\text{liquid}}}{[PPP^*]_{\text{liquid}}} = - \int_{t_1}^{t_2} k \cdot dt \quad [4]$$

which gives:

$$\text{Ln} \frac{[PPP^*]_{t_2}}{[PPP^*]_{t_1}} = -k \cdot (t_2 - t_1) \quad [5]$$

The first-order rate law for the exchange reaction can then be described by:

$$k = - \frac{\text{Ln} \frac{[PPP^*]_{t_2}}{[PPP^*]_{t_1}}}{t} \quad [6]$$

Equation 6 shows that in order to measure the exchange rate one should plot  $\text{Ln} ([PPP^*]_{t_2}/[PPP^*]_{t_1})$  against time and measure the gradient ( $-k$ ), as in Figure 5.

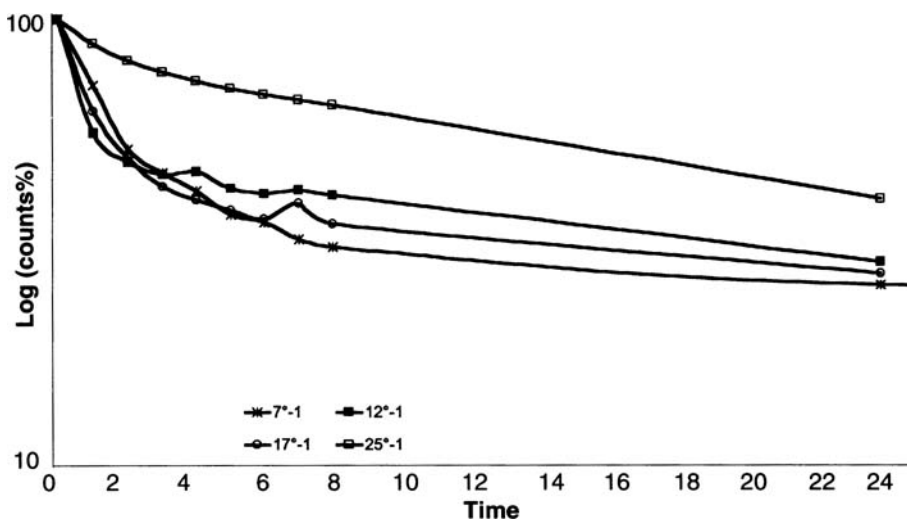


Fig. 5. Change in the solution concentration of radiolabeled PPP with time for 20 mg crystals from 7 to 25°C, \* 7°C, ■ 12°C, ○ 17 and 25°C. See Figure 2 for abbreviation.

The mechanism of the exchange reaction can thus be deduced. PPP from the crystals is dissolving and diffusing from the surfaces into the oil. At the same time, the dissolved  $^{14}\text{C}$ -PPP in the oil is diffusing toward the surface of the crystal and recrystallizing in the crystals. The total concentration of PPP plus  $^{14}\text{C}$ -PPP in the oil remains constant (note that the solution is always saturated). However the amount of dissolved  $^{14}\text{C}$ -PPP in the dispersion decreases constantly. If we assumed that the exchange rate is constant, the rate of loss of  $^{14}\text{C}$ -PPP should be directly proportional to the  $^{14}\text{C}$ -PPP concentration in solution.

The overall flow rate of the exchange reaction is dependent upon the rate of the dissolution of the solid material along with the rate of diffusion and crystallization of the dissolved PPP into the crystals. Analysis of the results at the other temperatures shows similar results, showing the same mechanism within this temperature range.

## Summary

A method has been developed that allows for the measurement of interactions between liquid and solid lipids. This is potentially a very powerful technique that allows for the monitoring of many transformations and exchange processes. Typical processes include crystallization and solid-liquid exchange. The use of the technique on exchange processes, such as occur in fat-bloom, has been demonstrated.

It has been shown that the interaction between solid and liquid PPP depends upon the diffusion of PPP in the liquid. This gives us information as to the exchange process in fats and starts to suggest the mechanisms that may be respon-

sible for fat-bloom in chocolate. Further research is necessary, but the importance of the speed of diffusion of the liquid oil must be considered. Further work using this technique should enable further elucidation of the mechanisms behind fat-bloom formation in chocolates containing oils.

### Acknowledgments

The authors are grateful to Jari Alander (Karlshamns AB), Martin Malmsten (YKI), and Thomas Arnebrant (YKI) for valuable discussions. We thank Annika Dahlman and Eva Lundgren for laboratory assistance. We gratefully acknowledge the financial support of the Future Technologies for Food Production Program (LiFT) and also Karlshamns AB for providing us with materials.

### References

1. Koyano, T., I. Hachiya, and K. Sato, Fat Polymorphism and Crystal Seeding Effects on Fat-Bloom Stability of Dark Chocolate, *Food Structure* 9: 231–240 (1990).
2. Bricknell, J., and R.W. Hartell, Relation of Fat Bloom in Chocolate to Polymorphic Transition of Cocoa Butter, *J. Am Oil Chem Soc.* 75: 1609–1615 (1998).
3. Hagemann, J.W., and J.A. Rothfus, Computer Modeling of Packing Arrangements and Transitions in Saturated-*cis*-Unsaturated Mixed Triglycerides, *Ibid.* 69: 429–435 (1992).
4. Yano, J., S. Ueno, and K. Sato, FTIR Study of Polymorphic Transformations in SOS, POP, POS, *J. Phys. Chem.* 97: 12967–12973 (1993).
5. Adenier, H., H. Chaveron, and M. Ollivon, Mechanism of Fat-Bloom Development on Chocolate, in *Shelf Life Studies of Foods and Beverages*, edited by G. Charalambous, Elsevier, Amsterdam, 1993, pp. 353–389.
6. Minifie, B.W., *Chocolate, Cocoa, and Confectionery: Science and Technology*, 2nd Edn., AVI, Westport, 1980, pp. 494–507.
7. Padley, F.B., *Chocolate and Confectionery Fats*, in *Lipid Technologies and Applications*, edited by F.D. Gunstone and F.B. Padley, Marcel Dekker, New York, 1997, pp. 391–432.
8. Ziegleder, G., C. Moser, and J. Geier-Greguska, Kinetics of Fat Migration in Chocolate Products, Part I: Ground Rules and Analysis, *Fett/Lipid* 98: 196–199 (1996).
9. Ziegleder, G., C. Moser, and J. Geier-Greguska, Kinetics of Fat Migration in Chocolate Products, Part II: Effects of Temperature, Diffusion Coefficient, and Fat Content, *Ibid.* 98: 253–256 (1996).
10. Ziegleder, G., and I. Schwingshandl, Kinetics of Fat Migration in Chocolate Products, Part III Fat Bloom, *Ibid.* 100: 411–415 (1998).
11. Haghshenas, N., P. Smith, and B. Bergenstahl, The Exchange Rate Between Dissolved Tripalmitin and Tripalmitin Crystals, *Colloids Surfaces B* (In Press).

## Chapter 15

# Application of Crystallization Technique for the Lipase-Catalyzed Solid-Phase Synthesis of Sugar Fatty Acid Monoesters

Youchun Yan<sup>a</sup>, Uwe T. Bornscheuer<sup>b</sup>, and Rolf D. Schmid<sup>a</sup>

<sup>a</sup>Institute of Technical Biochemistry, University of Stuttgart, Allmandring 31, D-70569 Stuttgart, Germany, and <sup>b</sup>Institute of Chemistry and Biochemistry, Department of Technical Chemistry and Biotechnology, University of Greifswald, Soldmannstrasse 16, D-17487 Greifswald, Germany

## Introduction

Sugar fatty acid monoesters are a class of biodegradable, nonionic surfactants, which are widely used in the food industry, cosmetics, and medical fields (1,2). Compared to classical surfactants, they have some advantages because they are tasteless, odorless, nontoxic, and nonirritant and are stable over a broad range of pH. A wide variety of structures are available by synthesis from inexpensive renewable materials. Much attention has focused on the synthesis of sugar fatty acid monoesters by enzymatic catalysis because of high regioselectivity encountered with biocatalysts and low energy consumption (for reviews see Refs. 3, 4).

Enzymatic reactions in organic synthesis are mostly performed using rather expensive activated esters (e.g., vinyl acetate) or modified sugars, allowing for an irreversible and/or rapid synthesis. Theoretically, sugar esters can be obtained by esterification/transesterification between a sugar and a cheap acyl donor such as free fatty acids or simple derivatives (e.g., methyl or ethyl esters). Accordingly, different processes for preparing mono- and disaccharide fatty acid monoesters with high regioselectivities and without requirement for laborious protection have been developed (5–13). In such a case, efficient removal of by-products (water, methanol, or ethanol) as well as crystallization of the product must be ensured to drive the reaction to completion at reasonable reaction times (14). However, the literature shows that relatively little attention has been paid to practical difficulties, e.g., how to efficiently remove the reaction water and the products from the solvent medium in the production of sugar fatty acid esters. Water removal from organic solvents on a large scale is quite difficult because the boiling point of organic solvent is usually lower than that of water. Recently, Gemert and Wilhelm (15) reported an enzymatically catalyzed process in which the reaction water formed was continuously removed through a nonporous, water-permeable membrane on which the enzyme was immobilized. However, in the process of solid-phase synthesis of sugar fatty acid esters, the membrane surface should not come

into direct contact with the solid particles because the membrane might be damaged.

The purpose of the present work was to develop a practical process for the synthesis of sugar fatty acid monoesters derived from sugar and free fatty acids.

## Materials and Methods

### Enzymes, Membrane, and Chemicals

Chirazyme® L-2 (E.C. 3.1.1.3 immobilized lipase B from *Candida antarctica*) was a gift from Roche Diagnostics GmbH (Penzberg, Germany). Novozyme® 435 (E.C. 3.1.1.3 immobilized lipase from *C. antarctica*) was provided by Novo Nordisk A/S (Bagsvaerd, Denmark). Pervap® 2200 membrane was donated by Sulzer Chemtech GmbH (Neunkirchen, Germany). Palmitic, stearic, and caprylic acids were obtained from Henkel KGaA (Düsseldorf, Germany). All other chemicals were purchased from Fluka (Buchs, Switzerland).

### Apparatus

A diagram of the apparatus is shown in Figure 1. A membrane reactor (containing the Pervap® 2200 membrane) with an area of 23 cm<sup>2</sup> was purchased from the Jülich Forschung GmbH (Jülich, Germany). Temperature was maintained by circu-

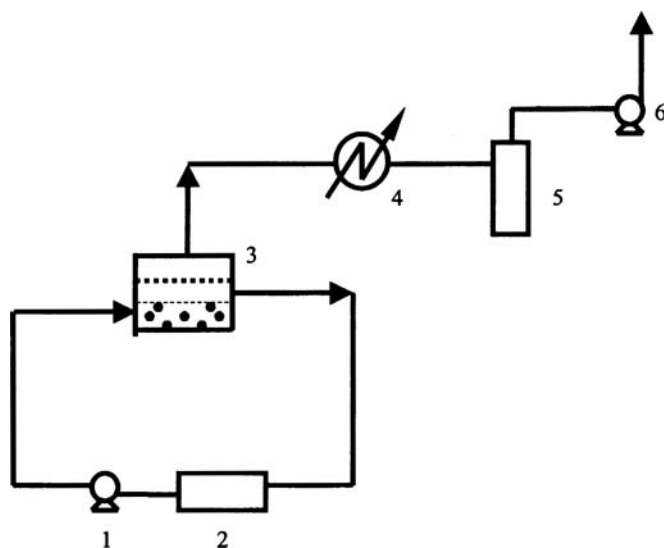


**FIG. 1.** Lipase-catalyzed esterification for the production of sugar fatty acid esters in a stirred-tank membrane reactor. 1, pump; 2, water bath; 3, membrane reactor; 4, condenser; 5, permeate container; 6, vacuum pump.

lating heated water. Before starting the reaction, the permeate container was cooled to  $-8^{\circ}\text{C}$  using a thermostat.

### ***Procedure for the Lipase-Catalyzed Esterification***

The reaction mixture consisted of equimolar amounts of sugar and fatty acid (usually 0.5 mmol) in a solvent mixture of ethyl methylketone (EMK) and hexane (1–2 weight equivalents of substrates) serving as adjuvants. The reaction mixture was incubated in the membrane reactor (Fig. 1) and agitated by a magnetic bar (650 rpm). The reaction temperature was kept at  $59^{\circ}\text{C}$ . At this temperature, the azeotropic mixture (b.p.  $56^{\circ}\text{C}$ ) of EMK, hexane, and water produced during esterification was vaporized. This gaseous mixture came in contact with the membrane Pervap® 2200 and water vapor passed through the membrane, leading to a break of the azeotrope. EMK and hexane vapor became liquid and returned to the reaction medium.

## **Results and Discussion**

### ***Continuous Removal of By-Product in the Solid-Phase Synthesis of Sugar Fatty Acid Monoesters***

To facilitate complete removal of by-product water/methanol, our initial experiments were performed *in vacuo* using a solvent-free mixture of fatty acid/fatty acid methyl ester and glucose at  $60^{\circ}\text{C}$  using Novozyme® SP 435 as a catalyst. We found that the reaction kinetics under these solvent-free conditions were very poor, even when 5–10% glucose fatty acid ester was initially added to increase the contact interface of both substrates, apparently due to low miscibility of the reactants. We successfully minimized this problem by adding a small amount of an organic solvent (*tert*-butanol or acetone) which partially dissolves the sugar and completely dissolves the fatty acid, thereby creating a catalytic liquid phase (8). In the solid-phase synthesis of sugar fatty acid esters, optimal conversion is obtained by removal of water liberated during esterification by azeotropic distillation. This requires that the water form an azeotrope with the solvent, followed by water recovery using membrane pervaporation (a membrane surface in contact with only with azeotrope) and returning the solvent to the reaction medium. Crucial for success is a suitable organic solvent which should (i) be nontoxic and cheap; (ii) dissolve enough substrate to carry out the reaction, but the product solubility should be low enough to favor crystallization and so prevent reversible reactions (iii) form an azeotrope with reaction water; and (iv) not affect the enzyme activity or stability. Only very few solvents meet most of these criteria. We found EMK or a mixture of EMK and hexane to be useful for the production of sugar fatty acid esters, because both solvents meet all criteria listed above and are allowed for use in the manufacture of foods by German authorities (16,17). Thus, the water content in the reaction medium can be kept as low as 0.1%.

### Crystallization of the Products in the Solid-Phase Synthesis of Sugar Fatty Acid Monoesters

Crystallization is a useful technique in chemical processes. It can be obtained by decreasing the temperature or minimizing solvent amount or changing solvent. Bornscheuer and Yamane applied this technology in the enzymatic synthesis of monoacylglycerols (18). Accordingly, in our ongoing project, we tried this approach in the synthesis of sugar fatty acid esters, which was carried out in a heterogeneous low-solvent reaction system in which most of the substrate was present as suspended particles (19–21). The present research was performed by means of varying the solubilization property of the solvent to favor crystallization of the product.

**Solvent Effects.** As described above, EMK and hexane served as an ideal solvent mixture, because EMK showed a slightly higher product solubility, whereas hexane hardly dissolve the product at all. Thus, sugar fatty acid esters were synthesized by lipase-catalysis at 59°C in a mixture of EMK and hexane. From Figure 2 it can be observed, that the addition of 20% hexane to the medium gave rise to a notable acceleration of the process, resulting in a 90% conversion to 6-*O*-palmitoyl- $\beta$ -D-glucose in 48 h starting from equimolar concentrations of reactants. This enhancement of monoester production could be related to a poor solubilization of glucose fatty acid ester in the medium containing hexane, thus leading to easy crystallization of the product from the reaction medium (solubility: 1.98 mg/mL 6-*O*-palmitoyl-glucose

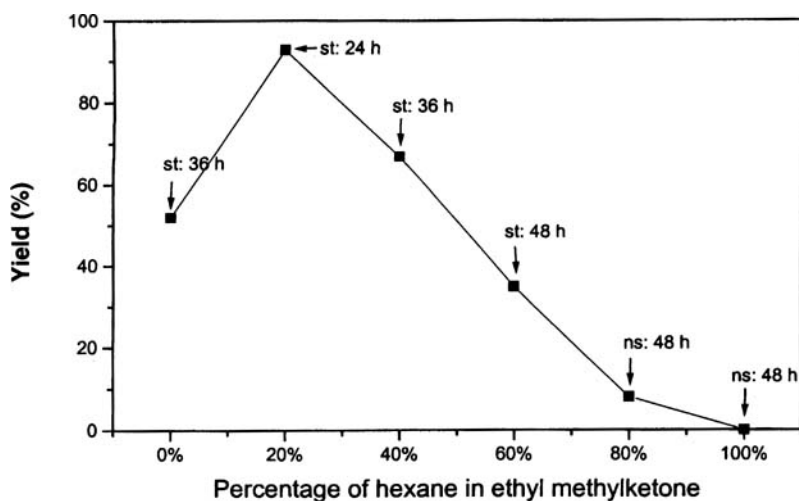


**FIG. 2.** Relationship between product yields and the percentage of hexane in ethyl methylketone. Reaction condition: 0.5 mmol glucose, 0.5 mmol fatty acids, 50 mg Chirazyme® L-2 lipase, 0–0.4 mL ethyl methylketone and/or hexane, 59°C, 650 rpm, 48 h. st: solidification time; ns: no solidification.

compared to 2.50 mg/mL in pure EMK, solidification time, 24 h). At  $\geq 80\%$  hexane, the reaction became very slow and no solidification took place. In contrast, reactions in pure EMK proceeded with high initial rates, but the maximum conversion to monoester did not exceed 52% (achieved only after 8 h). Presumably, solidification became the rate-limiting step suppressing higher yields.

*Effect of Solvent Amounts.* The solvent amounts in the reaction medium were also investigated. It was found that conversion and productivity increased with higher solvent amounts (optimum 140% w/w) until a maximum conversion was achieved. Conversion was decreased with increasing amounts of solvent (Fig. 3). This may be explained by an increased product amount in the liquid phase and lower precipitation of product. In addition, the fatty acid concentration in the liquid phase decreased during the course of the reaction; this may have led to a change in the polarity of the liquid phase and an increase in the solubility of the product in the liquid phase, which may have caused product inhibition at high product concentration in the liquid phase.

*Effect of Acyl Donors.* The synthesis of glucose fatty acid esters was investigated with continuous by-product removal in a stirred-tank membrane reactor by azeotropic distillation using EMK containing 20% hexane as reaction solvent and different fatty acids as acyl donors. From previous studies on the lipase-catalyzed synthesis of glucose esters in a solid-phase system (17,19,22,23), it was already known that the fatty acid chainlength had a considerable influence on product formation. This was due

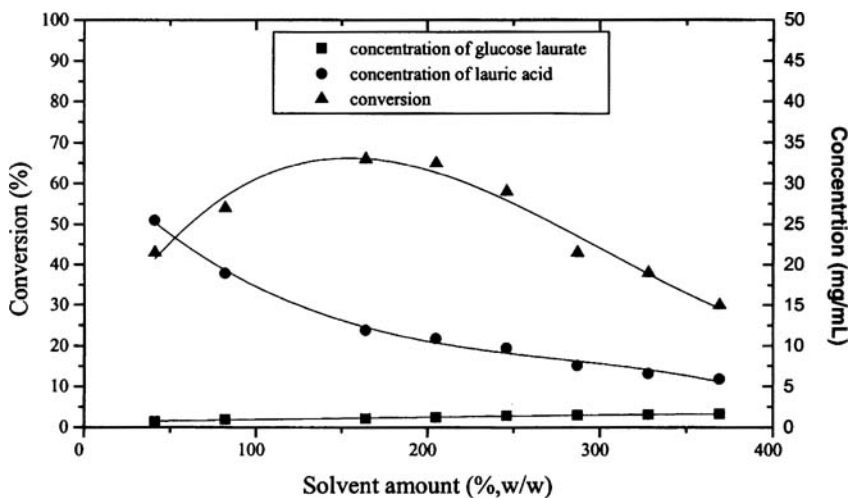


FIG. 3. Relationship between the concentration of fatty acid and solvent with conversion in the synthesis of 6-O-lauroyl-glucose. Reaction condition: 0.5 mmol glucose, 0.5 mmol lauric acid, 50 mg Chirazyme® L-2 lipase, 0.4 mL mixture of ethyl methylketone and hexane (4:1, vol/vol), 59°C, 650 rpm, 48 h.

mainly to the different solubilities of the glucose esters of fatty acids with different chainlengths in the reaction medium, causing different solidification times (Table 1). Using saturated long-chain fatty acids, such as stearic acid as acyl donor, it was observed that the reaction mixtures began to solidify at an early stage of the reaction (16–24 h), and the conversions achieved with stearic acid were 99%. With myristic and lauric acids, the mixture solidified after about 36 h. With short-chain fatty acids such as caprylic and caproic acids, no solidification of the reaction mixtures was observed. In this case, the products were totally solubilized, thus suppressing the crystallization of product and resulting in low conversions.

## Summary

The process for the enzymatic synthesis of sugar fatty acid ester as described demonstrates a successful application of crystallization technique. This process does not require prior modification of substrates—renewable sources of sugar and fatty acids. This process offers also a number of advantages such as high productivity (0.56–1.3 mmol/g · h), high ratio of product to reaction mixture and reaction rate. Furthermore, use of only very small amounts of organic solvents and high reaction rates leads to high space-time yield (0.047–0.122 g/mL · d), which is a very important factor for industrial application. In addition, recovery of solvent by membrane vapor permeation under mild and “environmentally friendly” reaction conditions results in low energy consumption and high enzyme stability. This technique performed with equimolar reactants, provides a simple downstream process.

## Acknowledgments

We would like to thank the companies listed in the Materials section for providing us with chemicals, lipase, and membrane, respectively. The award of the KAAD (Bonn, Germany) Graduate Fellowship to Yochun Yan is gratefully acknowledged.

**TABLE 1**  
Influence on Product Solubility with Different Fatty Acids as Acyl Donors<sup>a</sup>

Glucose ester	Conversion (%)	Saturated solubility (mg/mL)	Solidification time (h)
Stearate	99	0.78	16–24
Palmitate	88	1.98	16–24
Myristate	75	2.33	36
Laurate	69	3.55	36
Capronate	58	8.49	48
Caprylate	54	13.28	ns
Caproate	48	13.72	ns

<sup>a</sup>Reaction condition: 0.5 mmol glucose, 0.5 mmol fatty acids, 50 mg Chirazyme® L-2 lipase, 0–0.4 mL ethyl methylketone or/and hexane, 59°C, 650 rpm, 48 h. ns: no solidification.

## References

1. Fiechter, A., Biosurfactants: Moving Toward Industrial Application, *Trends Biotechnol.* 10: 208–217 (1992).
2. Hill, K., and O. Rhode, Sugar-Based Surfactants for Consumer Products and Technical Applications, *Fett/Lipid* 101: 25–33 (1999).
3. Bornscheuer, U.T., Enzymes in *Lipid Modification*, Wiley-VCH, Weinheim, 2000.
4. Sarney, D.B., and E.N. Vulfson, Application of Enzymes to the Synthesis of Surfactants, *Trends Biotechnol.* 13: 164–172 (1995).
5. Coulon, D., M. Girardin, and M. Ghoul, Enzymic Synthesis of Fructose Monooleate in a Reduced Pressure Pilot-Scale Reactor Using Various Acyl Donors, *Process. Biochem.* 34: 913–918 (1999).
6. Arcos, J.A., M., Bernabe, and C. Otero, Quantitative Enzymatic Production of 6-O-Acylglucose Esters, *Biotechnol. Bioeng.* 57: 505–509 (1998).
7. Grüning, B., and G. Hills, European Patent 0,965,645A2 (1999).
8. Cao, L., U.T. Bornscheuer, and R.D. Schmid, Lipase-Catalyzed Solid-Phase Synthesis of Sugar Esters, *Fett/Lipid* 98: 332–335 (1996).
9. Ducret, A., A. Giroux, M. Trani, and R. Lortie, Enzymatic Preparation of Biosurfactants from Sugars or Sugar Alcohols and Fatty Acids in Organic Media Under Reduced Pressure, *Biotechnol. Bioeng.* 48: 214–221 (1995).
10. Oguntimein, G.B., H. Erdmann, and R.D. Schmid, Lipase-Catalyzed Synthesis of Sugar Ester in Organic Solvents, *Biotechnol. Lett.* 15:175–180 (1993).
11. Oosterom, M.W., F. Rantwijk, and R.A. Sheldon, Regioselective Acylation of Disaccharides in *Tert*-Butyl Alcohol Catalyzed by *Candida antarctica* Lipase, *Biotechnol. Bioeng.* 49: 328–333 (1996).
12. Sarney, D.B., M.J. Barnard, M. Virto, and E.N. Vulfson, Enzymatic Synthesis of Sorbitan Esters Using a Low-Boiling-Point Azeotrope as a Reaction Solvent, *Ibid.* 54: 351–356 (1997).
13. Vlahov, I.R., P.I. Vlahova, and R.J. Linhardt, Regioselective Synthesis of Sucrose Monoesters as Surfactants, *J. Carbohydrate Chem.* 16:1–10 (1997).
14. Bosley, J., Turning Lipases into Industrial Biocatalysts, *Biochem. Soc. Trans.* 25: 174–178 (1997).
15. Gemert, V., and R. Wilhelm, World Patent 98/36,058 (1998).
16. Bundesministerium, *Verordnung über die Verwendung von Extraktionslösungsmitteln und anderen technischen Hilfsstoffen bei der Herstellung von Lebensmitteln (Technische Hilfsstoff-Verordnung-THV) vom 08.11.1991 (BGBl. I S.2100)*, Bundesdruckerei, Bonn, Germany, 1991, pp. 1–6.
17. Yan, Y., U.T. Bornscheuer, and R.D. Schmid, Efficient Water Removal in Lipase-Catalyzed Esterifications Using a Low-Boiling-Point Azeotrope, Submitted to *Biotechnol. Bioeng.* (2000).
18. Bornscheuer, U.T., and T. Yamane, Fatty Acid Vinyl Esters as Acylating Agents: A New Method for the Enzymatic Synthesis of Monoacylglycerols, *J. Am. Oil Chem. Soc.* 72: 193–197 (1995).
19. Cao, L., U.T. Bornscheuer, and R.D. Schmid, Lipase-Catalyzed Solid-Phase Synthesis of Sugar Esters, IV: Selectivity of Lipases Towards Primary and Secondary Hydroxyl Groups in Carbohydrates, *Biocatal. Biotransform.* 16: 249–257 (1998).

20. Otto, R., U.T. Bornscheuer, C. Syldatk, and R.D. Schmid, Lipase-Catalyzed Synthesis of Arylaliphatic Esters of  $\beta$ -D(+)-Glucose, Alkyl-, and Arylglucosides and Characterization of Their Surfactant Properties, *J. Biotechnol.* 64: 231–237 (1998).
21. Yan, Y., U.T. Bornscheuer, L. Cao, and R.D. Schmid, Lipase-Catalyzed Solid-Phase Synthesis of Sugar Fatty Acid Esters. Removal of By-Products by Azeotropic Distillation, *Enzyme Microb. Technol.* 25: 725–728 (1999).
22. Yan, Y., U.T. Bornscheuer, and R.D. Schmid, Lipase-Catalyzed Synthesis of Vitamin C Fatty Acid Esters, *Biotechnol. Lett.* 21: 1051–1054 (1999).
23. Yan, Y., U.T. Bornscheuer, G. Stadler, M. Reuss, and R.D. Schmid, Lipase-Catalyzed Solid-Phase Synthesis of Sugar Fatty Acid Esters in a Stirred-Tank Membrane Reactor, *J. Am. Oil Chem. Soc.* in press (2000).

## Chapter 16

# Relating Bulk-Fat Properties to Emulsified Systems: Characterization of Emulsion Destabilization by Crystallizing Fats

Shawn D. Campbell, H. Douglas Goff<sup>a</sup>, and D errick Rousseau<sup>b</sup>

<sup>a</sup>Department of Food Science, University of Guelph, Guelph, Ontario, Canada N1G 2W1, and <sup>b</sup>School of Nutrition, Ryerson Polytechnic University, 350 Victoria St., Toronto, Ontario, Canada M5B 2K3

## Introduction

The controlled destabilization of emulsified fats by intraglobular fat crystals plays a considerable role in the development of microstructure and sensory properties of many foods (e.g., butter, spreads, whipped toppings, and ice cream). During a cooling regime, under perikinetic or orthokinetic conditions, intraglobular fat may crystallize, and collisions between droplets may lead to flocculation. Crystals near or at the droplet interface may cause the disruption of droplets at rest, or as the result of collisions. With a disrupted interface, the available liquid oil preferentially wets protruding crystals, and a bridge is formed between the two droplets (1). Due to the structural rigidity of the crystals, the droplets are prevented from fully coalescing, a process known as partial coalescence (2,3). It has been shown that solid fat content (SFC), crystal structure, crystallization kinetics, shear, and tempering all impact the stability of emulsions containing solid fat (1,4).

Fat crystallization has been extensively studied in bulk fats and, to a lesser extent, in emulsified fats. It has been shown that the crystallization behavior of a fat will proceed quite differently, depending on whether it is in bulk or emulsified form (4,5). Authors have examined the effect of the state of dispersion on the crystallization mechanisms (nucleation, crystallization rate) and polymorphic behavior (6–11) of partial- and triglycerides in bulk and emulsified form. Understanding the mechanisms of emulsion nucleation and crystallization is one of the first steps in understanding the destabilization of emulsions and partial coalescence, e.g., stabilization of liquid fat emulsions by solid particles (fat) or control of the polymorphic form of crystals during the process of partial coalescence to control the size of aggregates and textural properties.

There are two approaches to nucleation kinetics that have been utilized to explain intraglobular fat crystallization—homogeneous and heterogeneous nucleation. During homogeneous nucleation, there are no impurities present to act as nucleation catalysts (6). Heterogeneous nucleation involves the presence of impu-

rities that serve as nucleation sites for intradroplet crystallization. After nucleation initiation, crystals may behave as secondary nucleation sites and promote further crystallization. Although an understanding of nucleation and crystallization has been established, it is clear that further insight into the relationship of crystallization kinetics, polymorphic behavior, and rheological properties is necessary to better understand the destabilization and/or stabilization of emulsified systems. The goal of this research was to determine the effects of two different fat systems on the crystallization behavior of fats in emulsified oil-in-water and bulk systems. Two fats, of similar final SFC, but different crystallization kinetics were chosen. The kinetics, polymorphism, rheology, and microstructural behavior of two fat systems in emulsified oil-in-water and bulk form were studied.

## Materials and Methods

### *Materials*

Refined, bleached, and deodorized palm stearine was obtained from CanAmera Foods (Toronto, Ontario, Canada); lard and canola oil were purchased from a local supermarket. Tween 80 was supplied by Quest International (Lachine, Quebec, Canada). Free fatty acid content was determined [as percentage oleic acid (w/w)] by titration (12). Free fatty acid contents were 0.03, 0.1, and 0.02%, respectively, for the lard, palm stearine, and canola oil.

### *Blend and Emulsion Preparation*

A 40% (w/w) palm stearine/60% (w/w) canola oil (PSCO) blend was made by heating the palm stearine to 90°C (to destroy crystal history) and blending it with canola oil. All emulsions were formulated by weight to be 20% (w/w) oil and 1% (w/w) Tween 80. The Tween was dissolved in the distilled water prior to emulsification, and emulsions were prepared by heating the ingredients to 90°C, to ensure that the fats were liquid, followed by high shear mixing (PowerGen 700 homogenizer; Fisher Scientific, Nepean, Ontario, Canada) at 27,000 rpm for 6 min. The temperature of the emulsion immediately after emulsification was 65°C. Samples were equilibrated at 60°C prior to analysis, quenched at 25°C, and held isothermally at 25°C during analysis. A canola oil emulsion was prepared and used as a control. Samples were prepared in triplicate.

### *Bulk and Emulsion Characterization*

Droplet distributions were measured by light scattering using a Mastersizer X particle size analyzer (Malvern, Worcestershire, United Kingdom). SFC and rheological measurements were collected using a Minispec Mq pulsed nuclear magnetic resonance (pNMR) spectrometer (Bruker, Milton, Ontario, Canada) and Carri-Med CSL100 rheometer (Dorking, Surrey, United Kingdom), with a 2°, 6 cm cone and plate fixture, respectively. Heat transfer rates were comparable for particle size,

SFC, and rheological experiments (results not shown). Calorimetry was performed using a Dupont Instruments DSC 2910 (Wilmington, DE). Microstructural characterization of bulk and emulsified fats was performed with a Carl Zeiss LSM-510 (Zeiss, Heidelberg, Germany) confocal laser-scanning microscope. The oil phase in these samples was stained with Nile Red (5 ppm) (Acros Organics, Nepean, Ontario, Canada), and the aqueous phase was stained with Rhodamine B (5 ppm) (Acros Organics). A Rigaku Geigerflex (Danvers, MA) X-ray diffraction (XRD) unit ( $\lambda = 1.79 \text{ \AA}$ ) was used to determine powder diffractograms of the polymorphic forms of the bulk and emulsified fats. Samples were placed into the unit at  $65^\circ\text{C}$ , allowed to cool to  $25^\circ\text{C}$ , and scanned from  $18$  to  $33^\circ 2\theta$  for 1 h at 5-min intervals.

## Results and Discussion

### *Droplet Size Distribution*

The oil-in-water emulsions studied in this experiment contained sufficient levels of crystallized fat to lead to droplet destabilization *via* partial coalescence. The role of intradroplet crystallization and its effects on emulsion stability and partial coalescence were determined by examining the evolution of droplet size distribution [volume weighted particle size distribution ( $d_{4,3}$ )] as a function of time. All freshly formed emulsions had mean  $d_{4,3}$  values of  $5 \pm 0.5 \mu\text{m}$ . At rest, destabilization of the PSCO emulsion occurred more rapidly relative to the lard and the canola oil control emulsions (Fig. 1). Comparison of particle size and SFC indicated that intradroplet crystallization occurred prior to the destabilization of the lard and PSCO emulsions.

### *SFC and Emulsion Destabilization*

SFC was monitored by pNMR and used as an indicator of nucleation and crystallization kinetics. Bulk and emulsified lard were found to have slower induction times and slower rates of crystallization than the bulk and emulsified PSCO blends (Fig. 2). The onset of crystallization in emulsified fats was longer than that of their respective bulk phases. The increase in the relative degree of undercooling required for the crystallization of emulsified fat has long been known to limit the rate of homogeneous nucleation (13). Emulsification of the fats used in this study also served to redistribute impurities in the oil phase to slow the rate of heterogeneous nucleation (14). Various accounts illustrating the effects of impurities on crystallization behavior have been reported in the literature. Kaneko *et al.* (15) studied the effect of impurities, hydrophobic surfactants, in the dispersed phase on surface nucleation. In the area of bulk fat behavior, Siew and Ng (16) reported a general increase in the "crystallization time" of palm olein due to the presence of diglycerides. Wright *et al.* (17) have reported a decrease in induction time after removal of mono- and diglycerides from milk fat. It is evident that not only the

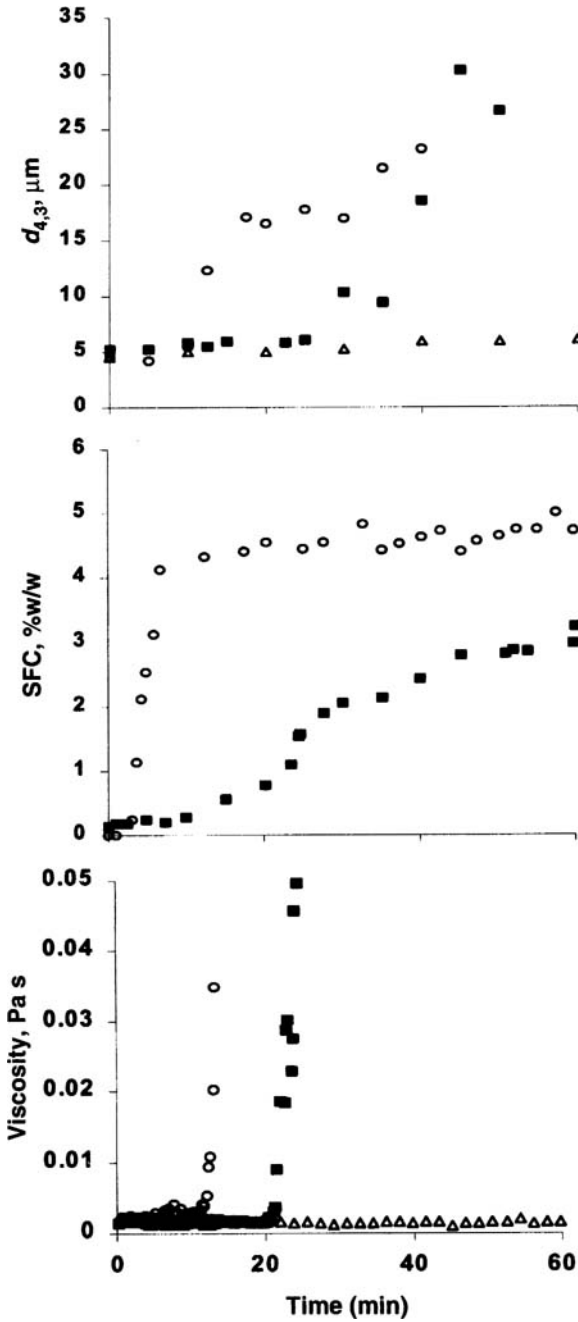


Fig. 1. Emulsion destabilization of lard  $\circ$ , palm stearin/canola oil (PSCO)  $\blacksquare$ , and canola  $\triangle$  emulsions monitored by  $d_{4,3}$ , solid fat content (SFC) and viscosity as a function of time at 25°C under quiescent conditions.

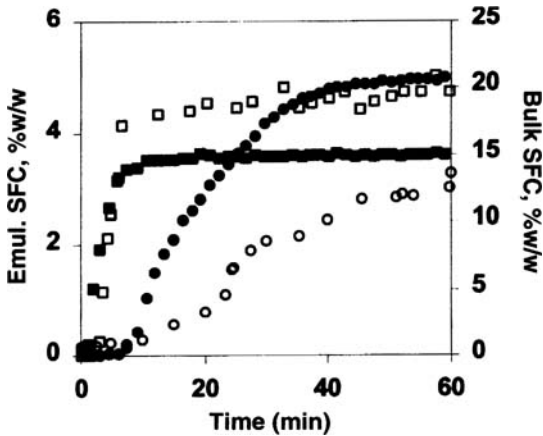


Fig. 2. SFC of bulk (lard ●, PSCO ■) and emulsified fats (lard ○, PSCO □) as a function of time, measured isothermally at 25°C. See Figure 1 for abbreviations.

purity of fats but also the distribution of impurities must be considered when studying crystallization behavior.

Onset of crystallization (defined in this experiment as the intercept with the time axis extrapolated from the initial slope of the SFC curve) and crystallization rate provided evidence of the degree of undercooling required for each fat. The undercooling of bulk lard and palm stearine was 5 and 25°C below their respective melting points as determined by differential scanning calorimetry (DSC). The induction time for crystallization of the emulsified PSCO was 2 min longer than the bulk fat, and the emulsified lard 5.5 min longer than bulk lard. The presence or absence of impurities will determine whether heterogeneous or homogeneous nucleation is prevalent, as well as the nature of crystal growth. Emulsified lard and PSCO had lower relative rates of crystallization compared to crystallization rate in bulk (Fig. 2), indicating that more undercooling was required to initiate crystallization in the emulsified fats. Crystallization of bulk and emulsified PSCO were complete within the same time frame after quenching, whereas the emulsified lard took considerably longer to reach similar SFC values. The SFC of the PSCO emulsion reached the final SFC of 4.6% quickly without evidence of destabilization by flocculation and/or coalescence. The droplets, however, did destabilize within the next 7.5 min. As expected, destabilization of both the lard and PSCO emulsion was observed only after the onset of crystallization (Fig. 1). Destabilization of the PSCO emulsion, as noted by a rapid increase in particle size, occurred quickly after the SFC of the emulsion had increased to near its final value. At this time, rapid flocculation and (partial) coalescence of droplets occurred as a result of collisions of droplets with fat crystals oriented at or protruding from the interface. The lard emulsion began to destabilize 22 min after quenching when the emulsion SFC reached 1%, as opposed to the final SFC of 4.4%. By comparison, a 20% canola oil emulsion remained stable to flocculation for the duration of the experiment under both perikinetic and orthokinetic conditions.

### ***Intraglobular Crystal Morphology Under Perikinetic Conditions***

The nature of the fat crystals found within the emulsified lard and PSCO played a key role in the destabilization kinetics of the emulsion droplets. Droplet SFC during the early stages of destabilization gave an indication of intraglobular fat behavior. PSCO droplets were stable for a short time as they approached their final SFC. The lard droplets, however, destabilized before reaching their final SFC, suggesting a difference in crystallization behavior within the droplets. The uniform growth, flocculation, and/or sintering of crystals (1,9) within the droplet environment maintained the stability of the droplet in the short term as a result of consolidation of the fat crystals within the droplet prior to outward growth. The long-term stability of the droplets, however, was compromised by an increase in the coalescence efficiency resulting from contact between droplets (18). The efficiency of coalescence was partially dictated by the amount and orientation of crystalline fat at the interface and how well the crystals are wetted by the oil phase. Fat crystals tend to be preferentially wetted by the liquid oil contained in droplets rather than the continuous phase. After reaching its final SFC, the crystal structure of the emulsified PSCO underwent changes induced by crystal sintering, crystal growth, and/or polymorphic transition. The resulting formations of large crystals or crystal networks are capable of deforming the droplet interface. Destabilization as a result of crystal protrusion and/or crystal growth from the interface was seen when microstructure development was examined in time sequences (Fig. 3). The nature of crystal growth is a crucial factor in destabilization of emulsified fat under quiescent conditions. The growth of crystals to the interface may occur from relatively few nucleation sites in the bulk and outward as needle-like structures to deform the droplet. Slow growth of these crystals will lead to a droplet that is susceptible to destabilization in relatively few locations (i.e., where the crystal touches the interface). Droplets are stable at rest when crystal formation is limited to small crystals confined within the native droplet geometry and not available at the interface. Droplets were observed to have freely rotating crystals mobile within the droplet bulk when observed over time (not shown). The location of the crystals within the droplet makes them less available to the interface, decreasing the chance that they will promote flocculation or coalescence of the droplet with another. Flocculation is therefore limited to interaction of liquid portions of the droplets.

Droplets that rapidly achieve a high SFC tend to contain many small crystals that flocculate within the droplet and continue to grow out toward the interface where they are available for promotion of coalescence. However, a greater destabilizing influence will result from the growth of crystals outward from the interfaces of droplets. Boode and Walstra (18) noted the importance of the disruptive influence of droplets containing protruding crystals and the importance of crystal morphology with respect to coalescence efficiency and droplet destabilization. Microscopic examination of emulsified lard showed slow growth of large crystallite structures outward from the bulk of the droplet (Fig. 4). The needle-like and

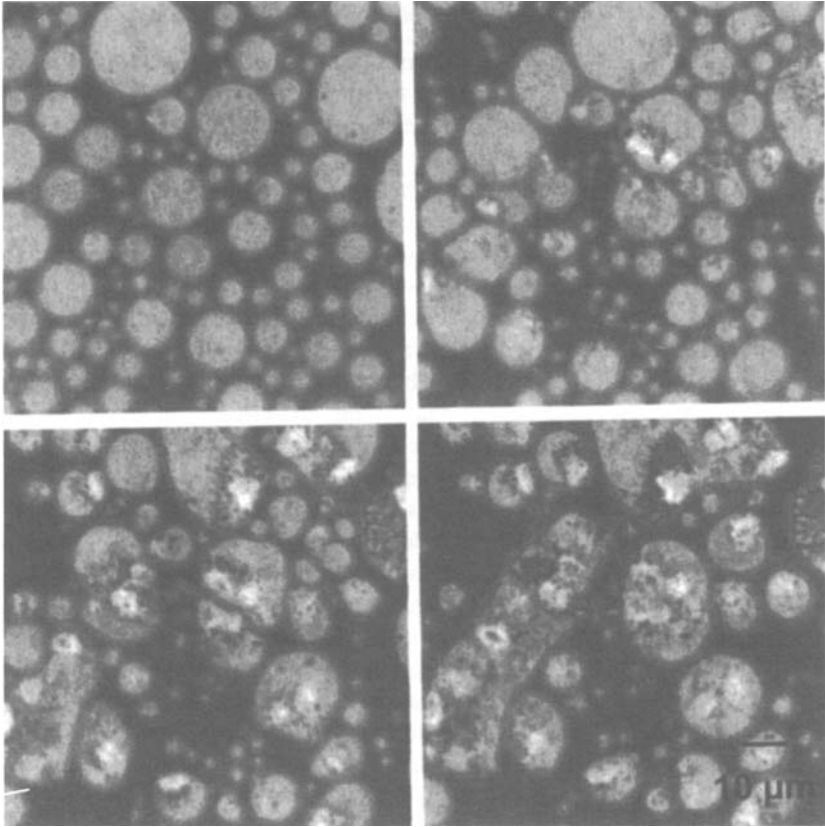


**Fig. 3.** Destabilization of PSCO emulsion over 20 min observed *via* confocal laser scanning microscope. See Figure 1 for abbreviation.

plate-like crystals distorted and pierced droplets; however, disruption occurred only when the crystals grew to the interface. The PSCO emulsion was destabilized more quickly due to crystal growth at the droplet surface, after the average SFC of the droplet population had reached its final value (Fig. 3). Few examples of droplet disruption were observed at rest when crystals were small and contained within droplets. It was the outward growth or projection of larger crystals that initiated the destabilizing action in these systems.

Initially, growth of crystals from the interior of fat droplets most likely follows a similar mechanism as was observed in the bulk. In the case of the PSCO system, fast nucleation of fine crystals within the bulk phase was followed by growth of larger crystals outward and growth at the interface (Fig. 3). In the lard system, slow growth of fine crystals was followed later by slower formation of larger crystals (Fig. 4). It was at sites where these larger crystal formations protruded to the exterior of the droplet that partial coalescence was observed by microscopy.

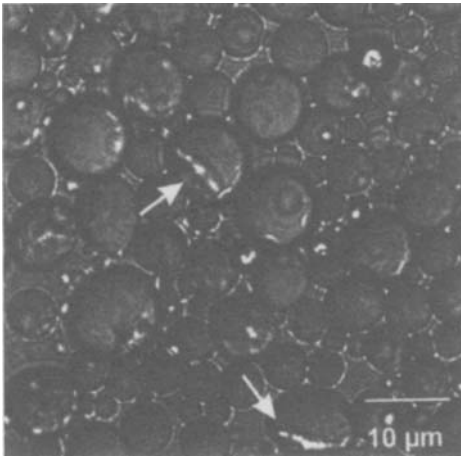


**Fig. 4.** Destabilized lard emulsion with droplets containing large crystal forms.

However, in the PSCO system, the delayed disruption (“blistering”) of the interface with large crystals appeared to be the primary source of destabilization. Interfacial “blistering” was also observed in the lard droplets, although much later than in the emulsified PSCO. This visual observation coincided with SFC and particle size measurements that indicated the SFC of the PSCO droplets had stabilized prior to the rapid increase in droplet size and destabilization.

Lard emulsion destabilization was less dependent on SFC, compared to the PSCO emulsion, and more dependent on crystal morphology. The average SFC of the droplets at the time of destabilization was observed to be lower than in the case of the PSCO emulsions although the minimum destabilizing SFC of emulsified PSCO was not determined. The difference in the rates of crystallization in the lard and PSCO was due to the inherent crystallization rate of the fat and to the region of nucleation in the droplet, whether in the droplet “bulk” or at the interface. Droplets with crystal nucleation at the interface would most likely promote partial coalescence (or at least disruption of the interface) more quickly than those with free-floating crystals within the droplet. It has been shown that collision of droplets containing solid fat is sufficient to induce nucleation in liquid droplets. McClements *et al.* (19,20,21) used pNMR and ultrasonic techniques to observe the effects of droplet collisions on the crystallization behavior of a mixture of solid and liquid droplets. Droplets were undercooled sufficiently to yield solid droplets, and then they were mixed with liquid droplets of identical chemical composition. The presence of the solid droplets was sufficient to induce crystallization in the liquid droplets, whereas a treatment of the emulsified liquid remained so for the duration of the experiment, illustrating the mechanism of collision-induced crystallization. The crystallization of the lard emulsion was limited by the degree of undercooling employed in the experiment, resulting in a population of partially solidified droplets. Subsequent crystallization may have been due to combined intradroplet crystallization of further undercooled fat and collision-induced crystallization. Collision with other droplets contain-

ing solid fat makes secondary nucleation of liquid fat and flocculation of existing crystallized droplets possible, thus inducing partial coalescence. Crystals held within droplets cause rupture upon the formation of sufficient intradroplet networks or transition of the crystals to a different morphology and/or polymorph. Impact at the interface of a liquid droplet by another droplet containing solid fat increases the degree of partial coalescence in the emulsion due to the greater coalescence efficiency of the (partially) solid droplet. Growth of a rigid crystal mass or a number of large crystals within droplets provides the required structural rigidity for protrusion of crystals from the interface and penetration into neighboring droplets. Crystallization kinetics of the lard emulsion are different from the bulk, possibly due to the distribution of impurities within the droplet or the number of large slow-growing crystals of emulsified fat. Large crystals were observed at the droplet interface in both fat systems, but their origin was not always discernible with the microscopic technique employed.

### ***Polymorphs in Bulk and Emulsified Fat***

Examination of the destabilization of emulsified fats was also monitored using X-ray diffraction in an attempt to determine the influence of emulsification on the polymorphic form and polymorphic transitions on the stability of emulsified fats. Attempts were also made to examine polymorphic behavior by DSC, but it became evident that the SFC in the emulsions was too low to reliably detect transitions. No detectable differences were found in the polymorphic transitions of bulk and emulsified lard by XRD (Fig. 5). The formation of  $\beta$ -type crystals was favored in both systems, although the  $\beta'$  structure was observed in the lard. The  $\beta$  peak appeared with greater intensity in the emulsified PSCO relative to the emulsified lard, which was not completely crystallized after the first hour of the experiment. The XRD experiment indicates that, in this instance, there was little or no difference in the polymorphic behavior of emulsified and bulk fats; however, as might be expected, the more  $\beta$ -tending PSCO generated large  $\beta$  crystals relatively quickly, leading to the least stable emulsion system.

### ***Emulsion Crystallization in a Shear Field***

The influence of a shear field on emulsion crystallization is of great interest as it relates to behavior during product processing and distribution. Emulsions can be destabilized under shear in a controlled manner to deliver desirable properties; uncontrolled or unintentional destabilization may lead to poor product performance. Comparisons of emulsions under perikinetic (at rest) and orthokinetic (under shear) conditions were made in an effort to understand the role of shear on the stability of the systems studied. Davies *et al.* (22) found stability of triglyceride emulsions containing crystals to be sensitive to both shear and crystal concentration. Crystal morphology also plays an important role in the destabilization of emulsions under shear. Boode and Walstra (4) reported the presence of needle-like

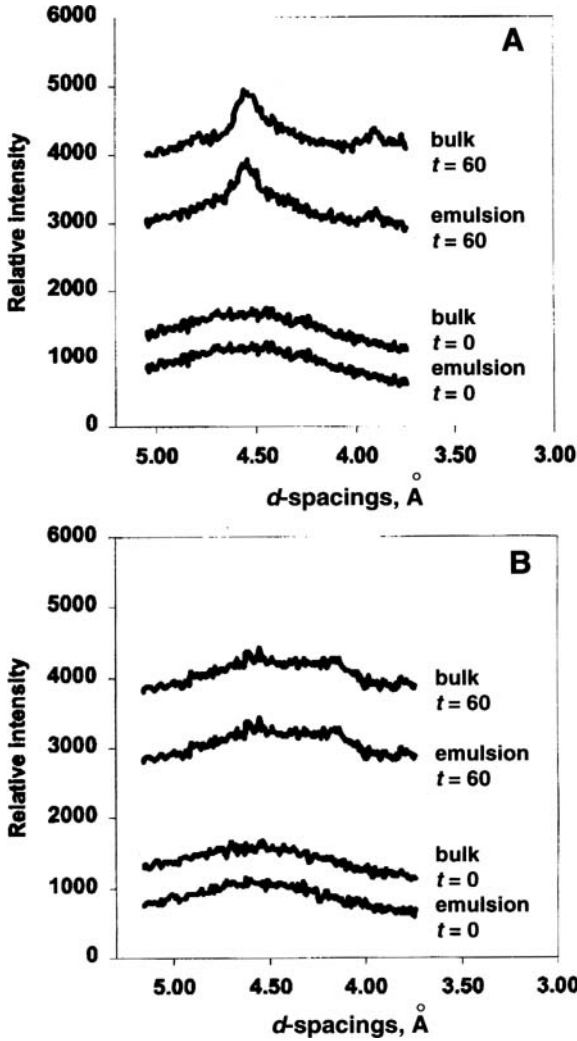


Fig. 5. X-ray diffractograms of bulk and emulsified (A) PSCO and (B) lard held isothermally at 25°C, measured at time zero and 60 min. See Figure 1 for abbreviation.

crystals to be important in the destabilization of milk-fat emulsions. Crystallization of fats at the droplet interface was observed followed by partial coalescence and interglobular crystallization on contact with other droplets.

Contact with other droplets was promoted during isothermal crystallization of the emulsified PSCO and lard in a shear field. During the initial stages of shear, the increase in emulsion viscosity was found to correlate well with the increase in particle size observed under quiescent conditions. Upon reaching a critical level of droplet aggregation or partial coalescence, the increase in viscosity and rate of droplet destabilization diverged rapidly from that observed under quiescent condi-

tions (Fig. 1). The initial viscosity increase was likely due to flocculation of droplets during shear and/or small crystal protrusion from the droplet interface, followed by the rapid increase in viscosity imparted by droplet destabilization and partial coalescence. In both the emulsified lard and PSCO systems, an increase in viscosity was observed as the emulsion destabilized in a low shear field. As stated previously, the stability of the lard emulsion does not appear to be dictated solely by SFC (Fig. 1). Microstructural characterization of the emulsified lard indicated its tendency to form fewer and larger crystals than the emulsified PSCO. This may have contributed to the fact that emulsified lard droplets did not require such a high SFC as the PSCO system for destabilization to occur. A control canola emulsion remained stable when treated in the same manner as the lard and PSCO emulsions, indicating the SFC dependence of emulsion stability under shear conditions.

Shear-induced crystallization had a much greater effect in bulk systems than emulsified systems (Fig. 6) and resulted in an accelerated rate of crystallization. Prior to, and during, the initial stages of crystallization, intradroplet fat is protected from interdroplet crystallization by the spherical shape and pressure of the droplet and is not directly available to the shear field, i.e., no protruding crystals. This observation is consistent with microstructure work where limited destabilization was observed in droplets with no visible crystals. Initially, droplet interfaces in the PSCO system showed that the crystallized fat was not available at the surface, limiting the occurrence of crystal-induced flocculation and coalescence. Droplets remained stable until their interfaces were disturbed by the shear field or crystal interaction.

Exposure to a shear field causes more rapid crystallization as the presence of protruding crystals leads to more aggregation of crystalline droplets, similar to bulk-fat behavior. The rapid increase in the rate of droplet destabilization following crystal growth and protrusion is due to the shear induced by the less spherical

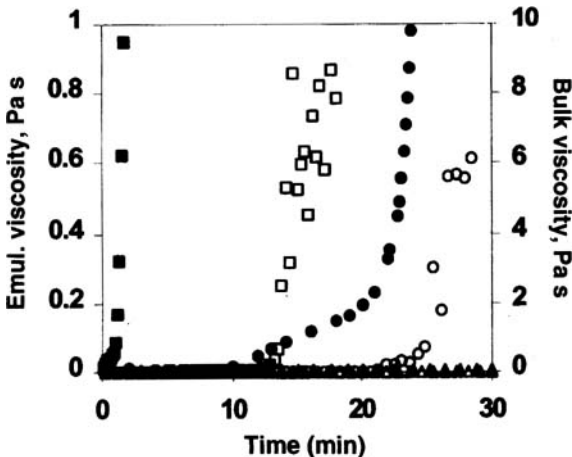


Fig. 6. Viscosity of bulk (lard ●, PSCO ■, canola ▲) and emulsified (Emul) fats (lard ○, PSCO □, canola △) measured at  $10 \text{ s}^{-1}$  as a function of time. Samples quenched and held isothermally at  $25^\circ\text{C}$ . See Figure 1 for abbreviation.

crystalline droplets and an increase in coalescence efficiency resulting from the availability of crystals at interfaces. This behavior was observed in the PSCO emulsion, which began to destabilize only after reaching its final SFC. Destabilization must therefore be induced not just by the increase in SFC of the droplet but by rearrangement, migration, or change in crystal morphology at the droplet interface, and/or change in crystal morphology. Stability of the emulsified fats at rest and under shear was similar until there was either sufficient crystal growth or sufficient energy applied to the system. Once sufficient shear is applied, crystals more easily break the interfacial energy barrier of neighboring droplets and destabilization occurs. Emulsified lard destabilized prior to reaching its final SFC under both orthokinetic and perikinetic conditions. This can be attributed to the slow growth of fewer and larger crystals within the droplet. The initial coalescence efficiency of droplets containing large single crystals is low relative to those filled with a network of fine crystals (18), as they require time to reach the dimensions necessary to span the droplet.

Flocculation of the droplets increases with shear rate (orthokinetic aggregation). The effect of the applied shear field is amplified by crystallization and crystal growth at the surface, hence the difference in behavior at rest and under shear. The shear field supplied the energy required to disrupt the interface during droplet collisions. As crystals protruded from the droplet, the shear rate applied to the emulsion combined with the roughened surface of the droplets contributed to the flocculation and destabilization of the emulsion. Prior to crystal growth out of the droplets, there is less resistance to flow and less shear applied by each droplet to its neighbor. Stability during early stages of shear is more analogous to that illustrated by the particle-size distributions under quiescent conditions as there was not yet sufficient energy supplied to the system to induce coalescence. Destabilization of emulsions at rest was observed as an increase in particle size coupled with slow creaming prior to complete crystallization of the PSCO and lard emulsions compared with the rapid destabilization of the emulsions under shear. As expected, orthokinetic conditions had a measurable impact on the stability of the emulsions. When coupled with an increase in droplet SFC, the increase in collision frequency resulted in an increase in coalescence efficiency and an accelerated rate of droplet destabilization.

Crystallization of lard and PSCO emulsions with similar initial droplet size distributions led to partial coalescence under perikinetic and orthokinetic conditions. The application of shear accelerated the destabilization of the emulsions after the achievement of a critical SFC. The SFC was found not to be the sole contributing factor to emulsion destabilization. Crystal morphology and distribution within the droplet are important factors in the destabilization of these emulsified fats. The emulsions are relatively stable in the short term when crystals are small and form quickly in a consolidated mass in the bulk of the droplet. Polymorphic transitions were not detectable as a source of destabilization in this experiment. The observation of the microstructure of bulk and emulsified fats gave insight into the mechanisms of emulsion destabilization.

## Acknowledgments

The authors would like to acknowledge the financial support of the Natural Sciences and Engineering Research Council (NSERC) of Canada and the Ryerson Polytechnic University Office of Research.

## References

1. Boode, K., C. Bisperink, and P. Walstra, Destabilization of O/W Emulsions Containing Fat Crystals by Temperature Cycling, *Colloids Surf.* 61: 55–74 (1991).
2. Goff, H.D., Instability and Partial Coalescence in Whipped Dairy Emulsions, *J. Dairy Sci.* 80: 2620–2630 (1997).
3. Rousseau, D., Fat Crystals and Emulsion Stability, *Food Res. Intl.* 33: 3–14 (2000).
4. Boode, K., and P. Walstra, Partial Coalescence in Oil–Water Emulsions 1: Nature of Aggregation, *Colloids Surf. A.* 81: 121–137 (1993).
5. Lopez, C., P. Lesieur, G. Keller, and M. Ollivon, Thermal Behaviour of Milk Fat: 1. Unstable Species of Cream, *J. Colloid Interface Sci.* 22: 62–71 (2000).
6. Kloek, W., P. Walstra, and T. van Vliet, Nucleation Kinetics of Emulsified Triglyceride Mixtures, *J. Am. Oil. Chem. Soc.* 77: 643–652 (2000).
7. Sato, K., S. Ueno, and J. Yano, Molecular Interactions and Kinetic Properties of Fats, *Prog. Lipid Res.* 38: 91–116 (1999).
8. Yano, J., and K. Sato, FT-IR Studies on Polymorphism of Fats: Molecular Structures and Interactions, *Food Res. Intl.* 32: 249–259 (1999).
9. Johansson, D., and B. Bergenstahl, Sintering of Fat Crystal Networks in Oil During Post-Crystallization Processes, *J. Am. Oil. Chem. Soc.* 72: 911–920 (1995).
10. Boistelle, R., Fundamentals of Nucleation and Crystal Growth, in *Crystallization and Polymorphism of Fats and Fatty acids*, edited by N. Garti and K. Sato, Marcel Dekker Inc., New York, 1988, pp. 189–226.
11. Skoda, W., and M. Van den Tempel, Crystallization of Emulsified Triglycerides, *J. Colloid Sci.* 18: 568–584 (1963).
12. *The Official Methods and Recommended Practices of the American Oil Chemists' Society*, 4th edn. (1994) Method Ca-5a-40, AOCS Press, Champaign, IL.
13. Turnbull, D., and R.L. Cormia, Kinetics of Crystal Nucleation in Some Alkane Liquids, *J. Chem. Phys.* 34: 820–831 (1961).
14. Mulder, H., and P. Walstra, Crystallization Behaviour in Milk Fat, in *The Milk Fat Globule*, Commonwealth Agricultural Bureaux, Centre for Agricultural Publishing and Documentation, Wageningen, The Netherlands, 1974, pp. 33–53.
15. Kaneko, N., T. Horie, S. Ueno, J. Yano, T. Katsuragi, and K. Sato, Impurity Effects on Crystallization Rates of *n*-Hexadecane in Oil-in-Water Emulsions, *J. Crystal Growth* 197: 263–270 (1999).
16. Siew, W.-L., and W.-L. Ng, Effect of Diglycerides on the Crystallization of Palm Oleins, *J. Sci. Food Agric.* 71: 496–500 (1996).
17. Wright, A.J., R.W. Hartel, S.S. Narine, and A.G. Marangoni, The Effect of Minor Components on Milk Fat Crystallization, *J. Am. Oil Chem. Soc.* 77: 463–475 (2000).
18. Boode, K., and P. Walstra, Kinetics of Partial Coalescence in Oil-in-Water Emulsions, in *Food Colloids and Polymers: Stability and Mechanical Properties*, edited by E. Dickinson and P. Walstra, Royal Society of Chemistry, Cambridge, 1993, pp. 23–30.

19. McClements, D.J., S.-W. Han, and S.R. Dungan, Interdroplet Heterogeneous Nucleation of Supercooled Liquid Droplets in Oil-in-Water Emulsions, *J. Am. Oil Chem. Soc.* 71: 1385–1389 (1994).
20. McClements, D.J., E. Dickinson, and M.J.W. Povey, Crystallization in Hydrocarbon-in-Water Emulsions Containing a Mixture of Solid and Liquid Droplets, *Chem. Phys. Lett.* 172: 449–452 (1990).
21. Davies, E., E., Dickinson, and R. Bee, Shear Stability of Sodium Caseinate Emulsions Containing Monoglyceride and Triglyceride Crystals, *Food Hydrocolloids* 14: 145 (2000).
22. McClements, D.J., and S.R. Dungan, Effect of Colloidal Interaction on Rate of Interdroplet Heterogeneous Nucleation in Oil-in-Water Emulsions, *J. Colloid Interface Sci.* 186: 17–28 (1997).

## Chapter 17

## Crystallization in Emulsion: Application to Thermal and Structural Behavior of Milk Fat

Christelle Lopez<sup>a,b</sup>, Pierre Lesieur<sup>c</sup>, Gérard Keller<sup>b</sup>, and Michel Ollivon<sup>b</sup>

<sup>a</sup>Arlait Recherches, 42, rue de Châteaudun, 75314 Paris cedex 09, France; <sup>b</sup>Equipe Physico-Chimie des Systèmes Polyphasés, UMR 8612 du CNRS, 5 rue J.B. Clément, 92296 Châtenay-Malabry, France; and <sup>c</sup>Laboratoire pour l'Utilisation du Rayonnement Electromagnétique, Bât. 209D Université Paris-Sud, 91898 Orsay, France

### Introduction

Milk, which is the starting point of many food products, is a natural oil-in-water emulsion. Natural milk fat, mainly composed of about 97% triacylglycerols (TG), is dispersed in globules with a mean diameter of 4  $\mu\text{m}$ , stabilized by a complex membrane. The concentration of fat globules in milk leads to cream. The increased knowledge of crystallization of natural milk-fat globules might be of a certain value for technical applications of milk-fat crystallization. Thus, it is interesting to compare crystallization of fat dispersed in emulsion, such as milk or cream, with crystallization of bulk milk fat, devoid of the physical barrier of membranes. To study the thermal and structural properties of TG in fat globules of cream and in anhydrous milk fat (AMF), experiments were conducted using X-ray diffraction as a function of temperature (XRDT) and differential scanning calorimetry (DSC) techniques at different cooling rates. Determination of the physical properties of TG dispersed in fat globules is much more challenging than the study of AMF since the presence of numerous compounds such as water and proteins decreases the intensity of the X-ray signal, at least by simple dilution effect. XRDT experiments were conducted both at small angles, to characterize the longitudinal stacking of TG also called "long spacings" (LS), and at wide angles, which give information on the cross-sectional packing of the aliphatic chains also called "short spacings" (SS). The polymorphic behaviors of TG in emulsion and in AMF were systematically compared in the same conditions. Using very low cooling rates, we studied the formation of stable crystalline varieties (Lopez *et al.*, manuscript submitted for publication). Medium-stability species were studied at intermediate cooling rates (Lopez *et al.*, manuscript in preparation). Very fast quenching from 50 to  $-8^{\circ}\text{C}$  in 3 s allowed us to obtain the most unstable varieties of TG dispersed in milk-fat globules (1). In this paper are presented the results of the later thermal process.

## Materials and Methods

### *Creams*

Concentrated creams [fat content (60% (wt/vol))] obtained after skimming of fresh whole milks originating from Brittany and/or Normandy (Laïta and Lactalis; France) were used for the experiments.

### *AMF*

AMF was extracted from fresh concentrated creams as previously described (2).

### *XRDT/DSC measurements*

Experiments were conducted with coupled time-resolved synchrotron X-ray diffraction as a function of temperature (XRDT) and high-sensitivity differential scanning calorimetry (DSC) (3). X-ray data and thermal measurements were collected simultaneously from the same sample by a single microcomputer. The experiments were carried out on D22 bench ( $\lambda = 1.5498 \text{ \AA}$ ) of DCI synchrotron of LURE (Laboratoire pour l'Utilisation du Rayonnement Electromagnétique). Two one-dimensional position-sensitive proportional detectors allowed XRDT detection simultaneously at small and wide angles (3,4). Crystalline  $\beta$  form of high-purity tristearin was used as reference for both small-angle ( $44.95 \pm 0.05 \text{ \AA}$ ) and wide-angle ( $4.59, 3.85, 3.70 \pm 0.01 \text{ \AA}$ ) channels for scattering vector  $q$  [ $q = \pi \cdot \sin(\theta) / \lambda$ ;  $q$  in  $1/\text{\AA}$ ,  $\theta$  in degrees is the angle of incidence of X-ray relative to the crystalline plane, and  $\lambda$  is the X-ray wavelength] calibration of the detectors.

The samples were loaded in thin Lindeman glass capillaries (GLAS, Muller; Berlin, Germany) with 0.01 mm of wall thickness and diameter ( $\varnothing = 1.4 \pm 0.10 \text{ mm}$ ) using a syringe and a small capillary tubing. The capillaries were heated at  $50^\circ\text{C}$  for 10 min in order to melt all existing crystals and nuclei. The samples were quenched by rapid introduction of the capillaries into the calorimeter coupled with XRD precooled to  $-8^\circ\text{C}$ .

An X-ray pattern has been recorded under isothermal conditions at  $-8^\circ\text{C}$  for 5 min prior to the heating of the sample of cream at  $2^\circ\text{C}/\text{min}$ . from  $-8$  to  $50^\circ\text{C}$  (2).

## Results and Discussion

The sample of concentrated cream was first maintained for 10 min at  $50^\circ\text{C}$  in order to melt all existing crystals and nuclei. At this temperature, all the TG are in a liquid state while proteins are not affected by heat treatment. The sample was quenched by rapid introduction of the capillary into the calorimeter cooled to  $-8^\circ\text{C}$  in order to study the formation of the less stable crystalline structures of TG within fat globules of cream. We can evaluate that quenching rate is about a thousand degrees per minute. The quenching temperature,  $-8^\circ\text{C}$ , was chosen low enough to study crystallized TG structures and high enough to avoid water crystallization during the whole experiments.

After quenching, an isothermal X-ray pattern was immediately recorded at  $-8^{\circ}\text{C}$  for 5 min in order to identify the crystalline structures created after the thermal treatment applied to the sample. Then, the sample of concentrated cream was heated at  $2^{\circ}\text{C}/\text{min}$ . from  $-8$  to  $50^{\circ}\text{C}$  in order to study the evolution of these less stable forms toward more stable varieties formed by TG in fat globules.

**(i) Isothermal conditioning at  $-8^{\circ}\text{C}$  after quenching**

An isothermal X-ray pattern has been immediately recorded at both small and wide angles at  $-8^{\circ}\text{C}$  for 5 min in order to characterize the crystalline structures formed in fat globules after the thermal treatment applied to the sample.

Figure 1 shows both the X-ray diffraction patterns recorded for cream and AMF, to allow a comparison. The small-angle XRD pattern recorded in emulsion shows four peaks corresponding to LS of 70.4, 47, 35.8, and 23.7 Å. As for AMF, which displays similar distances (70, 47, 36, 23.7 Å), they were attributed to the coexistence of two different lamellar phases with triple-chain length ( $3\text{L} = 70$  Å) and double-chain length ( $2\text{L} = 47$  Å) organizations of the TG molecules. The diffraction peak recorded at 23.7 Å may correspond to the third order of the 3L organization or the second order of the 2L variety, or both.

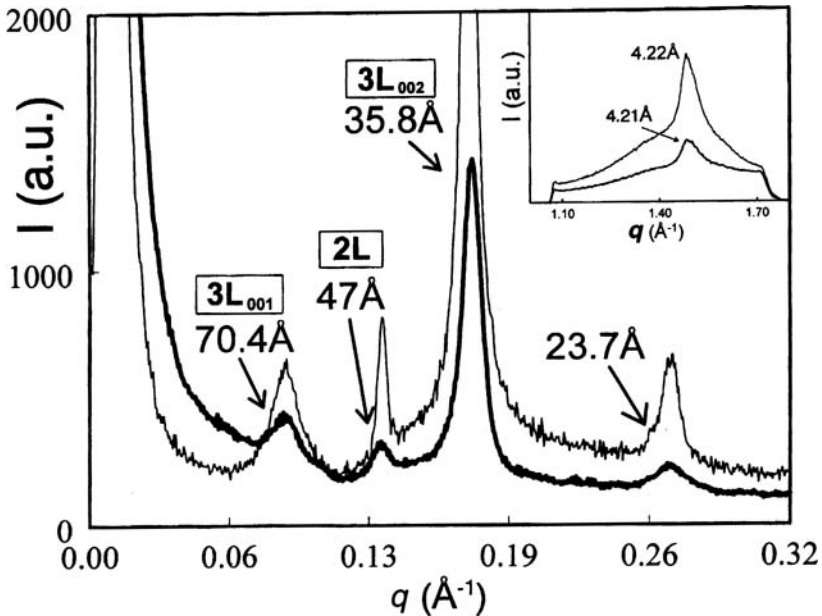


**Fig. 1.** Small- and wide- (insert) angle X-ray diffraction (XRD) patterns recorded at  $-8^{\circ}\text{C}$  after quenching of the samples of cream (thick line) and anhydrous milk fat (thin line) from  $50^{\circ}\text{C}$ .

The evolution, as a function of time, of the unstable crystalline structures formed after quenching, was recorded during 20 min. at  $-8^{\circ}\text{C}$  for cream (Fig. 2), as it was done for AMF (3) using XRDT facilities. The evolutions of the maximal intensities of the peaks were plotted vs. time on the same graph (Fig. 2, insert) in order to visualize the evolution, in isothermal conditions, of the different varieties formed in fat globules. A similar evolution, mainly consisting of the progressive vanishing of 2L (47 Å) and the development of 3L ( $3L_{001} = 70.4$  Å and  $3L_{002} = 35.8$  Å) organizations, was observed for cream and AMF. The results show that the destabilization of the 2L variety is not caused by the temperature increase but is due to the metastable character of this structure. The intensity of the peak at 23.7 Å stays nearly constant vs. time, which allowed us to conclude that it represents actually both the second order of the 2L variety and the third order of the 3L structure. The 2L  $\rightarrow$  3L isothermal transition observed in fat globules and in AMF indicates that the evolution of TG organization is independent of their dispersion state.

The simultaneous wide-angle XRD pattern recorded at  $-8^{\circ}\text{C}$  in emulsion (Fig. 1, insert) shows a single peak with a SS of 4.21 Å on a diffuse peak centered at about 4.5 Å corresponding to the X-ray signature of hydrocarbon chains in the liquid state (5). The single peak corresponds to the crystallization of the alkyl chains

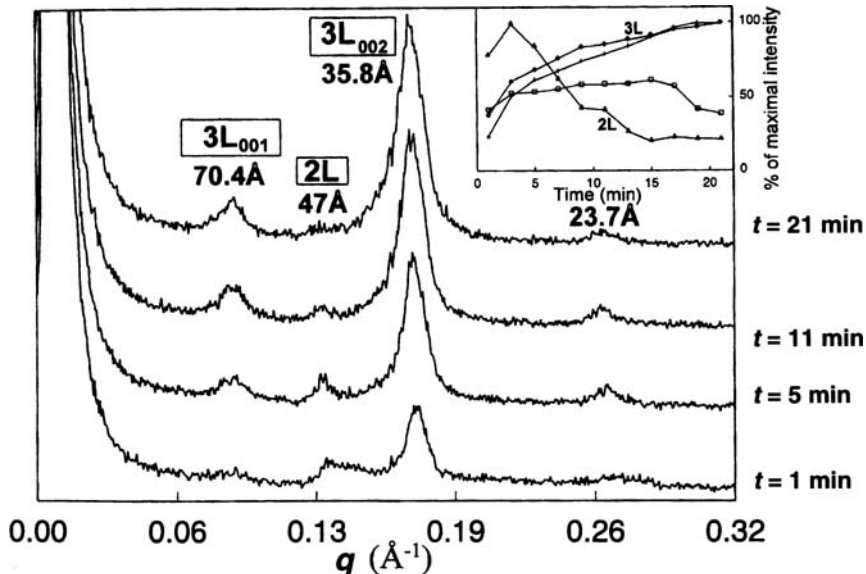


**Fig. 2.** Isothermal evolution at  $-8^{\circ}\text{C}$ , as a function of time, of small-angle XRD peaks recorded just after quenching of cream from  $50^{\circ}\text{C}$ . Insert: evolution of peak relative intensities vs. time (100% corresponds to the strongest peak) : (+) 70.4 Å, (▲) 47 Å, (◇) 35.8 Å, (□) 23.7 Å. 2L, double chainlength; 3L, triple chainlength. See Figure 1 for other abbreviation.

of TG in the unstable  $\alpha$  form (hexagonal packing) which is consistent with the thermal treatment applied to the sample.

As a summary, rapid cooling of both fat globules and AMF leads to the coexistence of a 3L and a 2L structures of unstable  $\alpha$  type.

### (ii) Heating at 2°C/min

After rapid cooling and identification of the unstable varieties formed at  $-8^{\circ}\text{C}$ , the sample of cream was heated to  $50^{\circ}\text{C}$  at  $2^{\circ}\text{C}/\text{min}$ .

**Structural Analysis.** Figure 3 shows the evolution of the crystalline varieties in fat globules, recorded simultaneously by XRD at small (Fig. 3A) and wide (Fig. 3B) angles, during heating of cream at  $2^{\circ}\text{C}/\text{min}$ . In order to delimit the domain of existence of each crystalline variety, it is necessary to analyze the evolutions of spacings and intensities of X-ray peaks as a function of temperature during the heating of the sample at  $2^{\circ}\text{C}/\text{min}$ .

The evolutions of the LS and SS vs. temperature of the diffraction peaks observed in Figure 3 are shown in Figure 4A and B. The LS of the 3L ( $70.4 \text{ \AA}$ ) and 2L ( $47 \text{ \AA}$ ) varieties do not show any significant evolution at  $T < 5^{\circ}\text{C}$  when observed (Fig. 4A). In the  $5 \leq T \leq 11^{\circ}\text{C}$  domain, a progressive  $3\text{L} \rightarrow 2\text{L}$  transition occurs. The thickness of the new 2L crystalline structure formed ( $37.5 \text{ \AA}$ ) increases up to  $40.8 \text{ \AA}$  in the range  $13.2\text{--}24^{\circ}\text{C}$  and increases again of about  $1 \text{ \AA}$  up to the final melting of TG in fat globules. This LS increase was attributable to the selec-

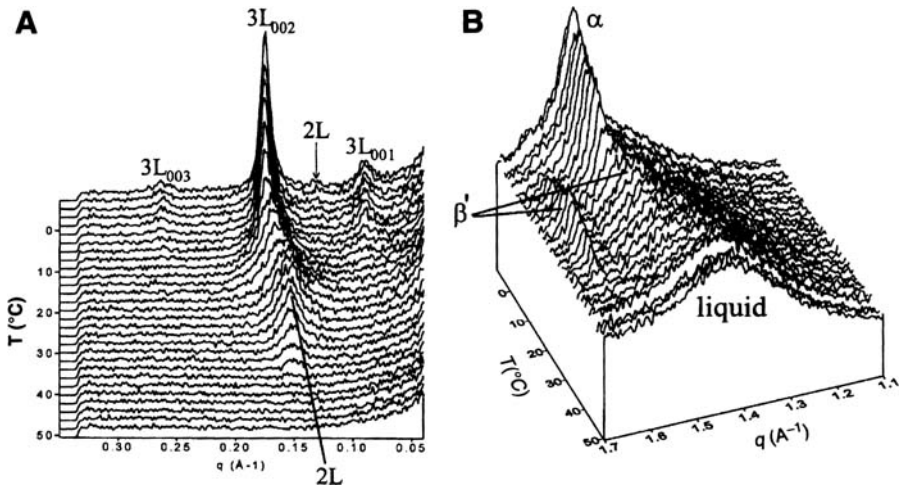


**Fig. 3.** Crystalline evolution of triacylglycerols in fat globules of cream. Three-dimensional plots of small- (A) and wide- (B) angle XRD patterns, recorded simultaneously with differential scanning calorimetry (DSC) experiments during heating of cream at  $2^{\circ}\text{C}/\text{min}$  from  $-8$  to  $50^{\circ}\text{C}$ . See Figure 1 for other abbreviation.

tive melting of TG constituted by shorter acylglycerol chains. The evolution of SS recorded at wide angles (Fig. 4B) shows, at  $T \geq 5^\circ\text{C}$ , a progressive transition from a hexagonal subcell ( $\alpha$ -form) into an orthorhombic packing ( $\beta'$  form) characterized by two diffraction lines (4.2 and 3.9 Å).

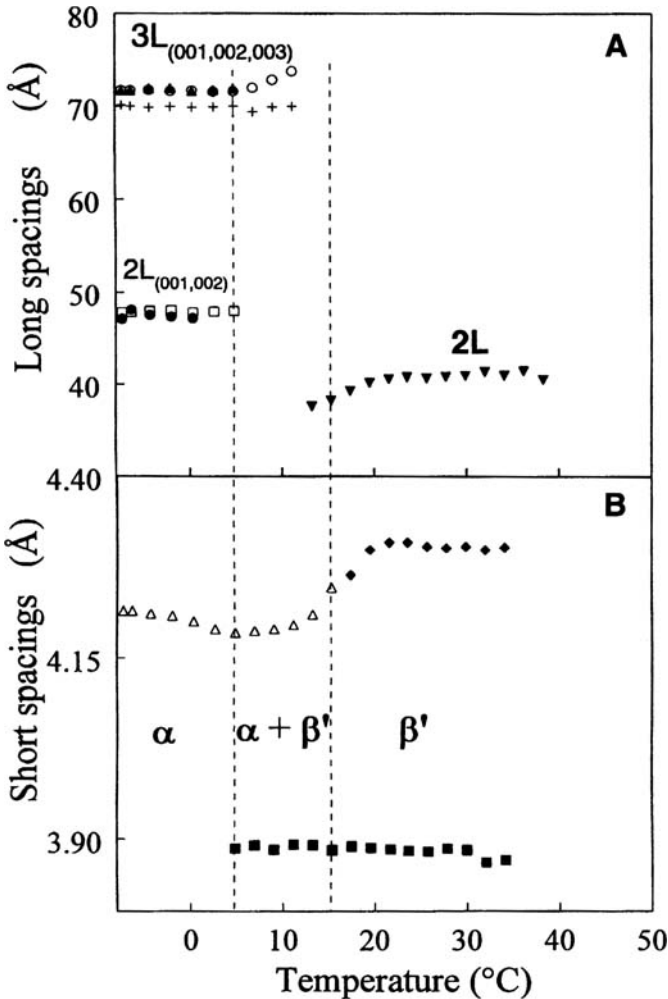


**Fig. 4.** Evolution of the long and short spacings (Å) of unstable crystalline varieties in fat globules of cream recorded by XRD, during heating at  $2^\circ\text{C}/\text{min}$ . from  $-8$  to  $50^\circ\text{C}$ . Reciprocal spacings of lamellar structures are multiplied by their corresponding diffraction order as reported in the figure. (A) Long spacings : (+)  $70.4 \text{ \AA}$ , ( $\square$ )  $47 \text{ \AA}$ , ( $\circ$ )  $35.8 \text{ \AA}$ , ( $\blacktriangle$ )  $23.7 \text{ \AA}$ (003), ( $\bullet$ )  $23.7 \text{ \AA}$ (002), ( $\blacktriangledown$ )  $37.5 \text{ \AA}$ . (B) Short spacings : ( $\triangle$ )  $\alpha$ , ( $\blacklozenge$ )  $\beta'$ ( $4.2 \text{ \AA}$ ), ( $\blacksquare$ )  $\beta'$ ( $3.9 \text{ \AA}$ ). See Figures 1 and 2 for other abbreviations.

The evolutions as a function of temperature of intensities of the XRD peaks observed during the heating of cream (Fig. 3) are shown in Figure 5A and B. Intensities were normalized to the more intense peak in order to allow the comparison of their thermal variations. The intensity evolution of the LS (Fig. 5A) shows the rapid

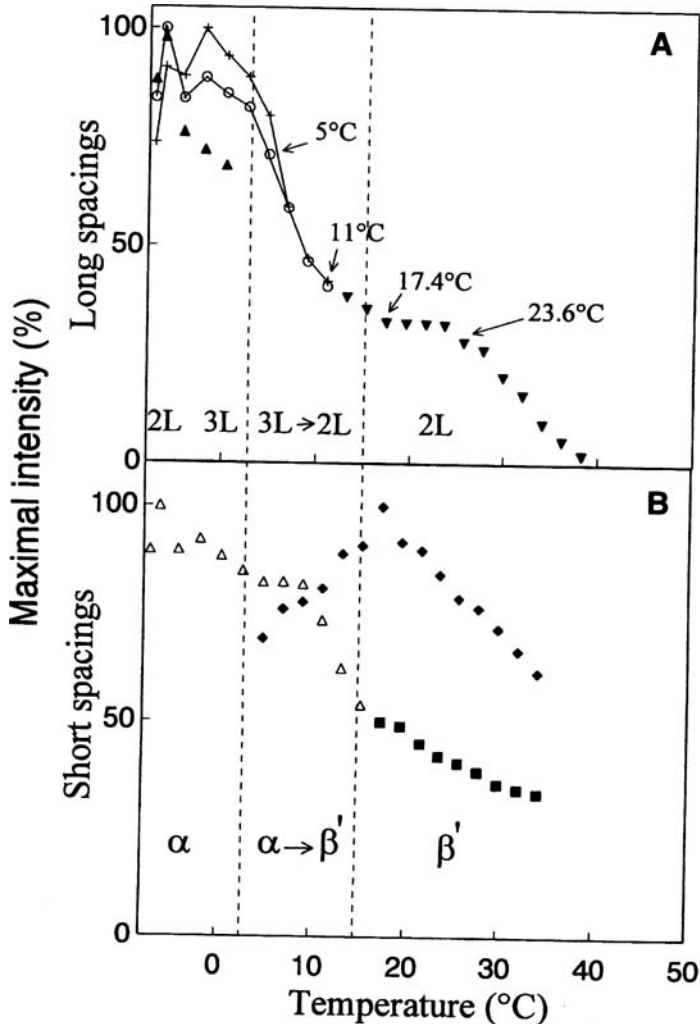


**Fig. 5.** Evolution of the relative intensities expressed as a percentage of the peak maximum of the (A) long and (B) short spacings, recorded by XRD, respectively at small and wide angles, vs. temperature (100% corresponds to the strongest peak). (A) Long spacings : (+) 70.4 Å, (O) 35.8 Å, (▲) 23.7 Å(003), (▼) 37.5 Å. (B) Short spacings : (Δ) α, (◆) β'(4.2 Å), (■) β'(3.9 Å). See Figure 3 for other abbreviations.

vanishing of the 2L (47 Å) structure, identified as a 2L → 3L isothermal transition (see previous discussion). In the  $-8 \leq T \leq 11^\circ\text{C}$  domain, the simultaneous decrease of the set of peaks associated with the 3L organization corresponds to the melting of this variety. From 13.2°C, the new 2L (37.5 Å) variety formed shows four regimes in the decrease of its intensity during heating. The SS intensity evolution recorded simultaneously at wide angles during heating (Fig. 5B) displays break points at identical temperatures as LS (5, 11, and 17.4°C). Thermal evolution of SS summarizes the observation of an  $\alpha$ -form from  $-8$  to about 17°C and of a  $\beta'$ -form from 5 to about 39°C and then the coexistence of  $\alpha$  and  $\beta'$  packings in the 5–17°C range.

The precise analysis of the data allowed delimiting of the domains of existence of the different varieties.

Except for LS peak widths of both unstable 2L and 3L organizations, which are significantly different (1), the overall variations observed in cream resemble that of AMF (2). The fact that this broadening was only observed in the dispersed state was interpreted as a selective influence of the interface curvature onto the less crystalline forms.

*Thermal Analysis.* The DSC curve recorded simultaneously with XRDT experiments on the same sample of cream during heating from  $-8$  to 50°C at 2°C/min is presented in Figure 6 with AMF thermal evolution in the same conditions. Only a comparison of the simultaneously recorded DSC and X-ray data makes it possible to associate the thermal events with the structural changes described above. The domains of existence of the different crystalline varieties identified in cream by X-ray analysis are delimited by vertical lines. The DSC curve clearly shows the end of a first endotherm (melting of 3L structure), an exothermic peak from 5 to 10°C (3L  $\alpha$  → 2L  $\beta'$  transition), and a set of endotherms overlapping each other (selective melting of the 2L structure) until melting of all TG dispersed in milk-fat globules at 39°C. The DSC curve recorded for AMF shows the same thermal events as cream. However, the final melting temperature of cream at about 39°C is repeatedly slightly higher than the final melting point of AMF (37°C). As the TG compositions of cream and AMF are supposedly identical due to the extraction mode of AMF from cream, we interpreted this difference as a structure of the more saturated TG layers by oil–water interface.

## Conclusion

In this study, it has been shown that (i) the brightness of a synchrotron beam is necessary for the study of dispersed systems and (ii) only the coupling of time-resolved XRD at both small and wide angles with DSC allows the interpretation of complex structural and thermal recordings observed during milk-fat globules crystallization.

The study of unstable crystalline varieties formed in milk-fat globules after quenching allowed the identification of a 2L (47 Å) unstable structure with a very

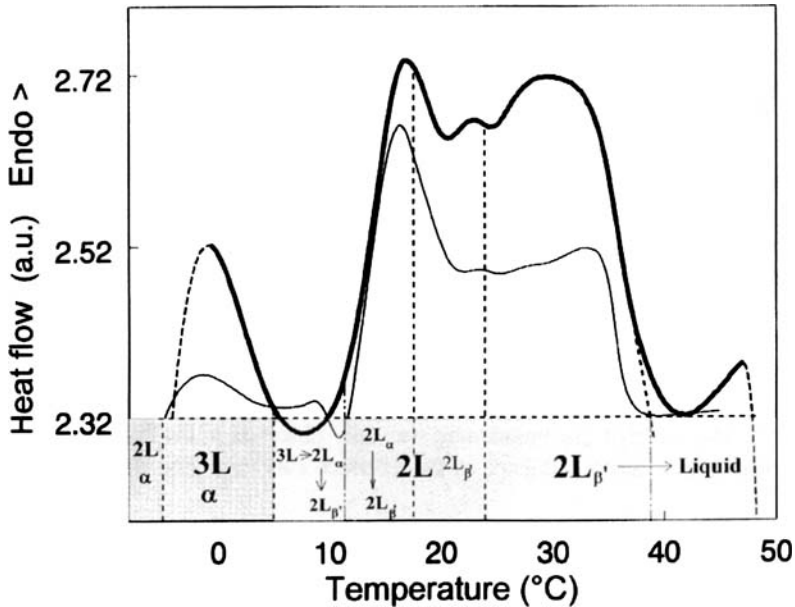


Fig. 6. DSC curves recorded simultaneously with XRD data during heating at  $2^{\circ}\text{C}/\text{min}$  of the samples of cream (thick line) and anhydrous milk fat (thin line). The crystalline varieties formed and their domains of existence deduced from XRD analysis are noted on the figure. See Figures 1 and 3 for other abbreviations.

small domain of existence in isothermal conditions. This result could be important for ice-cream processing. The comparison between cream and AMF fat showed that similar structures are formed in emulsion and in bulk after rapid cooling, but we also showed that TG crystallization is more disordered in emulsion: peak broadenings are attributed to constraints due to interface curvature in emulsion droplets.

### Acknowledgments

The authors thank Arilait Recherches and ANRT for supporting this research. They also thank Mrs. M.-H. Quemener (Laita, France) and Mr. Rabache (Lactalis, France) for supplying cream samples as well as all the members of the Steering Committee for Fat Research of Arilait Recherches.

### References

1. Lopez, C., P. Lesieur, G. Keller, and M. Ollivon, Thermal and Structural Behavior of Milk Fat. 1. Unstable Species of Cream, *J. Colloid Interface Sci.* 229: 62–71 (2000).
2. Lopez, C., F. Lavigne, P. Lesieur, G. Keller, and M. Ollivon, Thermal and Structural Behavior of Milk Fat. 1. Unstable Species of Anhydrous Milk Fat, *J. Dairy Sci.*, in press.

3. Keller, G., F. Lavigne, L. Forte, K. Andrieux, M. Dahim, C. Loisel, M. Ollivon, C. Bourgaux, and P. Lesieur, DSC and X-ray Diffraction Coupling. Specifications and Applications, *J. Thermal Anal.* 51: 783–791 (1998).
4. Keller, G., F. Lavigne, C. Loisel, M. Ollivon, and C. Bourgaux, Investigation of the Complex Thermal Behavior of Fats: Combined DSC and X-ray Techniques, *J. Thermal Anal.* 47: 1545–1565 (1996).
5. Larsson, K., Molecular Arrangement in Glycerides, *Fette Seifen Anstrich.* 74: 136–142 (1972).

## Chapter 18

# Emulsion Partial Coalescence and Structure Formation in Dairy Systems

H. Douglas Goff

Department of Food Science, University of Guelph, Guelph, ON, N1G 2W1, Canada

## Introduction

The process of controlled fat destabilization of an emulsion during whipping and air incorporation is responsible for the establishment of structure in two notable dairy products, whipped cream and ice cream, leading to complex products described both as protein-stabilized emulsions and fat-stabilized foams. This process has been studied by several researchers in whipped cream (1–10) and ice cream (11–13). Fat destabilization is also responsible for structure formation in a variety of whipped nondairy dessert toppings (14,15). “Fat destabilization” (sometimes “fat agglomeration”) is a general term that describes the summation of several different phenomena (16). These include: coalescence, an irreversible increase in the size of fat globules and a loss of identity of the coalescing globules; flocculation, a reversible (with minor energy input) agglomeration/clustering of fat globules with no loss of identity of the globules in the floc; and partial coalescence, an irreversible agglomeration/clustering of fat globules, held together by a combination of fat crystals and liquid fat, and a retention of identity of individual globules as long as the crystal structure is maintained (i.e., temperature-dependent, once the crystals melt, the cluster coalesces). Partial coalescence dominates structure formation in whipped, aerated dairy emulsions (13,17–19), and occurs because of the presence of fat crystals within the emulsion droplets (20).

## Stability of Dairy Emulsions

Raw milk is an oil-in-water emulsion comprised, at the time of secretion, of liquid oil droplets and a protein/phospholipid membrane derived from the secretory cell. Cooling causes temperature-dependent crystallization of the high-melting triglycerides. During processing of dairy emulsions, sufficient heating to melt the fat occurs during pasteurization and homogenization. The latter operation greatly increases surface area of the oil droplets and causes a large adsorption of amphiphilic materials to the oil–water interface. Further cooling again recrystallizes the high-melting triglycerides, but undercooling is a common occurrence, especially in homogenized emulsions given the large number of emulsion droplets per unit mass of fat present, so that attainment of equilibrium is time-dependent (21).

Emulsions are inherently unstable. The interfacial tension or surface free energy between fat and water surfaces is high. Rearrangements will lower the surface free energy as a thermodynamic system moves toward equilibrium by reducing the surface area. The equilibrium situation would be minimum free energy, minimum surface area, and two distinct layers, fat and water. In addition, density differences between the fat and water phases result in a driving force for the fat phase to rise, a process known as creaming. Therefore, coalescence and creaming are inevitable in unstabilized emulsions and both lead to loss of the dispersed state. However, amphiphilic molecules play an important role in emulsions. Proteins with hydrophobic regions or mono- and diglycerides are examples of such molecules as they contain segments that prefer solution into an aqueous environment and segments that prefer solution into a nonpolar environment (22,23). Thus, during the homogenization of oil into a solution in the presence of amphiphilic molecules, a membrane quickly forms around the fat globule. This membrane acts to lower the oil–water interfacial tension and, depending on the amount of surfactant adsorbed, to increase the density of the fat globule. Both have a stabilizing effect, slowing down the rate of coalescence and creaming that may have otherwise occurred.

In a noncrystallized oil-in-water emulsion, when the membrane between two approaching globules is ruptured, the oil generally coalesces. However, many of the triglyceride emulsions common in the food industry, particularly dairy emulsions, are stored at temperatures where fat crystallization occurs (17,24). Such globules show intricate patterns of crystals within the globule, both radial and tangential to the surface, and crystals actually growing or protruding through the membrane (18). If crystals are present in the oil phase, coalescence may be incomplete (partial), leading to the formation of irregularly aggregated globules that retain some of their original identity but are intricately linked (Fig. 1). Partial coalescence exhibits some important differences compared to coalescence of oil

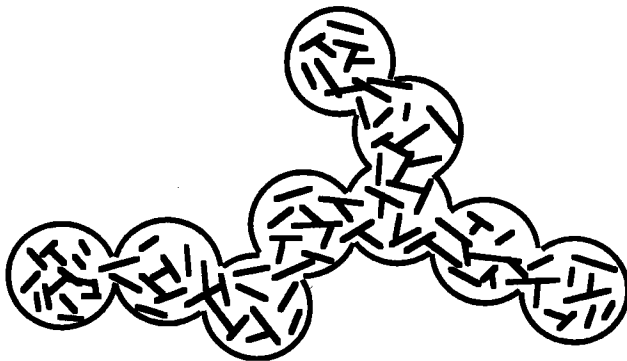


**Fig. 1.** A schematic representation of a network of partially coalesced fat globules, illustrating the important role of fat crystals in the coalescence globules (visualized as the straight lines within the globule).

droplets: the identity of the individual globules is still retained in the aggregates; due to the irregular form of the aggregates, the viscosity of the emulsion may increase; the aggregation can proceed until a continuous network is formed throughout the volume, thus giving the product solid properties (yield stress) and immobilizing other particles (e.g., air cells) present; the rate of aggregation greatly depends on agitation, while liquid droplets rarely show an appreciable dependence of coalescence on agitation; during flow or agitation, the stability to partial coalescence is orders of magnitude smaller than would be the case for coalescence, i.e., the globules containing no crystals (18,19,25). Air has also been shown to greatly affect the formation of fat clustering in partially crystalline emulsions, both when the emulsion is in the static state (e.g., sparging) and during agitation (21). Thus, the combination of air and agitation produces extremely rapid partial coalescence.

### Partial Coalescence in Whipped Cream

#### Structure Formation

Whipped cream is a dairy product that relies heavily on partial coalescence for the development of structure, as it is converted from a viscous liquid into a viscoelastic solid during the process of whipping. Figures 2 and 3 illustrate the build-up of the

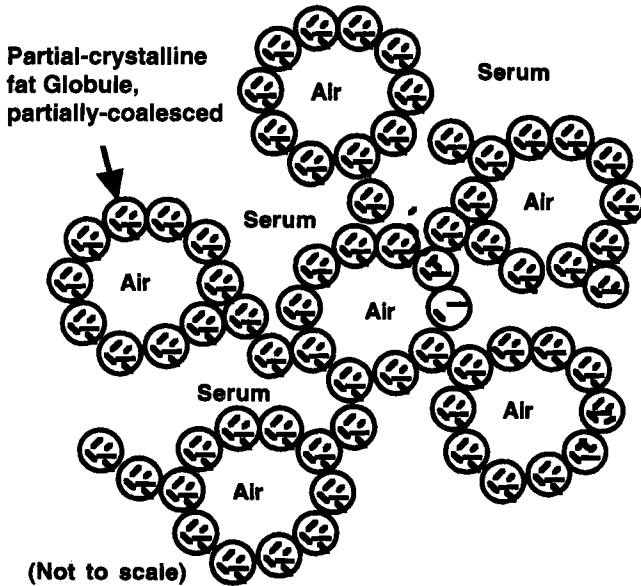
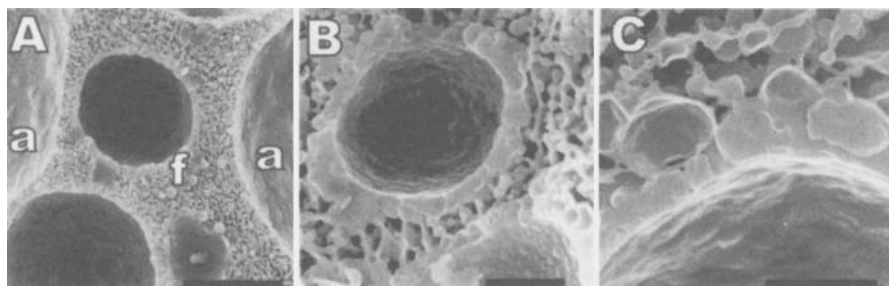


Fig. 2. A schematic representation of the structure of whipped cream, showing the role of fat crystals within the emulsion droplets and partial coalescence of the emulsion in stabilizing the air bubbles and trapping the serum phase into a continuous three-dimensional network.



**Fig. 3.** The structure of whipped cream as determined by scanning electron microscopy. A. Overview showing the relative size and prevalence of air bubbles (*a*) and fat globules (*f*); bar = 30  $\mu\text{m}$ . B. Internal structure of the air bubble, showing the layer of partially coalesced fat which has stabilized the bubble; bar = 5  $\mu\text{m}$ . C. Details of the partially coalesced fat layer, showing the interaction of the individual fat globules. Bar = 3  $\mu\text{m}$  (Ref. 16).

semi-continuous network of fat surrounding and stabilizing the air bubbles. In studying the whipping of heavy cream, Schmidt and van Hooydonk (1) stated that the proteinaceous membrane that envelops the air bubble is penetrated by fat globules as the whipping process proceeds, and this fat penetration offers foam stability to the whipped product. Brooker *et al.* (2) offered a more detailed explanation of the whipping and foam stabilization process in heavy cream. During the initial stages of whipping, air bubbles were stabilized primarily by  $\beta$ -casein and whey proteins with little involvement of fat. Adsorption of fat to air bubbles occurred when the fat-globule membrane coalesced with the air-water interface. Only rarely did fat spread at the air-water interface. The final cream was stabilized by a cross-linking of fat globules surrounding each air cell to adjacent air cells, thus building an infrastructure in the foam. In skim milk foams, the initial air-water interface is also formed by the serum proteins and soluble  $\beta$ -casein with little involvement of micellar casein. Micelles became attached as a discontinuous layer but were not deformed or spread (26). Thus, the important role of the protein, both in the serum phase and at the membrane, cannot be overlooked in the development of whipped cream structure. Bruhn and Bruhn (4) observed that ultra-high temperature (UHT) sterilized cream took about 40% longer to whip than raw or pasteurized cream. Research on the effects of UHT processing and the addition of stabilizer to cream for whipping on structure and rheological properties of whipped cream was extended by Smith *et al.* (8–10).

### **Manipulation of the Adsorbed "Membrane"**

We have recently studied the effect of the protein membrane composition on partial coalescence in 20% milk-fat emulsions (16). Emulsions were produced consisting of 20% fat (from sweet butter, 80% fat), and 0.085, 0.17, 0.25, 0.50, 0.75, 1.0, 1.5, or 2.0% whey protein isolate (WPI, 88% protein; Protose Separations, Teeswater, ON, Canada). The emulsions were heated to 70 or 90°C for 30 min,

continuously stirred with a hand mixer, and then homogenized at 20.7/3.4 MPa (Cherry Burrell Superhomo A125A) (Chicago, IL, USA). Emulsion stability was determined by measuring the fat depletion at the bottom of a 100-mL graduated cylinder in 48 h at 4°C by Babcock fat analysis. Emulsions were whipped with a kitchen mixer and aliquots removed each minute for overrun measurement, fat destabilization by spectroturbidity, and particle size analysis (Mastersizer X, Malvern Instruments, Malvern, Worcs, UK). Foam stability was assessed by removing aliquots after 2 min of whipping and measuring collapse and drainage after 24, 48, and 72 h.

As protein concentration was increased from 0.085 to 0.75%, the mean fat globule diameter decreased, leveling off at a  $d_{3,2}$  of 0.6  $\mu\text{m}$  at protein concentrations greater than 0.75%. Emulsions with greater than 0.25% protein were found to be stable to creaming under quiescent conditions. However, during whipping and agitation, considerable differences were seen in the behavior of the emulsions (Fig. 4). Less than 10% fat destabilization was seen with protein concentration of greater than 1%. However, with protein concentrations between 0.25 and 1%, substantial destabilization was noted during the time course of whipping. Between 0.25 and 0.5% protein, the resulting foams showed little collapse or drainage over 72 h. When the fat-globule size distribution in these emulsions was examined by a Malvern Mastersizer X, it was evident that a small number of larger globules/clusters had formed, which were responsible for the resulting foam stiffness. It was thus concluded that a range of protein concentrations existed where the initial size of the fat globule was small, the emulsion was stable to creaming in the quiescent state, the emulsion formed significant fat destabilization during whipping and agi-

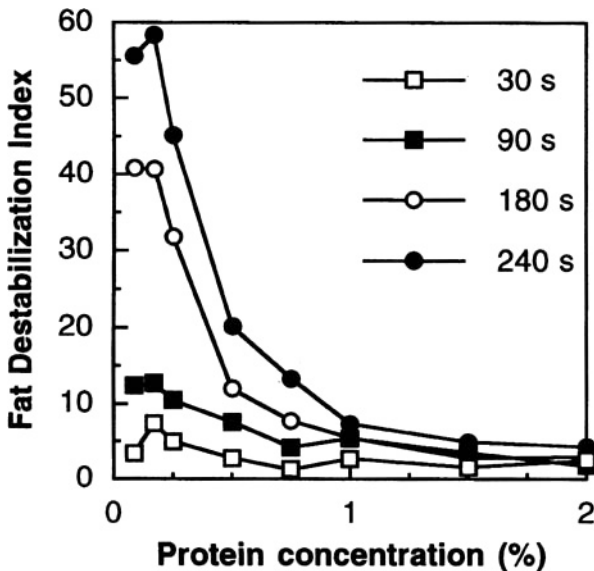


**Fig. 4.** Fat destabilization, determined by spectroturbidity, in 20% milk-fat emulsions as a function of protein concentration in the emulsion and time of whipping in a kitchen mixer at high speed (Ref. 16).

tation, and the resulting foam was stable to collapse and drainage. This is very significant, given that the fat content in these emulsions was only 20%.

The above research indicates the potential for the development of lower-fat whipping creams for the retail market. Preliminary work has been conducted by us to test the concept of altering the fat-globule membrane composition to affect whipped cream formation and stability (16). Emulsions were prepared containing 18% w/w butterfat from sweet butter, 0.175–0.55% whey protein isolate (92% protein), 4.0–6.0% milk solids-non-fat (skim milk powder, 97% solids), 5.0–8.0% sugar, and 0.45–0.60% stabilizer. The emulsions were prepared in two stages by heating the butterfat, WPI, and a portion of the water to 70°C for 30 min, homogenizing at 20.7/3.4MPa, cooling to 4°C, then blending with the skim milk powder, sugar, stabilizer and remainder of the water, which had previously been heated to 70°C for 30 min and cooled to 4°C. Emulsion stability was tested by examination of creaming after 24 h in a 100-mL graduated cylinder. Overrun and foam stability were examined by whipping the emulsions with a kitchen mixer for 2 min. Several combinations of WPI, sugar, and stabilizer produced emulsions that were stable to creaming before whipping and produced stable foams after whipping. None, however, matched the control (35% fat real cream) for foam stiffness or consumer mouthfeel. While this project was only a very preliminary examination of product-development applications, it suggests that application of a two-step process of membrane formation and post-homogenization blending with other desired ingredients, particularly milk proteins not wanted at the fat interface, produced a stable emulsion capable of being whipped into a stable foam.

## Partial Coalescence in Ice Cream

### *Structure Formation*

Ice cream is a complex food colloid that consists of air bubbles, fat globules, ice crystals, and an unfrozen serum phase. The structure of ice cream (Fig. 5) begins with mix as a simple emulsion, with a discrete phase of partially crystalline fat globules at refrigerated temperatures, *ca.* 1  $\mu\text{m}$  in size, surrounded by an interfacial layer comprised of proteins and surfactants. The continuous, serum phase consists of the unadsorbed casein micelles in suspension in a solution of sugars, unadsorbed whey proteins, salts, and high molecular weight polysaccharides. Homogenization is responsible for a reduction in the size and size distribution of the liquid oil droplets at hot temperatures, and begins the formation of the fat-globule membrane, which initially consists of a random mix of amphiphilic molecules. Crystallization of the fat droplets is initiated during cooling to aging temperatures (4°C), and membrane formation is completed in the aging process (4–24 h) with competitive displacement of proteins by added emulsifiers (27).

The mix emulsion is subsequently foamed in the continuous ice cream freezer, creating a dispersed phase of air bubbles, and is concomitantly frozen, forming another dispersed phase of ice crystals. Air bubbles and ice crystals are usually in

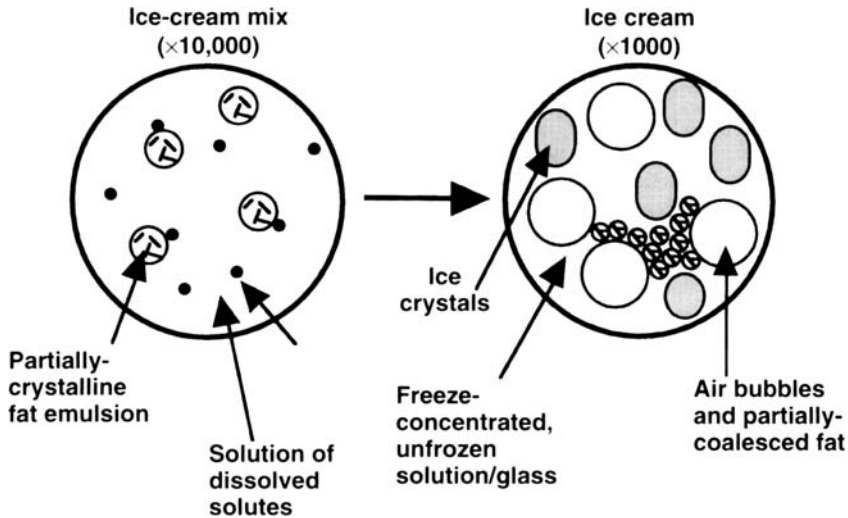


Fig. 5. A schematic representation of the structure of ice-cream mix and of ice cream.

the range of 20 to 50  $\mu\text{m}$ . The solutes and dispersed macromolecules in the serum phase become freeze-concentrated, establishing an ice/unfrozen solution equilibrium based on freezing-point depression considerations. The partially-crystalline fat phase undergoes partial coalescence during the concomitant whipping and freezing process, resulting in a network of agglomerated fat that interacts with the air bubbles and gives rise to a semi-continuous solid-like fat structure throughout the frozen product (27). This results in the beneficial properties of dryness upon extrusion during the manufacturing stages (aids in packaging and novelty molding, for example), a smooth-eating texture in the frozen dessert, and resistance to meltdown or good stand-up properties (necessary for soft-serve operations) (28–30).

### **Role of Surfactants**

Emulsifiers are used in ice cream for: enhancement of fat-crystal nucleation during cooling/aging; improvement of the whipping quality of the mix; production of a drier ice cream to facilitate molding, fancy extrusion, and novelty/impulse manufacture; superior drawing qualities at the freezer to produce a product with good stand-up properties; smoother body and texture in the finished product; and, enhancement of melting resistance (27). Their mechanism of action can be summarized as follows: they lower the fat/water interfacial tension in the mix, resulting in protein displacement from the fat-globule surface, which in turn reduces the stability of the fat globule to destabilization that occurs during the whipping and freezing process, leading to the formation of a fat structure in the frozen product that contributes greatly to texture and meltdown properties. The extent of protein displacement from the membrane, and hence the extent of dryness achieved, is a func-

tion of the emulsifier type and concentration. The loss of steric stability from the globule, which was contributed from protein adsorption, particularly casein micelles, accounts for its greater propensity for partial coalescence during shear (11,24,31,32).

Due to the importance of the fat destabilization phenomena in ice cream, it would be desirable to predict the extent of fat destabilization for a particular freezing process from measurement of colloidal properties in mix. This would allow ingredient suppliers and manufacturers to assess the impact of formulation changes without extensive pilot-plant work. Since the effect of emulsifiers on fat destabilization and the effect of emulsifiers on protein displacement from the interface of fat droplets in emulsions are well-known (27), it seems plausible that adsorbed protein measurements in mix should allow for the prediction of fat destabilization subsequently occurring during the freezing of that mix under constant processing conditions. Thus, the objectives of a recent research project in our laboratory were to study the effect of emulsifiers on the structure of fat in ice-cream mix and ice cream, the subsequent meltdown characteristics of the ice cream, and the correlation between colloidal ice-cream mix properties and properties of ice cream (30). A range of emulsifier types and concentrations was used to produce a series of ice-cream mixes. Adsorbed protein on fat globules and fat particle size were measured. After freezing, fat agglomeration index, solvent extractable fat, fat agglomerate size, microstructure in the frozen state, melting rate, and component analyses (protein and fat) of the melt were measured and correlated to mix property measurements.

Increasing levels of emulsification significantly depleted protein from the fat globule in the mix. The adsorbed protein content in the mix ( $\text{mg m}^{-2}$  of fat surface area) correlated with major characteristic analyses describing the fat structure in ice cream (fat agglomerate size, fat agglomeration index, solvent extractable fat; Fig. 6). Thus, the measurement of protein load in the mix can be used to predict ice-cream-fat stability and related structure. Structural analyses indicated enhanced interaction between fat and air as protein adsorption decreased. It was also observed that the fat content in the dripped portion collected from a meltdown test correlated well with other indices of fat destabilization.

Although the importance of fat destabilization to ice-cream structure is well-known (27), it is not clear whether the appropriate schematic model for destabilized fat networks is one of partially coalesced (clustered) fat globules adsorbed to air bubbles, or fat clusters primarily in the bulk, or both. The role of coalescence in fat destabilization is also not clear. Most of the measurements of fat destabilization are done on melted ice cream. Thus, we recently completed a study, by low-temperature scanning electron microscopy and freeze-substitution transmission electron microscopy with low-temperature embedding, of fat and air structures in ice-cream samples containing differing degrees of fat destabilization (13). Variations in fat destabilization were achieved by processing ice cream with three different emulsifier concentrations in the formulation (no emulsifier; mono- and diglyc-

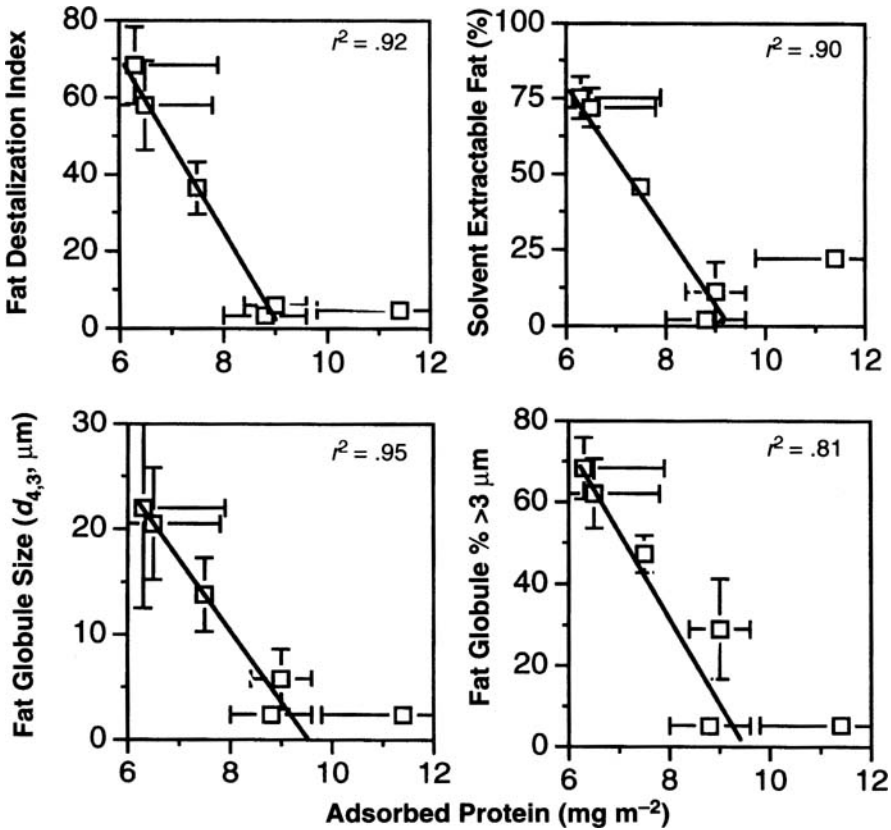
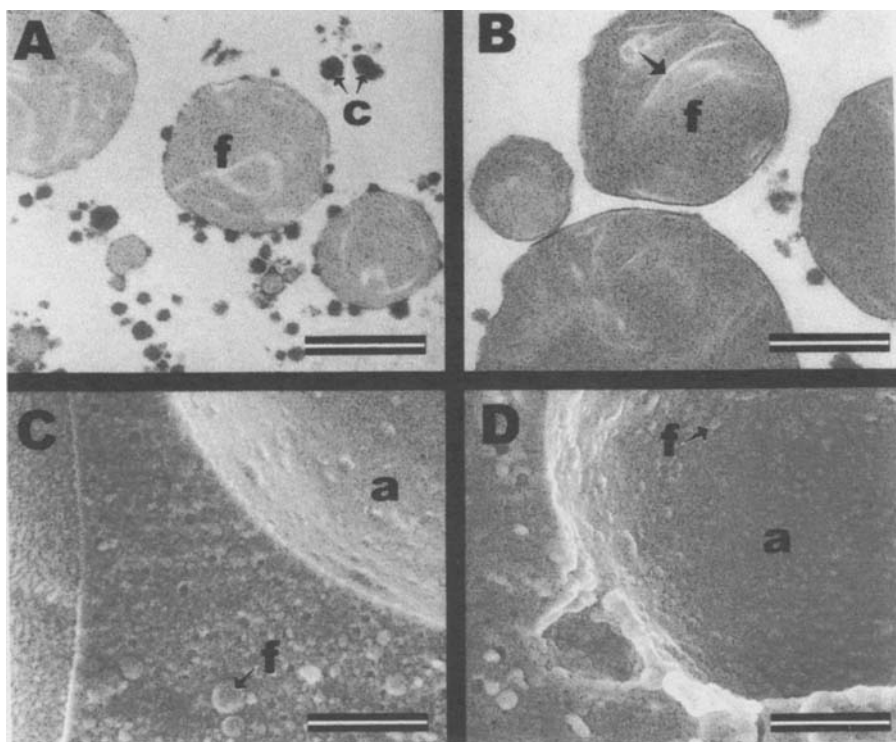


Fig. 6. The effect of adsorbed protein in the mix on fat agglomeration index, solvent extractable fat, and fat agglomerate size in ice cream (Ref. 30).

erides added; mono- and diglycerides plus polysorbate 80 added) and by three different freezing techniques (batch freezing, continuous freezing at low back pressure, and continuous freezing at high back pressure). Each of these variations was expected to have an impact on the formation of air bubbles and the degree of fat destabilization exhibited in the ice cream, hence on the fat and air structures created.

Figure 7 shows the effect of protein adsorbed to the surface of the fat globule on resulting ice-cream structure. High levels of adsorbed protein, especially casein micelles, in the mix (Fig. 7A) impede fat adsorption at the air interface (Fig. 7C), impede fat partial coalescence and network formation (Fig. 7E), leading to rapid meltdown with recovery of mostly intact fat globules (Fig. 7G). However, low levels of adsorbed protein in the mix (Fig. 7B) enhance fat adsorption at the air interface (Fig. 7D), promote fat partial coalescence and network formation (Fig. 7F), leading to slower meltdown as the fat network (Fig. 7H) must collapse after ice



**Fig. 7.** The effect of adsorbed protein on structure of ice-cream mix, ice cream, and melted ice cream. A–B, ice-cream mix with no surfactant and with added surfactant, respectively, as viewed by thin-section transmission electron microscopy. *f* = fat globule, *c* = casein micelle, arrow = crystalline fat, bar = 0.5  $\mu\text{m}$ . See Reference 24 for methodology. C–D, ice cream with no surfactant and with added surfactant, respectively, as viewed by low-temperature scanning electron microscopy. *a* = air bubble, *f* = fat globule, bar = 4  $\mu\text{m}$ . See Reference 34 for methodology. E–F, ice cream with no surfactant and with added surfactant, respectively, as viewed by thin-section transmission electron microscopy with freeze substitution and low-temperature embedding. *a* = air bubble, *f* = fat globule, *c* = casein micelle, *fc* = fat cluster, bar = 1  $\mu\text{m}$ . See Reference 13 for methodology. G–H, melted ice cream with no surfactant and with added surfactant, respectively, as viewed by thin-section transmission electron microscopy. *f* = fat globule, *c* = casein micelle, *fn* = fat network, bar = 1  $\mu\text{m}$  in G and 5  $\mu\text{m}$  in H. See Reference 24 for methodology.

crystals have melted. It could be concluded from this work that the appropriate schematic model for fat and air structures in ice cream includes a significant concentration of discrete fat globules and clusters at the air interface, an important role of protein at the air interface, clustered fat extending away from the air interface into the serum phase, and clustered fat in the serum phase independent of the air interface. Fat destabilization in ice cream includes both the processes of partial

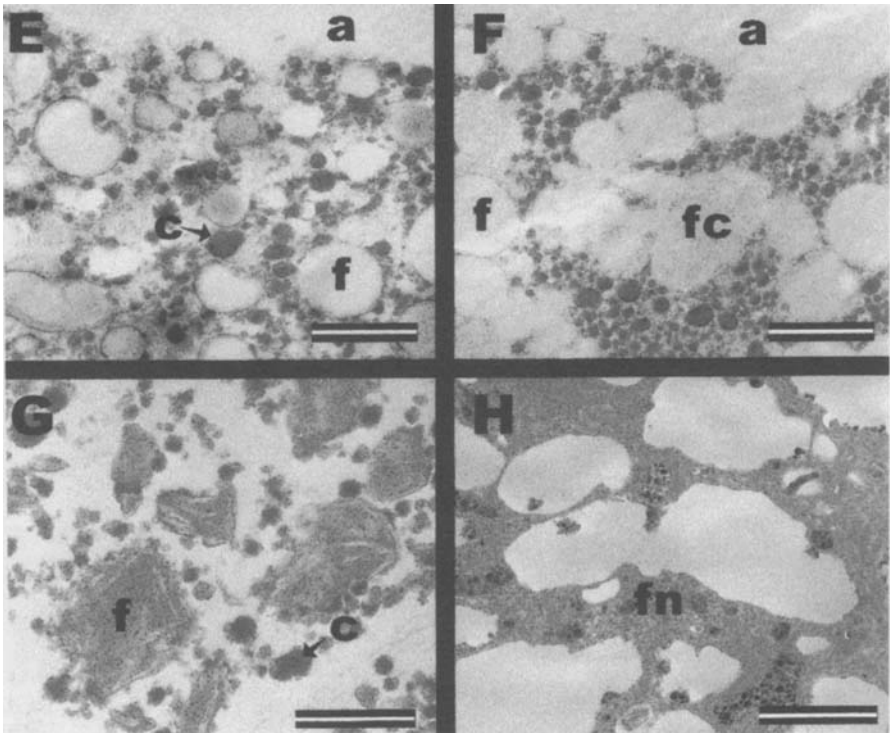


Fig. 7. (Cont.).

coalescence and coalescence, although examples of the former were much more apparent. Air interfaces were not completely covered by fat globules, even with the highest levels of fat destabilization. There did not seem to be significant fat spreading or continuous fat layers at the air interface. Air interfaces from continuous and batch freezing were similar.

#### ***Manipulation of the Adsorbed "Membrane"***

As discussed above, partial coalescence of emulsified fat droplets is critical for generating desirable ice-cream body and texture. In conventional ice-cream manufacture, the fat droplets are first stabilized by a thick coating of proteins, which is subsequently displaced by small-molecule surfactant as the mix is aged. The resulting thin coating of surfactant allows close association of droplets and is necessary for partial coalescence. We hypothesized in a recent research project that emulsifying butterfat with minimal concentrations of milk proteins would generate quiescently stable fat droplets but with a droplet membrane thin or fragile enough to undergo partial coalescence under conditions of shear (33). After homogenization of the fat with the desired type and concentration of protein to create an emulsion,

further ice-cream-mix components could be added as desired. Thus, emulsions created from butter oil (25%) and minimal amounts of WPI and sodium caseinate (0.2–0.7%) were characterized for particle size, protein surface concentrations, and relative stability under shear as a first step in such a process.

At the same mix protein concentration, sodium caseinate emulsions had a slightly smaller average particle size compared to WPI emulsions. Protein surface concentration increased for both protein types with increasing protein levels in the mix. Both proteins gave emulsions that were quiescently stable over the course of the experiment at protein levels higher than 0.2%. The amount of partial coalescence from shearing of the emulsions was found to decrease as the protein level increased regardless of the protein type (Fig. 8). Thus, the lower the surface concentration of protein, the greater the susceptibility to partial coalescence. At a given protein level, WPI emulsions appeared to undergo more partial coalescence than sodium caseinate emulsions when subjected to whipping action (Fig. 8). This is likely attributed to the amphiphilicity and flexibility of the casein molecules, allowing them to form a tighter coating on the fat droplets. As considerable partial coalescence is desirable in ice cream, the lower the protein surface concentration, the better for an ice-cream

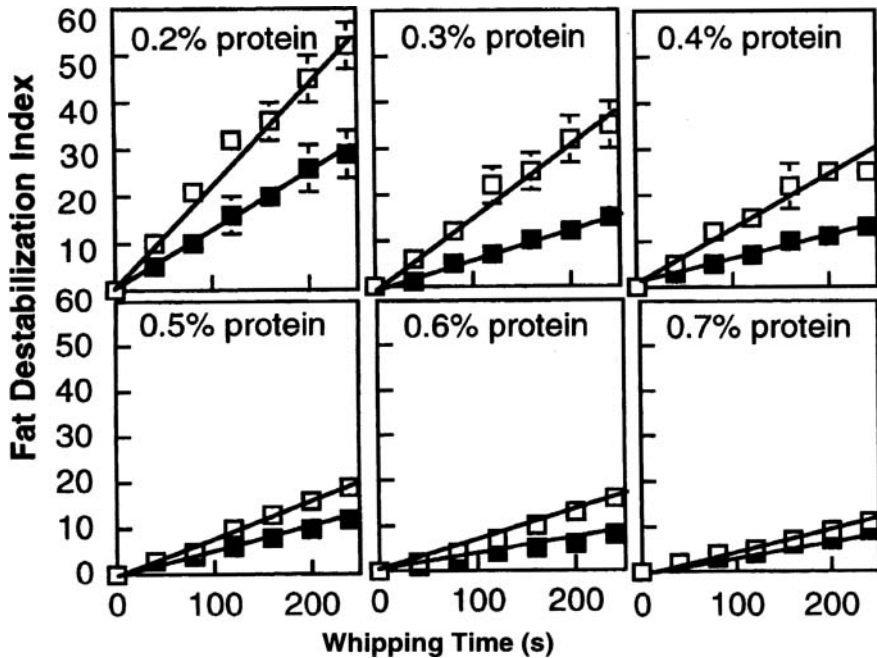


Fig. 8. The effect of adsorbed protein type and concentration on the destabilization of emulsions during whipping. □, whey protein isolate emulsions; ■, sodium caseinate emulsions (33).

emulsion. However, quiescent stability must also be considered, and as mentioned 0.3% protein was found to be the lower threshold for generating a quiescently stable emulsion under these experimental conditions. From the above experimentation, it appears that WPI at minimal surface concentration would be more suitable than sodium caseinate as an ice-cream emulsifier system.

## Conclusions

Emulsion stability is required in many dairy applications, but not all. In products like whipped cream and ice cream, the emulsion must be stable in the liquid form but must partially coalesce readily upon foaming and the application of shear. The structure and physical properties of whipped cream and ice cream depend on the establishment of a fat-globule network. In cream whipped to maximum stability, partially coalesced fat covers the air interface. In ice cream, partially coalesced fat exists both in the serum phase and at the air interface; also, there is more globular fat at the air interface with increasing fat destabilization. Partial coalescence occurs due to the collisions in a shear field of partially crystalline fat-emulsion droplets with sufficiently-weak steric stabilization (low level of surface adsorption of amphiphilic material to the interface per unit area). To achieve optimal fat crystallinity, the process is very dependent on the composition of the triglycerides and the temperature. It is also possible to manipulate the adsorbed layer to reduce steric stabilization to an optimal level for emulsion stability and rapid partial coalescence upon the application of shear. This can be done either by addition of a small-molecule surfactant to a protein-stabilized emulsion or by a reduction of protein adsorption to a minimal level through selective homogenization.

## Acknowledgments

Appreciation is expressed to the Ontario Ministry of Agriculture, Food and Rural Affairs, Unilever Research Colworth Laboratory, and Goodman Fielder Ingredients for financial support, and to Shanti Anant, Stephan Bolliger, Kevin Segall, Sandy Smith, and Edita Verespej for collaboration in the experimental studies.

## References

1. Schmidt, D.G., and A.C.M. vanHooydonk, A Scanning Electron Microscopical Investigation of the Whipping of Cream, *Scanning Electron Microscopy III*: 653–658 (1980).
2. Brooker, B.E., M. Anderson, and A.T. Andrews, The Development of Structure in Whipped Cream, *Food Microstruc.* 5: 277–285 (1986).
3. Noda, M., and Y. Shiinoki, Microstructure and Rheological Behaviour of Whipping Cream, *J. Texture Studies* 17: 189–204 (1986).
4. Bruhn, C.M., and J.C. Bruhn, Observations on the Whipping of Cream, *J. Dairy Sci.* 71: 857–862 (1988).
5. Brooker, B.E., The Adsorption of Crystalline Fat to the Air–Water Interface of Whipped Cream, *Food Struc.* 9: 223–229 (1990).

6. Needs, H.C., and A. Huitson, The Contribution of Milk Serum Proteins to the Development of Whipped Cream Structure, *Ibid.* 10: 353–360 (1991).
7. Stanley, D.W., H.D. Goff, and A.S. Smith, Texture–Structure Relationships in Foamed Dairy Emulsions, *Food Res. Internat.* 29: 1–13 (1996).
8. Smith, A.K., H.D. Goff, and Y. Kakuda, Whipped Cream Structure Measured by Quantitative Stereology, *J. Dairy Sci.* 82: 1635–1642 (1999).
9. Smith, A.K., H.D. Goff, and Y. Kakuda, Microstructure and Rheological Properties of Whipped Cream as Affected by the Heat Treatment and Addition of Stabilizer to the Cream, *Internat. Dairy J.* 10: 295–301 (2000).
10. Smith, A.K., H.D. Goff, and Y. Kakuda, Changes in Protein and Fat Structure in Whipped Cream Caused by Heat Treatment and Addition of Stabilizer to the Cream, *Food Res. Internat.* 33: 697–706 (2000).
11. Goff, H.D., and W.K. Jordan, Action of Emulsifiers in Promoting Fat Destabilization During the Manufacture of Ice Cream, *J. Dairy Sci.* 72: 18–29 (1989).
12. Gelin, J.-L., L. Poyen, J.-L. Courthadon, M. Le Meste, and D. Lorient, Structural Changes in Oil-in-Water Emulsions During the Manufacture of Ice Cream, *Food Hydrocoll.* 8: 299–308 (1994).
13. Goff, H.D., E. Verespej, and A.K. Smith, A Study of Fat and Air Structures in Ice Cream, *Internat. Dairy J.* 9: 817–829 (1999).
14. Buchheim, W., N.M. Barfod, and N. Krog, Relation Between Microstructure, Destabilization Phenomena and Rheological Properties of Whippable Emulsions, *Food Microstruc.* 4: 221–232 (1985).
15. Barfod, N.M., and N. Krog, Destabilization and Fat Crystallization of Whippable Emulsions (Toppings) Studied by Pulsed NMR, *J. Am. Oil Chem. Soc.* 64: 112–119 (1987).
16. Goff, H.D., Instability and Partial Coalescence in Dairy Emulsions, *J. Dairy Sci.* 80: 2620–2630 (1997).
17. Boode, K., C. Bisperink, and P. Walstra, Destabilization of O/W Emulsions Containing Fat Crystals by Temperature Cycling, *Colloids Surfaces* 61: 55–74 (1991).
18. Boode, K., and P. Walstra, Partial Coalescence in Oil-in-Water Emulsions 1. Nature of the Aggregation, *Colloids Surfaces A: Physicochem. Eng. Aspects* 81: 121–137 (1993).
19. Boode, K., P. Walstra, and A.E.A. deGroot-Mostert, Partial Coalescence in Oil-in-Water Emulsions 2. Influence of the Properties of the Fat, *Ibid.*: 139–151 (1993).
20. Rousseau, D., Fat Crystals and Emulsions Stability—A Review, *Food Res. Internat.* 33: 3–14 (2000).
21. Walstra, P., T.J. Guerts, A. Nooman, A. Jellema, and M.A.J.S. van Boekel, *Dairy Technology*, Marcel Dekker, Inc., New York, 1999, pp. 107–124, 410–425.
22. Aynié, S., M. Le Meste, B. Colas, and D. Lorient, Interactions Between Lipids and Milk Proteins in Emulsion, *J. Food Sci.* 57: 883–886,891 (1992).
23. Tomas, A., J.-L. Courthadon, D. Paquet, and D. Lorient, Effect of Surfactant on Some Physico-Chemical Properties of Dairy Oil-in-Water Emulsions, *Food Hydrocoll.* 8: 543–553 (1994).
24. Goff, H.D., M. Liboff, W.K. Jordan, and J.E. Kinsella, The Effects of Polysorbate 80 on the Fat Emulsion in Ice Cream Mix: Evidence from Transmission Electron Microscopy Studies, *Food Microstruc.* 6: 19–198 (1997).
25. van Boekel, M.A.J.S., and P. Walstra, Stability of Oil-in-Water Emulsions with Crystals in the Disperse Phase, *Colloids Surfaces* 3: 109–118 (1981).

26. Brooker, B.E., Observations on the Air Serum Interface of Milk Foams, *Food Microstruc.* 4: 289–296 (1985).
27. Goff, H.D., Colloidal Aspects of Ice Cream—A Review, *Internat. Dairy J.* 7: 363–373 (1997).
28. Berger, K.G., Ice Cream, in *Food Emulsions*, 3rd Edn., edited by S. Friberg and K. Larsson, Marcel Dekker Inc., New York, 1997, pp. 413–490.
29. Walstra, P., and Jonkman, M. (1998), The Role of Milkfat and Protein in Ice Cream, in *Ice Cream*, edited by W. Buchheim, Special Issue 9803, International Dairy Federation, Brussels, pp. 17–24.
30. Bolliger, S., H.D. Goff, and B.W. Tharp, Correlation Between Colloidal Properties of Ice Cream Mix and Ice Cream, *Internat. Dairy J.* 10: 303–309 (2000).
31. Goff, H.D., J.E. Kinsella, and W.K. Jordan, Influence of Various Milk Protein Isolates on Ice Cream Emulsion Stability, *J. Dairy Sci.* 72: 385–397 (1989).
32. Barfod, N.M., N. Krog, G. Larsen, and W. Buchheim, Effect of Emulsifiers on Protein–Fat Interaction in Ice Cream Mix During Aging I. Quantitative Analyses, *Fat Sci. Technol.* 93: 24–29 (1991).
33. Segall, K.I., and H.D. Goff, Influence of Adsorbed Milk Protein Type and Surface Concentration on the Quiescent and Shear Stability of Butteroil Emulsions, *Internat. Dairy J.* 9: 683–691 (1999).
34. Caldwell, K.B., H.D. Goff, and D.W. Stanley, A Low-Temperature Scanning Electron Microscopy Study of Ice Cream. I. Techniques and General Microstructure, *Food Struc.* 11: 1–9 (1992).

## Chapter 19

## Solidification Processes in Chocolate Confectionery Manufacture

Gregory R. Ziegler

Department of Food Science, Penn State University, 116 Borland Lab, University Park, PA 16802

### Introduction

The phenomena of crystallization and solidification when applied to chocolate confectionery can be conveniently separated into the unit operations of tempering, sometimes referred to as pre-crystallization, and cooling or bulk crystallization (Fig. 1). The objective of tempering is the production of the right amount of crystal “seed” (weight percentage) of the appropriate size (or number) in the proper polymorphic form—ideally, 1–3% of small crystals of form V ( $\beta$ ) evenly distributed throughout the mass. The precise path to obtaining these conditions is highly dependent on thermal history and shear, the effect of which is little understood.

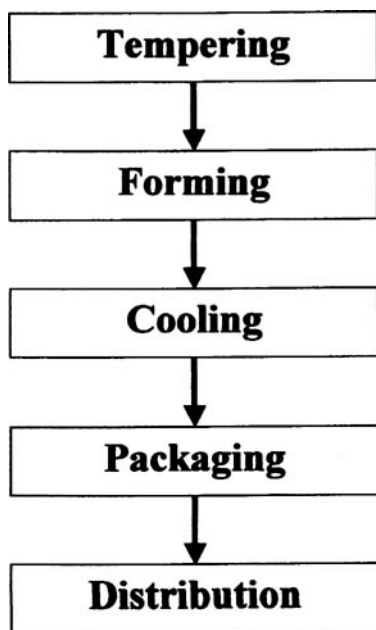


Fig. 1. Chocolate-forming operations.

During cooling, the bulk of the triacylglycerols is deposited on the “seed,” forming a coherent fat crystal network. However, crystallization is not completed with cooling (1). We routinely store chocolate at 19°C for at least 1 wk before measuring physical or sensory properties, since they are generally not stable before this time. Furthermore, re-crystallization occurs during storage and distribution, often resulting in the quality defect known as fat bloom. At room temperature, only about 75% of the cocoa butter in chocolate (or cocoa butter and milk fat in milk chocolate) is solidified. The presence of a liquid phase and a distribution in fat crystal size promote Ostwald ripening, where larger crystals grow at the expense of smaller ones.

Manufacturing confectionery is nothing short of controlling crystallization, and given the value of chocolate, it is not surprising that in the area of crystallization of lipids a large amount of attention will be directed to cocoa butter. Much has been written on the subject of polymorphism under both dynamic (tempering) and static (bloom) conditions. Therefore, here is presented a study strictly concentrating on a review of approaches to bulk crystallization. The correct model, at least for bulk crystallization, is probably not what you find in most chemical engineering texts, which seem to focus on crystallization for separations, but comes from the materials area, most particularly metals casting (2).

## Crystallization in Chocolate

Crystallization events in chocolate manufacture include tempering (pre-crystallization), cooling (bulk crystallization), and bloom (re-crystallization). These processes influence a number of important technological (economic) and sensorial attributes of chocolate (Table 1). Much attention has been focused on bloom formation and its influence on color and gloss, and for good reason, since a consumer may never even buy, let alone eat, a “moldy-looking” confection. However, we are less

**TABLE 1**

Important Attributes of Chocolate Confectionery Influenced by Crystallization Processes

---

Bloom Resistance (and hence shelf life)
Coating weight control (yield)
Color
Contraction from molds
Susceptibility to “fingerprinting”
Gloss
Melt rate (and hence flavor)
Productivity (production rates)
Smearing
Snap
Texture (hardness, grain)

---

able to quantitatively describe the crystal structure that leads to desirable attributes. For example, the failure properties, commonly referred to as “snap,” will depend on features of the fat crystal network and its interaction with the nonfat particulate phase. Texture will also depend on the “grain size”—the most obvious example being a badly bloomed chocolate with large fat crystals, often described as “crumbly.” But short of this extreme, we know very little of how the microstructure influences, for example, melt rate and flavor perception. Perhaps crystal morphology plays a role. Rousset and Rappaz (3) have observed several crystalline microstructures during the solidification of POS (the triacylglycerol 1-palmitoyl-2-oleoyl-3-stearyl-*sn*-glycerol) and have published the results in the form of morphology maps.

Reviewing and synthesizing the literature on chocolate solidification present some challenges, the first of which is to accurately define the system under study. Due to its complexity, little published information is available on chocolate *per se*. Instead, model systems usually consisting of purified triacylglycerols and mixtures thereof are the object of investigation. Figure 2 illustrates the hierarchy in these systems, with the degree of complexity increasing from bottom to top. The extrap-

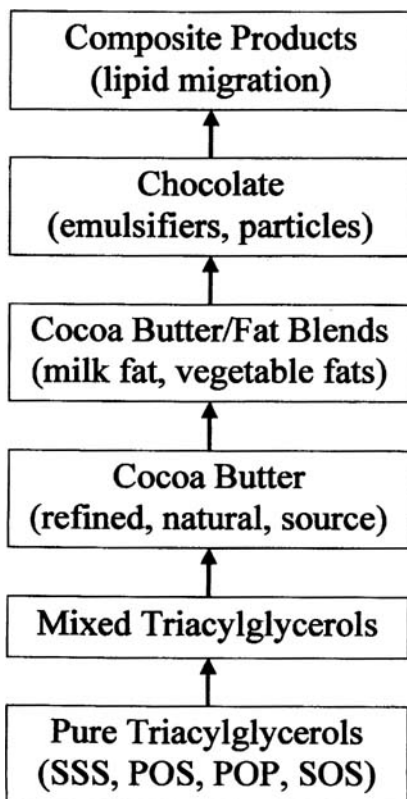


**Fig. 2.** Systems used for the investigation of crystallization in “chocolate.” The degree of complexity increases from bottom to top. Complicating factors are identified in parentheses.

olation of results obtained with pure triacylglycerols to chocolate is questionable. For example, the presence of a particulate phase with a large exposed surface area will undoubtedly alter crystallization kinetics. Rousset and Rappaz (4) reported that the simple substitution of aluminum pans for glass pans during differential scanning calorimetry (DSC) altered the crystallization kinetics of POS, and emulsification generates surfaces that promote polymorphic transformations (5). It is likely that nonfat particles in chocolate will have similar effects.

In addition to the compositional differences between the systems under study, environmental conditions vary. Thermodynamics and kinetics are both required for a complete understanding of crystallization, i.e., both temperature and cooling rate are important. Crystallization kinetics is often followed using DSC in either an isothermal (quenched) or time-variant mode. Furthermore, with this technique, the sample experiences static conditions, i.e., no mechanical shear, and in this respect is unrepresentative of commercial practice. The dramatic effect of shear is illustrated by the process of chocolate panning, where because of the shear during tumbling of the centers a “self-tempering” occurs in the pan (6). A shortening of induction time for crystallization and an acceleration of polymorphic transitions have been demonstrated in chocolate under shear (7,8). Local temperatures may vary due to evolution of the latent heat of crystallization. The effect of shear may be partly explained by its influence on local heating/cooling rates. The effects of shear are most significant in the tempering process and for bulk crystallization can probably be ignored, although this may not be the case with frozen cone molding. It is generally assumed that crystallization processes occur at a constant pressure close to atmospheric. However, the injection molding of chocolate operates at about 15 MPa (9), and pressure tempering machines operating between .17–1.0 MPa are available (10). However, little published information exists on the pressure-dependence of the phase or state diagrams of cocoa butter.

## Solidification of Chocolate

After forming, bulk crystallization is generally accomplished in a cooling tunnel (Fig. 3). Solidification proceeds through the deposition of triacylglycerols onto the

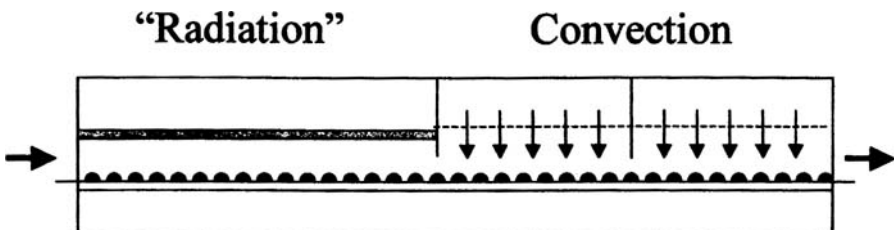


Fig. 3. Cooling tunnel. Product flow is from left to right. First zone is equipped with a “radiation plate” or heat sink.

previously formed “seed” crystals. The function of the cooling tunnel is the efficient removal of the latent heat released during this crystal-growth phase. Cooling is usually accomplished in zones. For chocolate products (vis-à-vis coatings), a gradual initial cooling is recommended to avoid nucleation of unstable polymorphs that may cause fat bloom later. Some tunnel manufacturers claim to use “radiant” cooling in this first zone. However, radiation as a mode of heat transfer is really only efficient at large  $\Delta T$ ; calculations estimate that only about 7% of the cooling load would be transferred radiantly in a chocolate cooling tunnel (11). In the first zone, heat is transferred principally by conduction and natural convection from the product to the surrounding air at *ca.* 25°C. A second zone employing forced convection at 10–15°C removes the bulk of the heat from the crystallizing product. The final zone is operated at slightly warmer temperatures to avoid condensation of moisture onto the product as it leaves the cooling tunnel.

## Modeling Chocolate Solidification

A comprehensive model for solidification would necessarily require fully-coupled, three-dimensional fluid flow, heat transfer, and solidification kinetics. For operations like drop forming and enrobing, the geometry is free form, and so finite element modeling would seem the best approach.

With the object of making the bulk solidification of chocolate a less empirical process, several models for the temperature distribution or heat evolution during cooling have been proposed. The challenge is to account for the latent heat of fusion that is evolving as a function of the degree of crystallization. This has been accomplished by either including an internal heat generation term (12),  $Q$ , or by modeling an effective specific heat (13),  $C_{p,eff}$  (Eqs. 1 and 2, respectively).

$$\rho C_p \frac{\partial T}{\partial t} = \nabla(k\nabla T) + Q \quad [1]$$

$$\rho C_{p,eff} \frac{\partial T}{\partial t} = \nabla(k\nabla T) \quad [2]$$

Franke (12) proposed a model for the calculation of the bulk crystallization and temperature variation within a chocolate coating during cooling with the intent to relate cooling kinetics to the finished product quality. The final quality of an enrobed product is generally evaluated on the basis of gloss, degree of solidification (propensity for fingerprinting and smearing), and coating thickness. The goal was optimization of product quality and tunnel productivity (minimized cooling time). Franke’s (12) model was a numerical calculation in one dimension of the unsteady-state temperature distribution. The enrobed center and the chocolate coat-

ing were assumed to be even, infinite slabs. Franke assumed that the coating was well-tempered, with an initial uniform temperature between 30–32°C. The initial center temperature was assumed uniform between 18–26°C. Heat transfer coefficients and the dependence of the thermal conductivity of the chocolate on temperature were taken from literature values. The heat flux at the coating-center interface was calculated from an energy balance. The most unique aspect of the model was Franke's approach to calculating the specific enthalpy of crystallization per unit time.

Franke (12) assumed: (i) that no sharp crystallization front occurs within the coating and, therefore, temperature and crystallinity change simultaneously throughout the coating, (ii) no additional nucleation occurs during cooling, and (iii) the specific enthalpy of crystallization can be expressed as a function of temperature and the sum of the heat already evolved  $[q(T, Q)]$ . These assumptions lead to the conditions:  $q = 0$  for  $T(t, x) > T_m$  (i.e., no heat evolved above the melting temperature), and  $q = 0$  for  $Q > Q_m$  (i.e., no more heat evolved when the total evolved equals the latent heat of crystallization). These conditions were then implemented as the product of two functions  $f_1(Q)$  and  $f_2(T)$ . The form of  $f_1(Q)$  is shown in Figure 4. The dependence on temperature,  $f_2(T)$ , was modeled as a simple linear function of the degree of undercooling,  $f_T(T_m - T)$  (Fig. 5). The ultimate result was a model with 3–5 adjustable parameters (depending on whether  $T_m$  and  $Q_m$  are fit or measured independently).

The model parameters were estimated by fitting cooling curves of enrobed model bodies cooled in a laboratory tunnel under different conditions (12). Using the best fit parameters, the model was able to reproduce the cooling curve (temperature curve) for chocolate reasonably well, including the "plateau phase," where the bulk of the latent heat is released. The maximum rate of cooling on the coating surface was correlated to coating gloss; excessively high cooling rates are related to diminished gloss. Simulations of the cooling of chocolate-coated cookies in either a one- or two-zone cooling tunnel, with or without forced convection, predicted the general profile of heat evolved as a function of time (distance) in the cooling tunnel, and suggested optimal time-temperature combinations for zone 1 and zone 2, as well as, optimal initial center temperature.

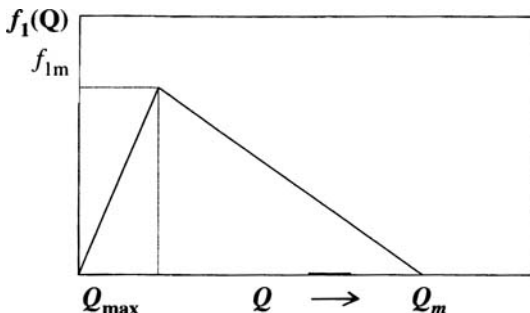


Fig. 4. Dependence of the specific enthalpy of crystallization on the heat of fusion already released (after Ref. 12).

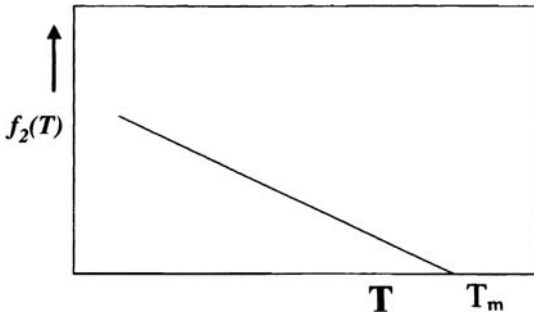


Fig. 5. Dependence of the specific enthalpy of crystallization on temperature (after Ref. 12).

Franke's model suffers from the drawback that it is highly empirical in nature and relies on five adjustable parameters. Since it assumes the chocolate entering the cooler is well tempered, it cannot provide insight into the behavior of poorly tempered products. The assumption that there is no sharp crystallization front limits its utility to thin geometries. Finally it assumes a single melting point and constant total heat of fusion, but these values have been shown to vary with cooling rate (7).

Employing the approach in Equation 2 and the finite element method, Tewkesbury *et al.* (13) modeled the cooling of chocolate. The effect of temperature on physical properties was determined from linear interpolation of known data. An initial uniform temperature was assumed, and heat transfer coefficients at the upper and lower boundary were calculated from cooling curves using paraffin wax. Two methods were used to model the latent heat release: (i)  $C_p(T)$  at a single cooling rate corresponding to the nominal cooling rate of the tunnel and (ii)  $C_p(T, dT/dt)$ , with the cooling rate at an integration point calculated from the difference in the temperature at the current and previous time steps. The local cooling rate was smoothed using a simple moving average of six points to avoid oscillations.

The use of  $C_p(T)$  at a constant average cooling rate was unable to accurately predict the experimental temperature profile in the "plateau zone" (13), with temperature deviations as high as  $2.7^\circ\text{C}$ . The accuracy of the model, especially in the phase change region, was improved so that deviations were less than  $0.7^\circ\text{C}$  by incorporating the cooling rate dependence of  $C_p$ . However, experimental and predicted temperature profiles diverged at the lowest ( $0.5^\circ\text{C}/\text{min}$ ) and highest ( $4.0^\circ\text{C}/\text{min}$ ) cooling rates. The authors suggested that at an average cooling rate of  $0.5^\circ\text{C}/\text{min}$  local cooling rates may have fallen outside the range of their experimental  $C_p(T, dT/dt)$  data (i.e., to  $<0.1^\circ\text{C}/\text{min}$ ), especially in the phase-transition region, and this extrapolation caused significant error. The error at high cooling rates was attributed to inherent inaccuracies in the model, i.e., cooling rate is a path function and cannot be expected to estimate a state function such as enthalpy with total accuracy (13).

In the absence of a full kinetic description of the crystallization process, the assumption that the solidification of chocolate can be modeled using effective heat capacity data as a function of temperature and cooling rate is an acceptable engi-

neering approximation over the cooling rate range of commercial concern (13). However, large volumes of data would be required to account for all the potential changes in formula that may influence  $C_p$  (e.g., cocoa butter source and milk-fat level).

Rousset and Rappaz (3) have attempted to provide a kinetic description of the crystallization of triacylglycerols using an Avrami-type expression (Eq. 4):

$$Q = F(f_s) \quad [3]$$

$$f_s(t) = 1 - \exp(-bt^n) \quad [4]$$

$$f_{s,i} = 1 - \exp[-b(T_i)(\theta_i + \delta t)^{n(T_i)}] \quad [5]$$

where  $b(T_i)$  and  $n(T_i)$  are determined from isothermal DSC data. The temperature dependence of  $f_s$  under nonisothermal conditions was based on the decomposition of the cooling curve into small time steps,  $\delta t$ , where the temperature was assumed constant. This additivity principle using empirical data from time-temperature-transformation (TTT) diagrams was able to predict solidification times for non-isothermal cooling trajectories.

Rudnicki and Niezgodka (14) modeled temperature-induced phase transitions (crystallization and melting) in cocoa butter during DSC analysis employing a phenomenological rate model to predict heat flow and a cellular three-dimensional model to describe spatial distribution of temperature. The transition between the liquid and crystalline states is described by a bistable thermodynamic potential, with the equilibrium distribution given by the difference in the thermodynamic potential of the two states according to the Boltzmann distribution. Process dynamics are controlled by a barrier height according to an Arrhenius-type relationship (15). The model assumed that phase transitions between polymorphic forms I–V are not direct but occur through the liquid phase (a point repeatedly discussed during the symposium). It also assumed that form VI cannot form directly from the melt, so melting of this form is the only process to be accounted for, and that different triacylglycerols crystallize in various polymorphic forms, determined only by the temperature and the rate of cooling. Only the melting temperature and heat of fusion are required, with the time scale of the experiment varied by the choice of the Arrhenius coefficient.

Rudnicki and Niezgodka (14) produced reasonably accurate simulated DSC scans including those of varying initial phase content. For example, a system initially containing 70% form V and 30% of form IV revealed two endothermic peaks, with an exothermic crystallization peak between them. Complex thermograms initially containing 25% each of forms I–IV predicted the actual formation of form V via polymorphic transformation during the DSC experiment. This is something we have actually observed and should be considered by all who use DSC to evaluate the solid state of lipids. Segregation of triacylglycerol species accompanies bulk crystallization and results in a melting range for crystallites of

the same polymorphic form due to the varying composition. Under some circumstances, crystallization may even lead to phase separation (16). These conditions are not accounted for in this simple model.

## Rheology in the Semi-Solid State

Tewkesbury *et al.* (13) assumed that negligible fluid movement occurs during cooling since chocolate is a highly non-Newtonian fluid with very high viscosity at low shear rates. While this might be the case for solid molded items, flow does occur during the drop forming, enrobing, and frozen cone molding, and a complete model of solidification may require coupled fluid flow equations. Here, too, an approach from the metallurgical literature may help (17–20).

## Conclusions

The hope is that quantitative process modeling will lead to general insights or specific information that would help manufacturers optimize processes. In this regard, the approach of Franke (12) to link the quantitative modeling to product quality is noteworthy. Modeling may be particularly helpful in the analysis of new technologies, like frozen cone molding, that have not been optimized through years of experience.

## References

1. Seguine, E.S., It Ain't Over Until... A Review of Post Cooling Tunnel Changes in the Cocoa Butter Phase of Chocolate, in *Proceedings of the Annual Production Conference*, Pennsylvania Manufacturing Confectioners' Association, Hershey, PA, 1995, pp. 60–64.
2. Rappaz, M., and Ph. Rousset, Solidification Processes and Modeling, in *Confectionery Science, Proceedings of an International Symposium*, edited by G.R. Ziegler, Penn State University, University Park, PA, 1997, pp. 177–208.
3. Rousset, Ph., and M. Rappaz,  $\alpha$ -Melt-Mediated Crystallization of 1-Palmitoyl-2-Oleoyl-3-Stearoyl-*sn*-Glycerol, *J. Am. Oil Chem. Soc.* 74: 693–697 (1997).
4. Rousset, Ph., and M. Rappaz, Crystallization Kinetics of the Pure Triacylglycerols Glycerol-1,3-Dipalmitate-2-Oleate, Glycerol-1-Palmitate-2-Oleate-3-Stearate, and Glycerol-1,3-Distearate-2-Oleate, *Ibid.* 73: 1051–1057 (1996).
5. Sato, K., Fat Polymorphism: How Its Structures and Kinetic Behavior Are Modified, Conference on Crystallization and Solidification Properties of Lipids, American Oil Chemists' Society, Toronto, Canada, 2000.
6. Aebi, M., Chocolate Panning, in *Industrial Chocolate Manufacture and Use*, edited by S. Beckett, Blackwell Science, Oxford, 1999, pp. 285–301.
7. Stapley, A.G.F., H. Tewkesbury, and P.J. Fryer, The Effects of Shear and Temperature History on the Crystallization of Chocolate, *J. Am. Oil Chem. Soc.* 76: 677–685 (1999).
8. Rossi, A., K.J. Roberts, M. Wells, M. Polgreen, and I. Smith, Polymorphism in Cocoa Butter Under Shear, in *Confectionery Science II, Proceedings of an International Symposium*, edited by G.R. Ziegler, Penn State University, University Park, PA, 1999, pp. 121–132.

9. Mackley, M., Flexible Chocolate, in *Confectionery Science II, Proceedings of an International Symposium*, edited by G.R. Ziegler, Penn State University, University Park, PA, 1999, pp. 15–24.
10. Nelson, R.B., Tempering, in *Industrial Chocolate Manufacture and Use*, edited by S. Beckett, Blackwell Science, Oxford, 1999a, pp. 231–258.
11. Nelson, R.B., Enrobers, Moulding Equipment, and Coolers, in *Industrial Chocolate Manufacture and Use*, edited by S. Beckett, Blackwell Science, Oxford, 1999b, pp. 259–286.
12. Franke, K., Modelling the Cooling Kinetics of Chocolate Coatings with Respect to Finished Product Quality, *J. Food Engng.* 36: 371–384 (1998).
13. Tewkesbury, H., A.G.F. Stapley, and P.J. Fryer, Modelling Temperature Distribution in Cooling Chocolate Moulds, *Chem. Engng. Sci.* 55: 3123–3132 (2000).
14. Rudnicki, W.R., and M. Niezgodka, Phase Transitions in Cocoa Butter, in *Proceedings of International Conference on Free Boundary Problems, Theory and Application*, Gakuto International Series, Mathematical Sciences and Applications, Vol. 14, edited by N. Kenmochi, Gakkotosho, Tokyo, Japan, 2000, pp. 409–417.
15. Porter, D.A., and K.E. Easterling, *Phase Transformations in Metals and Alloys*, Chapman & Hall, London, 1992, pp. 55–56.
16. Ollivon, M., Simultaneous Examination of Structural and Thermal Behaviors of Fats by Coupled X-Ray Diffraction and DSC Techniques: Application to Cocoa Butter Polymorphism, Conference on Crystallization and Solidification Properties of Lipids, American Oil Chemists' Society, Toronto, Canada, 2000.
17. Kumar, P., C.L. Martin, and S. Brown, Shear Rate Thickening Flow Behavior of Semisolid Slurries, *Metallurgical Trans. A* 24(A): 1107–1116 (1993).
18. Martin, C.L., S.B. Brown, D. Favier, and M. Suery, Shear Deformation of High Solids Fraction (>0.60) Semi-Solid Sn-Pb Under Various Structures, *Mater. Sci. Engng. A* 202: 112–122 (1995).
20. Ngygen, T.G., D. Favier, and M. Suery, Theoretical and Experimental Study of the Isothermal Mechanical Behavior of Alloys in the Semi-Solid State, *International J. Plasticity* 10: 663–693 (1994).

## Chapter 20

**Polymorphism and Texture of Fats**J.M. deMan<sup>a</sup>, and L. deMan<sup>b</sup><sup>a</sup>Department of Food Science, University of Guelph, Guelph, ON Canada N1G 2W1, and<sup>b</sup>DEMAN Food Technology Services Inc., Guelph, ON Canada N1H 6B5**Introduction**

The texture of fat is influenced by a number of factors, including fatty acid and glyceride composition, solid fat content, crystal size and shape, nature of the crystal network, polymorphism, mechanical treatment, and temperature history (1). Many of these factors are interrelated, making it difficult to establish the independent effect of each. It is well recognized that different fats preferentially occur in either  $\beta'$  or  $\beta$  form (Table 1).

The three main polymorphic forms are  $\alpha$ ,  $\beta'$ , and  $\beta$  (Fig. 1). The  $\alpha$  form is very unstable and may be present during processing, but processed fat products, such as margarines and shortenings, are present in either  $\beta'$  or  $\beta$  form, or both. The metastable  $\beta'$  form may persist in such products almost indefinitely or change slowly into the stable  $\beta$  form. For margarines and most shortenings, the  $\beta'$  form is the preferred one because the crystals are small, whereas conversion to the  $\beta$  form results in formation of very large crystals. The transformation from  $\beta'$  to  $\beta$  may proceed in the solid state or *via* the liquid form as indicated in Figure 2. The mechanism of the transformation has been suggested by Riiner (2); it involves the rotation of the fatty acid chains (Fig. 3). Considering the massive change in crystal size that is often observed when  $\beta$  crystals are formed, it is unlikely that it is happening as a solid-state conversion.

**Effect on Texture**

The most noticeable effect of  $\beta$  crystal formation is the increase in crystal size, which leads to an increase in hardness and loss of spreadability. In extreme cases

**TABLE 1**

Crystal Form of Fully Hydrogenated Fats in Their Most Stable State

$\beta'$	$\beta$
Cottonseed	Soybean
Palm	Sunflower
Tallow	Canola
Rape	Lard

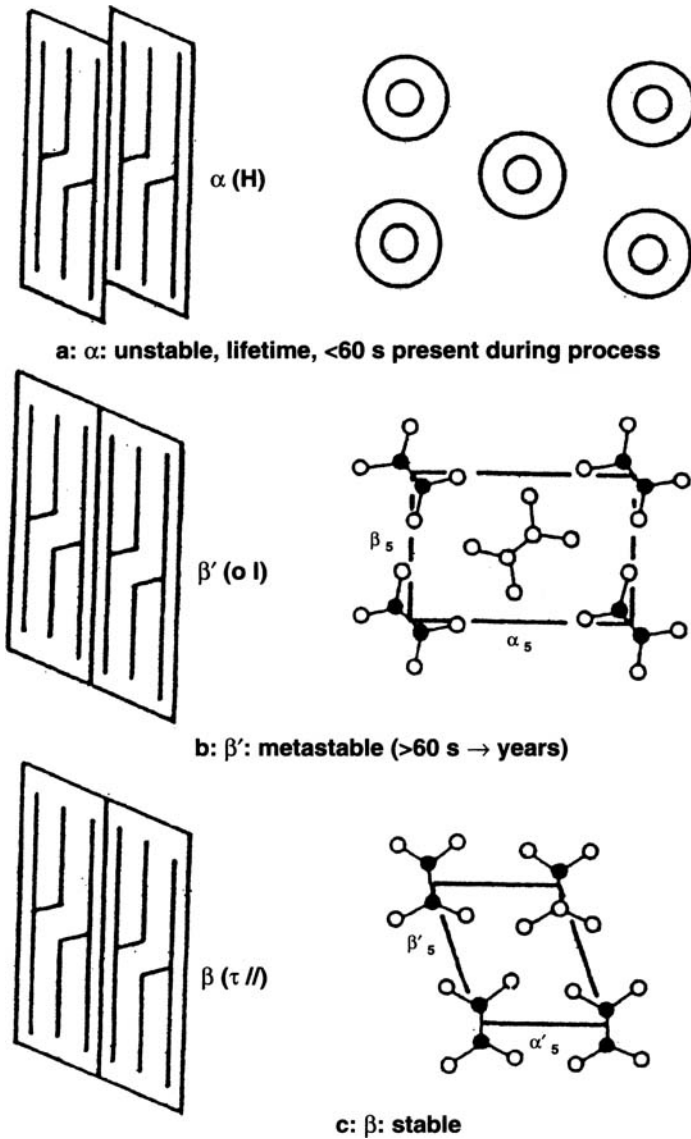


Fig. 1. Polymorphic forms of fats.

the product becomes brittle and crumbles under applied pressure. Other consequences of this increased crystal size are changes in appearance and flavor release. When crystals grow, the color is moved into the liquid position and the size of the crystals may become visible to the naked eye. A similar change affects flavor. As

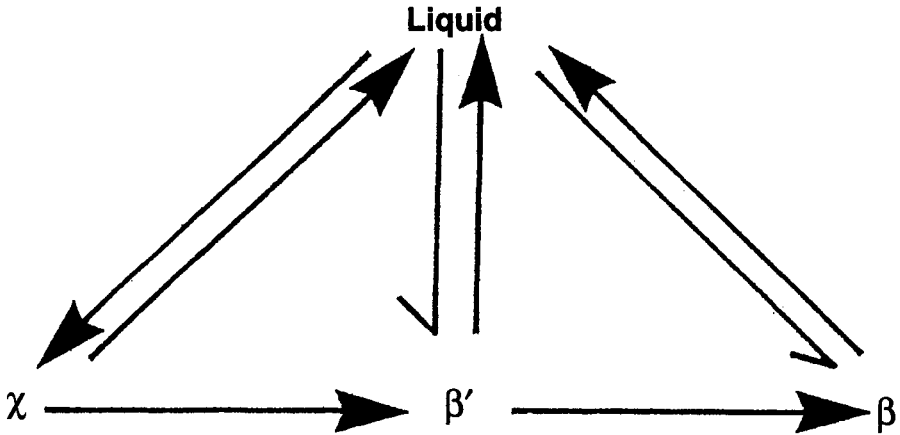


Fig. 2. Polymorphic transition pathways.

the crystals grow, it becomes more difficult to perceive the flavor in the mouth. In shortenings, creaming properties may be diminished. In soft (tub) margarines, the change to the  $\beta$  form can also be perceived by the naked eye, the initial surface gloss of the product changes into a dull appearance.

### Factors Affecting $\beta$ Crystal Formation

A great deal of information about polymorphic changes has been obtained from studying pure triacylglycerols (TAG). However, in commercial fats, especially if they contain several ingredients, it may be more difficult to predict the likelihood of  $\beta$  crystal formation to occur. Factors that influence the stability of the  $\beta'$  poly-

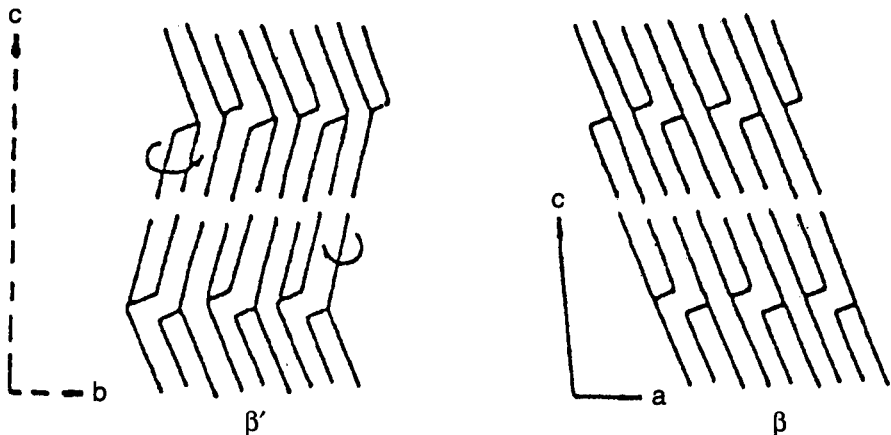


Fig. 3. Mechanism of the  $\beta'$  to  $\beta$  transformation of fats according to Riiner (Ref. 2).

morph are: fatty acid chain-length diversity, TAG carbon-number diversity, TAG structure, presence of specific TAG-PSP and PEP, level of liquid oil present, temperature fluctuations during storage.

Plastic fats contain solid fat crystals and varying levels of liquid oil. Most of the factors mentioned above relate to the solid portion of the fat, but the liquid portion also plays a role in determining  $\beta'$  stability. Indirectly, therefore, high solid fat content is a factor in determining  $\beta'$  stability.

It is well known that sunflower oil, when partially hydrogenated, produces a margarine with very poor texture. Before the development of canola from rapeseed, the polymorphic properties of partially hydrogenated rapeseed oil were very desirable. Canola margarine was found to be prone to form  $\beta$  crystals as does sunflower margarine. Examination of the fatty acid composition of these oils (Table 2) indicates that rapeseed oil had much greater fatty acid chain-length diversity than canola oil. Table 3 demonstrates the similarity in fatty acid chain-length distribution of canola and sunflower oils. For most oils and fats used in the food industry, chain-length diversity relates to the ratio of 16 and 18 carbon fatty acids. The higher the level of palmitic acid, the more likely the fat will be stable in the  $\beta'$  form. Table 4 lists the palmitic acid content of some vegetable and animal fats. Cottonseed and palm oil have the highest palmitic acid content. Most animal fats, including human fat, con-

**TABLE 2**  
Fatty Acid Composition of Rape and Canola Oils

Fatty acid	Rape	Canola
16:0	3	4
18:0	1	2
18:1	17	58
18:2	14	21
18:3	9	11
20:1	11	2
22:1	45	<1

**TABLE 3**  
Fatty Acid Composition of Canola and Sunflower Oils

Fatty acid	Canola	Sunflower
16:0	4	4
18:0	2	3
18:1	58	34
18:2	21	59
18:3	11	—
20:1	2	—
22:1	<1	—

**TABLE 4**  
Palmitic Acid Content of Some Fats and Oils (%)

Canola	4
Soybean	11
Olive	14
Cottonseed	29
Palm	44
Chicken	24
Beef	28
Milk	25
Human	27

tain 25–27% palmitic acid. The lower the palmitic acid content of an oil, the higher will be the level of 54 carbon glycerides in the solids after partial hydrogenation. Table 5 lists the polymorphic tendency of the major solid TAG in vegetable margarines and shortenings of 16 and 18 carbon chain lengths. The 48 and 54 carbon TAG are  $\beta$  formers; the 50 and 52 carbon ones are  $\beta'$  formers. The TAG composition by carbon number of some vegetable oils is shown in Table 6. As the number of 54 carbon TAG decreases, there has to be an increase in 50 and 52 carbon TAG, resulting in increased  $\beta'$  stability of the crystals in the hydrogenated oil.

There is another effect of  $\beta$  crystal formation that has received far less attention than the change in crystal morphology. This is the change in melting point. When TAG change into the  $\beta$  form, there is a considerable increase in melting point (Table 7). The TAG PSP is unique in that it does not have a  $\beta$  form. The presence of PSP in a fat, therefore, will be an important factor in stabilizing the  $\beta'$  form. Closer examination of the melting points of the polymorphs of TAG (Table 8) shows that the melting point increase varies for different TAG from a low of 4.5 to a high of 16.9°C. In the case of SOO (for abbreviations of TAG, see Table 5), the melting point increases from 8.8 to 23.7°C, which undoubtedly influences the solid fat content and texture of a product containing this TAG. We found that the hardness of a fat containing solids with a lower melting point is lower than a fat containing the same percentage of solid fat with a higher melting point.

**TABLE 5**  
Polymorphic Tendency of the Major Solid Triacylglycerols (TAG) in Vegetable Margarines and Shortenings of 16 and 18 Carbon Chain-Length Fatty Acids<sup>a,b</sup>

Carbon	Triacylglycerol	Polymorphic form
48	PPP	$\beta$
50	PSP	$\beta'$
52	PSS	$\beta'$
54	SSS	$\beta$

<sup>a</sup>Elaidic acid can replace stearic acid (S) to yield the same polymorphic form, P, S.

<sup>b</sup>For TAG shorthand description: P = palmitic acid; S = stearic acid; O = oleic acid; L = linoleic acid; U = unsaturated fatty acid.

**TABLE 6**  
TAG (carbon number) Composition of Vegetable Oils<sup>a</sup>

	50	52	54	56	58
High-oleic sunflower	2.0	15.0	80.6	1.0	1.3
Sunflower	2.8	20.2	75.1	.7	.9
Olive	4.7	27.7	66.7	.9	—
Peanut	5.5	30.9	54.2	5.3	3.0
Main TAG	16-18-16	16-18-18	18-18-18	18-18-20	18-18-22

<sup>a</sup>See Table 5 for abbreviation.

The transformation of crystals from the  $\beta'$  to the  $\beta$  form takes place in the solids present in a fat. However, the rate of this transformation is greatly influenced by the amount of liquid oil in the fat. A suitable method to estimate the  $\beta'$  stability of a fat is temperature cycling. An example is given in Table 9, where palm oil products were subjected to temperature cycling between 4 and 20°C. A cycle may take two or more days. The polymorphic forms can be measured at the end of each cycle. A product such as hydrogenated palm oil or palm olein will show no presence of  $\beta$  polymorphs after four cycles. Palm oil and palm stearin will

**TABLE 7**  
Melting Points of the  $\beta'$  and  $\beta$  Form of Some TAG<sup>a</sup>

TAG	Carbon number	$\beta'$	$\beta$
PPP	48	56.7	66.2
SSS	54	64.2	73.5
PSP	50	68.8	—
POP	50	30.5	45.3

<sup>a</sup>See Table 5 for abbreviations.

**TABLE 8**  
Melting Points of the  $\beta'$  and  $\beta$  Form of TAG<sup>a</sup>

TAG	$\beta'$	$\beta$	$\Delta$
SSS	64.2	73.5	9.3
PPP	56.7	66.2	9.5
PSP	68.8	—	—
SOS	36.7	41.2	4.5
SOO	8.8	23.7	14.9
POP	30.5	35.3	4.8
OOO	-11.8	5.1	16.9
LOO	-28.3	-23.3	5.0
LLO	-3.02	-25.2	5.0

<sup>a</sup>See Tables 5 and 7 for abbreviations.

**TABLE 9**Polymorphic Forms of Some Palm Oil Products Temperature Cycled Between 4 and 20°C<sup>a</sup>

Product	DP	Polymorphic form	
		Cycle 1	Cycle 4
Palm oil	38.6	β'	β' >>> β
Palm stearin	53.5	β' >> β	β' >> β
H-palm oil	54.9	β'	β'
H-palm olein	54.6	β'	β'

<sup>a</sup>DP = dropping point; H = hydrogenated.

show the presence of β crystals after four cycles. When some of these products are diluted with liquid canola oil (Table 10), hydrogenated palm olein remains in the β' form after four cycles even if diluted in a 20:80 ratio with liquid canola oil. Hydrogenated palm oil shows development of β crystals at a dilution ratio of 25:75. This trend is even more pronounced for palm oil even after only one cycle.

The difference in β' stability of palm oil, palm olein, and palm stearin can be explained by differences in TAG composition. Palm oil contains about 6% of tri-palmitin, a β former, which upon fractionation goes mostly into the stearin, leaving the olein with mostly 50 and 52 carbon TAG, which after hydrogenation are all β' formers (Table 11). One of the major TAG in palm oil (and olein) is POP, which on hydrogenation yields PSP. This is the TAG with exceptional β' stability. Upon partial hydrogenation, POP is transformed into PEP (E = elaidic acid), which we have found to have the same β' stabilizing effect as PSP (3,4). This was confirmed by Elisabettini *et al.* (5), who synthesized PEP, EPP, and PEE and found no β form in any of these TAG.

**TABLE 10**Polymorphic Behavior of Hydrogenated Palm Oils Diluted with Canola Oil<sup>a</sup>

H-palm olein	Liquid oil	Polymorphic form	Cycle
40	60	β'	4
30	70	β'	4
20	80	β'	4
<hr/>			
H-Palm oil			
30	70	β'	4
25	75	β' = β	4
<hr/>			
Palm oil			
80	20	β' >> β	1
60	40	β > β'	1

<sup>a</sup>See Table 9 for abbreviation.

**TABLE 11**  
Major TAG of Palm Oil<sup>a</sup>

TAG	Carbon number	%	Melting points	
			$\beta'$	$\beta$
PPP	48	6.0	56.7	66.2
PPS	50	.0	59.9	62.9
PSP	50	0.5	68.8	—
POP	50	26.0	30.5	35.5
PPO	50	6.0	35.4	40.4
PLP	50	7.0	18.6	NA
POO	52	19.0	14.2	19.2
POS	52	3.0	33.2	38.2
PLO	52	4.0	NA	NA
OOO	54	3.0	-1.8	5.1

<sup>a</sup>NA, not applicable. See Table 5 for abbreviations.

In addition to hydrogenated palm olein, hydrogenated palm mid fraction is an excellent ingredient for high-stability plastic fat products. Palm mid fraction is even higher in POP than palm olein.

It has been found that the recommended cycling temperatures for different types of plastic fat products depend on the nature of the product (Table 12). An example is given in Table 13 of a cycling experiment with a corn-canola oil soft margarine using temperature cycles 4–15 and 4–20°C. The product is  $\beta'$  stable using the 4–15°C cycling but shows development of  $\beta$  crystals when using the 4–20°C cycling.

The level of 54 carbon TAG is important in establishing the  $\beta'$  stability of plastic fat products made from commonly used vegetable oils and as a consequence the textural quality of these products. Table 14 shows the TAG composition of a variety of stick margarines and its effect on polymorphism (6). Products that are  $\beta'$  stable have 54 carbon TAG levels in the high melting glycerides (HMG) of below 50%. At levels over 50% the product will crystallize in the  $\beta$  form (7). Table 15 gives the relationship between 54 carbon TAG in the high melting glycerides of soft margarines and their polymorphic forms (8). In this case the influence of the high liquid oil content of the

**TABLE 12**  
Recommended Cycling Temperatures for Testing  $\beta'$  Stability of Plastic Fat Products

	Formulation	Cycling Temperatures (°C)
Margarines	Soft	15–4
	Soft stick	20–4
	Normal stick	25–4
Shortening		30–20

**TABLE 13**

Polymorphism of a Corn-Canola Oil Soft Margarine Temperature Cycled Between 4 and 15°C and 4 and 20°C

	Cycled between 4 and 15°C	Cycled between 4 and 20°
Cycle 1	$\beta'$	$\beta'$
Cycle 2	$\beta'$	$\beta < \beta'$

margarines is evident. None of these products is completely in the  $\beta'$  form. The canola soft margarine is completely in the  $\beta$  form. The canola-palm soft margarine contains insufficient nonhydrogenated palm oil to reduce the TAG 54 in the high-melting glycerides to below 50%. The nonhydrogenated margarine is unusual in that it contains only 9.3% TAG 54 in the solid fraction and 1.1% in the HMG. This is because the solids are made up of modified palm and palm kernel oils in 90% of liquid oil.

The TAG 54 levels in the high melting glycerides of some shortenings and their polymorphic forms are listed in Table 16. Products with TAG 54 levels in the high-melting glycerides of less than 25% are  $\beta'$  stable. This is usually achieved by incor-

**TABLE 14**

TAG Carbon Number Composition (%) of the High-Melting Glycerides of (HMG) Stick Margarines and Their Polymorphic Form<sup>a</sup>

Ingredient oils	TAG—carbon numbers				Polymorphic form of margarine
	48	50	52	54	
Canola	—	2.2	19.8	69.2	$\beta$
Canola-palm	3.1	3.1	15.5	68.9	$\beta$
Canola-H palm	7.3	12.8	20.2	51.1	$\beta'$
Soy	—	7.7	38.2	50.8	$\beta'$
Corn	—	7.6	42.6	46.8	$\beta'$

<sup>a</sup>See Table 5 for abbreviations.

**TABLE 15**

TAG 54 Levels (%) in the High-Melting Glycerides of (HMG) Soft Margarines and Their Polymorphic Form<sup>a</sup>

Ingredient oils	TAG 54 in HMG		Polymorphic forms of margarine solids
	Solids	HMG	
Soy	58.9	56.8	$\beta' \gg \beta$
Canola	71.7	68.4	$\beta$
Canola-palm	58.3	56.9	$\beta' = \beta$
Nonhydrogenated	9.3	1.1	$\beta' = \beta$

<sup>a</sup>See Table 5 for abbreviations.

**TABLE 16**

TAG 54 Levels (%) in the High-Melting Glycerides of (HMG) Shortenings and Their Polymorphic Form

Ingredient oils	TAG 54 in HMG	Polymorphic form
Soy	53.9	$\beta$
Soy-palm	19.4	$\beta'$
Canola-palm	44.3	$\beta \ll \beta'$
Canola-soy-palm	21.5	$\beta'$
Palm-vegetable	10.1	$\beta'$

poration of hydrogenated palm oil. The importance of chain-length diversity in improving the physical properties of margarines has been emphasized (9). They concluded that oils that contain a high level of palmitic acid containing TAG contribute to products with favorable melting characteristics and crystallization behavior.

The TAG 54 level in a fat is an important factor in establishing  $\beta'$  stability or the lack of it. Fatty acid chain-length diversity in an oil is the determining factor in TAG 54 levels. Interestingly, chain-length diversity within glycerides is not the only factor. Chain-length diversity between glycerides also plays a role. In a fat that is high in TAG 54 and, therefore, a  $\beta$  former, inclusion of palm stearin which contains high levels of tripalmitin (C48), also a  $\beta$  former, will promote greater  $\beta'$  stability (3).

The distribution of fatty acids in the TAG of natural fats also determines their polymorphic behavior and, therefore, the texture of these fats. This is exemplified by the difference between lard and tallow (Table 17). Lard has none of the symmetric SUS glycerides, whereas in tallow there is 21%. The result (Table 18) indicates that lard crystallizes in the  $\beta$  form and tallow in the  $\beta'$  form. The levels of TAG 54 and 16:0 in the high-melting glycerides of these fats are roughly similar.

**TABLE 17**Positional Distribution of Fatty Acids in the TAG of Lard and Tallow (%)<sup>a</sup>

	SSU	USU	SUS
Lard	29	36	0
Tallow	11	3	21

<sup>a</sup>See Table 5 for abbreviations.

**TABLE 18**TAG Composition (%) and Polymorphic Form of Lard and Tallow<sup>a</sup>

	TAG 54 in HMG	16:0 in HMG	Polymorphic form
Lard	12.9	36.4	$\beta$
Tallow	17.1	33.2	$\beta'$

<sup>a</sup>See Table 5 for abbreviations.

**TABLE 19**  
Polymorphic Form in Tempered Shortening

Treatment temperature (°C)	Week 1		Week 5	
	$\beta'$	$\beta$	$\beta'$	$\beta$
23°—isothermal	100%	—	100%	—
26.5°—9 d	100%	—	62%	38%
30°—9 d	73%	27%	64%	36%
10°—9 d	100%	—	100%	—

Temperature treatment of fats can have a profound influence on the  $\beta'$  stability of fats. Even usually  $\beta'$  stable fats may transform wholly or partially to the  $\beta$  form when subjected to temperature fluctuations during storage. It is customary to temper shortenings for several days, usually at a temperature above which they are processed, but not higher than 28°C. Ideally, tempering should not lead to the formation of  $\beta$  crystals. A tempering experiment with a commercial shortening (Table 19) indicated that at 23°C there is no  $\beta$  crystal formation, and this is also true for storage at 10°C. Tempering at 26.5°C causes the formation of  $\beta$  crystals after week 5 and tempering at 30°C results in  $\beta$  crystal formation within the first week of tempering (10).

## References

1. deMan, J.M., *Principles of Food Chemistry*, 3rd Edn., Aspen Publishers Inc., Gaithersburg, Maryland, 1999, p. 311.
2. Riiner, U., Phase Behavior of Hydrogenated Fats. II. Polymorphic Transitions of Hydrogenated Sunflower Seed Oil and Solutions, *Lebensm. Wiss. Technol.* 4: 113–117 (1971).
3. deMan, L., and J.M. deMan, Functionality of Palm Oil in Margarines and Shortenings, *Lipid Technol.* 6: 5–10 (1994).
4. deMan, J.M., and L. deMan, Palm Oil as a Component for High-Quality Margarine and Shortening Formulations, *Malaysian Oil Sci. Technol.* 4: 56–60 (1995).
5. Elisabettini, P., G. Lognay, A. Desmedt, N. Istasse, E. Deffense, and F. Durant, Synthesis and Physicochemical Characterization of Mixed Diacid Triglycerides That Contain Elaidic Acid, *J. Am. Oil Chem. Soc.* 75: 285–291 (1998).
6. D'Souza, V., L. deMan, and J.M. deMan, Chemical and Physical Properties of the High-Melting Glyceride Fraction of Commercial Margarines, *Ibid.* 68: 153–162 (1991).
7. D'Souza, V., J.M. deMan, and L. deMan, Chemical and Physical Properties of the Solid Fat in Commercial Margarines, *Ibid.* 69: 1198–1205 (1992).
8. deMan, L., V. D'Souza, J.M. deMan, and B. Blackman, Polymorphic Stability of Some Shortenings as Influenced by the Fatty Acid and Glyceride Composition of the Solid Phase, *Ibid.* 69: 246–250 (1992).
9. Zeitoun, N.A.M., W.E. Neff, G.R. List, and T.L. Mounts, Physical Properties of Interesterified Fat Blends, *Ibid.* 70: 467–471 (1993).
10. Mozziar, C., J.M. deMan, and L. deMan, Effect of Tempering on the Physical Properties of Shortenings, *Can. Inst. Food Sci. Technol. J.* 22: 238–242 (1989).

# INDEX

---

<u>Index Terms</u>	<u>Links</u>		
<b>A</b>			
$\alpha$ form	1	4	9
of fully hydrogenated fats	225		
of SLS	12		
Acyl donors			
effect on crystallization	172		
influence on product solubility	173		
Adsorbed "membrane"			
effect on fat agglomeration	208		
manipulation of	203	210	
Agglomeration, effect of adsorbed			
protein on fat	208		
Anhydrous milk fat (AMF)	190	197	
fractional crystallization of	126		
shortenings based on binary blends			
with palm oil	42		
Arrhenius equation	71		
Atom-atom approach, to calculation of			
intermolecular interactions	19		
Attachment energy model, growth form			
according to	23		
Avrami equation plots, for refined,			
bleached, deodorized palm oil	113		

## Index Terms

## Links

Avrami exponent				
effect of DSC cooling rate on				
determination of	115			
for various types of nucleation and				
growth mechanisms	112			
Avrami model	63	70	73	
<i>See also</i>				
Index of Avrami				
for DSC measurement	111			
<b>B</b>				
$\beta$ form	1	4	10	13
	116			
of fully hydrogenated fats	225			
$\beta'$ form	1	4	116	
of fully hydrogenated fats	225			
of SRS	12			
in TAG	8			
testing stability of plastic fat products	232			
transition to $\beta$ form	227			
BFDH law	22			
growth form according to	23			
Blocking				
additives for	25			
growth	24			
Blooming. <i>See</i> Fat-blooming				
Buckingham (B) potential	18			

## Index Terms

## Links

### Bulk fats

measurements of	136
polymorphism in	184
properties of, in relation to emulsified systems	176
SFC of	180
viscosity of	186
X-ray diffractograms of	185

## C

Calorimetry. *See* Differential scanning calorimetry

### Canola oil

emulsion destabilization of	179
fatty acid compositions of	228
viscosity of	186

CB. *See* Cocoa butter

Cerius2 modeling software 29

### Chainlength structures

diverse	234
typical	2

### Chocolate

crystallization in	216
differential scanning calorimetry for predicting fat-blooming in	79
phases coexisting in tempered	35
rheology of, in the semi-solid state	223
ultrasonic velocity on cooling	138

## Index Terms

## Links

Chocolate confectionery manufacture		
operations in	215	
solidification processes in	215	
Chocolate solidification	218	
modeling	219	
Coalescence		
emulsion, partial	200	
schematic representation of	201	206
Cocoa butter (CB)		
dynamic and static crystallization of	96	
effect of cooling rates on latent heat of	106	
HMF and LMF of	37	
liquid crystalline structures of	37	
phases coexisting in	35	
polymorphism in	34	
Colloidal aggregate networks,		
microstructure of a fractal	155	
Commercial margarine spread		
oils, solid fat content in	147	
Computer modeling, of dynamic and static crystallization of cocoa butter	96	
Confectionery fat. <i>See also</i> Chocolate confectionery manufacture		
speed of sound during cooling in	142	
ultrasonic reflectance amplitude in	139	
Conjugate gradient algorithm	28	
Consistency measurement, of shortenings	43	

This page has been reformatted by Knovel to provide easier navigation.

## Index Terms

## Links

Cooling	
in confectionery fat, speed of	
sound during	142
in various studies of lipid	
crystallization	123
Cooling rate	
differential scanning calorimetry	115
effect on crystallization	62
effect on latent heat of cocoa butter	106
Cooling tunnel, for solidification	
of chocolate	218
Corn-canola oil soft margarine,	
polymorphism of	233
Coupled x-ray diffraction,	
examination of structural and	
thermal behaviors of	
fats by	34
Crude palm oil (CPO)	
Avrami equation plots for	113
polymorphic forms of	115
Crystal interface, growth of	24
Crystal morphology	
of fully hydrogenated fats in their	
most stable state	225
intraglobular, under	
perikinetetic conditions	181
periodic bond chains governing	22
shape calculation of	22

## **Index Terms**

## **Links**

Crystalline evolution, of TAGS	
in cream	194
Crystalline structures	6
liquid, of cocoa butter	37
Crystallization	
in chocolate	216
controlling	216
dynamic and static, of cocoa butter	96
effect of acyl donors in	172
effect of viscosity and cooling	
rate on	62
in emulsion	190
of fats, emulsion destabilization by	176
fractal organization of TAG during	74
induction period for	69
for lipase-catalyzed solid-phase	
synthesis of sugar fatty	
acid monoesters	168
molecular modeling applications	
in lipid	17
of palm oil products	110
shear-induced	186
solvent effects in	171
specific enthalpy of	220
supercooling and supersaturation in	55
triacylglyceride, in vegetable oils	53
Crystallization induction times,	
determination of	122

## Index Terms

## Links

Crystallization kinetics, of mixtures		
of <i>n</i> -hexadecane	143	
Crystallization rate		
constant for blends of palm stearin and sesame oil	63	
of vegetable ghee	87	
Crystallization thermograms, isothermal, obtained by differential scanning calorimetry	59	
Crystallization time, reduced		
crystallinity as a function of	69	
Cycling temperatures	232	
<b>D</b>		
DAG. <i>See</i> Diacylglycerol		
Dairy formations, stability of	200	
DCL. <i>See</i> Double chainlength structure		
Destabilization		
emulsion, by crystallization of fats	176	
emulsion, during whipping	211	
fat, determined by spectroturbidity	204	
Diacylglycerol (DAG), milk-fat	126	
Differential scanning calorimetry (DSC)		
in assessment of crystallization rate of vegetable ghee	88	
Avrami model for measurement using examination of structural and thermal behaviors of fats by	111	115
	34	

## Index Terms

## Links

Differential scanning calorimetry (DSC) ( <i>Cont.</i> )			
isothermal crystallization thermograms			
obtained by	59	67	89
for predicting chocolate			
fat-blooming	79		
Dilatometry, for measuring solids			
in hydrogenated soybean oil	146		
Discriminant analysis,			
in assessment of fat-blooming	83		
Disruption of growth	24		
Double chainlength (DCL) structure	2	4	
DSC. <i>See</i> Differential scanning calorimetry			
Dynamic crystallization			
of cocoa butter	96		
morphology maps of	103		
temperature-time-transformation			
diagram of	101		
Dynamic onset time, as function of			
average shear rate	104		
<b>E</b>			
Elaidic acid, polymorphic occurrence of	14		
Elasticity, of fractal aggregate networks	153		
Electrostatic interactions	20		
EMK. <i>See</i> Ethyl methylketone			
Emulsified fats			
polymorphism in	184		
SFC of	180		

## **Index Terms**

## **Links**

Emulsified fats ( <i>Cont.</i> )	
ultrasonic velocity in n-hexadecane	140
viscosity of	186
X-ray diffractograms of	185
Emulsifiers	
effect on solid fat index	149
oil-soluble	87
Emulsion crystallization	190
in a shear field	184
and thermal and structural behavior of milk fat	184
Emulsion destabilization	
by crystallization of fats	176
SFC and	178
during whipping	211
Emulsion partial coalescence, and structure formation in dairy systems	200
Enthalpy	
of polymorphic transformations of SSS, SOS, SRS, and SLS	10
specific, of crystallization	220
Entropy, of polymorphic transformations of SSS, SOS, SRS, and SLS	10
Equilibrium melting temperature	
determination, for blends of palm stearin and sesame oil	57

## Index Terms

## Links

Esterification, lipase-catalyzed	169	
Ethyl methylketone (EMK), solvent		
action of	170	
Evolution. <i>See</i> Crystalline evolution;		
Isothermal evolution		
<b>F</b>		
Fat agglomeration, effect of adsorbed protein on	208	
Fat-blooming	167	216
development of	84	
differential scanning calorimetry for pre-		
dicting in chocolate	79	
visual assessment of	80	
Fat crystallization. <i>See</i> Lipid crystallization		
Fat destabilization, determined by		
spectroturbidity	204	
Fat polymorphism	225	
defined	2	
molecular aspects in	1	
Fats. <i>See also</i> Plastic fat products		
radiolabeled	161	
structural and thermal		
behaviors of	34	
texture of	225	
Fatty acid compositions		
of rape, sunflower, and canola oils	228	
of TAG, diversity in	3	

## Index Terms

## Links

Fatty acid monoesters, rystallization for lipase-catalyzed solid-phase synthe- sis of sugar	168	
Fisher-Turnbull equation	58	120
effect of viscosity and cooling rate	62	
nucleation kinetics of blends of palm stearin and sesame oil	61	
Fletcher-Powell algorithm	28	
Floc packing	156	
Food materials, interactions of sound waves with	134	
Formylurea, simulated packing arrangement of	29	
Fourier transform-infrared (FT-IR) spectra polarized, of SRS	11	
Fractal aggregate networks elasticity of	153	
microstructure of a colloidal	155	
Fractal organization, of TAG during crystallization	74	
Fractional crystallization, of milk-fats	126	
Free energy for nucleation, and crystallization in blends of palm stearin and sesame oil	63	
FT-IR. <i>See</i> Fourier transform- infrared spectra		
Fully hydrogenated fats, crystal form of, in their most stable state	225	
Functions, potential	18	

## Index Terms

## Links

### **G**

$\gamma$ form	4	9
of SLS	12	
Glycerides. <i>See</i> High-melting glycerides		
Glycerol conformations	6	
Growth blocking	24	
Growth disruption	24	
Growth forms, according to various models	23	
Growth mechanisms, Avrami exponent for various types of	112	
Growth slice adsorption	24	

### **H**

Hard sphere (HS) potential	18	
Heat sink, in chocolate cooling tunnel	218	
Heterogeneous nucleation	61	
<i>n</i> -hexadecane crystallization kinetics of mixtures of	143	
ultrasonic velocity in emulsified	140	
Hexane, solvent action of	170	
High-melting fraction (HMF), of cocoa butter	37	
High-melting glycerides (HMG), of stick and soft margarines	233	

## **Index Terms**

## **Links**

Hydrogen bonding interactions	20		
Hydrogenated fats			
fully, crystal form of	225		
measuring solids in soybean oil	146		
polymorphic behavior of	231		
<b>I</b>			
Ice cream			
partial coalescence in	205		
role of surfactants in	206		
structure formation in	205		
Image analysis studies, cooling			
curves for	123		
Index of Avrami, and crystallization in			
blends of palm stearin			
and sesame oil	63		
Induction period, for crystallization	69		
Intermolecular interactions,			
calculation of	19		
Intraglobular crystal morphology, under			
perikinetiic conditions	181		
Isothermal conditioning	192		
Isothermal crystallization			
Avrami equation plots for palm oil			
products under	113		
thermograms obtained by			
differential scanning calorimetry	59	67	89
Isothermal evolution	193		

## Index Terms

## Links

### **J**

“Jackknife classification” 83

### **L**

Lamellar organization, effect of  
    cooling rate on TAG  
    crystallization 64

#### Lard

    emulsion destabilization of 179  
    TAG composition of 234  
    viscosity of 186  
    X-ray diffractogram of 185

Latent heat, of cocoa butter,  
    effect of cooling rates on 106

Lattice energy 21

Lecithins, sucrose polyester,  
    effect on crys-  
    tallization rate of vegetable ghee 87

Lennard-Jones (LJ) potential 18

Light-scattering studies  
    cooling curves for 123  
    of fractional crystallization of  
    milk fats 127

Linear viscoelastic region (LVR) 65

#### Linoleic acid

$\alpha$  and  $\gamma$  form of 12  
    enthalpy and entropy of polymorphic  
    transformations of 10

## Index Terms

## Links

Linoleic acid ( <i>Cont.</i> )	
melting of $\gamma$ of	13
subcell structures of polymorphic	
forms of	9
X-ray diffraction spectra of -	
transformation of	13
Lipase-catalyzed esterification	169
procedure for	170
Lipase-catalyzed solid-phase synthesis,	
crystallization for, of sugar	
fatty acid monoesters	168
Lipid crystallization	
comparative experimental techniques	
used in studies of	120
measurements of	136
molecular modeling applications in	17
ultrasonic characterization of	132
Lipid crystals, measuring	
exchange with oils	160
Liquid crystalline structures	
of cocoa butter	37
of TAG	40
Liquid soybean oil, solid fat content in	148
LJ. <i>See</i> Lennard-Jones potential	
Longitudinal waves	134
Low-melting fraction (LMF), of	
cocoa butter	37

## Index Terms

## Links

### M

Margarine spread oils. *See also* Vegetable

margarines and shortenings

polymorphism of corn-canola oil 233

solid fat content in commercial 147

trans-free 62

Medium-chain triglyceride (MCT) oil 161

Melting profiles

in assessment of fat-blooming 81

of  $\beta'$  and  $\beta$  form of TAG 230

Microscopy

of shortenings 43

thresholded polarized light 125

Milk fat, thermal and structural

behavior of 190

Milk-fat DAG (MF-DAG), fractional

crystallization of 126

Milk-fat TAG (MF-TAG) 110

fractional crystallization of 126

polarized light micrographs of 125

Minimization

in polymorphism 30

in surface studies 27

Mixed-acid TAG 3

molecular structures of 5

polymorphic occurrence of

saturated-elaidic 14

saturated-unsaturated 8

## Index Terms

## Links

### Modeling

attachment energy, growth form	
according to	23
molecular applications, in lipid	
crystallization	17
Molecular aspects, in fat polymorphism	1
Molecular dynamics simulations	27
Molecular interactions in TAG	3
promoting structural stabilization	4
Molecular mechanics	17
Molecular modeling applications, in lipid	
crystallization	17
Molecular structures, of mixed-acid TAG	5
Mono-acid TAG	3
Monoesters, synthesis of sugar fatty acid	168
Morphology maps	
of dynamic crystallization of cocoa butter	103
of static crystallization of cocoa butter	100

## N

Networks. *See* Fractal aggregate networks

### Nucleation

Avrami exponent for various types of	112
on a foreign particle	60
heterogeneous	61
Nucleation kinetics	
of blends of palm stearin and sesame oil	61
free energy for	63

## Index Terms

## Links

### **O**

Oil-in-water (O/W)emulsion state	1
Oleic acid	
enthalpy and entropy of polymorphic transformations of	10
lattice energy of	21
polymorphic forms of	4
subcell structures of polymorphic forms of	9

### **P**

Packing arrangement, simulated,	
of formylurea	29
Palm kernel oil (PKO)	42
Avrami equation plots for refined	114
Palm oil (PO)	
Avrami equation plots for crude	113
Avrami equation plots for refined, bleached, deodorized	113
crystallization of products from	110
major TAG of	232
polymorphic forms of	
products from	231
shortenings based on binary blends with anhydrous milk fat	42
Palm stearin/canola oil (PSCO)	
emulsion destabilization of	179    182
viscosity of	186
X-ray diffractograms of	185

## Index Terms

## Links

Palm stearin (PS)	
Avrami equation plots for refined	114
thermograms for blends with	
sesame oil	56
Palmitic acid content, of various	
fats and oils	229
Partial coalescence	
emulsion, in dairy systems	200
in ice cream	205
in whipped cream	202
Particulate aggregate network, structural	
hierarchy of	153
PBC. <i>See</i> Periodic bond chains	
Perikinetic conditions, intraglobular crystal	
morphology under	181
Periodic bond chains (PBC), governing	
crystal morphology	22
Periodic boundary conditions, in a Monte	
Carlo simulation	26
Phase-separation theory	79
Physical properties, of shortenings	
based on binary blends with palm	
oil and anhydrous milk fat	42
PKO. <i>See</i> Palm kernel oil	
Plastic fat products	53
testing $\beta'$ stability of	232
pNMR. <i>See</i> Pulsed nuclear magnetic reso-	
nance studies	

## Index Terms

## Links

PO. <i>See</i> Palm oil		
Polarized Fourier transform-infrared spectra of SRS	11	
Polarized light micrographs, thresholded, of milk-fat TAG	125	
Polymorphic transformations, of SSS, SOS, SRS, and SLS, enthalpy and entropy of	10	
Polymorphic transition pathways	227	
Polymorphism	29	
in bulk and emulsified fat	184	
cluster analysis of	30	
in cocoa butter	34	
confirmation of	30	
of corn-canola oil soft margarine	233	
in fats, molecular aspects of	1	226
minimization in	30	
Monte Carlo simulation of	29	
in palm oil-anhydrous milk fat shortenings	51	
in palm oil products	115	
in $PP_n$	5	
of saturated-elaidic mixed-acid TAG	14	
of SOS, SRS, and SLS, subcell structures of	9	
in tempered shortening	235	
and texture of fats	225	

## Index Terms

## Links

Potential functions	18
Powder, structure solution from	28
PP2 $\beta$ , crystal structure of	5
PP14 $\beta'_2$ , crystal structure of	5
Protein membrane composition, adsorbed	203
PS. <i>See</i> Palm stearin	
PSCO. <i>See</i> Palm stearin/canola oil	
Pulsed nuclear magnetic resonance (pNMR)	
cooling curves for	123
of fractional crystallization of milk fats	126
for measuring solids in hydrogenated soybean oil	146
<b>Q</b>	
Quantum mechanics	17
<b>R</b>	
“Radiation plate,” in chocolate cooling tunnel	218
Rape oil, fatty acid compositions of	228
Refined, bleached, deodorized (RBD) palm oil	
Avrami equation plots for	113
polymorphic forms of	115

## Index Terms

## Links

Refined palm kernel oil	
Avrami equation plots for	114
polymorphic forms of	115
Refined palm stearin	
Avrami equation plots for	114
polymorphic forms of	115
Rheology	
of blends of palm stearin	
and sesame oil	67
of chocolate in the semi-solid state	223
Ricinoleic acid	
$\beta'$ form of	12
enthalpy and entropy of polymorphic	
transformations of	10
polarized Fourier transform-infrared	
spectra of	11
subcell structures of polymorphic	
forms of	9
X-ray diffraction spectra of	11
Rietveld refinement, rigid-body	28
<b>S</b>	
Saturated-elaidic mixed-acid TAG,	
polymorphic occurrence of	14
Saturated-unsaturated mixed-acid TAG	8
Scanning calorimetry. <i>See</i> Differential	
scanning calorimetry	
Semi-solid state, rheology of	
chocolate in	223

## Index Terms

## Links

Sesame oil, thermograms for blends with		
palm stearin	56	
SFC. <i>See</i> Solid fat content		
SFI. <i>See</i> Solid fat index		
Shear-induced crystallization	184	
Shear longitudinal waves	134	
Shear rate		
dynamic onset time as function of average	104	
effect on dynamic-static		
crystallization	105	
Shortenings. <i>See also</i> Vegetable		
margarines and shortenings		
analysis and evaluation of	43	
based on binary blends of palm oil and		
anhydrous milk fat	42	
HMG of	234	
polymorphic form in tempered	235	
production of	42	
Slice boundary	19	
Small-angle XRD patterns	36	192
Soft margarines		
HMG of	233	
polymorphism of corn-canola oil	233	
Soft sphere (SS) potential	18	
Solid fat content (SFC)		
changes in, during storage	46	
in commercial margarine		
spread oils	147	
in liquid soybean oil	148	

## Index Terms

## Links

Solid fat content (SFC) ( <i>Cont.</i> )		
measuring by pNMR	120	
in palm oil-anhydrous milk fat	46	
of shortenings	43	148
vs. solid fat index	146	
Solid fat index (SFI)		
effect of emulsifiers on	149	
vs. solid fat content	146	
Solid-phase synthesis, of sugar fatty acid		
monoesters	168	
Solidification, of chocolate	218	
Solidification processes	93	
in chocolate confectionery		
manufacture	215	
Sound waves		
fundamentals of	133	
interactions with food materials	134	
measurement methods using	135	
Soybean oil, solid fat content in liquid	148	
Specific enthalpy, of crystallization	220	
Spectroturbidity, fat destabilization		
determined by	204	
Speed of sound, during cooling in confec- tionery fat	142	
SR-XRD. <i>See</i> Synchrotron radiation		
X-ray diffraction spectra		
SSS. <i>See</i> Tristearoylglycerol		
Stabilization		
of dairy formations	200	
structural, of TAG	4	

This page has been reformatted by Knovel to provide easier navigation.

## **Index Terms**

## **Links**

Static crystallization	
of cocoa butter	96
morphology maps of	100
temperature-time-transformation	
diagram of	99
Stearic acid	
as acyl donor	173
BFDH and attachment energy results for	23
unit cell of	23
Steepest descent algorithm	28
Stick margarines, HMG of	233
Storage	
changes in solid fat content of	
shortenings during	46
of shortenings based on binary blends	
with palm oil and anhydrous	
milk fat	42
Structural behaviors of fats	
application of crystallization in emulsion to	190
simultaneous examination of, by cou-	
pled x-ray diffraction and DSC	34
Structural stabilization	10
of TAG	4
Structure formation	
in dairy systems	200
in ice cream	205
in whipped cream	202

## **Index Terms**

## **Links**

Structure solution, from powder	28
Subcell arrangements	
hybrid-type	7
typical	2
Subcell structures, of polymorphic	
forms of SOS, SRS, and SLS	9
Sucrose polyesters, effect on	
crystallization rate of vegetable ghee	87
Sugar fatty acid monoesters, crystallization	
for lipase-catalyzed solid-	
phase synthesis of	168
Sunflower oil, fatty acid	
compositions of	228
Supercooling	
in blends of palm stearin and	
sesame oil	64
in crystallization	55
Supersaturation, in crystallization	55
Surface studies	23
minimization in	27
molecular dynamics of	27
using Monte Carlo simulations	26
Surfactants, role in ice cream	206
Sutherland (S) potential	18
Synchrotron radiation X-ray diffraction	
(SR-XRD) spectra	12
Synchrotron X-ray diffraction, time-	
resolved	36

## Index Terms

## Links

### T

TAG. <i>See</i> Triacylglycerol		
Tallow, TAG composition of	234	
TCL. <i>See</i> Triple chainlength structure		
Temperature-time-transformation (TTT)		
diagram		
of dynamic crystallization of cocoa butter	101	222
of static crystallization of		
cocoa butter	99	
Tempered chocolate, phases		
coexisting in	35	
Tempered shortening, polymorphic		
forms in	235	
Tempering	235	
different conditions of	81	
effects on shortenings based on		
binary blends with palm oil		
and anhydrous milk fat	42	
micrograph of shortenings	49	
and yield values	44	
Texture of fats, polymorphism and	225	
Thermal behaviors of fats		
application of crystallization in		
emulsion to	190	
simultaneous examination of, by		
coupled x-ray diffraction		
and DSC	34	

## Index Terms

## Links

Thermodynamic drive, for crystallization	55
Thermograms	
for blends of palm stearin and sesame oil	56
DSC, for blends of palm stearin and sesame oil	67
isothermal crystallization	59
Thresholded polarized light micrographs, of milk-fat TAG	125
Time-resolved synchrotron X-ray diffraction	36
Transition pathways, polymorphic	227
Triacylglyceride crystallization	
effect of cooling rate on lamellar organization of	64
fractal organization during	74
in vegetable oils	53
Triacylglycerol (TAG)	
crystal birefringence of	72
crystalline evolution of, in cream	194
diversity in fatty acid compositions of	3
in liquid crystalline form	40
major, of palm oil	232
melting points of $\beta'$ and $\beta$ form of	230
molecular interactions in	3
structural stabilization of	4

## Index Terms

## Links

Triacylglycerol (TAG) ( <i>Cont.</i> )		
subcell structures of polymorphic		
forms of	9	
in vegetable margarines and		
shortenings	229	
Triglycerides, interactions		
between solid and liquid	160	162
Triple chainlength (TCL) structure	2	4
Tristearoylglycerol (SSS), enthalpy and		
entropy of polymorphic		
transformations of	10	
TTT. <i>See</i> Temperature-time-		
transformation diagram		
Turbidimetric studies, cooling		
curves for	123	127
Turbidity time, of fat used in vegetable ghee	93	
<b>U</b>		
Ultrasonic characterization		
future of	143	
instrument used in	141	
of lipid crystallization	132	
principles of	133	
Ultrasonic reflectance amplitude,		
in confectionery fat	139	
Ultrasonic velocity		
on cooling in chocolate	138	
in emulsified <i>n</i> -hexadecane	140	

## **Index Terms**

## **Links**

Undertempering	81	
Unsaturated TAG. <i>See</i> Saturated-unsaturated mixed-acid TAG		
<b>V</b>		
Vegetable ghee (vanaspati)		
crystallization rate of	87	
turbidity time of fat used in	93	
Vegetable margarines and shortenings,		
TAG in	229	
Vegetable oils		
TAG composition of	230	
TAG crystallization in	53	
Velocity. <i>See</i> Ultrasonic velocity		
Viscosity, effect on crystallization	62	
<b>W</b>		
Wetting angles, nucleation on a foreign		
particle for different	60	
Whipped cream, partial coalescence in	202	
Wide-angle XRD patterns	192	194
<b>X</b>		
X-ray diffraction (XRD) analysis. <i>See also</i>		
Coupled x-ray diffraction		
of bulk and emulsified fats	185	
of shortenings	43	
small-angle	37	192

## **Index Terms**

## **Links**

X-ray diffraction (XRD) spectra	
of $\alpha$ - $\gamma$ transformation of SLS	13
of SRS	11
XRD. <i>See</i> X-ray diffraction	

## **Y**

Yield values, effect of tempering on	44
Young's modulus	157